



Casado Magaña, Enrique Juan (2016) *Trajectory prediction uncertainty modelling for Air Traffic Management*. PhD thesis.

<http://theses.gla.ac.uk/7700/>

Copyright and moral rights for this thesis are retained by the author

A copy can be downloaded for personal non-commercial research or study, without prior permission or charge

This thesis cannot be reproduced or quoted extensively from without first obtaining permission in writing from the Author

The content must not be changed in any way or sold commercially in any format or medium without the formal permission of the Author

When referring to this work, full bibliographic details including the author, title, awarding institution and date of the thesis must be given

Glasgow Theses Service

<http://theses.gla.ac.uk/>

theses@gla.ac.uk

TRAJECTORY PREDICTION UNCERTAINTY MODELLING FOR AIR TRAFFIC MANAGEMENT



University
of Glasgow

A thesis submitted in fulfilment of the requirements for the Degree of Doctor of
Philosophy

Division of Aerospace Sciences
School of Engineering
University of Glasgow

By
Enrique Juan Casado Magaña
April 2016

© Enrique Juan Casado Magaña, 2016

This page intentionally left blank

*This work is dedicated to
the most resilient person I've ever met, my mom.*

This page intentionally left blank

*“The more precisely the position is determined,
the less precisely the momentum is known in this instant,
and vice versa.”*

The Uncertainty Principle

Werner Heisenberg (1927)

This page intentionally left blank

ABSTRACT

The anticipated growth of air traffic worldwide requires enhanced Air Traffic Management (ATM) technologies and procedures to increase the system capacity, efficiency, and resilience, while reducing environmental impact and maintaining operational safety. To deal with these challenges, new automation and information exchange capabilities are being developed through different modernisation initiatives toward a new global operational concept called Trajectory Based Operations (TBO), in which aircraft trajectory information becomes the cornerstone of advanced ATM applications. This transformation will lead to higher levels of system complexity requiring enhanced Decision Support Tools (DST) to aid humans in the decision making processes. These will rely on accurate predicted aircraft trajectories, provided by advanced Trajectory Predictors (TP). The trajectory prediction process is subject to stochastic effects that introduce uncertainty into the predictions. Regardless of the assumptions that define the aircraft motion model underpinning the TP, deviations between predicted and actual trajectories are unavoidable.

This thesis proposes an innovative method to characterise the uncertainty associated with a trajectory prediction based on the mathematical theory of Polynomial Chaos Expansions (PCE). Assuming univariate PCEs of the trajectory prediction inputs, the method describes how to generate multivariate PCEs of the prediction outputs that quantify their associated uncertainty. Arbitrary PCE (aPCE) was chosen because it allows a higher degree of flexibility to model input uncertainty. The obtained polynomial description can be used in subsequent prediction sensitivity analyses thanks to the relationship between polynomial coefficients and Sobol indices. The Sobol indices enable ranking the input parameters according to their influence on trajectory prediction uncertainty.

The applicability of the aPCE-based uncertainty quantification detailed herein is analysed through a study case. This study case represents a typical aircraft trajectory prediction problem in ATM, in which uncertain parameters regarding aircraft performance, aircraft intent description, weather forecast, and initial conditions are considered simultaneously. Numerical results are compared to those obtained from a Monte Carlo simulation, demonstrating the advantages of the proposed method. The thesis includes two examples of DSTs (Demand and Capacity Balancing tool, and Arrival Manager) to illustrate the potential benefits of exploiting the proposed uncertainty quantification method.

This page intentionally left blank

ACKNOWLEDGEMENTS

I wish to express my gratitude to my supervisor, Dr. Euan McGookin, for his support, advice, and help during the most critical part of this research. His effort to manage all difficulties I caused has been invaluable.

I also want to thank my former supervisor, Dr. Colin Goodchild, who selected me as the most appropriate candidate to develop the proposed research.

I express a very special appreciation to my industrial supervisor, Dr. Miguel Vilaplana. He is one of the brightest, most encouraging, and energetic persons I have met. His global understanding of the ATM environment, his broad technical knowledge and his capability to motivate has guided my research to a singular outcome, and helped me to overcome the toughest moments. On top of that, I really appreciate his friendship.

I would like to extend my gratitude to my Boeing Mentor, Dr. Marco La Civita. His technical expertise, pragmatic view of complex problems, and most especially his friendship, are somehow part of this thesis.

A special thanks to Luis P. D'Alto, he always found a couple of minutes to discuss my thoughts just to let me vent my worries. I sincerely appreciate his contribution to the process of importing weather forecast data that boosted my work significantly, and, mostly, his friendship.

My gratitude to Dr. Javier López Leonés, not only because this research is founded in his work relative to a formal aircraft intent description, but also for his support and friendship. He advocated my application to Boeing Research and Technology Europe (BR&T-E), what is actually the inception of this research.

My thanks to David Esteban and David Scarlatti for the time we spent together discussing innovative and leading-edge inventions, and, most importantly, for their friendship.

I especially appreciate the contribution of Dr. Sergey Oladyshkin, who explained me how to apply the arbitrary Polynomial Chaos Expansions theory. I want also to thank Dr. Bruno

Sudret and Óscar García Cabrejo, who provided me with alternative PCE-based solutions that were of high interest in supporting the selection of the final implemented solution.

My thanks also to Paco Navarro for sharing with me some of the plots included in this thesis that strongly facilitate the understanding of the trajectory prediction lifecycle.

I want to thank SESAR JU for recognizing me with the SESAR Scientist Award 2014 for the contribution of this research to the modernisation of Air Traffic Management, and AIAA for awarding the paper presented at Infotech@Aerospace 2013 Conference that described a model to assess the impact of aircraft performance uncertainties in trajectory prediction as Best Student Technical Paper.

I sincerely appreciate the contribution of Pam Arkebauer, who helped me with the English style writing and the document edition. She strongly improved the document readability and clarity, which finally facilitates significantly the dissemination of the research outcomes.

Thanks to Elaine McNamara, for her willingness to help me with all painful financial and administrative issues required to get registered and to extend the standard academic period.

My lifelong gratitude to my parents, Juan and Carolina, for their love, trust, and example. They have always encouraged me to take my own decisions and warmly took care of me when I failed.

My gratitude also to my siblings, Carlos R. and Lorena M., for their love, patience, and understanding.

I especially want to thank my beloved Eva for her love and kindness. I sincerely appreciate the sacrifices you have made to help me finding more time to dedicate to this thesis.

And, finally, thanks to Marcela and Marco for bringing unexpected uncertainty to my life every day. This research has been cosponsored by HALA! (Higher Automation Levels in ATM) SESAR Research Network and The Boeing Company.

CONTENTS

Acknowledgements.....	ix
Declaration of Originality.....	xxiii
List of Abbreviations	xxv
Nomenclature	xxxiii
CHAPTER 1 Introduction	1
1.1 Preface.....	1
1.2 Aims and Objectives	4
1.3 Contribution of the Research	4
1.3.1 Papers	5
1.3.2 Patents.....	6
1.4 Dissertation Outline	6
CHAPTER 2 Background & Literature Review	9
2.1 Introduction.....	9
2.2 Air Traffic Management Definition and Historical Evolution	10
2.3 Towards a New ATM Paradigm	15
2.3.1 Trajectory Management.....	18
2.3.2 Advanced Decision Support Tools.....	19
2.4 The Role of Aircraft Trajectory Prediction in ATM.....	20
2.5 The Trajectory Prediction Process	23
2.5.1 Trajectory Prediction Accuracy.....	29
2.6 Uncertainty Quantification in Trajectory Prediction	33
2.7 Summary	36
CHAPTER 3 Uncertainty Sources Affecting Aircraft Trajectory Prediction	37
3.1 Introduction.....	37
3.2 Aircraft Trajectory Prediction.....	38

3.3	Initial Aircraft State	42
3.4	Aircraft Motion Modelling	43
3.4.1	Aircraft Motion Modelling Uncertainties	49
3.5	Earth Surface Modelling.....	49
3.5.1	Earth Surface Modelling Uncertainties	50
3.6	Gravitational Force Modelling	50
3.6.1	Gravitational Force Modelling Uncertainties	51
3.7	Aircraft Performance Modelling	51
3.7.1	EUROCONTROL Base of Aircraft Data.....	52
3.7.2	Aircraft Performance Modelling Uncertainties.....	53
3.8	Weather Modelling	54
3.8.1	Atmosphere Modelling	55
3.8.1.1	Atmosphere Modelling Uncertainties	57
3.8.2	Wind Modelling	58
3.8.2.1	Wind Modelling Uncertainties	58
3.9	Aircraft Intent Uncertainties	59
3.10	Uncertainty in Model-Based Decision Support Applications	62
3.10.1	Trajectory Prediction Uncertainties Modelling.....	65
3.11	Summary.....	66

CHAPTER 4 Impact of Aircraft Performance Uncertainty on Trajectory

Prediction	69
4.1	Introduction	69
4.2	Aircraft Performance in Trajectory Prediction	70
4.2.1	Aerodynamics	71
4.2.1.1	Lift.....	71
4.2.1.2	Drag.....	73
4.2.2	Propulsion	76
4.3	Aircraft Performance Modelling in Trajectory Prediction	79

4.3.1	BADA Aircraft Performance Models.....	82
4.3.2	Aerodynamic Model.....	83
4.3.3	Propulsion Model.....	86
4.4	Aircraft Performance Modelling Uncertainty.....	89
4.4.1	Aerodynamic Modelling Uncertainty.....	90
4.4.2	Propulsion Modelling Uncertainty.....	92
4.5	Assessment of APM Uncertainty Impact on Prediction.....	93
4.5.1	Cruise.....	96
4.5.2	Climb.....	98
4.5.3	Descent.....	99
4.6	Trajectory Prediction Uncertainty Model due to APM Uncertainty.....	101
4.7	Summary.....	102
CHAPTER 5 Impact of Weather Uncertainty on Trajectory Prediction.....		105
5.1	Introduction.....	105
5.2	Weather Data in Trajectory Prediction.....	107
5.2.1	Aircraft Dynamics.....	108
5.2.2	Aircraft Performance.....	108
5.2.3	Aircraft Speeds Transformations.....	109
5.2.4	Altitude Transformations.....	110
5.2.4.1	Tropopause.....	112
5.3	Weather Forecast Uncertainty.....	113
5.3.1	Forecast Ensemble.....	115
5.4	Weather Forecast Uncertainty in Trajectory Prediction.....	117
5.4.1	Forecast Ensembles in Trajectory Prediction.....	119
5.5	Assessment of Trajectory Prediction Uncertainty due to Forecast Ensembles....	120
5.5.1	Trajectory Prediction Uncertainty Identification.....	121
5.6	Summary.....	126

CHAPTER 6 Impact of Aircraft Intent Uncertainty on Trajectory Prediction	129
6.1 Introduction	129
6.2 The Aircraft Intent Description Language	130
6.2.1 AIDL Alphabet	131
6.2.2 AIDL Grammar	135
6.3 Description of AI Uncertainties.....	136
6.3.1 Instruction Uncertainty	137
6.3.2 Initial Conditions Uncertainty.....	139
6.3.3 Continuity Uncertainty.....	140
6.4 AI Uncertainty Modelling	141
6.4.1 Instruction Uncertainty Model	141
6.4.1.1 Trigger Uncertainty Model	142
6.4.1.2 Effect Uncertainty Model.....	148
6.4.2 Initial Conditions Uncertainty Model	154
6.4.2.1 Lateral Profile	155
6.4.2.2 Vertical Profile	159
6.5 Uncertainty Propagation between Operations	166
6.6 Summary.....	167
CHAPTER 7 Quantification of Trajectory Prediction Uncertainty	169
7.1 Introduction	169
7.2 Uncertainty Quantification Based on Polynomial Chaos Expansions	170
7.2.1 One-dimensional PCE.....	172
7.2.2 Multi-dimensional PCE.....	172
7.2.3 PCE Based on Statistical Moments.....	174
7.2.4 Non-intrusive Determination of PCE Coefficients	177
7.3 Global Sensitivity Analysis Based on Polynomial Chaos Expansions	180
7.3.1 Sobol Sensitivity Indices.....	181
7.4 Application of PCE-based Uncertainty Quantification to Trajectory Prediction	183

7.4.1	Case Study Description	184
7.4.1.1	Sources of Uncertainty	187
7.4.2	Numerical Results	193
7.4.2.1	Results from Monte Carlo Simulation.....	193
7.4.2.2	Results from aPCE Method.....	195
7.4.2.3	Comparison of Results	197
7.4.2.4	Sensitivity Analysis	198
7.5	Trajectory Prediction Uncertainty in Decision Support Tools	200
7.5.1	Demand and Capacity Balancing	201
7.5.2	Arrival Manager	203
7.6	Summary	206
CHAPTER 8 Conclusions and Future Work		209
8.1	Conclusions.....	209
8.2	Future Work.....	212
References		215
Appendix A Aircraft Performance Degradation Modelling Using Recorded Flight Data		227
Appendix B Trajectory Prediction Uncertainty Due to Uniformly Distributed APM Uncertainty		231
B-1.	Cruise.....	231
B-2.	Climb	232
B-3.	Descent	233
Appendix C AIDL Alphabet & Grammar Summary		235
Appendix D Trigger and Effect Uncertainty Models.....		237
D-1	Trigger Uncertainty Modelling.....	237
D-2	Effect Uncertainty Modelling.....	245

Appendix E Polynomial Chaos Expansions	253
E-1 Orthonormal Basis Used in gPCE.....	253
E-2 Computation of ϕ_j^k	253

LIST OF TABLES

Table 3-1 – Summary of the Identified Uncertainty Sources	67
Table 4-1 – Performance Uncertainty Coefficients	95
Table 4-2 – Cruise Phase Initial Conditions	97
Table 4-3 – Climb Phase Initial Conditions	98
Table 4-4 – Descent Phase Initial Conditions	100
Table 4-5 – Prediction Uncertainty Due to APM Uncertainty	102
Table 5-1 – Descent Phase Initial Conditions	125
Table 6-1 – AIDL Instruction Groups and Profiles	134
Table 6-2 – AIDL Lexical Rules	136
Table 6-3 – AIDL Syntactical Rules	136
Table 6-4 – Impact of Instruction Type on Uncertainty	138
Table 6-5 – Trigger Uncertainty - AI Descriptions Used in Monte Carlo Runs	143
Table 6-6 – Trigger Uncertainty – Monte Carlo Parameters Ranges	144
Table 6-7 – Subset of Studied Aircraft State Variables	146
Table 6-8 – Trigger Uncertainty Propagation Model - RMSE Metric	147
Table 6-9 – Effect Uncertainty - AI Descriptions Used in Monte Carlo Runs	149
Table 6-10 – Effect Uncertainty – Monte Carlo Parameters Ranges	150
Table 6-11 – Effect Uncertainty Propagation Model - RMSE Metric	153
Table 6-12 – Values of the Identified Mass Uncertainty Model Coefficients	161
Table 7-1 – Case Study – Initial Aircraft State	187
Table 7-2 – Case Study – AI Uncertainties (Triggers A to D)	188
Table 7-3 – Case Study – AI Uncertainties (Triggers E to K)	188
Table 7-4 – Case Study – AI Uncertainties (Triggers L)	190

Table 7-5 – Case Study – AI Uncertainties (Instructions Effects)	190
Table 7-6 – Case Study – Initial Conditions Uncertainties	191
Table 7-7 – Case Study – Initial Conditions Uncertainties	193
Table 7-8 – Monte Carlo Simulation Results	194
Table 7-9 – aPCE Results	196
Table 7-10 – Case Study – Initial Aircraft State.....	197
Table 7-11 – Sensitivity Analysis Based on Total Sobol Indices.....	199
Table 7-12 – DCB - Uncertainty Sources.....	201
Table 7-13 – Departure Time Uncertainty.....	202
Table 7-14 – DCB – Sensitivity Analysis.....	203
Table 7-15 – AMAN – Sensitivity Analysis.....	206

LIST OF FIGURES

Figure 2-1 – Trajectory Lifecycle Scheme.....	18
Figure 2-2 – AP-16 Common Trajectory Prediction Framework	24
Figure 2-3 – Intent Generation Process.....	27
Figure 2-4 – Representation of the Spatial Trajectory Prediction Accuracy	32
Figure 2-5 – CTAS Trajectory Synthesis Architecture.....	35
Figure 3-1 – Aircraft Trajectory Prediction Architecture	39
Figure 3-2 – Progressive Transition Between Determinism and Total Indeterminacy.....	64
Figure 4-1 – Dependencies of the Lift Coefficient	72
Figure 4-2 – Dependencies of the Drag Polar Curve	75
Figure 4-3 – Airspeed Effect on Thrust	78
Figure 4-4 – Net Thrust Behaviour	81
Figure 4-5 – Drag Polar Curve.....	85
Figure 4-6 – Boeing 767-200 Fuel Consumption Coefficient for Non-Idle Regimes	88
Figure 4-7 – Boeing 767-200 Fuel Consumption Coefficient for Idle Regimes	89
Figure 4-8 – Triangular Distribution of f_I^+	96
Figure 4-9 – Aircraft Mass Variability (Cruise Case).....	97
Figure 4-10 – Elapsed Time Variability (Climb Case)	99
Figure 4-11 – CAS Variability (Descent Case).....	100
Figure 5-1 – Weather Uncertainty Propagation in Trajectory Prediction	119
Figure 5-2 – Ensemble of Trajectories – h vs. t	123
Figure 5-3 – North and East Wind Components Speed	124
Figure 5-4 – Ensemble of Trajectories – Δh Boxplot	124

Figure 5-5 – Trajectory Uncertainty Described by ECDFs	125
Figure 5-6 – Correlation Between Along-Track Wind Speed and Ground Speed Standard Deviations	126
Figure 6-1 – Initialisation of a TPPC Problem	140
Figure 6-2 – Mass and Flown Distance Uncertainty Distributions at the End of the Execution Interval due to Gaussian Trigger Uncertainty	144
Figure 6-3 – CMB3 – Comparison Between Modelled and Raw Uncertainty Data due to Trigger Uncertainty	148
Figure 6-4 – Mass and Flown Distance Uncertainty Distributions at the end of the Execution Interval due to Gaussian Effect Uncertainty	151
Figure 6-5 – CMB3 – Comparison Between Modelled and Raw Uncertainty Data due to Effect Uncertainty.....	154
Figure 6-6 – Propagation of Initial Speed and Altitude Uncertainties in Cruise Trajectory Prediction at Constant Speed	156
Figure 6-7 – TLP - Position Uncertainty	157
Figure 6-8 – Heading Uncertainty in CL Instructions	158
Figure 6-9 – AF, γ_{TAS} and ROC Uncertainties in Climbs at Constant Speed.....	163
Figure 6-10 – AF, γ_{TAS} and ROC Uncertainties in Descents at Constant Speed.....	165
Figure 6-11 – Mass Uncertainties in Climbs and Descents at Constant Speed.....	166
Figure 7-1 – Case Study – Aircraft Intent Description.....	185
Figure 7-2 – DCB - Estimated Time and Elapsed Time Uncertainties	202
Figure 7-3 – AMAN – Fuel Burnt and Pressure Altitude Uncertainties	205
Figure 7-4 – AMAN – CAS and Ground Speed Uncertainties	205
Figure A-1 – Aircraft Performance Degradation Modelling	227
Figure B-1 – Uniform Distribution of f_l^+	231
Figure B-2 – Aircraft Mass Variability (Cruise Case).....	232

Figure B-3 – Elapsed Time Variability (Climb Case)	233
Figure B-4 – CAS Variability (Descent Case).....	234
Figure D-1 – CASE CRZ1	238
Figure D-2 – CASE CRZ2	238
Figure D-3 – CASE CRZ3	239
Figure D-4 – CASE CMB1	240
Figure D-5 – CASE CMB2	241
Figure D-6 – CASE CMB4	242
Figure D-7 – CASE DES1	243
Figure D-8 – CASE DES2	244
Figure D-9 – CASE CRZ2	245
Figure D-10 – CASE CRZ3	246
Figure D-11 – CASE CMB4	247
Figure D-12 – CASE CMB5	248
Figure D-13 – CASE CMB6.....	249
Figure D-14 – CASE DES2	250
Figure D-15 – CASE DES3	251

This page intentionally left blank

DECLARATION OF ORIGINALITY

I hereby declare that the entire work presented in this thesis has been personally carried out. Where sources of information or the work of others have been used, they are fully cited and referenced and/or appropriate acknowledgement is given.

.....

Enrique Juan Casado Magaña

This page intentionally left blank

LIST OF ABBREVIATIONS

4D	Four Dimensional
AATMSP	Australian ATM Strategic Plan
ACARS	Aircraft Communications Addressing and Reporting System
ADS-B	Automatic Dependent Surveillance-Broadcast
AF	Acceleration Factor
AG	Altitude Guidance
AI	Aircraft Intent
AIDL	Aircraft Intent Description Language
AIP	Aeronautical Information Publication
AL	Altitude Law
AM	Atmospheric Model
AMAN	Arrival Managers
AMM	Aircraft Motion Model
ANP	Aircraft Noise and Performance
ANSP	Air Navigation Service Provider
AOC	Airline Operating Centre
aPC	arbitrary Polynomial Chaos
aPCE	arbitrary Polynomial Chaos Expansion
APDM	Aircraft Performance Degradation Model
APM	Aircraft Performance Model
ASM	Airspace Management
ATC	Air Traffic Control
ATFM	Air Traffic Flow Management
ATM	Air Traffic Management
ATR	Along Track
AV	Air Vehicle
BADA	Base of Aircraft Data
BM	Behavioural Model
BOD	Bottom of Descent
BR&T-E	Boeing Research and Technology - Europe
BUFR	Binary Universal Form for Representation of Meteorological Data

CAR	Civil Air Regulations
CARATS	Collaborative Actions for Renovation of Air Traffic Systems
CAS	Calibrated Airspeed
CDM	Collaborative Decision Making
CDoF	Configuration Degrees of Freedom
CFMU	Central Flow Management Unit
CG	Centre of Gravity
CI	Cost Index
CINTIA	Control of Inbound Trajectories for Individual Aircraft
CITRAC	Common Interface for Trajectory Computation
CL	Course Law
CMB1	Climb 1 (Constant Speed @ Maximum Climb Rating)
CMB2	Climb 2 (Constant Speed @ Constant Path Angle)
CMB3	Climb 3 (Constant Acceleration @ Maximum Climb Rating)
CMB4	Climb 4 (Constant Acceleration @ Linear Altitude Law)
CNS	Communications, Navigation and Surveillance
CNTL	Control Forecast
ConOps	Concept of Operations
CRZ1	Cruise 1 (Constant Speed & Altitude)
CRZ2	Cruise 2 (Constant Acceleration @ Constant Altitude)
CRZ3	Cruise 3 (Constant Deceleration @ Constant Altitude)
CT	Computed Trajectory
CTAS	Center/TRACON Automation System
CV	Coefficient of Variation
CVS	Control Variable Subsystem
DAE	Differential Algebraic Equations
DASC	Digital Avionics Systems Conference
DCB	Demand and Capacity Balancing
DES1	Descent 1 (Constant Speed @ Low Idle Rating)
DES2	Descent 2 (Constant Speed @ Linear Path Angle Law)
DFS	Deutsche Flugsicherung GmbH
DME	Distance Measuring Equipment
DoF	Degrees of Freedom
DSR	Deviated Specific Range
DST	Decision Support Tool

EA	Enterprise Architecture
EAS	Equivalent Airspeed
ECAC	European Civil Aviation Conference
ECDF	Empirical Cumulative Density Function
ECEF	Earth Centred Earth Fixed
ECMWF	European Centre for Medium-Range Weather Forecasts
EDA	Ensemble of Data Assimilation
EG	Energy Guidance
EGM96	Earth Gravitational Model 1996
EM	Ensemble Mean
ES	Ensemble Spread
EPP	Extended Projected Profile
EPR	Engine Pressure Ratio
ERAM	En-Route Automation Modernization
ETA	Estimated Time of Arrival
ETMS	Enhanced Traffic Management System
EU	European Union
EUROCAE	European Organisation for Civil Aviation Equipment
EUROCONTROL	European Organisation for the Safety of Air Navigation
FAA	Federal Aviation Administration
FAB	Functional Airspace Block
FANS	Future Air Navigation Systems
FDM	Finite Difference Method
FDP	Flight Data Processing
FDR	Flight Data Recorder
FDRS	Flight Data Recorder System
FEM	Finite Elements Method
FI	Flight Intent
FL	Flight Level
FMS	Flight Management System
FOM	Figure of Merit
FORM	First-Order Reliability Method
FP	Flight Plan
FPPM	Flight Planning & Performance Manual
FS	Flight Script

GEFS	Global Ensemble Forecast System
GMT	Greenwich Mean Time
gPCE	generalised Polynomial Chaos Expansion
GRS	Geodetic Reference System
GSA	Global Sensitivity Analysis
HA	Hold Altitude
HALA!	Higher Automation Levels in ATM
HC	Hold Course
HLC	High Lift Configuration
HPA	Hold Path Angle
HRES	High Resolution
HS	Hold Speed
HSG	Horizontal Speed Guidance
HT	Hold Throttle
IATA	International Air Transport Association
IC	Initial Condition
ICAO	International Civil Aviation Organisation
IFR	Instrument Flight Rules
IGP	Intent Generation Process
ILS	Instrument Landing System
ISA	International Standard Atmosphere
INM	Integrated Noise Model
JPDO	Joint Planning and Development Office
KPA	Key Performance Area
KPI	Key Performance Indicator
KVM	Kinetic Vertical Modelling
LDC	Lateral Directional Control
LDG	Lateral Directional Guidance
LGC	Landing Gear Configuration
LIDL	Low Idle
LLS	Local Level System
LPG	Lateral Positional Guidance
LSA	Local Sensitivity Analysis
MADIS	Meteorological Assimilation Data Ingest System
MCMB	Maximum Climb

MCNT	Maximum Continuous
MCRZ	Maximum Cruise
MDCRS	Meteorological Data Collection and Reporting System
MDoF	Motion Degrees of Freedom
MFP	Metering Fix Point
MM	Mathematical Model
MSL	Mean Sea Level
MTKF	Maximum Take-Off
MUAC	Maastricht Upper Area Control Centre
NATCA	National Air Traffic Controllers Association
NAS	National Airspace System
NextGen	Next Generation Air Transportation System
NM	Network Manager
NM	Nautical Mile
NOAA	National Oceanic and Atmospheric Administration
NOMADS	National Operational Model Archive and Distribution System
NOP	Network Operations Plan
NOSA	NOAA Observing System Architecture
NOTAM	Notice to Airmen
NWP	Numerical Weather Predictions
OAT	Outside Air Temperature
OCM	Operational Context Model
ODE	Ordinary Differential Equations
OLT	Open Loop Throttle
OP	Operation
PAC	Path Angle Control
PAG	Path Angle Guidance
PAL	Path Angle Law
PAM	Probabilistic Atmospheric Model
PC	Polynomial Chaos
PCE	Polynomial Chaos Expansion
PCM	Probabilistic Collocation Method
PDF	Probability Density Function
PE	Primitive Equation
PMM	Point Mass Model

PP	Preparation Process
PRB	Performance Review Body
PRC	Performance Review Commission
PRU	Performance Review Unit
QFE	Query: Field Elevation
QNH	Query: Nautical Height
R&D	Research and Development
RCRV	Reduced Centred Random Variable
RDP	Radar Data Processing
RMS	Root Mean Square
RMSE	Root Mean Square Error
RO	Research Objective
ROC	Rate of Climb
ROC	Relative Operating Characteristic
RTCA	Radio Technical Commission for Aeronautics
RUC	Rapid Update Cycle
S-TP	Stochastic Trajectory Predictor
SA	Sensitivity Analysis
SAE	Society of Automotive Engineers
SBC	Speed Breaks Configuration
SC	Special Committee
SES	Single European Sky
SESAR	Single European Sky ATM Research programme
SDR	Sequential DAE Resolution
SG	Speed Guidance
SID	Standard Instrument Departure
SIS	State Initialization Subsystem
SL	Speed Law
SM	Spectral Method
SNOWTAM	Snow Warning to Airmen
SORM	Second-Order Reliability Method
SPA	Set Path Angle
SRS	Spherical Reference System
SSR	Secondary Surveillance Radar
STAR	Standard Terminal Arrival Route

SWIM	System Wide Information Management
SV	Singular Vector
TAS	True Airspeed
TBO	Trajectory Based Operations
TC	Throttle Control
TC	Trajectory Computation
TCE	Trajectory Computation Engine
TE	Trajectory Engine
TFM	Traffic Flow Management
TL	Throttle Law
TLP	Track Lateral Path
TM	Trajectory Management
TMA	Terminal Manoeuvring Area
TOA	Time of Arrival
TOC	Top of Climb
TOD	Top of Descent
TE	Trajectory Engine
TP	Trajectory Predictor
TPEP	Trajectory Prediction Export Process
TPP	Trajectory Prediction Process
TPPC	Trajectory Prescribed Path Control
TRACON	Terminal Radar Approach Control
TRJC	Trajectory Computed
TRJR	Trajectory Real
TS	Trajectory Synthesiser
TSC	Trajectory Selection Criterion
TUP	Trajectory Update Process
TVP	Track Vertical Path
UPM	User Preference Model
URET	User Request Evaluation Tool
US	United States
VER	Vertical
VFR	Visual Flight Rules
VHF	Very High Frequency
VOR	VHF Omnidirectional Range

VPG	Vertical Positional Guidance
VSG	Vertical Speed Guidance
WFS	Wind Fixed System
WG	Working Group
WM	Weather Model
XTR	Cross Track

NOMENCLATURE

v_{CAS}	Calibrated airspeed [m/s] ¹
v_{TAS}	True airspeed [m/s]
F_n	Thrust [N]
D	Drag [N]
L	Lift [N]
W	Weight [kg]
m	Aircraft mass [kg]
λ	Longitude [rad]
φ	Latitude [rad]
C_D	Drag Coefficient [-]
C_L	Lift Coefficient [-]
C_T	Thrust Coefficient [-]
δ	Local Pressure [Pa]
V	Magnetic declination [rad]
M	Mach number [-]
κ	Adiabatic index [-]
a	Speed of sound [m/s]
a_0	Speed of sound at MSL [m/s]
T	Air temperature [K]
ΔT	Temperature deviation at MSL [K]
R	Specific air constant [J/(K·mol)]
GM	Earth Gravitational Constant [N·m ² /kg ²]
h	Geodetic Altitude [m]
H_p	Geopotential Pressure Altitude [m]
γ_{TAS}	Aerodynamic path angle [rad]
μ_{TAS}	Aerodynamic bank angle [rad]
χ_{TAS}	Aerodynamic yaw angle [rad]

¹ International System of Units

<i>F</i>	Fuel Consumption [kg/s]
<i>w_i^{WFS}</i>	Wind components referred to the WFS of reference [m/s]
<i>%N_I</i>	Rotational speed of the engine's low-pressure compressor and turbine [-]
<i>δ_T</i>	Throttle Coefficient [-]
<i>θ</i>	Temperature ratio [-]
<i>g</i>	Gravity model [m/s ²]
<i>S</i>	Aerodynamic surface [m ²]
<i>V</i>	Magnetic declination [rad]
<i>ρ</i>	Air density [kg/m ³]
<i>P</i>	Air pressure [Pa]
<i>ΔP</i>	Pressure deviation at MSL [Pa]
<i>LHV</i>	Fuel Lower Heating Value [J/mol]
<i>e</i>	Terrain elevation [m]
<u><i>P_{qp}</i></u>	Normalised Legendre functions degree q and order p [-]
<u><i>C_{qp}</i></u>, <u><i>S_{qp}</i></u>	Normalised gravitational coefficients [-]
<i>p</i>	Order [-]
<i>q</i>	Degree [-]
<i>α</i>	Angle of attack [rad]
<i>β</i>	Sideslip angle [rad]
<i>d</i>	PCE order [-]
<i>A_i</i>	Univariate PCE coefficients [-]
<i>B_i</i>	Multivariate PCE coefficients [-]
<i>n</i>	Number of random variables [-]
<i>m</i>	Size of the polynomial basis [-]

CHAPTER 1

INTRODUCTION

1.1 Preface

Current Air Traffic Management (ATM) worldwide is shifting its paradigm in order to accommodate increasing air traffic demands with higher levels of safety and efficiency. This transformation relies on the provision of high fidelity predictions in the air traffic flow that supports enhanced traffic management capabilities.

A sound knowledge of how trajectory prediction uncertainties affect Decision Support Tools (DST) using such predictions is paramount for a robust design of the capabilities of the future ATM system. It is expected that in the future Trajectory Based Operations (TBO), the DSTs will require not only the nominal trajectory predictions generated by a Trajectory Predictor (TP), but also additional information about their suitability in support of client traffic management applications, such as trajectory uncertainty information.

Nowadays, trajectory prediction relies upon a deterministic process that returns the same outputs when initialised with the same set of inputs. However, in reality there will be differences between the predicted and actual trajectories due to the influence of a variety of uncertainty sources.

Although the influence of the uncertainty sources affects all state variables, from an ATM perspective, different DSTs may focus on different state variables. For instance, the traffic flow management only considers kinematic variables (speed, altitude, longitudinal distance, and time at designated waypoints). These variables enable any of the ATM procedures, such as conflict detection and resolution, sequencing, or arrival and departure management. The kinetic variables are mainly used for environmental impact assessments, trajectory optimisations, or air traffic efficiency analysis.

Depending on the flight phase, the effects of some uncertainty sources are more prominent than others. For instance, during cruise or level segments, the accuracy of the aircraft

performance model² does not affect the predicted aircraft dynamic, while for descents and climbs, the uncertainty of these models strongly influence the accuracy of the predictions.

During the cruise phase, the horizontal positioning uncertainty has been described in the literature by an ellipse whose centre is the deterministic position of the aircraft calculated at a specific instant in time. This simplification, which models the input uncertainty as normally distributed [1], is broadly accepted and derives from the lateral and longitudinal control loops executed by the Flight Management System (FMS). The FMS evaluates the cross-track root mean square (RMS) prediction error and maintains it approximately constant between 0.5 and 1 NM of deviation with respect to the nominal path. The longitudinal control involves throttle adjustments to compensate headwinds or tailwinds variations, which translates into Mach number control. In such situations, the along-track RMS error grows approximately linearly with the look-ahead time [2]. Assuming this FMS behaviour, the corresponding uncertainty ellipses have their major principal axis in the along-track direction and their minor principal axis in the cross-track direction, which means that the location uncertainty is greater in the longitudinal than in the lateral position due to the effect of the control loops.

The trajectory prediction uncertainty can be measured by the spread of possible predictions, according to the spread of the inputs, by means of the standard deviation of the state variable distributions. This process allows the quantification of prediction uncertainties based on the knowledge of the variability of inputs to the trajectory prediction process. The standard deviation of the aircraft state variables can be used to assess the sensitivity of the predicted trajectory to the considered uncertainty sources. For instance, the variability of the initial mass is a high contributor to the climb prediction uncertainty, especially for heavy aircraft. Instead, descent prediction uncertainty is mainly driven by the speed schedule and thrust settings' uncertainties. Regardless the aircraft type, operational environment, and flight phase, it is possible to obtain a measure of the related uncertainty by the combination of standard deviations of input [3].

² Depending on the selected turn modelling, a detailed description of the aircraft performance could be necessary

In addition to those purely prediction uncertainties, the process of exporting the trajectory to be used by further DSTs generates additional inaccuracies. DSTs consume trajectory predictions based on an internal data format and structure. The translation between these data types and the TP native output formats diminishes the prediction accuracies. This is of high importance during the air-ground synchronisation, where the FMS generates a trajectory prediction as a continuum but it can broadcast only a reduced dataset (not all trajectory attributes managed by the FMS are useful for ground DSTs) at a reduced set of trajectory points (bandwidth limits the capability of data transmission). Depending on how the flight has been executed between two consecutive reporting points, the errors between them may vary. For instance, if no acceleration information is available in a segment where the speed changes, the option is to estimate a constant acceleration. The error produced by this assumption is directly proportional to the duration of the segment [4]. Hence, defining a consistent trajectory sampling reduces the associated uncertainty and, therefore, limits its impact on trajectory synchronisation.

Although there can be strategies to reduce prediction uncertainties to the minimum, it is clear that some levels of uncertainty are unavoidable. For instance, a value of 0.13 NM/min look-ahead time with a 65 percent confidence level is assumed a reasonable lower limit for the along-track uncertainty [5]. This result relies on a speed accuracy of 1 percent, a 7-kt RMS wind speed uncertainty, and a standard deviation of the atmospheric temperature of 2°C.

However, there is no a common approach to quantify the uncertainty of a trajectory prediction to be used afterwards by interested DST. Current methodologies, especially those based on Monte Carlo simulations, demand a high computational effort and, therefore, are not suitable to generate timely information that help the decision making processes.

The research presented in this thesis proposed a novel approach to formally quantify trajectory prediction uncertainty in the context of future ATM applications. This new method based on the application of the Polynomial Chaos (PC) theory will facilitate the use of enhanced prediction information in support of advanced DST. The thesis exposes the mathematical foundation upon which a formal framework to quantify uncertainty is developed. A main improvement of this approach is the ability to assess the sensitivity of the predictions to the considered inputs removing the need of defining dedicated simulations to study the effect of each input individually.

“This research will provide means for enhancing the DST’s capabilities by the introduction of prediction uncertainty into the ATM functions, providing increased levels of efficiency, robustness and reliability.

1.2 Aims and Objectives

The work carried out in this research aims to investigate methods to quantify the uncertainty associated with an aircraft trajectory prediction in the context of ATM. The main research objectives (RO) can be summarised as follows:

- Detailed study and classification of the stochastic factors affecting trajectory prediction in ATM (RO#1).
- Provision of practical methods and tools to evaluate the impact of the different stochastic factors on trajectory prediction accuracy, with a view to facilitating the development of requirements for advanced automation tools regarding uncertainty management in future TBO (RO#2).
- Quantification of the impact of the identified stochastic factors by the characterisation of individual uncertainty models (RO#3).
- Development a formal theoretical framework for the analysis of trajectory prediction uncertainty in the context of trajectory management applications (RO#4).
- Development of global sensitivity assessment capabilities based on the developed framework that enable ranking the input variables in accordance with their impact on trajectory prediction uncertainty (RO#5).

1.3 Contribution of the Research

The main contribution of the research presented in this thesis is a methodology for modelling and quantifying the uncertainty affecting the prediction of an aircraft trajectory based on the use of Polynomial Chaos Expansions. The use of this methodology provides an unprecedented capability to quantitatively describe the trajectory prediction uncertainty in pseudo-real time. In addition, the proposed method enables straightforward sensitivity

assessment capabilities based on the computed analytical representation of the prediction uncertainty. The extended use of the proposed uncertainty quantification method will facilitate the development of more robust DSTs and support more sophisticated air traffic efficiency analyses. For instance, environmental impact assessments could provide stochastic noise and emissions footprints, improving the decision-making process that may derive from such analyses.

The output of the research also includes an assessment of the most relevant uncertainty sources that impact the prediction process. For each of the identified sources, an individual uncertainty model is proposed. These models provide insight into the importance and relevance of each factor in the prediction outputs when considered individually.

The lists of papers published in peer-review conferences, and patents filed and awarded to date as a result of this research, are presented next.

1.3.1 Papers

- Casado, Enrique, Miguel Vilaplana, and Colin Goodchild. "Application of the Theory of Formal Languages to the Modelling of Trajectory Uncertainty and the Analysis of its Impact in Future Trajectory-Based Operations." 1st International Conference on Application and Theory of Automation in Command and Control Systems (ATACCS'2011). Barcelona (SP). September 2011.
- Casado, Enrique, Miguel Vilaplana, and Colin Goodchild. "Formal Modelling of Trajectory Prediction Uncertainty in Future Trajectory Based Operations." 5th International Conference on Research in Air Transportation (ICRAT 2012). University of Berkeley (California, US). May 2012.
- Casado, Enrique, Miguel Vilaplana, and Colin Goodchild. "Identification and Initial Characterization of Sources of Uncertainty Affecting the Performance of Future Trajectory Management Automation Systems." 2nd International Conference on Application and Theory of Automation in Command and Control Systems (ATACCS'2012). Imperial College (London, UK). May 2012.

- Casado, Enrique, Miguel Vilaplana, and Colin Goodchild. "Sensitivity of Continuous Climb Departure Predictions to Aircraft Intent Uncertainties." 3rd International Conference on Application and Theory of Automation in Command and Control Systems (ATACCS'2013). University of Naples Federico II (Naples, IT). May 2013.
- Casado, Enrique, Colin Goodchild, and Miguel Vilaplana. "Sensitivity of Trajectory Prediction Accuracy to Aircraft Performance Uncertainty." In AIAA Infotech@ Aerospace (I@ A) Conference, p. 5045. 2013. Awarded as Best Student Paper in the 5th Intelligent Systems Student Paper Competition.
- Casado, Enrique, Luis P. D'Alto, and Miguel Vilaplana. "Analysis of the Impact of Intent Uncertainty on the Accuracy of Predicted Trajectories for Arrival Management Automation." 6th International Conference on Research in Air Transportation (ICRAT 2014). Istanbul Technical University, (Istanbul, Turkey). 2014.

1.3.2 Patents

- Magaña, Enrique Juan Casado. "Method for Modelling Aircraft Performance through Adaptive Aircraft Performance Models." US Patent Application 14/525,418, filed October 28, 2014.
- Casado Magaña, Enrique Juan, Luis Pedro D'Alto, and Miguel Vilaplana Ruiz. "Determining a Descent Trajectory Described by an Aircraft Intent Description Language (AIDL)." US Patent No. 20,150,338,853, filed November 6, 2015.

1.4 Dissertation Outline

The chapters of this dissertation are organized as follows:

CHAPTER 1 describes the trajectory prediction process that is presented later in the dissertation as framework for analysing and modelling the uncertainty sources. This chapter also includes an identification of the main factors introducing uncertainty to the prediction

process. The influence of these factors will be studied in the following chapters, which will propose different alternatives to model their effect on the prediction uncertainty.

CHAPTER 2 provides a literature review from the origins of the ATM system to the different initiatives that aim at the Trajectory-Based Operations (TBO) concept, with a special focus on the impact of prediction accuracy in future Decision Support Tools (DST). This chapter also presents a revision of the state-of-the-art techniques used for representing the aircraft trajectory prediction uncertainty.

CHAPTER 4 develops a new method for evaluating the influence of the aircraft performance uncertainty into the trajectory prediction. The use of generic performance models leads to deviations between the values provided by the models and the actual performance. These deviations are not only due to the effect of aging on the airframe and engine, but are also due to the performance model itself that it is just an approximation of the actual performance of a specific aircraft (usually the models represent the performance of a brand new aircraft as it rolls out of the factory). This chapter proposes a model to capture deviations in aircraft performance and how to use it to analyse the sensitivity of trajectory prediction to those deviations.

CHAPTER 5 studies the effect of weather forecasts on trajectory prediction and how the stochastic behaviour of the atmosphere can be introduced by means of the weather forecast ensembles. The atmospheric conditions and the wind are variables considered in the definition of the aircraft motion problem and, therefore, their variability adds uncertainty to trajectory predictions. Their evolution with time and location is described by a set of weather forecasts generated by perturbing the system of equations and initial conditions that describe the atmosphere state. This set encompasses the ensembles that represent possible atmosphere evolutions. The use of those ensembles to predict an aircraft trajectory leads to an ensemble of trajectories that can be used to represent the trajectory uncertainty due to weather variability.

CHAPTER 6 leverages the Aircraft Intent Description Language to assess the impact on trajectory prediction of aircraft intent uncertainties. According to the alphabet and grammar rules of this formal language it is possible to model the uncertainty introduced by different factors and how this uncertainty is propagated throughout the state variables according to

the description of the aircraft intent. In this chapter, several models are proposed to evaluate the deviations with respect to the deterministic prediction as a function of the language elements that describe the trajectory to be predicted.

CHAPTER 7 proposes an innovative method to cope with trajectory prediction uncertainty. Arbitrary Polynomial Chaos theory is applied to the trajectory prediction problem. This theory is widely applied to the analysis of dynamic systems affected by stochastic inputs and models. This process applied to trajectory prediction enables the capability of quantifying the prediction uncertainty due to the simultaneous effect of multiple uncertainty sources in a high efficient manner. This chapter introduces the concept of Arbitrary Polynomial Chaos and describes how to implement a non-intrusive approach to obtain a quantitative description of the trajectory uncertainty that can be exploited by subsequent advance automation tools.

CHAPTER 8 gathers the main conclusions of the dissertation and makes some recommendations for further research.

CHAPTER 2

BACKGROUND & LITERATURE

REVIEW

2.1 Introduction

Nowadays, ATM is commonly considered to encompass all the activities required to provide the capabilities to ensure safe and ordered air traffic operations [6]. The ATM functions include Air Traffic Control (ATC), Air Traffic Flow Management (ATFM), and Airspace Management (ASM). These functions are organized at national or regional levels while they are coordinated worldwide by the International Civil Aviation Organisation (ICAO). The ATC function represents all functions aimed at maintaining separation between aircraft, and between aircraft and ground obstacles, to avoid collisions at any time and under any circumstances. This safety objective must also expedite the air traffic flow while meeting, to the best extent possible, the airspace user preferences. The ATFM function includes the processes and procedures required to regulate the flow of aircraft efficiently to prevent congestions of the airspace and airports without jeopardising safety. Finally, the ASM function is concerned with how the airspace is structured to facilitate ATC services and how the use of the airspace is allocated to the different users (e.g., civil and military coordination of airspace use).

This chapter summarises the birth of the ATM system and its evolution throughout the past decades. It also describes the different initiatives that aim at developing the new processes, procedures, and automation tools required for implementing the TBO concept.

The role of aircraft trajectory prediction in the current and future ATM environments is also provided, with a special focus on the impact of prediction accuracy in client DST.

A comprehensive revision of the state-of-the-art methodologies used for representing the aircraft trajectory prediction uncertainty is also part of this chapter.

2.2 Air Traffic Management Definition and Historical Evolution

The origins of ATM trace back to 1929 at the St. Louis Airport, in Missouri. At that time, Archie W. League was hired as the first air traffic controller to prevent aircraft collision in the vicinity of the airport. He was basically equipped with a red and a chequered flags to indicate whether the approaching aircraft should *hold* or *go*. League joined the federal service in 1937. He eventually became the Federal Aviation Administration's (FAA) Air Traffic Service director and retired as an Assistant Administrator in 1973 [7].

By 1932, the advent of two-way communication capability onboard removed the need for *flag men* and enabled new capabilities and associated responsibilities on radio-equipped airport traffic control towers. In the event of possible conflicts, the arrivals were coordinated between the involved airline dispatchers and the control tower by means of a local airport interphone.

A major milestone in the modernisation of aviation in the United States (US) was the Civil Aeronautics Act of 1938, which formulated the Civil Air Regulations (CAR) and is considered the origin of the so-called First Generation of the ATM system. The CAR-60 [8] established a comprehensive set of rules that differentiate between the Visual Flight Rules (VFR) and Instrument Flight Rules (IFR) procedures. This was the first time pilots were mandated to comply with the instructions issued by the Air Traffic Control centres, which were previously merely advisory.

The evolution of the ATM system was propelled forward at the end of the 1940s by two disruptive technologies: the use of direct communications between pilots and controllers and the extensive use of radar for civil air traffic surveillance, based on military experience gained during World War II. The direct pilot-controller communication led to more efficient and safer operations enabled by real-time knowledge of pilot intent and controller instructions. The use of radar provided dynamic representations of aircraft movement, which replaced the pseudo-aircraft movement representations by means of aircraft markers on a map table. This transformation marks the so-called Second Generation of the ATM system. During this period, additional improvements related to the navigation capabilities were deployed. For instance, the VHF omnidirectional range (VOR) US nationwide programme

ran until the late 1940s. The initial deployment of the distance measuring equipment (DME) and instrument landing system (ILS) infrastructure also dates from those days [9].

After more than a decade of exploiting the benefits provided by radio communications, primary radar surveillance, and radio navigation, the controller's need for better target identification became a strong requirement. In early 1960s, secondary surveillance radar (SSR) solved the aircraft identification issue by providing reply codes with an additional radar pulse to be transmitted at the controller's request [10]. SSR mode A enabled aircraft identification while other modes such as mode C returned, for instance, additional information about pressure altitude³. This technology improvement reduced the number of communications between controllers and pilots, contributed to the optimised use of airspace during climb and descent procedures, and supported controllers in their aircraft vertical separation monitoring duties.

In parallel to the deployment of the SSR, traffic volumes in the United States started to exceed the capacity of the ATM system, which was related to excessive controller workload. Airspace sectorisation was first established to respond to this need for additional capacity. The objective was to reduce the airspace volume allocated to each controller so as to limit the amount of traffic under his/her responsibility. As the number of sectors increased, the complexity of air traffic management operations grew exponentially, demanding improved and enhanced communications and coordination to facilitate the cross cooperation amongst controllers and with sector coordinators. The need for more automation to support all of these activities became crucial for the development of the ATM system [11].

During this decade in Europe, the need for coordinated ATC procedures to cope with new fleets of jet airplanes led to the founding of the European Organisation for the Safety of Air Navigation (EUROCONTROL). Its main objective was to create a single pan-European upper airspace. In the course of those years, EUROCONTROL concurrently developed major support functions that enhanced the quality of ATC service [12].

³ Years later, the SSR mode S was developed to improve the quality and integrity of the detection, identification, and altitude reporting by selective and addressed interrogations [15].

In the early 1970s, the introduction of automation in the ground-based ATM infrastructure initiated what is referred to as the Third Generation of the ATM system [13]. The main concept was to substitute some of the controller's manually executed activities (e.g., flight plan predictions, traffic conflict detection, flight data transfer between centres) with computer-based processes that returned the expected outputs faster and in a more efficient and reliable manner, while reducing human errors significantly. Automation reduced the controllers' workload and supported their responsibilities, although the ultimate executive decision remained on the controller's side.

Radar data processing (RDP) and weather subsystem display are examples of the automation capabilities achieved during this third generation [14]. The former provided automatic aircraft tracking and computer-generated alphanumeric displays by exploiting available digitalised radar data. The latter provided controllers with up-to-date severe weather awareness, enabling better advisories for air traffic during the controller's shift.

Meanwhile, Europe in the 1970s experienced high complexity and fragmentation of its airspace structure. The challenge during this period was to deliver common, consolidated, and more efficient air traffic control services in busy airspace volumes over several European states. In 1972, one of the most important events in the history of EUROCONTROL occurred: the Maastricht Upper Area Control Centre (MUAC) became operational. Its mission was to provide seamless air navigation services to the central Europe upper airspace. More than four decades after its initial operations, MUAC has grown into one of the best performing air navigation service providers in Europe, with excellent safety records, first-rate cost efficiency, and the highest controller productivity on the continent [16].

During the 1980s, the increased air traffic in Europe and the United States forced the global ATM system to its limits. According to the International Air Transport Association (IATA) survey on summer journeys in 1981, 25 percent of the flights through southern and south-eastern Europe were delayed by air traffic services for an average of 33 minutes [17]. The European air traffic congestion crisis led to the decision to create the Central Flow Management Unit (CFMU), the first centralised air traffic flow management service and a milestone for European airspace integration. Although not fully operative until 1996, the

CFMU reduced the delays by half compared to those of 1989 by coordinating air traffic flows across Europe [18].

In 1983, the International Civil Aviation Organization (ICAO) Council established the Special Committee on Future Air Navigation Systems (FANS) to develop recommendations for the future development of air navigation for civil aviation. FANS provides the means for direct communication between the pilot and ATC, using data link technology to share flight information such as oceanic clearances, pilot requests, or position reporting [19]. In September 1991, the 10th Air Navigation Conference endorsed the FANS concept.

In 1999, the European Commission launched the Single European Sky (SES) initiative to create a legislative framework for European aviation, which enables an enhanced pan-European ATM system capable of coping with the foreseen increase in capacity demand [20]. The cornerstone of the concept was to develop a centrally coordinated European airspace that leveraged seamless European air traffic management services.

By the beginning of the new millennium, EUROCONTROL released The ATM 2000+ Strategy [21] aimed at outlining the required ATM developments required during the period 2000 to 2015 towards the envisioned SES. The challenge was to generate extra capacity to meet the demand, while reducing unit costs and simultaneously increasing safety levels. The strategy proposed key operational improvements [22] that would lead to achieving the proposed operational targets.

The SES project promotes an airspace organisation based on the definition of Functional Airspace Blocks (FAB) instead of national borders. These functional blocks will be designed dynamically, according to the foreseen air traffic flows to be managed within. The FABs concept was developed in the first Legislative Package of the SES (SES I), launched by the European Commission in 1999 (enacted in 2004), as one of the primary means for reducing European airspace fragmentation.

In 2005, the Definition Phase of the Single European Sky ATM Research programme (SESAR) was launched to coordinate and concentrate all European Union (EU) research and development (R&D) activities in ATM.

At the same time in the United States, a similar evolution of the ATM system was promoted although motivated not by airspace fragmentation, since a single authority, the FAA, manages the complete airspace, owns the ATM infrastructure, defines the procedures, and deploys the resources to enable air traffic operations within US territory. In June 2007, the Joint Planning and Development Office (JPDO) released the Concept of Operations (ConOps) [23] and Enterprise Architecture (EA) [24] that defines the master design and development of the Next Generation Air Transportation System (NextGen).

Following the regulations promoted by SES I in Europe in 2007, the second regulatory package on the Single European Sky (SES II) was launched by the European Commission (enacted in 2009). SES II implemented a comprehensive performance-based framework and defined the capabilities of the European Network Manager (NM).

In 2010, the EUROCONTROL's Performance Review Commission (PRC), supported by the Performance Review Unit (PRU), was designated by the European Commission as the Performance Review Body (PRB). The PRB's main objectives are advising the European Commission in setting EU-wide performance targets and monitoring the performance of the European ATM system in four key performance areas⁴ (KPs): Safety, Capacity, Environment, and Cost-Efficiency. These overall targets, which are reviewed and updated periodically, are transposed into binding national/FAB targets that are incorporated into national/FAB performance plans. The SES Performance Scheme defines a set of Key Performance Indicators (KPIs) for each of the KPs, which provide common metrics to evaluate the performance of the European ATM system based on recorded air traffic-related data. The European Network Manager, established in July 2011, is considered an evolution of the CFMU where all ATFM responsibilities are centrally coordinated and executed, and its main goal is to promote collaborative decision-making (CDM) among all European ATM stakeholders.

⁴ The ICAO KPs are grouped in three different categories according to the relevance of the expected impact of the associated improvement: societal (Safety, Security and Environmental Sustainability), operational (Capacity, Predictability, Efficiency, Flexibility and Cost-Effectiveness), and enablers (Access and Equity, Participation and Interoperability). The KPs Efficiency, Flexibility, and Predictability are considered to be Quality of Service indicators of the system.

Both NextGen and SESAR have recognised the need for an interoperable global ATM system that provides seamless ATM services to airlines operating on both sides of the Atlantic Ocean [25]. Interoperability means to integrate the air and ground ATM systems by addressing efficiency needs of flight trajectories planning and execution, and the seamless sharing of accurate information.

Additionally, there are some other initiatives running worldwide that aim to move the current ATM system forward to increase system capacity, improve operational efficiency, and reduce costs while maintaining the focus on operational safety. The most relevant ones are both in the Asia-Pacific area—the Australian ATM Strategic Plan (AATMSP) in Australia [26] and the Collaborative Actions for Renovation of Air Traffic Systems (CARATS) in Japan [27].

The ATM system is currently embarked on a major modernisation worldwide. This transformation will take many years, although some of the foreseen operational improvements are already becoming a reality thanks to the use of leading edge technologies. In April 2015, the Ornskoldsvik airport in northern Sweden was operated using the world's first remote-control air traffic control tower. The technology leap from the flagman procedures to remotely controlled airports would be almost unfathomable to Archie League.

2.3 Towards a New ATM Paradigm

The current ATM system is already reaching maximum operating capacity in many parts of the world, resulting in high levels of inefficiency (mainly increased delays and additional fuel burn) that produce increasingly unacceptable burdens on the operational costs of the airlines. To solve this problem, the ATM community has agreed to shift from the current tactical, surveillance-based operations to strategic, more predictable operations based on sharing trajectory information between stakeholders. The objective is to evolve from an airspace-focused management toward a trajectory-based management of the air traffic. This transformation relies on the concept of Trajectory-Based Operations (TBO), which encompasses a set of new processes, procedures, and technologies that will support the capability of flying a previously negotiated trajectory while taking both operator preferences and optimal airspace system performance into consideration [28].

TBO is expected to bring substantial and tangible benefits to the global capacity and efficiency of the ATM system. The FAA has estimated that the benefits of the initial deployment of TBO will produce a short-term cumulative benefit until 2018 equivalent to \$23 billion due to a 35 percent reduction in time delays using current values. This would imply an associated and approximate reduction in fuel consumption of 1.4 billion gallons, and therefore, a decrease in CO₂ emissions of 14 million tons during the aforementioned period [29]. Although these figures are promising, the major advantages of the envisioned new system are expected in the long term. The European Commission estimates that air traffic demand in Europe will grow to approximately 25 million of commercial flights yearly by 2050, compared to 9.4 million in 2011. It has established ambitious performance targets for year 2050, with a maximum delay of 1 minute per flight, a reduction of 75 percent in CO₂ emissions per passenger and kilometre, 90 percent in NO_x emissions, and less than one accident per 10 million flights, considering a heterogeneous traffic mix of manned and unmanned aircraft [30].

Although the implementation of TBO may differ slightly according to individual local requirements, the global interoperability among systems will be ensured by the guidance and supervision provided by ICAO. For instance, the implementation of the TBO concept adopted by SESAR relies on two basic elements: the definition of the business trajectory and the ownership of such trajectory.

The business trajectory describes the sequence of aircraft states that represent the aircraft's movement, according to user preferences and airline business strategies, while complying with the operational context restrictions. In the future ATM environment, the business trajectories should stay untouched (no ATC interventions) as much as possible, as long as no safety parameters are violated. Any possible trajectory modification or update will be analysed in advance to determine both the effects on the airspace sector where the aircraft is currently flying and the effects on downstream traffic. Trajectory Management (TM) encompasses the process and procedures to negotiate, agree, update, and modify the business trajectory throughout its complete life cycle [31].

The second element is the ownership of the business trajectory. Each airspace user is the responsible agent for generating the expected trajectory that fulfils its business goals. Once this trajectory is agreed upon with the Air Navigation Service Providers (ANSPs), it is

considered a contractual agreement that has to be respected as long as there are no safety issues that prevent it. This information has to be available to any interested stakeholder who needs it for elaborating its own plans or for providing advisory indications to other stakeholders. In this scenario, the aircraft will be operated according to the previously agreed business trajectory, ensuring that deviations from the nominal path are always within predefined boundaries. Since no special circumstances other than the expected are faced by the aircraft, the execution of the actual trajectory will be very close to that generated during the planning phase. The flight crew will be in charge of maintaining the operational requirements while ATC will monitor the overall traffic to ensure it is delivered conflict free, avoiding unnecessary over-constraints.

This new ATM system based on trajectory management needs to be supported not only by new processes and procedures, but also by the development of an infrastructure of automation tools capable of enabling the new required features. There are many foreseen activities that will be performed automatically by the automation tools, decreasing the controllers' workload, and therefore, optimising the system resources. The underlying communication infrastructure will evolve from fragmented point-to-point communications toward integrated network-centric, service-oriented information management, which will enable all TM functionalities among the involved ATM stakeholders. These mechanisms will be supported by a common infrastructure, the System Wide Information Management (SWIM), to which the stakeholders will be connected and where all required information will be continuously accessible according to the credentials of each user [32]. This infrastructure will provide the information regarding the system state, which includes trajectory data of all planned and actual flights, weather forecasts or airspace organisation. Any stakeholder will have the obligation of sharing the information that needs to be known by others and maintaining its up-to-date status.

In addition, enhanced CDM capabilities [33] for taking actions on the system performance based on the information shared through SWIM are an essential part of the planned transformation. CDM will harmonise the requirements and needs of the stakeholder in a collaborative manner, enabling the interaction among all interested actors when an action on a business trajectory has to be taken for the global benefit of the system. This new approach will describe the mechanisms for planning, managing, and updating the aircraft trajectory using the CDM as tool for integrating all stakeholders' requirements, preferences, and

system needs. For that purpose, new separation modes and automation tools need to be developed to ensure the proper situational awareness of pilots and controllers, maintaining at the same time respective workloads below safe thresholds.

2.3.1 Trajectory Management

The implementation of TBO requires infrastructures, processes, and procedures to collaboratively plan trajectories, as well as the capability on board the aircraft to adhere to the agreed trajectory. The provision of them is under the responsibility of the ANSP organisations, while the adequate execution of the trajectory relies on the aircraft: basically, on the flight crew and/or the Flight Management System (FMS) [34].

TM encompasses the process and procedures that establish how this provision and execution have to be performed. This also includes the roles and responsibilities of all involved actors according to their respective levels of involvement, and the mechanisms for trajectory planning, negotiation, updating, and reviewing [35]. Figure 2-1 depicts schematically the main TM processes and the interaction among ATM stakeholders throughout the trajectory lifecycle.

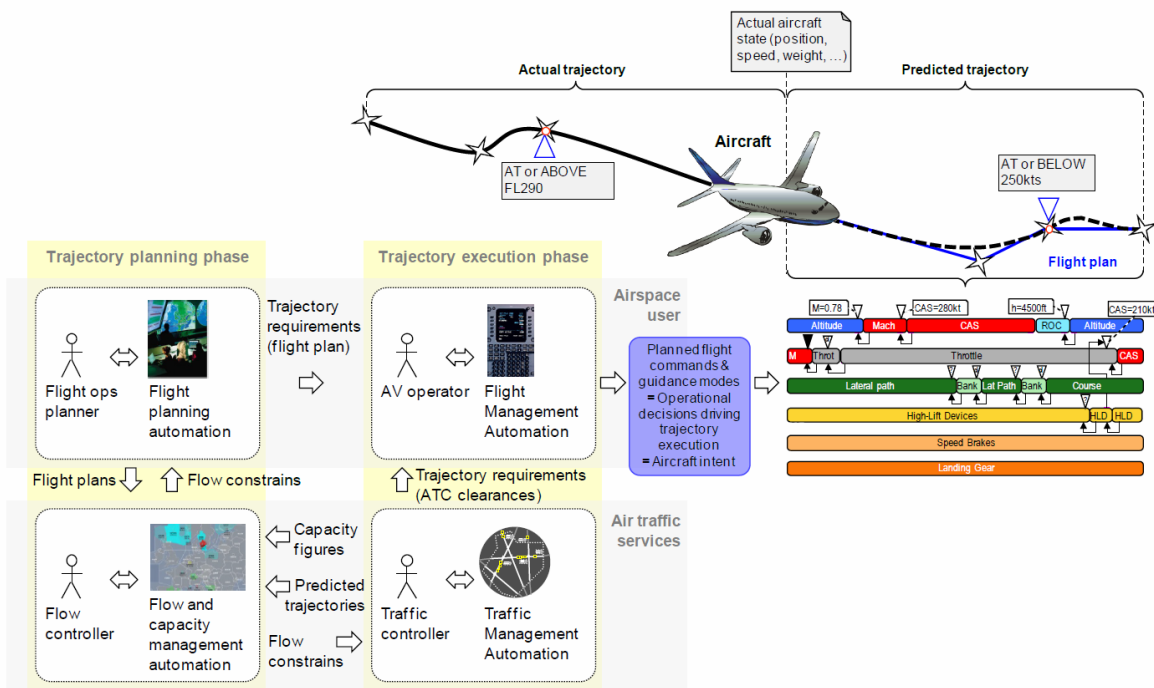


Figure 2-1 – Trajectory Lifecycle Scheme

The TM procedures are established to enable the definition of the aircraft trajectory throughout its complete life cycle from initial planning until execution. TM gathers all the processes required for adding information once the knowledge about how to execute the plan has improved. These processes are represented by successive planning phases from long term to medium and short terms, and involve the ATM stakeholders who collaboratively interact to progressively build, what is called in Europe, the Network Operations Plan (NOP) [36].

The NOP is a dynamic rolling plan that provides a detailed overview of the whole ATM system. The information contained in the NOP includes traffic demand, airspace structure, and airports capacity or current airspace constraints. It can be seen as a facilitator whose aim is to catalyse the negotiation process between airspace users and ANSPs. The NOP also provides both a qualitative and quantitative impact assessment of overall plan updates and modifications on the performance of the European ATM network.

All TM activities will use enhanced aircraft trajectory data (e.g., prediction uncertainty quantifications), which will be exploited by advanced automation tools. This improved set of trajectory data will enable more robust predictability and, therefore, will lead to an increase of system capacity.

2.3.2 Advanced Decision Support Tools

Under the current ATM paradigm, controllers and air traffic flow managers are viewed as the central authority with total responsibility for short-term safety issues and long-term traffic flow scheduling. However, the new TBO paradigm will distribute these responsibilities according to each stakeholder's level of involvement along the life cycle of the trajectory [37].

To provide these new functionalities, ATC will require improved and enhanced applications that ensure the safety of operations whilst enabling and supporting the TM functionalities. The development of advanced DSTs will take into account the most relevant technical requirements needed for the implementation of TBO, such as, distributed conflict detection and resolution, or user preferred trajectories. These tools can be part of a wider ground-based automation infrastructure, or be included into the onboard system as well. In both cases, all these advanced applications will help and support CDM processes. The main advantage

provided by advanced automation is the capability of speeding up the analysis and identification of complex situations (e.g., conflict detection) and the provision of optimal solutions (e.g., conflict resolution) considering the user preferences and ATM system requirements.

The foreseen automation infrastructure required to support TBO will be aligned with the concept of human-centred automation [38] where the actual capabilities of the controllers (i.e. collaborative negotiation and problem solving) will be augmented and enhanced; and where the weaknesses (i.e. reduction of situational awareness due to higher traffic density and complexity) are overcome or at least reduced significantly.

2.4 The Role of Aircraft Trajectory Prediction in ATM

As defined by the FAA/EURCONTROL R&D Action Plan 16 [39],

“a trajectory is a four dimensional (i.e., latitude, longitude, altitude and time) description of an aircraft’s flight path”.

ICAO extends the definition to ground operations, stating that a trajectory is

“a description of the movement of an aircraft, both in the air and on the ground, including position time and, at least, via calculation, speed and acceleration” [28].

While the RTCA5 Special Committee-214 (SC-214) in coordination with the EUROCAE6 Working Group 78 (WG78) introduces the concept of uncertainty by defining a 4D trajectory as

“a precise description of an aircraft path in space and time: the centreline of a path plus the position uncertainty, using waypoints to describe specific steps along the path” [40].

An aircraft trajectory description may include additional details about the aircraft motion:

- Geometric aspects, which refer to the position of the aircraft’s centre of mass in relation to a certain reference coordinate system and to the aircraft’s attitude, generally given by the Euler angles.

⁵ Radio Technical Commission for Aeronautics

⁶ European Organisation for Civil Aviation Equipment

- Kinematical aspects, which refer to the time evolution of the position and velocity of the centre of gravity and of the aircraft attitude and angular velocities.
- Kinetic aspects, which refer to the forces and moments acting on the aircraft, direct causes of its motion, as well as to the flight controls influencing those forces and the time evolution of the aircraft mass.

Depending on the requirements of the client applications, the description of the aircraft trajectory may be represented with different levels of detail and accuracy. Some applications may discard aspects of the trajectory that are valuable for other applications. For instance, environmental assessment tools make use of kinetic aspects (basically, thrust and fuel consumption data), which are not of any interest for sequencing and metering applications.

In addition, a predicted trajectory is defined by a time-ordered set of mathematically calculated aircraft states that represents an estimate of the path to be followed by the aircraft through the airspace [41]. Such description usually may require the knowledge of the current aircraft state, a forecast of the environmental condition expected along the flight path, a model of the aircraft performance, and estimates of how the aircraft is to be commanded, either by the pilot or the FMS, to comply with the ATC requirements.

Ground-based ATM applications exploit trajectory prediction to enable different functionalities, such as flight planning, conflict detection and resolution, traffic flow management (TFM), or flight data processing (FDP). Trajectory prediction facilitates the process of managing the traffic safely as it enables anticipating its evolution with time. For instance, breaches of separation minima can be anticipated and, therefore, solutions can be issued in advance to solve such foreseen conflicts. The main limitations of current trajectory prediction capabilities on the ground are the reduced aircraft performance data availability and the lack of precise knowledge of the aircraft intent (e.g., how the aircraft is to execute a climb procedure).

The trajectory predictions computed on board by the FMS are used for monitoring how the original flight plan is being executed and for commanding the aircraft throughout the remaining planned flight path. The FMS has at its disposal the most accurate aircraft performance data and uses the most updated representation of the intent (command and control instructions whose execution lead the aircraft to fly the planned trajectory). However,

the weather forecast used for computing those predictions lacks accurate updates. The forecast is basically uploaded into the FMS by the flight crew prior to the departure and updated by the Aircraft Communications Addressing and Reporting System (ACARS) [42] at some reference flight points. Additional limitations are introduced from the use of coarse wind and temperature information by the native FMS trajectory model.

Currently, there is a huge variety of trajectory predictor (TP) implementations that support a wide range of ATM applications (e.g., traffic flow optimisation, traffic monitoring, identification of short/medium-term conflicts, effective conflict resolution, or computation of estimated times of arrival at specific metering fix points). Each implementation considers a set of assumptions and simplifications that strongly influence the output of the trajectory prediction process.

Due to such disparity of applications, the DSTs' requirements over trajectory predictions are diverse in terms of accuracy, integrity, and availability [43].

- Accuracy is defined as the difference between the actual aircraft trajectory and the prediction generated by the considered automated tool as a function of the look-ahead time. Such discrepancies are assumed as prediction uncertainties that cannot be considered precisely by the TP in advance when a prediction is computed. Section 2.5.1, below, provides exhaustive details about how to assess the accuracy of aircraft trajectory predictions.
- Integrity represents the likelihood of providing misleading information to a DST without the appropriate alerting. The acceptable levels of integrity are directly related to the consequences on safety due to the undetected use of such erroneous data. According to this criteria, there are two integrity levels: nonessential for applications with less sensitivity to undetected erroneous inputs, such as traffic load managers; and essential for applications that cannot tolerate unknown erroneous information due to its relevant safety impact in the traffic operations, such as arrival managers.
- Availability refers to the percentage of time during which the prediction is available for providing acceptable quality information to the specified DST. The most common factors affecting availability are the ATC directives that impact the originally planned flight path and the rapid changes in environmental conditions.

These high-level requirements, considered as quality measurements of the TP outputs, are soundly dependent on the quality of the inputs and the theoretical approach used to model the aircraft motion.

2.5 The Trajectory Prediction Process

One of the cornerstones of future TBO will be the ability to share trajectory information among different automation systems in a timely, robust, and reliable manner. The generation of trajectory information will be performed by trajectory predictors, which will provide data to the decision support tools used to enable strategic, more efficient ATM.

Despite the fact that not all TPs are developed similarly and do not make use of the same data sources, for ATM interoperability purposes the FAA/EUROCONTROL Action Plan 16 proposed a generic TP model (Figure 2-2), including a set of common architectural concepts upon which TBO capabilities can be defined [39]. The core of the models is the Trajectory Prediction Process (TPP), which encompasses the process of obtaining a computed trajectory (CT) by means of a set of methods and algorithms implemented by the Trajectory Engine (TE). The input to the TPP is the Flight Script (FS), which can be defined as a blueprint of the planned trajectory. The TE requires information about weather and aircraft performance to properly instantiate the mathematical representation of the Aircraft Motion Model (AMM). In addition, there are some external processes that enable the capability of dynamically updating the trajectory (Trajectory Update Process [TUP]), facilitate the process of defining the FS based on available flight plan data or ATC constraints (Preparation Process [PP]), and format the output to be used by other applications (Trajectory Prediction Export Process [TPEP]).

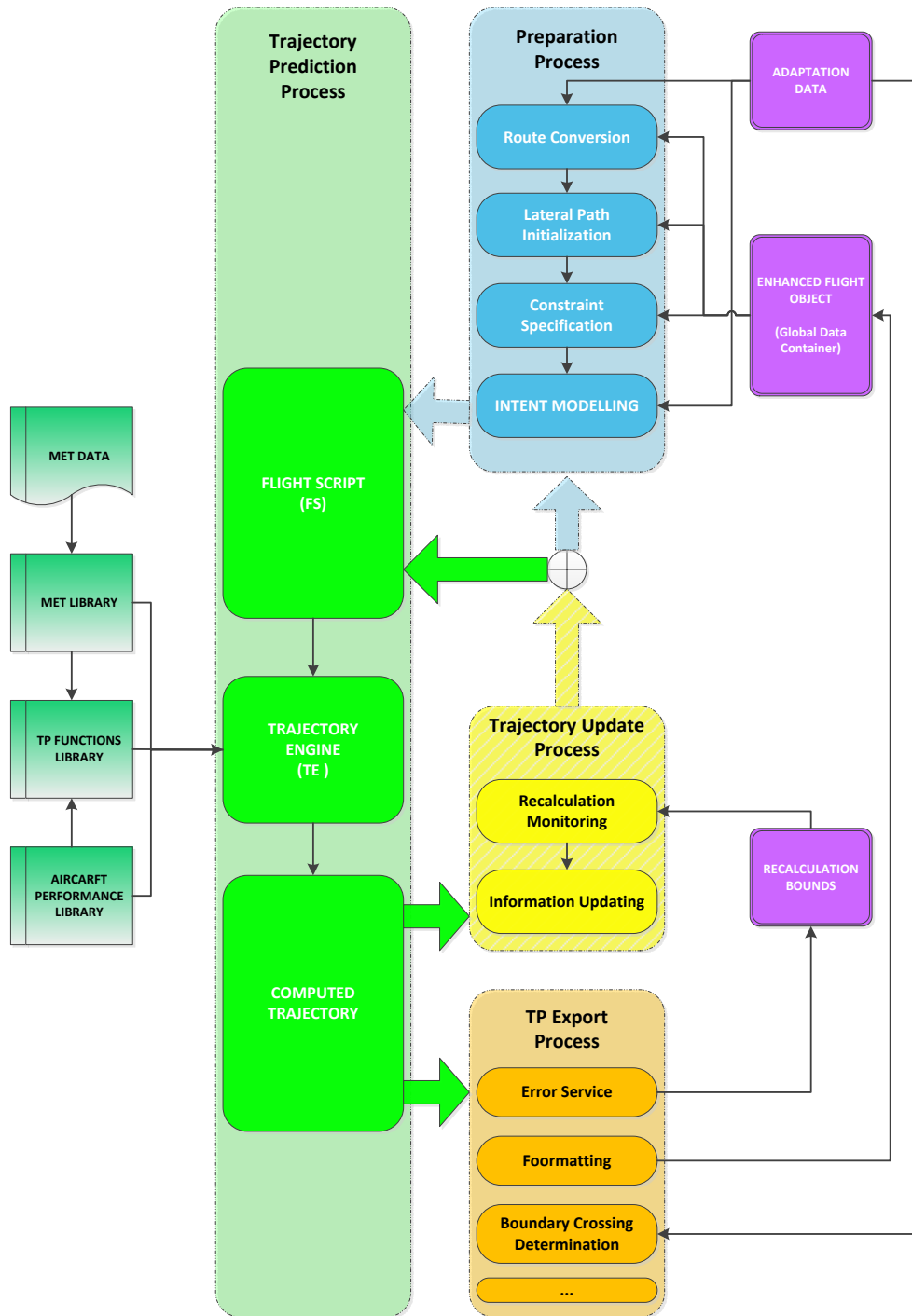


Figure 2-2 – AP-16 Common Trajectory Prediction Framework

The four main processes that govern the trajectory prediction process depicted in Figure 2-2 are:

- Preparation process. It is the initial step that is triggered by the requirement of a predicted aircraft trajectory under certain conditions. The input data range from flight plan information, ATC constraints, ATM procedures, or weather forecasts. From the initial inputs, the route information is translated into latitude and longitude points

(Route Conversion). This list of points defines the lateral path to be flown by the aircraft (Lateral Path Initialisation) and allows allocating the speed, altitude, and time constraints to be fulfilled along the flight (Constraint Specification). Finally, the intent or description of how to operate the aircraft to perform the envisioned trajectory compliant with all ATC constraints is described based on the available information (Intent Modelling).

- Trajectory prediction process. This process represents the kernel functionality of a TP. Using the information gathered by the Preparation Process and encapsulated in the Flight Script (FS), the Trajectory Engine (TE) integrates the system of equations of the implemented AMM⁷. The TE may have access to meteorological and aircraft performance databases for accurate and up-to-date trajectory computations.
- Trajectory update process. Once flight related information is updated due to the release of new constraints or a modification of the intent, the process of re-computing the prediction is launched. The recalculation monitoring is the service responsible for triggering the update process when a tolerance is exceeded, or when the considered valid time interval is finished. This process can imply the generation of a new complete set of inputs or just a minor modification of the former ones (Information Updating Service). In both cases, the entire prediction process must be rebooted with the updated information.
- TP export process. After a new trajectory prediction, the last stage is to share the output with any client application (Formatting Service). Additional features of this process would include the capability to monitor computation error and prediction accuracy (Error Service), or the function of verifying if the computed trajectory respects a specific ATC constraint when flying within a determined airspace volume (Boundary Crossing Determination).

This generic architecture provides a high-level overview of the main methods and data sources involved in the trajectory prediction process. The FS represents a trajectory

⁷ In the case of a kinetic approach.

compliant with the applicable ATC restrictions and, as much as possible, with the user preferences. These trajectory requirements represent the Flight Intent (FI), which can be thought of as a generalisation of the concept of flight plan. The FI gathers key operational requirements and constraints that must be fulfilled by a predicted trajectory (e.g., intended route, operator preferences, standard operational procedures, ATC constraints). In general, an FI instance does not unambiguously determine the aircraft motion and, in principle, there may be many trajectories (potentially infinite) that fulfil the defined set of operational requirements and constraints [44].

To remove the ambiguity contained in the FI, the introduction of additional information regarding the strategies used for commanding the aircraft during a time interval leads to the definition of the aircraft intent (AI). An AI instance is considered an unambiguous description of how the aircraft is to be operated to execute a trajectory compliant with the operational requirements and constraints established in an FI instance [45].

Depending on the type of information used for initiating the process of predicting an aircraft trajectory, the uncertainty associated with the process will vary. The FI may range from a complete description of the intent similar to that provided by an AI instance, to a rough blueprint in which the majority of the aircraft motion is unspecified. The process of completing the information contained in an FI instance to obtain an AI instance is known as the Intent Generation Process (IGP). As shown in Figure 2-3, the IGP entails the heuristics, methods, and algorithms required to univocally determine the aircraft motion based on the information contained in the Operational Context Model (OCM) and the User Preference Model (UPM) [46]. The OCM is a representation of the static and dynamic ATC constraints. This model not only includes the information provided in the Aeronautical Information Publication (AIP), but also Notices to Airmen (NOTAMs) that contain updates to the essential flight operation information not sufficiently known in advance (e.g., changes to charts, procedures, and airspace usage), or SNOWTAMs (special NOTAMs announcing the presence, or removal, of hazardous conditions due to snow, ice, slush, or standing water). The UPM provides information about the user's business strategy, optimisation criteria, or particular goals and objectives when available. Typical information included in the UPM could be the cost index, preferred routes, or desired alternative procedure in case of trajectory conflicts.

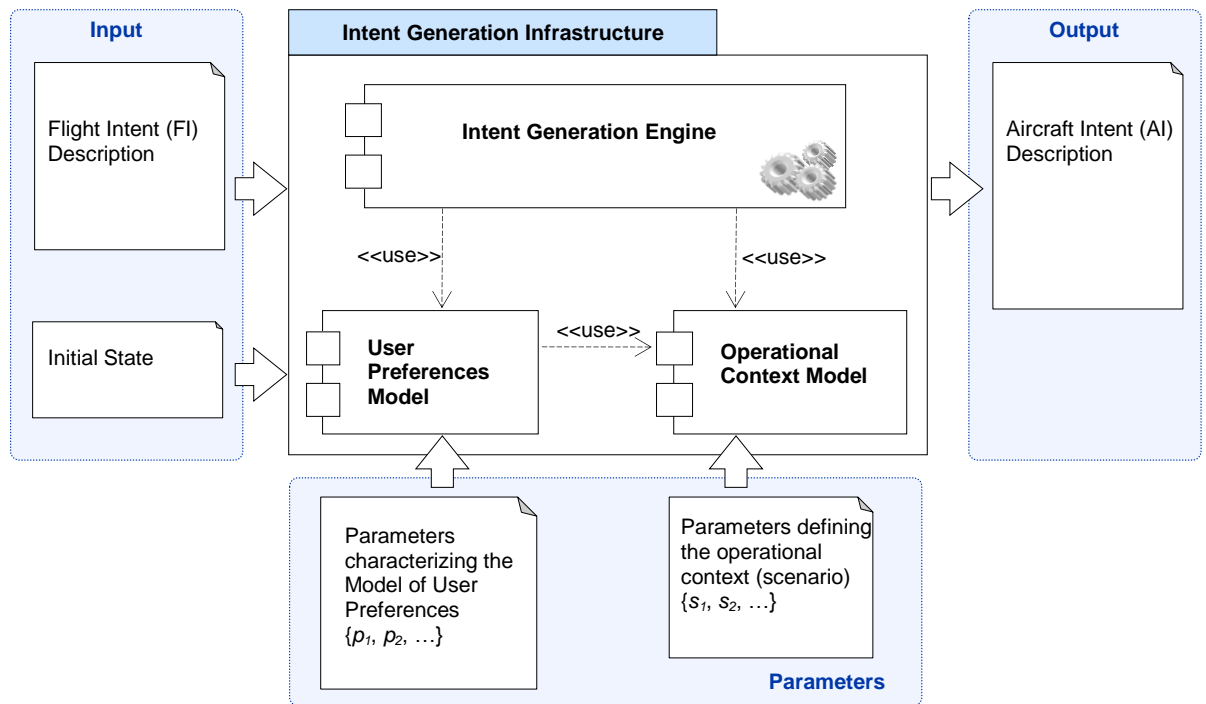


Figure 2-3 – Intent Generation Process

Since the FI does not univocally define a trajectory, the methodology applied for including the remaining information to obtain an AI instance will strongly influence the final prediction. This process is affected by the heuristics and algorithms applied to determine the open AI parameters. Different implementations of the IGP could return different AI instances and, therefore, disparate trajectory predictions. However, both AI instances and trajectory predictions will be representations of potential trajectories compliant with the input FI.

According to the definition of the AP-16, the outcome of the IGP is an AI instance that represents a synthesis of the trajectory to be predicted. Based on this AI and additional information including aircraft performance and weather conditions, the TE is capable of generating a trajectory prediction that observes the established requirements and constraints.

The TP kernel can be implemented following a kinematic or a kinetic approach, which basically describes how the aircraft performance is to be modelled and used throughout the predictions process [5].

The kinematic approach considers the aircraft behaviour as modelled by a set of look-up tables, which provide information about admissible vertical speeds, cruise speeds, or climb/descent profiles. These data do not explicitly consider the underlying physics that

govern the aircraft motion. This approach omits the influence of external forces on the aircraft motion by modelling their impact through descriptions of aircraft speed under the considered flight conditions. Examples of kinematic-based TPs are the En-Route Automation Modernisation (ERAM) [47], User Request Evaluation Tool (URET) [48], the Enhanced Traffic Management System (ETMS) [49], and the Control of Inbound Trajectories for Individual Aircraft (CINTIA) TP [45].

The kinetic approach requires an explicit description of the forces acting on the aircraft centre of gravity (drag, lift, thrust and weight) that enable the integration of the Newtonian equations of motion. Examples of kinetic-based TP are the FMS predictor [50], the Center/TRACON Automation System (CTAS) Trajectory Synthesizer (TS) [51], the HYBRIDGE project TP [52], the EUROCONTROL Integrated Aircraft Noise and Emissions Modelling Platform (IMPACT) [53], and the ERAM Kinetic Vertical Modelling (KVM) [54].

In light of the generic TP framework proposed by the AP-16, different approaches can be found in the literature formulating the intent information in accordance with their internal kernel requirements.

- The CTAS TP developed by NASA decouples the intent (FI) into the horizontal and vertical profiles. The horizontal profile establishes a sequence of straight lines and circular arcs representing the route. The vertical profile is split into flight segments. The flight segments are characterised by holding constant the value of one of the state variables that can be managed by the pilot/FMS. The state variable to be maintained constant depends on the flight phase. For instance, during cruise, the rate of climb would be assumed zero and during the final approach, the path angle would be maintained at 3° . The transition between consecutive flight segments is determined by a capturing condition. This condition is reached when the value of any of the state variables, rather than the one that is on hold during the flight segment, surpasses the pre-established threshold [51].
- The Behavioural Model (BM) is an alternative method for describing FI data [55]. The BM encodes intent information in a way that can be organised formally regardless of the mathematical formulation considered for the implementation of a specific TP. This model is structured in layers according to the level of detail used

for describing the planned flight. The lowest level descriptions establish a relationship with the underlying Mathematical Model (MM), which leads to a univocal trajectory prediction. The high-level description of the manoeuvres requires a decomposition process that enriches the initial description of the manoeuvre down to the granularity required by the MM.

- The Common Interface for Trajectory Computation (CITRAC) [56] was proposed as a standard framework for sharing intent information among DSTs. CITRAC organises the intent in flight segments characterised by a set of parameterised primitives. The logical combination of these primitives defines both the horizontal and vertical profiles. The horizontal profile can be formulated by means of geometric paths (e.g., ARINC 424 legs), while the vertical profile is described by the speed and altitude targets at the end of each segment and a model of the pilot intent (how the segments are to be flown).
- The AIDL is a formal language intended to univocally formulate AI instances to be used as direct input to a dedicated TE [57]. The language was designed to describe AI information in an unambiguous and interoperable manner. Any trajectory to be predicted can be organised as a chronological sequence of operations. Each operation establishes the basic command and guidance modes used by the pilot/FMS to steer the aircraft during a time interval. Like any other formal language, the AIDL is composed of an alphabet (minimal and indivisible pieces of information that identify command, control, and guidance inputs) and grammar rules (used for generating a well-formed string). The utilisation of this language allows the rigorous and systematic definition of any possible AI instances (any possible trajectory), while potentially facilitating the air-ground synchronisation [58].

2.5.1 Trajectory Prediction Accuracy

Regardless of the methodology applied for predicting an aircraft trajectory, knowledge of the accuracy of the predictions is paramount for its exploitation by the client DSTs. This accuracy can be measured by calculating the deviations between the actual and predicted aircraft states. Although there is a wide range of TP implementations, the main factors that affect the accuracy of the predictions can be grouped as follows [59][43]:

- Initial conditions. These are represented by the differences between the aircraft initial state (e.g., position, speed, and mass) information used for prediction and the actual aircraft state. The former can be obtained from surveillance information, so then the accuracy is limited by the accuracy of the surveillance data (e.g., radar tracks provide lower accuracy due to larger refresh rates than ADS-B⁸). A critical factor is the aircraft mass, which is usually unknown to the ground-based automation. This lack of accurate information may strongly impact the accuracy of predictions, especially in climbs and descents.
- Intent description. In order to predict a trajectory accurately, it is necessary to have knowledge about how the aircraft is going to be operated to execute the planned flight. The common information at the disposal of the TP is the flight plan, which contains some details about the planned trajectory (e.g., climb/descent speeds, cruise altitude, list of waypoints). However, such information does not univocally determine the trajectory. Thus, additional intent generation assumptions are required to predict a complete trajectory. These assumptions are usually not tailored to each flight and, therefore, result in inaccuracies due to the lack of knowledge of users' operational strategy. Intent data synchronisation is expected to lead to improvements of prediction accuracy.
- Dynamic intent updates. Changes to the original FP due to new altitude clearances, or route changes issued by the controllers to avoid future conflicts, or to facilitate the traffic flow, strongly affect the accuracy of the predictions. They are modifications on the trajectory not considered during the original prediction. Their impact cannot be evaluated a priori because the interventions depend on the current traffic state and unexpected circumstances that force controllers to take action on specific trajectories.
- Weather forecasting. These errors are deviations between the actual wind and atmosphere conditions (temperature and pressure deviation with respect to the International Standard Atmosphere) and the forecast used for trajectory prediction.

⁸ Automatic Dependent Surveillance-Broadcast

Their influence mainly impacts the along-track accuracy coupled with altitude deviations during climbs and descents.

- Aircraft performance. This factor gathers the effect on the accuracy introduced by the models that represent aircraft performance. The differences between the actual performance (affected by airframe and engine aging) and the model used for representing it (either kinematic or kinetic) are unavoidable and strongly depend on the considered operational conditions.
- Trajectory modelling implementation. All hypotheses assumed for the mathematical formulation of the aircraft motion problem impact prediction accuracy.
- Flight technical errors. Differences between the actual trajectory flown and the onboard reference due to inherent limitation of the flight control system. This effect cannot be modelled because it is unpredictable and does not depend on specific parameters or simplifications.

For a coherent accuracy assessment, it is required to define the data sampling at which the actual and predicted trajectories are to be compared, and the metrics to be applied to measure such accuracy. The data sampling basically ensures that the variables to be compared represent the aircraft state at the same location (temporal accuracy) or at the same instant (spatial accuracy). Depending on the type of comparison, a different set of metrics may be required to evaluate the accuracy of trajectory predictions. Typical metrics are the cross- and along-track deviations that can be measured with respect to the closest flight segment or a time-matched segment [60], or the estimated time of arrival (ETA) deviation at a given waypoint [61].

The prediction accuracy can be represented by spatial or geometric accuracy and temporal accuracy. The former indicates the deviation between the actual and predicted aircraft position at a fixed time. This accuracy measures the horizontal and vertical distances between the two considered positions. Temporal accuracy describes the time difference measured between the predicted and actual instant at which a trajectory event is achieved (e.g., time at which the aircraft reached the TOC).

Spatial accuracy can be decomposed into three orthogonal directions: cross track (XTR) or lateral accuracy, along track (ATR) or longitudinal accuracy, and vertical (VER) accuracy. This orthogonality does not imply decoupled effects. For instance, vertical errors during climbs at constant CAS generate deviations in TAS that affect the along track accuracy. As depicted in Figure 2-4, spatial accuracy can be represented by the covariance ellipsoid.

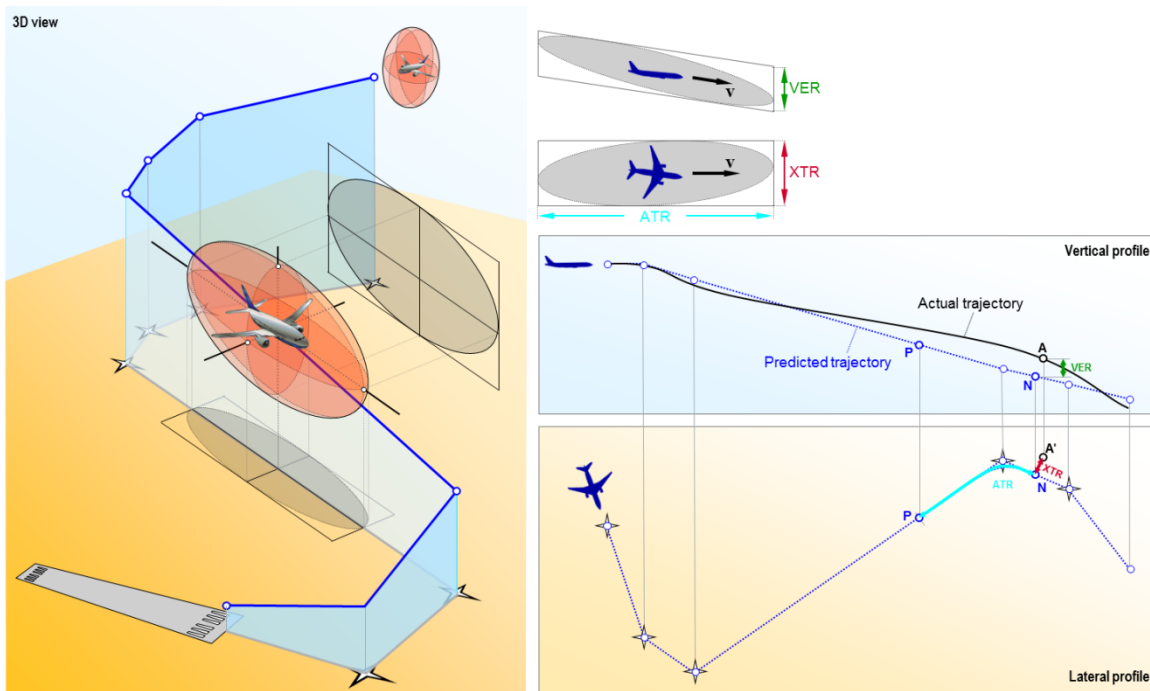


Figure 2-4 – Representation of the Spatial Trajectory Prediction Accuracy

The volume V of the covariance ellipsoid is determined by the size of its axes as follows:

$$V = \frac{4}{3} \pi XTR \cdot ATR \cdot VER \quad (2-1)$$

This volume contains all possible aircraft positions for the considered time and represents the accuracy of the predictions referred to in the actual trajectory. The ellipsoid can be obtained by historical analysis of previously recorded trajectories of the same aircraft types, flying the same procedures in similar weather conditions. The total volume consumed by an aircraft is usually used as a sector complexity indicator that assesses not only the traffic complexity, but also the impact of trajectory prediction uncertainty on the controllers' workload [62].

To relate the predicted (P) and actual (A) positions at time (t) shown in Figure 2-4, which are time-coincident, we need to find out a third position N , called *nominal position*, which is spatially correspondent to A over the predicted trajectory, i.e., the nearest predicted position corresponding to the actual one. Thus, the distance between points P and N along the horizontal path determines ATR, while the horizontal distance between N and A identifies XTR, and the vertical distance between N and A is VER.

The accuracy is strongly affected by the knowledge of the inputs considered in the prediction process. The higher fidelity of the measurements used, the increased levels of prediction accuracy. For instance, accurate values of take-off weight, speed profile, and engine type specification can significantly reduce the error of climb predictions [63]. However, not all inputs provide same increases of prediction accuracy. Thus, the capability of analysis the sensitiveness of the prediction to variability of inputs is of high interest.

2.6 Uncertainty Quantification in Trajectory Prediction

The definition of the accuracy ellipsoid proposed in previous Section 2.5.1 can be extended to the description of trajectory uncertainties. In this case, the calculation of the ellipsoid axes is not driven by the comparison between recorded and predicted trajectories, but by the comparison between the nominal prediction obtained from a deterministic trajectory computation and the set of stochastic predictions obtained by coherent random perturbations of the TP inputs and models.

The covariance analysis of prediction uncertainty provides the standard deviation of the distribution that characterises the variation between the nominal and stochastic predictions as a function of the statistical properties of the disturbances. There are two types of disturbances: parametric and time-varying [64]. The covariance of these disturbances and the autocorrelation of time-varying ones are used to build the covariance matrix of any state variable throughout the prediction.

The covariance matrix can be obtained by designing a series of Monte Carlo simulations that evaluate the variability of inputs and model disturbances into the prediction process. For that purpose, it is required to enhance the capability of a deterministic TP to cope with the stochasticity of inputs and models. The application of statistical methods to the outputs computed as a result of the Monte Carlo runs will provide a quantification of the prediction

uncertainty of the considered trajectory. This uncertainty will reflect the effect of all uncertainty sources that model the stochastic behaviour of the input parameters.

This approach relies on a high computationally demanding and time consuming process. The accuracy respect to the actual system response improves with the inverse of the square root of the number of runs $\left(\frac{1}{\sqrt{n}}\right)$, thus to reduce the error between the simulated and actual system outcomes by a half, it is required to increase the number of runs by four. Moreover, this approach does not provide a flexible and scalable framework for sensitivity analyses. The study and identification of most influencing factors on trajectory prediction uncertainty requires dedicated Monte Carlo experiments in which all stochastic parameters are considered as deterministic except those under study. Specific metrics to rank the influence of each individual parameter (or a collection of them) need to be developed in addition to the design of Monte Carlo simulations. The Stochastic Trajectory Predictor (S-TP) [65] proposed by Navarro and Valls is an example of this type of approach.

Other approaches are computationally more efficient and simultaneously provide physical insight into the effects of uncertainty sources on the predictions. The semi-analytical method proposed by Jackson [66] applies closed-loop sensitivity analysis to trajectory predictions in the presence of pilot/FMS feedback control actions. The sensitivity is defined as the relative change of differences between actual and computed trajectories with respect to modelled uncertainties. These uncertainties are considered to be parametric or time-varying disturbances. Both aircraft motion equations and control laws are linearised along reference trajectories, resulting in a linearised system of equations that enables obtainment of analytical expression for the proposed sensitivity analysis with respect to input uncertainties. The selection of control methods significantly affects the impact of the uncertainty sources among different state variables. The proposed method returns approximate values for the covariance matrix that represents spatio-temporal uncertainty of the trajectory.

Results of applying the closed-loop sensitivity analysis to different control modes enable the analytical identification of most impacting sources according to the defined trajectory and the variability of state variables at a fixed time or event [64]. Figure 2-5 shows the use of CTAS architecture to validate the proposed methodology, in which the indicated sources of uncertainty (highlighted in red) were modelled and their impact assessed.

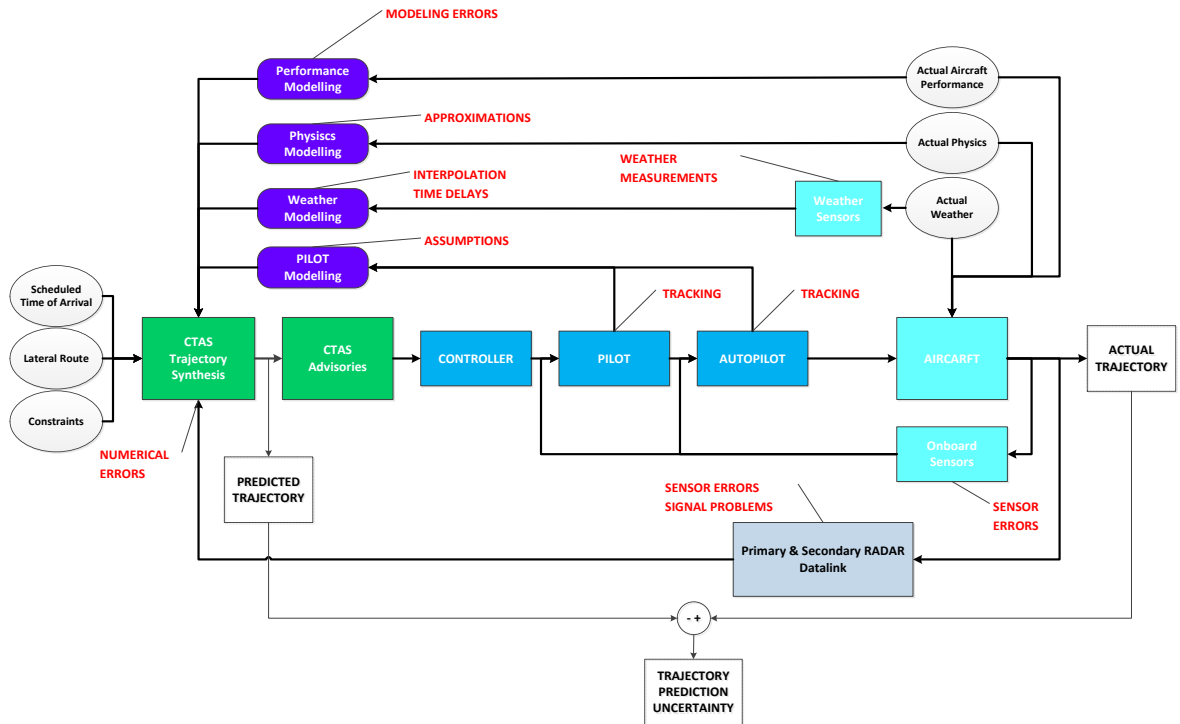


Figure 2-5 – CTAS Trajectory Synthesis Architecture

The trajectory prediction uncertainty is computed as the difference between the actual trajectory, flown by the aircraft following the control objectives consistent with those used to predict the trajectory, and the prediction computed by the Trajectory Synthesiser (TS). This difference is produced by the effect of numerical errors, the assumptions considered to defined the AMM (i.e., modelling errors, approximations, interpolations, time delays, assumption, and pilot modelling assumptions) and the external sources of error (i.e., tracking, sensor errors, and weather measurements).

However, the presented approaches applied to quantify trajectory prediction uncertainty require a very high computational effort (S-TP) or do not provide very accurate representations of the uncertainty (linearised approach). In both cases, the sensitiveness of the uncertainty due to the effect of different stochastic inputs implies the definition of dedicated study cases. The solution proposed in this thesis aims at overcoming these main drawbacks, proposing different models that represents the variability of the predicated state variables, and describing a framework that provides a formal representation to this variability regardless the type of trajectory to be predicted and the capability of assessing the influence of the considered CTAS input parameters in the prediction uncertainty.

2.7 Summary

With the goals of higher capacity, efficiency, and safety, and lower environmental impact, the ATM system is evolving worldwide from tactical airspace management to strategic trajectory management. This paradigm shift is founded on the introduction of the TBO concept, which establishes the procedures for TM thanks to the use of advanced automation tools. These tools will rely on the capability of accurately knowing the actual aircraft position and the intended aircraft trajectory for precisely predicting the future evolution of the aircraft position with the time. In future TBO contexts, onboard and on-ground systems will be able to predict aircraft trajectories based on the best knowledge of the aircraft intent, weather conditions, aircraft performance, and initial aircraft state. However, uncertainties related to such data cannot be fully eliminated and, thus, deviations between the actual and predicted trajectories are unavoidable. The study of prediction uncertainties will allow to evaluate their effects on the predicted trajectories and, therefore, will improve the strategic and collaborative decision making process by providing relevant information about most likely future aircraft states.

Regardless of the methodology applied to solve the aircraft trajectory prediction problem, the ability to determine the accuracy of the predictions is paramount. Accuracy is measured as the error between the actual and predicted aircraft states. The analysis of what stochastic factors influence this accuracy will improve the capabilities of DST thanks to the knowledge of the associated prediction uncertainty. In ATM applications, trajectory predictions are mainly affected by the variability of the initial aircraft state, the description of the intent and its dynamic updates, the modelling of the aircraft performance, the weather conditions, and the definition of the aircraft motion model. The study of their stochasticity leads to the quantification of the individual and collective impacts on trajectory prediction uncertainty.

CHAPTER 3

UNCERTAINTY SOURCES

AFFECTING AIRCRAFT

TRAJECTORY PREDICTION

3.1 Introduction

The trajectory uncertainty can be described as the probabilistic distribution of aircraft state variables, produced by the impact of probabilistic distributions of the uncertainty sources affecting trajectory prediction.

The process of identifying and characterising the uncertainty sources affecting trajectory prediction strongly depends on the formulation of the prediction problem. Kinetic approaches provide higher levels of trajectory accuracy for all types of operational procedures. This is the common approach followed by most sophisticated TPs for obtaining more realistic representations of the aircraft trajectory. It is expected that in future TBO, advanced DSTs will be required for managing highly detailed and accurate trajectory descriptions. Only kinetic TPs will be able to provide the expected levels of fidelity.

However, deviations between actual and predicted trajectories are unavoidable. Those discrepancies are produced by different error sources that can be classified as follows:

- Data errors. Incomplete, inaccurate, or corrupted information (e.g., filed flight plans or airspace databases) available throughout the system.
- Modelling errors. Simplifications assumed during problem formulation and hypotheses considered for identifying aircraft performance and environmental models.
- Operational errors. Unpredictable command and control instructions motivated by unexpected events or even by non-planned updates of the pilot/FMS intent.

The influence and effect of those errors determine the trajectory prediction uncertainty. The analysis of their variability provides insight into the uncertainty propagation along the predicted trajectory.

This chapter is devoted to identifying and quantitatively characterising the uncertainty sources affecting trajectory prediction. This approach will support the quantitative analysis proposed in further chapters.

First, the TP architecture used for the proposed analysis is exposed. This approach facilitates the identification of the uncertainty sources because it decouples the different data models required for predicting an aircraft trajectory.

Then, a detailed description of the influence and effect of each individual model on the uncertainty propagation is provided.

Finally, a generic uncertainty modelling framework applied to model-based decision support applications is particularised to the case of the trajectory prediction uncertainties.

3.2 Aircraft Trajectory Prediction

Aircraft trajectory prediction is a well-known problem that has been studied for years. As discussed in Section 2.5, although there are different alternatives to address the problem, some elements are common among TP implementations. Regardless of the approach followed to obtain a prediction, the aircraft motion is usually expressed as a function of the current aircraft state, an estimation of pilot/FMS intent, meteorological forecasts, and the knowledge of the aircraft performance. The main difference between current TP implementations and those envisioned in the future TBO environment is the knowledge of the aircraft intent. The synchronisation of intent information between onboard and ground systems will increase the reliability of predictions because of a better awareness about aircraft behaviour in the short and medium term.

A typical architecture of a kinetic TP is depicted in Figure 3-1, where input datasets are clearly identified. This solution considers that at least a basic knowledge of the aircraft intent is available. The process of generating an aircraft intent instance from a flight intent instance or a flight plan is out of the scope of the present research. The aircraft intent generation

process is affected by different sources of uncertainty (e.g., the operation context or the user preferences) that finally impact the formulation of the aircraft intent instance used for prediction. Due to the univocal relationship between aircraft intent and predicted trajectory, the proposed uncertainty analysis only considers variations of the parameters that describe a previously generated aircraft intent instance.

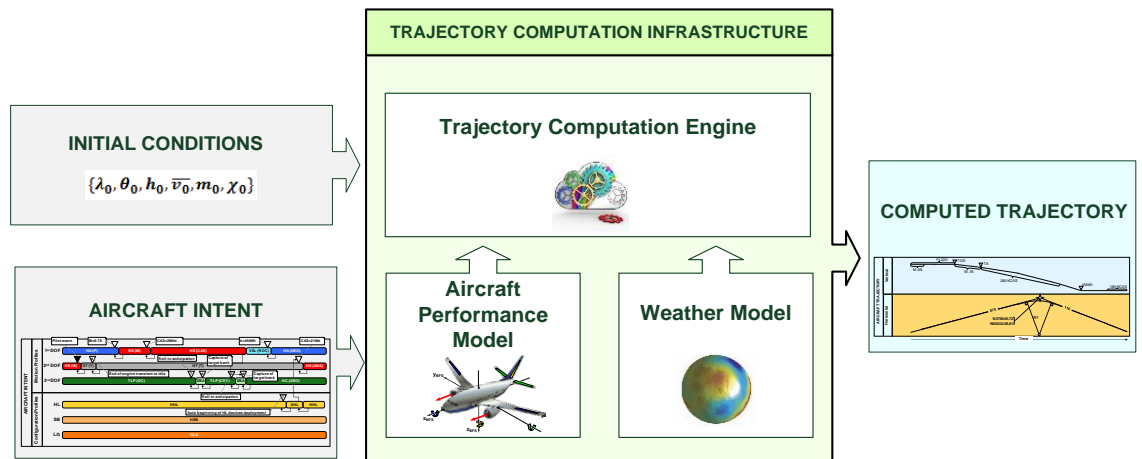


Figure 3-1 – Aircraft Trajectory Prediction Architecture

The proposed architecture for aircraft trajectory prediction requires the initial aircraft state and description of how the aircraft will be operated by the pilot/FMS (a description of the aircraft intent [67]). With this information, a prediction of the trajectory can be calculated once the aircraft performance (which defines the capabilities of aircraft that will execute the planned trajectory) and the environmental conditions (including a model of the Earth surface and gravitational forces) are known.

The main advantage of this approach is the capability to decouple the uncertainty sources, leading to separate and uncorrelated analyses of their individual influences.

The sources of uncertainty can be related to the datasets required by the trajectory computation engine (TCE), the modelling assumptions taken into account for defining the aircraft motion problem, and the deviations between the actual and planned aircraft intents (e.g., difference between the actual cruise Mach number and the Mach number measured and controlled on board). The sources to be studied are classified as follows:

- **Initial Conditions Uncertainties.** The mathematical system of equations that poses the aircraft motion problem requires a set of initial conditions that describe the initial aircraft state from which the trajectory is going to be predicted. Deviations between the actual and assumed initial conditions will be propagated throughout the prediction. The influence of such uncertainties depend on the description of the trajectory. For instance, for predicting the cruise phase of a flight, if the aircraft maintains the Mach speed used at the end of the climb phase, the trajectory uncertainty will depend directly on such target speed (initial speed for the cruise phase). However, if the cruise Mach speed is set to a fixed value, the uncertainty will not depend on the initial value, it will depend on the capability of controlling the cruise speed accurately (flight technical capabilities).
- **Aircraft Motion Modelling Uncertainties.** The mathematical system assumes a set of hypotheses that limit the fidelity of the solution. These hypotheses lead to solvable problems that provide the required levels of accuracy, especially for ATM purposes. The differences between the real aircraft behaviour and its mathematical representation are directly translated into uncertainties in the problem solution. Depending on the type of formulation used for describing the aircraft motion, the set of output variables will be affected by the uncertainty in different ways. For instance, aircraft simulators use aircraft motion models that capture the aircraft attitude while traffic simulators only take into account the movement of the aircraft centre of gravity. In the former, the uncertainty related to the pitch, yaw, and roll angles will influence the predicted trajectory, while in the latter, those uncertainties do not exist.
- **Aircraft Performance Model Uncertainties.** Accurate models for representing the aircraft performance, basically the aerodynamic drag, thrust, and fuel consumption as a function of the flight conditions, are compulsory in the case of kinetic-based TP. However, the most accurate performance datasets are only available to the aircraft manufacturers and aircraft's owners (airliners). Different initiatives have aimed at developing aircraft performance model specifications to provide the community with reliable performance information by removing the need to use manufacturers' datasets. Although there are highly accurate models such as BADA 4 Family [68], the use of generic performance models inevitably introduce uncertainty to the process. This effect is not only produced by the differences between the models and

raw performance data, but also by the lack of performance degradation models that evaluate the negative impact of aircraft life cycle on performance (e.g., years of service, number of flight hours, number of operations, or maintenance cycles). These differences represent the errors between the nominal model valid for an aircraft type and the actual performance of each specific aircraft of a type, in addition to the impossibility of modelling the performance of all existing aircraft types.

- **Weather Model Uncertainties.** The main parameters that determine the weather conditions in which the flight will take place are the atmospheric conditions (basically, temperature and pressure) and the wind. Weather forecasts are widely used as the most accurate representation of the evolution of the weather with time. Although the forecasts provided by the weather forecast agencies, e.g., the European Centre for Medium-Range Weather Forecasts (ECMWF), are deterministic, the process of computing a forecast is intrinsically stochastic. Hence, the weather models required for trajectory prediction add certain levels of uncertainty that can be evaluated a priori.
- **Aircraft Intent Uncertainties.** The aircraft intent represents the command and control actions issued by the pilot, or the FMS, to execute the planned trajectory according to aircraft performance, safety, airline business objectives, and passengers' comfort requirements[69]. A description of such aircraft intent leads to a univocal description of the trajectory to be flown. In general terms, different descriptions of aircraft intent will provide different predicted trajectories. The uncertainty related to aircraft intent represents variations on how the aircraft is finally operated compared to the original plan. Such variation may range, for instance, from deviations at the top of climb (TOC) location to a different flap retraction schedule than originally planned. These uncertainties also account for differences between the pilot/FMS behavioural models used for trajectory prediction and the actual guidance strategy applied by that pilot/FMS.

Moreover, flight technical errors also generate discrepancies with respect to the predicted trajectory. These discrepancies are produced by errors in the flight control system, i.e., these values represent the lack of adherence to the aircraft track [70]. Flight technical errors are considered noise around the nominal trajectory prediction. Due to its erratic nature, their

analysis is considered out of the thesis scope. It is assumed that the long-term effect on a predicted trajectory is negligible compared with the influence of other sources of uncertainties. If this effect becomes noticeable, it is assumed that the aircraft is not being operated according to its nominal capabilities and, therefore, the assumption used for predicting its trajectory is not valid, leading to predictions incoherent with actual aircraft capabilities.

3.3 Initial Aircraft State

The aircraft state at the beginning of the trajectory (or segment thereof) to be predicted represents the initial conditions. The definition of this initial aircraft state depends on how the aircraft motion problem is defined. Kinematic approaches require only initial position and speed since they do not consider the causes of motion for describing the aircraft motion. In contrast, kinetic approaches that take into account the external forces require additional information (especially the aircraft mass) for solving the prediction problem.

A typical set of initial conditions usually comprises the following information:

- Initial time, which represents the first time stamp from which the trajectory is predicted.
- Aircraft position (latitude, longitude, and altitude), which represents the position of the aircraft centre of gravity referenced to the Earth.
- Aircraft dynamic, basically speed and attitude.
- Aircraft mass, basic input in kinetic formulations of the aircraft motion problem.
- Aircraft configuration, position of the landing gear, high lift devices and speed breaks at the beginning of the trajectory to be predicted.

The close relationship between the initial aircraft state and the formulation of the mathematical problem used for predicting the aircraft motion facilitates the analysis of its effect in conjunction with the uncertainty sources identified in the formulation of the aircraft motion model.

3.4 Aircraft Motion Modelling

The problem of predicting an aircraft trajectory requires the formal definition of an Aircraft Motion Model (AMM). Following a kinetic approach, the AMM represents the application of Newton's Laws to the movement of an aircraft within an air mass. Those laws can be expressed as a system of differential equations that describe the evolution of the aircraft subject to external forces (aerodynamics, propulsion, and weight forces) with the time. According to the required level of fidelity, the mathematical problem is typically posed by means of a 6- or 3-degrees-of-freedom (DoF) formulation. The former establishes three force equations and three moment equations, while the latter only considers the first three equations, dismissing the influence of the angular speeds on calculation of the predicted trajectory. The 6-DoF approach is used in aircraft simulators that aim to reproduce the aircraft movement with high fidelity under specific flight conditions. This approach returns not only the aircraft position referred to the selected system of reference, but also the aircraft attitude referred to the Euler system of reference. The obtained state vector includes aircraft vertical and longitudinal position and speed, and aircraft attitude and angular speeds as well. This solution provides the most accurate representation of the aircraft trajectory. From the ATM perspective, the instantaneous information about aircraft attitude does not give any special benefit that can be exploited for a more efficient traffic management. On the contrary, this approach requires detailed information only available on board (e.g., the actual angle of attack) for determining the aircraft motion, and requires extensive computational effort. Thus, for ATM applications, the aircraft motion problem can be simplified to a Point Mass Model (PMM), which considers the following main assumptions [71]:

- Aircraft is considered as rigid solid. This is equivalent to consider that the airframe does not modify its structural shape (structural flexibility is not allowed), and that all points maintain their relative positions at all times.
- Aircraft is considered as symmetric. The orientation of the inertia tensor remains constant and, therefore, independent of the aircraft state. This assumption includes geometrical and mass symmetry, as well as symmetric mass distribution (airframe, fuel, passengers, and cargo) during the complete flight.

- Aircraft mass variation with time only due to fuel consumption. The aircraft mass decreases monotonically as flight evolves due to the fuel consumed by the power plant.
- Thrust force is parallel with respect to the airspeed.
- The variation with time of the aircraft path angle is small when compared with the other terms in the dynamic equations, so the path angle rate can be removed from the corresponding differential equation, converting it into an algebraic expression.
- Limited manoeuvrability. The motion problem is restricted to airborne movement at low angles of attacks and subsonic Mach speeds. Manoeuvres are slow enough to consider steady aerodynamics effects.
- Symmetric Flight. Flight is assumed to be always symmetric and, therefore, there is no sideslip (the sideslip angle is equal to zero) and no aerodynamic lateral force.
- Coordinated Flight. Coordinated flight implies that the roll and yaw dynamics are controlled simultaneously. Then, the aircraft control inputs are reduced to the longitudinal control, which acts over the elevator, and the lateral-directional control, which acts over the ailerons and rudder.
- The deflection of the aerodynamic control surfaces only produces effect on the aerodynamic moments but not on aerodynamic forces. The variation of the module of the aerodynamic forces due to the deflection of such control surfaces is negligible compared to the aerodynamic force produce by the wings, tail, and airframe. However, it heavily influences the aerodynamic moments, which determine the aircraft attitude (and, in turn, affect the resultant aerodynamic force).

Based on the above set of assumptions, it is possible to pose a mathematically solvable system of ordinary differential equations (ODE) for calculating the aircraft motion with the time as an independent variable. The ODE system is obtained by applying Newton's Second Law (3-1), the aircraft mass variation (3-2), and the navigation equations (3-3)

$$\sum \bar{\mathbf{F}} = \frac{d(m \cdot \bar{\mathbf{v}})}{dt} \quad (3-1)$$

$$\frac{dm}{dt} + F = 0 \quad (3-2)$$

$$\frac{dx}{dt} = \mathbf{T}^{GRS,LLS} \mathbf{R}^{LLS,WFS} \mathbf{v} \quad (3-3)$$

to an aircraft subject to the gravitational, aerodynamic, propulsive, and inertial forces ($\sum \bar{\mathbf{F}}$) projected into a Wind Fixed System (WFS)⁹ of reference, while the position of the centre of mass is referred to in terms of the Geodetic Reference System (GRS)¹⁰. Navigation equations transform the airspeed vector $\bar{\mathbf{v}}$ referred to WFS into derivatives of the aircraft position $\frac{dx}{dt}$ referred to the GRS, making use of the intermediate Local Level System (LLS)¹¹ of reference. $\mathbf{T}^{GRS,LLS}$ is the aircraft speed transformation matrix between GRS and LLS, while $\mathbf{R}^{LLS,WFS}$ is the rotation matrix between LLS and WFS. The fuel consumption (F) determines the variation of the aircraft mass with the time.

The aerodynamic forces depend on the actual aircraft speed and configuration. The latter can be expressed as a function of the position of the landing gear (δ_{LG}), high lift devices (δ_{HL}), and speed breaks (δ_{SB}). Then, the aerodynamic forces Drag (D) (3-4) and Lift (L) (3-5), and their dimensionless drag and lift coefficients (C_D [(3-6), C_L) will straightaway depend on the selected aerodynamic configurations as stated below,

$$D = \frac{1}{2} \kappa p_0 \delta M^2 S C_D \quad (3-4)$$

⁹ WFS is defined as follows: axis x directed at every moment along the aircraft airspeed vector, looking forward; axis z contained in the plane of symmetry of the aircraft, perpendicular to x pointing downward; axis y normal to x and z in such a way that they form a right-hand system, with origin in the aircraft's centre of gravity.

¹⁰ GRS defines the coordinates Longitude λ (angle formed between a point meridian plane and the Greenwich meridian plane), Latitude ϕ (angle formed between the line that passes through a point and is perpendicular to the Earth's surface and the equator plane), and Altitude h (distance above the Earth measured along a line perpendicular to its surface), with origin in the Earth's centre of gravity.

¹¹ LLS defines its three axes along the North, East, and down directions, with origin in the aircraft's centre of gravity.

$$L = \frac{1}{2} \kappa p_0 \delta M^2 S C_L \quad (3-5)$$

$$C_D = C_D(M, C_L, \delta_{LG}, \delta_{HL}, \delta_{SB}) \quad (3-6)$$

while the propulsive force thrust F_n (3-7) depends on the aircraft maximum weight (W_{MTOW}), the pressure ratio (δ), and its associated dimensionless thrust coefficient (C_T). The coefficient C_T (3-8) depends in turn on the selected engine rating (δ_T) and aircraft Mach speed (M).

$$F_n = W_{MTOW} \delta C_T \quad (3-7)$$

$$C_T = C_T(M, \delta_T) \quad (3-8)$$

Finally, the fuel consumption (F) (3-9) can be expressed as a function of the sound speed (a_0), the aircraft maximum weight (W_{MTOW}), the pressure (δ) and temperature (θ) ratios, and the Fuel Lower Heating Value (L_{HV}) and its associate dimensionless fuel consumption coefficient (C_F). The coefficient C_F (3-10) can be expressed in turns as a function of the thrust coefficient (C_T) and Mach number (M) as follows,

$$F = \frac{a_0 W_{MTOW}}{L_{HV}} \delta \sqrt{\theta} C_F \quad (3-9)$$

$$C_F = C_F(M, C_T) \quad (3-10)$$

The aircraft motion mathematical problem has one independent variable, the time [t], 10 dependent variables: true airspeed [v_{TAS}], aerodynamic path angle [γ_{TAS}], heading [χ_{TAS}], mass [m], longitude [λ], latitude [φ], altitude [h], throttle parameter [δ_T], aerodynamic bank angle [μ_{TAS}], and lift [L], and seven equations, as exposed next.

$$\frac{dv_{TAS}}{dt} - \frac{F_n - D - mg \sin \gamma_{TAS}}{m} + \frac{dw_1^{WFS}}{dt} = 0 \quad (3-11)$$

$$\frac{d\gamma_{TAS}}{dt} - \frac{1}{v_{TAS}} \left[\frac{L \cos \mu_{TAS} - mg \cos \gamma_{TAS}}{m} + \left(\frac{dw_3^{WFS}}{dt} \cos \mu_{TAS} + \frac{dw_2^{WFS}}{dt} \sin \mu_{TAS} \right) \right] = 0 \quad (3-12)$$

$$\frac{d\chi_{TAS}}{dt} - \frac{1}{v_{TAS} \cos \gamma_{TAS}} \left[\frac{L \sin \mu_{TAS}}{m} + \left(\frac{dw_3^{WFS}}{dt} \sin \mu_{TAS} - \frac{dw_2^{WFS}}{dt} \cos \mu_{TAS} \right) \right] = 0 \quad (3-13)$$

$$\frac{dm}{dt} + F = 0 \quad (3-14)$$

$$\frac{d\lambda}{dt} - \frac{v_{TAS} \cos \gamma_{TAS} \sin \chi_{TAS} + w_2^{WFS}}{(N + h) \cos \varphi} = 0 \quad (3-15)$$

$$\frac{d\varphi}{dt} - \frac{v_{TAS} \cos \gamma_{TAS} \cos \chi_{TAS} + w_1^{WFS}}{(M + h)} = 0 \quad (3-16)$$

$$\frac{dh}{dt} - v_{TAS} \sin \gamma_{TAS} = 0 \quad (3-17)$$

This is a 3-DoF problem whose output is the seven state variables $[v_{TAS} \gamma_{TAS} \chi_{TAS} m \lambda \varphi h]$ for a given set of 3 input variables $[\delta_T \mu_{TAS} L]$. The described system of equations is valid for a fixed aerodynamic configuration (i.e., fixed values of δ_{LG} , δ_{HL} , δ_{SB}). Consequently, in addition to this three Motion DoF (MDoF), the aircraft configuration needs to be also defined by three more DoF, named Configuration DoF (CDoF), determining together the aircraft motion.

Applying the Space-State formulation [72], the system can be expressed in a compact form:

$$\dot{\mathbf{X}} = \mathbf{f}(\mathbf{X}, \mathbf{u}, \mathbf{E}, \Delta, t) \quad (3-18)$$

where $\mathbf{X} = [v_{TAS} \ \gamma_{TAS} \ \chi_{TAS} \ m \ \lambda \ \varphi \ h]$ is the state vector, $\mathbf{u} = [\delta_T \ \mu_{TAS} \ L]$ is the control vector, $\mathbf{A} = [\delta_{LG} \ \delta_{HL} \ \delta_{SB}]$ is the configuration vector, and $\mathbf{E} = [\delta \theta \ V \ \mathbf{g} \ \mathbf{w}^{WFS}]$ is the environmental model vector. Given the initial conditions, the control parameters \mathbf{u} and the configuration parameters \mathbf{A} , the integration of the differential problem returns a trajectory \mathbf{X} .

The main problem of the above formulation is that, from the ATM perspective, it is almost impossible to determine the control parameters \mathbf{u} that define the aircraft motion. The simplest way of obtaining a well-posed, closed mathematical problem whose solution is a unique trajectory from the equations introduced above, is to define the time evolution of the three control and the three configuration parameters. However, this solution does not allow modelling the guidance modes applied in the ATM context in a straightforward manner. This is the reason why the inverse formulation of the problem (constrained mechanical model based on the specification of the constraints or control objectives that limit the system output) is more appropriate and useful. Thus, the problem can be solved by the definition of three motion constraints,

$$g_i(\mathbf{X}, \mathbf{u}, \mathbf{E}, t) = 0, i = \{1, 2, 3\} \quad (3-19)$$

and three configuration constraints.

$$d_i(\delta_i) = c_i(\mathbf{X}, \mathbf{E}, t), i = \{LG, HL, SB\} \quad (3-20)$$

The motion constraints represent the restrictions (mathematical formulation of guidance and control objectives) that the trajectory is required to fulfil, while the configuration constraints are the expressions that determine the aerodynamic configuration to be considered at each flight condition. The proposed set of six constraints represents a description of the aircraft intent (AI). An AI instance gathers in a formal data structure all command and control instructions released by the pilot/FMS to guide the aircraft according to the filed Flight Plan under the current weather conditions, while respecting all ATC constraints established along the planned trajectory [73].

This constrained formulation leads to a transformation of the ODE system into a differential algebraic equations (DAE) system. Hence, the DAE system describes the evolution of the

aircraft motion with time for known aerodynamics conditions within a specified time interval, compliant with ATC restrictions at any flight point. Such an interval starts at the considered initial conditions and ends when an event on the trajectory happens, for instance, when the aircraft reaches the cruise altitude. The aircraft trajectory can therefore be described as a sequential succession of DAE systems. The process of solving a sequence of DAE systems is known as Sequential DAEs Resolution (SDR).

3.4.1 Aircraft Motion Modelling Uncertainties

The uncertainties introduced by the aforementioned modelling of the aircraft motion model are founded in the assumptions considered for posing the mathematical problem. Those uncertainties come from the simplifications used for the formulation of a 3+3 DoF system, although it is required to distinguish between the intrinsic uncertainty derived from the formulation of the PMM, the solvability uncertainty coming from the description of the Motion and Configuration constraints used for coherently closing the mathematical problem, and the uncertainty in the selected time interval in which those constraints are applied.

The effect of the intrinsic uncertainty is independent of the type of trajectory to be predicted and will always lie with the same variables in the same manner. This uncertainty does not show any stochastic behaviour. Thus, this should be considered an intrinsic prediction error.

The solvability uncertainty depends on the type and definition of the constraints selected for obtaining a solvable DAE system; the time interval in which the DAE system is integrated; and the sequence of concatenated DAE systems that lead to a complete trajectory description. This uncertainty is equivalent to the aircraft intent uncertainty that will be detailed in the following Section 3.9.

3.5 Earth Surface Modelling

The location of the aircraft obtained from the navigation equations (3-3) is usually referred to as the GRS system. However, this does not take into account the position with respect to the Earth's surface, which determines how high the aircraft is flying in reference to the local ground level. The terrain elevation “e” is defined as the geodetic altitude of the terrain. Based on this definition, aircraft height can be calculated by the difference between the aircraft altitude and the terrain elevation.

The standard model used in cartography, geodesy, and navigation is the World Geodetic System (WGS), which comprises a standard coordinate system for the Earth, a standard spheroidal reference surface (the reference ellipsoid), and a gravitational equipotential surface (the geoid) that defines the nominal Mean Sea Level (MSL).

The latest version WGS84¹² defines Earth's surface as an ellipsoid where the MSL is typically defined by the EGM96 (Earth Gravitational Model 1996) geoid [74]. The undulation N is the difference between the ellipsoid and geoid surface at each longitude and latitude.

3.5.1 Earth Surface Modelling Uncertainties

The WGS84 is the most accurate representation currently available for describing Earth's surface [75]. Although the model assumes some inaccuracies, the effect of using it for aircraft trajectory predictions is limited and relatively small regarding other more important effects.

If other different models are considered, the accuracy representing the Earth surface will determine its impact on trajectory prediction.

In the case of the WGS84 (selected model used in this research), the model error is not considered a source of uncertainty because it does not show a stochastic behaviour.

3.6 Gravitational Force Modelling

The gravitational force represents the attraction force that the Earth applies to any other body. This is a particularisation of the Newton's theory of gravitation for the case of the Earth planet. This force not only influences the weight force applied to the aircraft, but also the atmospheric properties' variation with the altitude. The atmosphere is an air mass that surrounds the Earth and is in equilibrium with respect to the Spherical Reference System (SRS).

¹² World Geodetic System (WGS) 1984, last revised in 2004, defines a reference frame for the earth, for use in geodesy and navigation.

The Earth Gravitational Model 1996 (EGM96) [76] associated to WGS84 provides the gravitational potential U_g functions as a development of Legendre polynomials up to the degree (q) and order (p) 360. The following expression represents the most sophisticated fashion of the proposed model.

$$U_g(\lambda, \varphi, r) = \frac{GM}{r} \left[1 + \sum_{q=2}^{q_{max}} \sum_{p=0}^q \left(\frac{a}{r}\right)^q P_{qp} \cos \varphi (\underline{C}_{qp} \cos(m\lambda) + \underline{S}_{qp} \sin(m\lambda)) \right] \quad (3-21)$$

Here λ , φ , and r are the coordinates referenced to the SRS.

Due to the complexity of such a definition, simplifications of the model are widely used, especially in the case of aircraft trajectory predictions. It is possible to define a constant gravitational acceleration assuming independence regarding the longitude, latitude, and altitude; or considering the most detailed geoidal representation that instantiate a 3D model as a function of the SRS coordinates.

3.6.1 Gravitational Force Modelling Uncertainties

Each possible model instantiation introduces disparate accuracy in the description of the gravity force. The influence of the deviations between the actual and modelled gravity affects all the predictions in the same manner and are always contained within a boundary.

Nevertheless, the common models used by most TPs provide enough accuracy so that the error introduced is smaller in comparison with those produced by other models. In addition, its nature is purely non-stochastic. Hence, this bias introduced in the prediction process due to the use of gravitational models is not considered a source of uncertainty.

3.7 Aircraft Performance Modelling

The AMM exposed in Section 2.1 requires a description of the aircraft performance. This description provides inputs about the aerodynamic drag force (D), the propulsive thrust force (F_n), and the fuel consumption (F). Other information about common operational speeds and altitudes, performance envelope, kinematic and environmental limitations or flaps, and

landing gear deflection and retraction schedules are also valuable for ensuring flyable solutions¹³, although they are only provided by the most sophisticated performance models.

Onboard systems have access to up-to-date information about the aircraft performance, which is used for computing onboard trajectory predictions. This information is usually collected within the manufacturer's performance databases. These datasets contain the tables that provide performance data for any possible flight condition, including take-off and landing requirements, inoperative engine procedures, or thrust de-rate strategies.

However, such precise information is not available on ground. Instead, DSTs make use of generic Aircraft Performance Models (APM) that represent the best approximation to the nominal performance of a specific aircraft type.

3.7.1 EUROCONTROL Base of Aircraft Data

BADA (Base of Aircraft Data) is an aircraft performance model developed and maintained by EUROCONTROL through active cooperation with aircraft manufacturers [77]. The information and data contained in BADA is designed for use in aircraft trajectory modelling, including simulation and analysis of air traffic operations and non-safety critical DSTs for air traffic control. BADA is broadly considered the international standard aircraft performance model for ATM applications, providing means for aircraft manufacturers to furnish the ATM community with accurate aircraft performance information in a manner that protects their sensitive proprietary information and within a framework validated and controlled by a neutral international entity.

There are two versions of the BADA model, BADA 3 and BADA 4, each with a different model specification and different datasets.

BADA 3 provides aircraft performance information within the nominal part of the flight envelope. Although its accuracy and flexibility are limited, it is considered the basic standard model to support the requirements of trajectory simulation applications addressing current

¹³ Under some circumstances, the integration of ODE or DAE systems may provide a mathematically coherent solution that cannot be flown by the considered aircraft because it breaches some of the performance limitations.

air traffic operations. BADA 3 covers 90 percent of the current fleet, i.e., EUROCONTROL provides BADA 3 datasets for 90 percent of the aircraft types currently in operation.

BADA 4 is the latest generation of the BADA model and is intended to meet the accuracy and flexibility requirements of the research and validation initiatives aimed at supporting the development of the future ATM system. Currently, there are BADA 4 datasets available for 60 percent of the fleet (including all Boeing and Airbus types). BADA 4 provides accurate aircraft performance characteristics over the entire flight envelope and supports simulation of advanced ATM concepts.

The model specification consists of a set of polynomial expressions used to calculate aircraft performance parameters such as the drag coefficient (C_D), fuel consumption (F), or engine thrust coefficient (C_T). The polynomials are parameterised by a set of coefficients that particularise the polynomial expressions for specific aircraft types. These coefficients are the BADA datasets. Each aircraft type (airframe-engine combination) is associated with a specific BADA dataset. The BADA dataset of an aircraft type used with the BADA model specification provide approximate values of the aircraft performance characteristics of that aircraft. BADA 4 specification and datasets provide an unprecedented degree of fidelity with respect to manufacturers' performance data [78].

Both BADA 3 and BADA 4 model specifications define the polynomials that describe the Equations (3-6), (3-8), and (3-10), although disparately. For instance, the drag polar specification in BADA 3, contrary to BADA 4, does not take into account compressibility effects, thus, the influence of the Mach Number is not considered.

3.7.2 Aircraft Performance Modelling Uncertainties

Despite the fact that parametric aircraft performance models are becoming increasingly accurate (with respect to manufacturers' reference data), they introduce a bias with respect to the raw performance data resulting from the fitting techniques used for identifying the corresponding coefficients. Moreover, there are some effects that are not considered by the identification process, which lead to higher deviations between the modelled and actual performance. For instance, the raw drag values used for fitting the drag coefficient polynomial are based on nominal values of atmospheric pressure and temperature. However, if the actual flight conditions are off those nominal values, the actual drag needs to be

corrected by the Reynolds number correction ΔC_D^{Re} . This correction takes into account the viscosity of the airflow over the aerodynamic surface, which basically indicates the location of the boundary layer transition from laminar to turbulent. Although in most cases this correction is relatively small compared to value of the drag coefficient C_D , its influence needs to be considered for high fidelity trajectory predictions.

All deviations between the actual performance of a specific aircraft and the performance information provided by the models make up the aircraft performance modelling uncertainty.

3.8 Weather Modelling

The aircraft motion is determined by the surrounding air mass state (i.e., temperature, pressure, and density) and the speed of the air mass with respect to Earth (wind). Hence, the conditions that characterise the surrounding air mass play a paramount role in trajectory prediction.

Weather forecasts are obtained from meteorological models formulated in terms of differential equations that describe the behaviour of the atmosphere within certain temporal and spatial domains, and are characterised by some initial and boundary conditions. Such equations correspond to simplifications of the general Navier-Stokes laws that govern the fluid dynamics that are usually numerically solved over a discretisation of the space and time domains.

The chaotic nature of this problem makes its solution extremely sensitive to the following aspects:

- Domain definition: the grid shape, cell size, coordinate system, resolution, and accuracy of the terrain elevation model, moving surfaces (water) and soil characterisation, and time horizon.
- Model and solver: spatial and temporal discretisation of the equations that embody physical laws of fluid mechanics, integration time step, and solver method.
- Initial/boundary conditions: initial conditions are taken from best current knowledge of the atmospheric status at initial time, whereas boundary conditions are taken at the

limits of the spatial domain all along the time interval that span the initial time until the time for which the solution is required.

From the ATM perspective, the weather information required for solving the AMM are the atmospheric conditions (temperature, pressure, density, and speed of sound) and the wind field that will affect the aircraft trajectory. The remaining weather variables, although they might play a role in trajectory prediction (e.g., air humidity), are not considered uncertainty sources because they are not considered in the proposed AMM, in Section 3.4.

3.8.1 Atmosphere Modelling

Although there are a variety of atmosphere models tailored to specific applications, the International Standard Atmosphere (ISA) is broadly accepted by the ATM community as the standard model that provides atmosphere information when an aircraft trajectory needs to be predicted.

The atmosphere conditions not only influence the aircraft performance (e.g., the thrust provided by the power plant at different ratings depends on the atmosphere's temperature), but also the flight conditions (e.g., the Mach number depends on the speed of sound at the considered atmosphere conditions). This influence is especially relevant in the definition of the geopotential pressure altitude H_p . Commercial aircraft fly at constant pressure altitudes during cruise, which refer to a constant atmospheric pressure level (isobaric level). Depending on the atmosphere conditions, the geodetic altitude h (referred to the GRS) in cruise will vary among flights flying at the same H_p .

Any atmosphere model returns the evolution of the air pressure, temperature, and density with the time as a function of the longitude, latitude, and geodetic altitude,

$$P, T, \rho = f(\lambda, \varphi, h, t) \quad (3-22)$$

while the speed of sound is given by the following expression.

$$a = \sqrt{\kappa R T} \quad (3-23)$$

MSL conditions occur at the geopotential equipotential surface that better fit the average sea level. If those conditions are referenced to ISA conditions, they are known as MSL standard conditions.

$$\begin{aligned}
 P_0 &= 1013.25 \text{ hPa} \\
 T_0 &= 288.15 \text{ K} \\
 \rho_0 &= 1.225 \text{ kg/m}^3 \\
 a_0 &= 340.294 \text{ m/s}
 \end{aligned}
 \tag{3-24}$$

For non-standard conditions, the MSL conditions are described by the temperature (ΔT) and pressure (ΔP) deviations regarding ISA conditions. Thus, the expression that provides atmosphere conditions is

$$P, T, \rho = f'(\lambda, \varphi, h, t, \Delta T, \Delta P) \tag{3-25}$$

Equation (3-25) provides the atmospheric information required for defining the aircraft speeds that are commanded and controlled by the pilot/FMS for flying the planned trajectory. These speeds need to be transformed into the true airspeed v_{TAS} , which is the state variable used in the formulation of the AMM.

- Mach number. This refers to the ratio between the true airspeed and the speed of sound at the considered atmospheric conditions.

$$M = \frac{v_{TAS}}{a} \tag{3-26}$$

- Calibrated Airspeed (CAS). This is the airspeed shown by conventional onboard airspeed indicators after considering the static pressure measurement errors.

$$v_{CAS} = \sqrt{\frac{2\kappa}{\kappa-1} \frac{P_0}{\rho_0} \left\{ \left(1 + \frac{P}{P_0} \left[\left(1 + \frac{\kappa-1}{2\kappa} \frac{\rho}{P} v_{TAS}^2 \right)^{\frac{\kappa}{\kappa-1}} - 1 \right] \right)^{\frac{\kappa-1}{\kappa}} - 1 \right\}} \tag{3-27}$$

- Equivalent Airspeed (EAS). This airspeed represents the speed at MSL, under ISA conditions, that would produce the same incompressible dynamic pressure that is produced at the true airspeed and altitude at which the aircraft is flying. Airspeed limits caused by structural limitations are directly proportional to the square of the EAS value.

$$v_{EAS} = v_{TAS} \sqrt{\frac{\rho}{\rho_0}} \quad (3-28)$$

Although the AMM does not explicitly consider these airspeed definitions, the most common approach is to use them for defining the motion constraints $g_i(\mathbf{X}, \mathbf{u}, \mathbf{E}, t) = 0$ that describe the AI and, finally, the aircraft motion.

3.8.1.1 Atmosphere Modelling Uncertainties

The deviations between the actual and the modelled atmosphere conditions lead to trajectory predictions uncertainties whose effect is basically twofold:

- Altitude uncertainties. Depending on the type of altitude to be controlled during the flight (which is directly related to the flight phase), the uncertainties will impact the geodetic or the geopotential pressure altitudes. Since the former is the state variable used with the AMM formulation, the uncertainties introduced by ΔT and ΔP in the case of off-ISA conditions will affect the relationship between the pressure altitude at which the aircraft is being operated and the geodetic altitude that refers to the geometric height with respect to the MSL.
- Airspeed uncertainties. The atmosphere parameters that describe the actual atmosphere conditions relate the airspeeds' definitions to each other. Therefore, the uncertainties introduced by these modelled atmosphere parameters generate deviations in those relationships, which finally are translated into trajectory prediction uncertainties.

In addition, uncertainty in the atmosphere conditions affects the aircraft performance. For instance, the thrust provided by the engine directly depends on the air intake temperature

and pressure. This indirect effect influences the performance data provided by the aircraft performance model in use.

3.8.2 Wind Modelling

The wind is one of the most influential inputs in the aircraft trajectory prediction process. The AMM is basically referenced to the WFS and then, the output is translated to the GRS for positioning the trajectory data with respect to the Earth surface model.

The wind description required by the definition of the AMM only needs to include information about the components of the wind at each pressure level. Especially interesting is the effect of the wind gradient (variation with respect to altitude) that directly affects the rate of climb or descent. When subject to a headwind, neglecting this gradient places the estimated flight below the actual flight. Errors of 1 kt/1000 ft in the wind gradient during descent trajectories report approximately a deviation of 3.5 percent in the rate of descent [79][80].

3.8.2.1 Wind Modelling Uncertainties

Any TP requires knowledge from the three components of the wind field at any time (t) for all the positions (P) over which the flight will progress. Thus, this field is a function $w(t,P): \mathbb{R} \times \mathbb{R}^3 \rightarrow \mathbb{R}^3$ where $t \in \mathbb{R}$ and $P \in \mathbb{R}^3$. A basic wind model can be represented by two components: the nominal wind $W(t,P)$ and a random disturbance $N(t,P)$. The former is the temporal and spatial forecast wind data provided by any weather forecast agency (for instance, the Rapid Update Cycle [RUC]¹⁴ developed by NOAA [81]). The latter is a stochastic variation applied to all wind components, which finally is the component that adds uncertainty to the predicted trajectories [82].

If a Gaussian representation is assumed for describing the stochastic component of the wind field, the average of such distribution can be considered as the forecasted magnitude and the standard deviation as the wind uncertainty. In “Performance of trajectory models with wind

¹⁴ The RUC is a NOAA operational weather prediction system running every hour out to at least 18h comprised primarily of a numerical forecast model (using isentropic-sigma hybrid vertical coordinate) and an analysis/assimilation system to initialise that model.

uncertainty,” a new method for calculating both parameters is proposed [83]. The procedure uses a time-lagged ensemble of weather model forecasts from an hourly updated RUC system. Uncertainty is estimated based on the spread amongst several successive RUC forecasts of different lengths that are valid at the same time. The time-lagged ensemble is built by 2-, 3-, 4-, 5-, 6-, and 7-hour RUC wind predictions. The average wind at every point is defined by the ensemble average, while the standard deviation of the wind distribution among ensemble members is defined as the wind uncertainty. A key advantage of this approach is that it identifies regional variations of uncertainty that are related to actual weather phenomena. On the other hand, the two main drawbacks are that the use of older forecasts usually adds greater uncertainty and the correlation between different ensemble members is also larger than the correlation generated by other techniques. However, the proposed methodology for obtaining wind uncertainty has been proven as appropriate for defining more accurate separation buffers in en route flight predictions at constant heading and fixed altitude.

3.9 Aircraft Intent Uncertainties

The pilot/FMS actions on the command and control system determine the trajectory flown by the aircraft under the actual weather conditions within the considered operational context. These actions define how the aircraft is operated to meet the business goals and ATC restrictions, while ensuring flight safety during a time interval. The set of guidance instructions that are required for executing the planned trajectory specifies the aircraft intent. In general, such instructions capture basic commands and guidance modes at the disposal of the pilot/FMS to steer the aircraft.

In the aircraft trajectory prediction formulation exposed in Section 3.4, the aircraft intent is a basic input that describes the trajectory to be flown. This input is represented by the motion (3-19) and configuration (3-20) constraints. The remaining inputs provide information required for computing the prediction, but do not provide any data about the expected aircraft behaviour. Therefore, the aircraft intent must be formulated so that the AMM is univocally determined and results in a unique mathematical solution of the trajectory prediction problem.

The formalism adopted in thesis for describing the aircraft intent is the Aircraft Intent Description Language (AIDL) [71]. The AIDL is a formal language intended to express aircraft intent information in a univocal, rigorous, and standardised manner.

As any formal language, the AIDL is defined over a finite set of instructions, which comprise the AIDL alphabet. The AIDL grammar encompasses the set of rules according to which the instructions (or alphabet symbols) can be combined into valid instances of aircraft intent (or language strings). It contains rules governing how to combine instructions both sequentially (instructions with contiguous, non-overlapping execution intervals) and simultaneously (instructions with overlapping action intervals). The development of these rules, which are based on the DAE formulation of the AMM, ensures that the resulting aircraft intent defines the trajectory, unambiguously leading to a solvable mathematical problem.

The words of the AIDL are called operations. An operation represents an elemental aircraft behaviour that determines its motion univocally during a specific time interval. Such words are the result of a set of compatible instructions simultaneously active during the corresponding operation interval. The syntactical rules in the AIDL govern the definition of sentences, which are formed by sequences of operations. Each operation defines a unique solvable DAE system whose computation returns a segment of the trajectory valid during the specified time interval. For computing a sequence of operations, which actually represent a complete trajectory, the SDR methodology is applied (as studied in Section 2.1). Thus, the complete trajectory computation process is posed as a sequence of closed DAE problems sequentially solved. The shift from one DAE to the next one is triggered by the occurrence of certain events, for instance, when the aircraft reaches a certain altitude or the speed gets a specific target. These events are represented in the AIDL as trigger elements that describe when the effect of a specific instruction is over and, therefore, the effect of the following instructions in the sequence.

The AIDL can be considered a formal framework for expressing any possible behaviour that can be adopted by an aircraft operating within the ATM context.

The main advantages of assuming this solution are twofold:

- The use of a structured framework that decouples the influence of the AI in the trajectory prediction process from other sources of uncertainty.

- The capability of systematically modelling the uncertainties introduced by the AI description.

According to the definition of AIDL, the aircraft intent can be formulated as a chronologically ordered sequence of operations. Each well-formed operation requires three motion profiles that describe the aircraft behaviour and three configuration profiles that determine the aircraft configuration within the specified execution interval. Each profile is defined by an instruction that is characterised by an effect and a specifier. The effect of an instruction represents the mathematical expression that describes the influence of a constraint on the aircraft motion, while the specifier complements the instruction by indicating the specific aspect of the aircraft motion that is to be constrained. The execution interval runs from the initial instant to the achievement of the selected event. This event is formulated as a trigger condition that represents a condition on the predicted trajectory (e.g., a target speed), used for deactivating the instruction and activating the following one in the sequence.

Hence, this approach facilitates the identification of the uncertainty sources that affect the description of the aircraft intent. All uncertainties derived from the process of generating an aircraft intent instance from the information contained in a flight intent instance or in a flight plan are not considered hereafter. The focus is on the uncertainty sources affecting the description of the aircraft intent, not its generation. Based on this approach, the aircraft intent uncertainties can be classified as:

- Continuity conditions uncertainties. These are algebraic equations that relate the variables of two consecutive aircraft intent operations and that ensure continuity of the evolution of aircraft state variables in two consecutive operations. Contrary to the ODE formulation that admits any possible value for the state variables for initialising the mathematical problem, the DAE approach requires some continuity conditions that guarantee the coherent initialisation of the DAE system based on the outputs of the preceding operation. If those conditions are not imposed, it might be possible to obtain discontinuities in some variables that do not represent any realistic aircraft behaviour. For example, 3D position and mass require from a continuity condition to obtain a realistic trajectory prediction. The uncertainty introduced by those conditions is considered the same as the uncertainty introduced by the initial

conditions, because in fact, both represent the stochastic behaviour of the aircraft state variables at the beginning of an individual operation.

- **Instruction effect uncertainties.** The effect represents the mathematical formulation of the motion and configuration constraints that close the DAE system, and determines how an aircraft state variable has to be controlled to obtain the expected aircraft behaviour. The stochastic variability of these constraints translates into the variability of the controlled state variable.
- **Trigger uncertainties.** There are different alternatives for describing events that establish the end of an operation. For instance, it is possible to define a target altitude (floating trigger), an aircraft configuration modification (default trigger), an open condition that depends on an optimisation loop (auto trigger), or a specific time (fixed trigger). Nevertheless, all of them can be translated into a fixed trigger during the integration of the DAE system. Time is the independent variable of the mathematical problem, and therefore, any condition can be expressed in terms of elapsed time from the initial condition. This approach helps the process of uncertainty analysis because it reduces all alternatives just to the analysis to the instruction's execution interval variability.

3.10 Uncertainty in Model-Based Decision Support Applications

Deterministic models of real systems are widely used to help decision makers with their tasks. These models can provide highly accurate representations of reality, providing valuable hints to facilitate the process of evaluating the risks behind a decision. In most cases, the decision-making process is driven by the potential impact of a wrong decision, especially when safety is a critical aspect to be considered. The precautionary approach [84] states that in circumstances in which safety must prevail and, therefore, any potential adverse effect may occur, the decision should be not to proceed. Any likely harm has to be anticipated to avoid negative consequences. The uncertainty of the outcomes forces decision makers to act with precaution, which intrinsically means to practise caution in the context of uncertainty. The precautionary principle can be understood as a criterion guided by scientific knowledge, which considers the scientific uncertainty as a temporary lack of knowledge [85]. This approach is extensively applied in policy, health, and environmental decision

support processes. An enlightening example of application is the eruption of the Eyjafjallajökull volcano, during which many European airspace sectors were closed to prevent traffic from flying through the ash cloud because of an unknown impact on flight safety [86].

The uncertainty related to the models used in decision-making processes is characterised by three dimensions: location, level, and nature [87].

- Location. This dimension establishes where the uncertainty manifests its impact. Location refers to the logical structure in which it is possible to evaluate the sources of uncertainty and their effects. According to this, there are five possible locations:
 - Context, which refers to the conditions that define the boundaries of the system.
 - Inputs, which describe the reference systems and the external driving forces applied to the system.
 - Parameters, which are elements assumed as constant or invariant.
 - Model uncertainty, which is composed of the model structure uncertainty (lack of sufficient understanding of the model) and the technical uncertainty (deviations due to erroneous algorithms definition and/or implementation).
 - Outcome uncertainty or prediction error, which is the induced effect on the outputs driven by the propagation of the uncertainty introduced by the other locations.
- Level. The knowledge about system locations may vary from determinism to total ignorance. The spectrum between these two extremes determines the uncertainty level. Determinism is an unachievable and ideal state, which acts as delimiting boundary. From this state, the variety of the uncertainty levels can be expressed by means of the following transitional stages (Figure 3-2):

- Statistical uncertainty. Mathematical description of the behaviour of any locations of the model. Measurement inaccuracy or sampling errors are typical statistical uncertainties. This term is what is usually understood as *uncertainty* in the natural science.
 - Scenario uncertainty. A plausible description of how a system evolves due to the action of external forces comprises a scenario. A set of assumptions and hypotheses are necessary for a complete and detailed description of the scenario. However, there are no analytical expressions to characterise these assumptions and hypotheses, and therefore, additional uncertainty needs to be considered.
 - Recognised ignorance. The lack of knowledge about functional relationships, statistical descriptors, or scientific basis leads to increased levels of uncertainty. Under some circumstances, the ignorance can be mitigated by conducting an extensive research and analysis of the system (reducible ignorance). In other cases, such uncertainty cannot be reduced (irreducible ignorance or indeterminacy).
 - Total ignorance. This is the opposite extreme to determinism, when it is not known which locations are unknown.
- Nature. This dimension distinguishes between whether the uncertainty comes from imperfect knowledge (epistemic uncertainty) or from intrinsic variability or randomness (variability uncertainty) of the phenomena.



Figure 3-2 – Progressive Transition Between Determinism and Total Indeterminacy

3.10.1 Trajectory Prediction Uncertainties Modelling

With the advent of the new ATM paradigm, decision making will shift to a highly complex and sophisticated process. In this new environment, the advanced DSTs will exploit trajectory data (predicted and actual) to help and advise ATM stakeholders in their responsibilities. A sound understanding of the uncertainty affecting such a process will facilitate it, while enabling additional capabilities unauthorized today (e.g., autonomous self-separation). The trajectory modelling and prediction will be the core functionality of any DST. Thus, an analysis of the three uncertainty dimensions that characterised such functionality will enable its quantification, therefore enabling more reliable DST outcomes.

According to the framework described above, the main trajectory prediction uncertainties can be categorised as stochastic sources since they can be represented by random processes. The epistemic uncertainty is almost negligible. Thorough research has been conducted on the subject, and there is deep scientific knowledge of the trajectory prediction problem [88][89]. The inputs may be represented by statistical distributions that identify the behaviour of driving forces and data sources.

Considering the above, the uncertainties affecting prediction of an aircraft trajectory can be structured as follows:

- Context uncertainty. The prediction is circumscribed to the prediction of an aircraft trajectory under specific flight conditions (i.e., symmetric flights, no side-slip angles, and small angles of attack).
- Model uncertainty. Implementation of the TP in use, that is, the mathematical representation of the aircraft motion.
- Input uncertainty. Accuracy of the underlying models (aircraft performance or aircraft intent models) and the quality of the datasets required to predict a trajectory (aircraft mass, flight/aircraft intent, initial aircraft state, or weather forecasts).
- Parameter uncertainty. Invariants during a prediction such as the gravity, earth, or atmosphere models.

- Outcome uncertainties. Variability of trajectory predictions as a function of the expected variability of other uncertainty locations and the look-ahead time.

3.11 Summary

This chapter proposes a qualitative classification of the main sources of uncertainty that affect the aircraft trajectory prediction process. Those sources have been identified according to the proposed aircraft motion model in Section 3.4. This approach, based on the formulation of a DAE system, leads to the definition of the AIDL and the associated trajectory prediction approach. The main advantage of considering this alternative is the capability of decoupling the required input sources, removing correlated dependencies, and allowing the individual analysis of the sources of uncertainty.

Although the chapter provides a detailed study of all possible sources of uncertainty, not all of them introduce comparable levels of uncertainty to the prediction process. The following Table 3-1 gathers the identified sources, indicating their applicability to the study of the uncertainty propagation in aircraft trajectory predictions.

Table 3-1 – Summary of the Identified Uncertainty Sources

Uncertainty Source		Applicable	Description
<i>Flight Technical Uncertainties</i>		NO	Errors produced by the onboard command and control system
<i>Initial conditions uncertainties</i>		YES	Description of the initial aircraft state at the beginning of the trajectory Considered as part of the analysis of the AI uncertainties
<i>Aircraft Motion Modelling Uncertainties</i>			
	Modelling intrinsic uncertainty	NO	Errors introduced by the assumptions considered in the formulation of the aircraft motion problem
	Solvability uncertainty	YES	Definition of the constraints selected for obtaining solvable DAE systems Considered as part of the analysis of the AI uncertainties
	Earth surface model	NO	Differences between actual and modelled Earth surface
	Gravitational model	NO	Differences between actual and modelled gravitational force
<i>Aircraft Performance Modelling Uncertainties</i>		YES	Differences between actual and modelled aircraft performance
<i>Weather Forecast Uncertainties</i>			
	Atmosphere model uncertainties	YES	Differences between actual and forecasted atmosphere conditions
	Altitude description uncertainties	YES	Influence of the atmosphere conditions on the definition of the pressure altitude
	Airspeed description uncertainties	YES	Influences of the atmosphere conditions on the definition of the airspeed
	Wind model uncertainties	YES	Differences between actual and forecasted wind field
<i>Aircraft Intent Uncertainties</i>			
	Continuity conditions uncertainties	YES	Description of the initial aircraft state at any of the consecutive operations in the sequence
	Instruction effect uncertainties	YES	Mathematical definition of the applicable constraints at each individual operation, which lead to solvable DAE systems
	Trigger uncertainties	YES	Difference between the actual and modelled trigger that defines the end of an operation and the beginning of the next one in the sequence

All the uncertainty sources identified as *Applicable* will be studied and modelled in the remaining chapters of this thesis.

This page intentionally left blank

CHAPTER 4

IMPACT OF AIRCRAFT PERFORMANCE UNCERTAINTY ON TRAJECTORY PREDICTION

4.1 Introduction

Aircraft performance comprises the operational capabilities of an aircraft type equipped with a specific power plan. If available, the best source of performance information is the performance databases released by the manufacturers, for instance, those included in the Flight Planning and Performance Manual (FPPM). If this is not the case, the use of generic performance models is the only alternative.

The most accurate performance datasets, though, introduce certain levels of uncertainty in the process of providing aircraft performance information. The performance datasets are basically tables that return performance information for different values of the input state variables. Those tables are built on the flight test outcomes performed for certifying any aircraft. For those state variables' values not explicitly included in the tables, interpolation algorithms are usually applied. This translates into deviations between the actual and calculated performance, which can be seen as sources of uncertainty.

On the other hand, the use of generic aircraft performance models leads to broader uncertainties because the models are only representations of the performance of an aircraft at specific conditions (usually at delivery). Independently of the model's fidelity to the reference performance data, such models provide outputs with higher uncertainty than the performance outputs obtained from the manufacturers' performance datasets.

This chapter presents the role of aircraft performance models in trajectory prediction, especially in the case of kinetic formulations of the aircraft motion model.

Although most accurate performance datasets are owned by manufacturers, from the ATM perspective, generic models can be used for predicting a trajectory in a real environment. It is usually considered that the impact in prediction accuracy introduced by those models is moderate in the case of most sophisticated alternatives.

Following sections propose a methodology for introducing the aircraft performance degradation in the trajectory prediction process, providing means for modelling it. In addition, a formulation for characterising the trajectory uncertainty as a function of the aircraft performance uncertainty is also included in this chapter.

4.2 Aircraft Performance in Trajectory Prediction

The aircraft trajectory prediction relies on the availability of accurate aircraft performance information. According to the mathematical formulation of the AMM, the information required for solving the mathematical system of equations can be sorted into the following categories described below.

- **Aerodynamics.** Those are the forces and moments produced mainly by the wings, fuselage, and tail due to the movement of the aircraft within the surrounding air mass.
- **Propulsion.** Thrust provided by the installed engines and its associated fuel consumption under the considered atmosphere conditions and aircraft state.
- **Operational limitations.** Maximum and minimum values of the aircraft state variables that delimit the flyable conditions under which the aircraft can be safely operated.

Regardless the type of source considered for calculating the aircraft performance at specific flight conditions, uncertainty effects cannot be neglected when computing information about aerodynamics or propulsion.

The performance models also provide information about operational limitations, which are numerical thresholds that establish the boundaries in which the aircraft can safely fly. If

those thresholds are above the actual performance, predictions might be unrealistic. In contrast, there could be real trajectories outside those boundaries if thresholds are set below the actual performance. For instance, there could be aircraft flying at altitudes higher than Maximum Operating Altitude. In any case, from the uncertainty assessment point of view, it is assumed that the predictions are well within the performance envelopes and, therefore, their influence is considered further in the following sections.

4.2.1 Aerodynamics

The two main aerodynamic forces and moments produced by the movement of the aircraft within the air mass are the lift (L) and drag (D), and the longitudinal (M_L) and lateral directional (M_{LD}) moments. Both the forces and the moments are usually referred to as the Wing Fixed System (WFS).

Due to the adopted assumptions that considered the simplification of the point mass model formulation (Section 3.4), the influences of the moments M_L and M_{LD} are not required for predicting an aircraft trajectory. Thus, it is not necessary to model such aerodynamics moments.

4.2.1.1 Lift

The lift force L is produced by the different pressure and flow air speed above and below the airfoil in the direction orthogonal to the airfoil cord. This force is basically opposite the aircraft weight, hence, when the lift compensates the weight force, the aircraft starts to fly.

The lift force is commonly analysed by means of the lift coefficient C_L , which is defined in Equation (3-5) as follows:

$$C_L(\alpha, M, \delta_{HL}, \delta_{SB}, R_e) = \frac{L}{\frac{1}{2} \kappa p_0 \delta M^2 S} \quad (4-1)$$

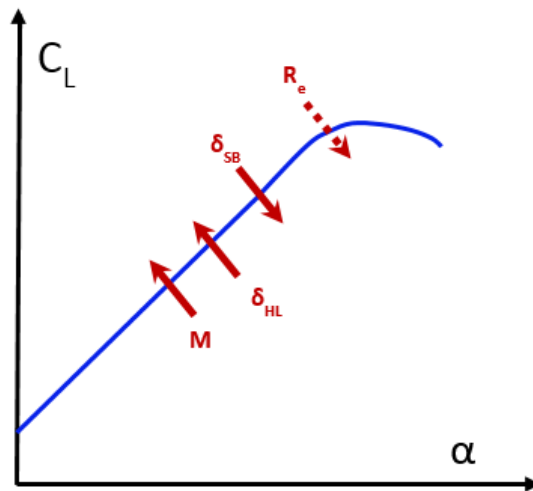


Figure 4-1 – Dependencies of the Lift Coefficient

The behaviour of the C_L depends on the following variables depicted in Figure 4-1:

- Angle of attack (α). The main factor influencing the C_L is the angle of attack, which is the angle between the chord of the airfoil at the wing root and the airflow. For non-symmetric airfoils (which is the case for all commercial aircraft), at zero angle of attack, the airfoil provides a small amount of lift that increases linearly as the angle of attack increases. At high angles of attacks, the airflow starts to separate from the airfoil's upper surface. From this point, the behaviour of the C_L is no longer linear, and therefore, the slope of the lift curve decreases until reaching the maximum value. Beyond this point, the airfoil is said to be stalled. Just before this point, the turbulent flow from the wing strikes the airplane fuselage and horizontal tail, causing a condition called buffet and is characterised by a shaking of the aircraft.
- Mach number (M). Although the lift L itself is strongly affected by the Mach number, the influence of such a parameter on the C_L is not of the same order of magnitude. Higher Mach numbers provide slightly higher C_L curves with almost identical slopes.
- High lift configuration parameter (δ_{HL}). The deployment of the high lift devices is equivalent to considering a larger wing, which is equivalent to having higher C_L curves with almost identical slopes.

- Speed breaks control parameter (δ_{SB}). The speed breaks are used for degrading the aerodynamics features of the wing, producing increased drag. Such degradation implies lower C_L values.
- Reynolds Number (Re). The air viscosity defines where the boundary layer starts to separate from the wing surface according the considered airspeeds. The boundary separates earlier at high airspeeds, which in turn produces lower C_L values.

The C_L mainly determines the aerodynamics forces to be considered for calculating the aircraft motion at each flight condition and establishes certain speed limits in which the aircraft can be operated.

According to the formulation of the AMM posed previously from Equations (3-11) to (3-17), the lift is an input to the system that needs to be known at every aircraft state. This information is not only necessary for integrating the mathematical system of equations, but also for obtaining other basic aerodynamic information such as the aerodynamic drag.

4.2.1.2 Drag

The second aerodynamic force is the drag force D which impedes the movement of the aircraft through the air. This force is a backward longitudinal force acting in opposition to the propulsive force.

The total drag comprises different aerodynamic effects that can be identified within one of the following categories.

- Compressibility drag. At high speeds (sufficiently high Mach numbers), the airflow around the upper airfoil surface may reach locally supersonic values. This produces an oblique shock wave whose effect is increased drag due to the growth of the boundary layer thickness produced by a pressure increase across the shockwave and a loss of the air flow energy.

- Excrescence drag. This is produced by the sum of all elements that impact the smoothness and sealed airframe surface (e.g., antennas, masts, gaps in skin joints or doors, surface roughness).
- Form drag. This is considered part of the pressure drag due to the growth and/or separation of the boundary layer from the airfoil surface.
- Induced drag. This is generated by the pressure difference between the upper and lower wing surfaces. There is airflow circulation around the wing tips from the lower to the upper surface that is added to the total drag.
- Interference drag. The integration of different bodies (e.g., body, wing, or engine) impacts the airflow around the intersection, producing a drag increase. The drag of the bodies together is much higher than the sum of the individual drags.
- Skin friction drag. This effect comes from the viscous shear force produced when the air passes over the aircraft surface. Maintaining the laminar flow over the wing surface as much as possible helps reduce skin friction drag.
- Trim drag. The nose-down effect derived from the aircraft centre of gravity (CG) placed forward of the wing centre of lift is compensated for by a nose-up momentum produced by the horizontal tail. The trim drag represents the drag produced by the deflection of the horizontal stabiliser and elevator required to generate the downward force that creates such nose-up momentum.

There are other elements such as the landing gear, spoilers, or control surfaces whose effects on drag need to be considered as well when they are operative.

Based on those aforementioned effects, total drag can be considered as composed of:

- Pressure drag, caused by the pressure distribution over the three-dimensional surface of the airplane. The compressibility, induced, and trim drags comprise the pressure drag.

- Parasite drag, caused by other effects rather than lift or compressibility. The excrescence, form, interference, and skin friction drags comprise the parasite drag.

The total drag D is usually represented by the drag coefficient (C_D) as defined in Equation (3-4):

$$C_D(M, C_L, \delta_{HL}, \delta_{SB}, \delta_{LG}, R_e) = \frac{D}{\frac{1}{2} \kappa p_0 \delta M^2 S} \quad (4-2)$$

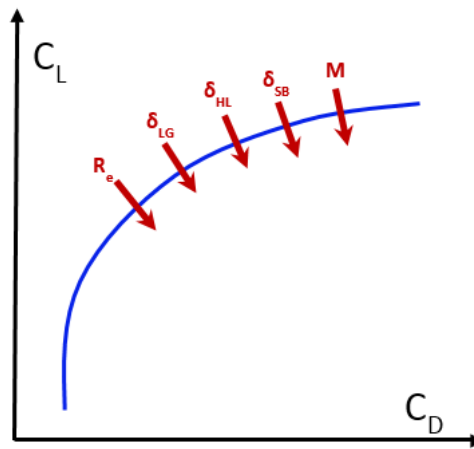


Figure 4-2 – Dependencies of the Drag Polar Curve

The behaviour of the C_D depends on the following variables, as depicted in Figure 4-2.

- Mach Number (M): The curve moves down and right as the Mach number increases, which means that at higher airspeeds the same C_L results into higher C_D . The degradation of the drag polar curve is motivated by the increasing influence of the airflow compressibility effect when M is approaching very high subsonic values.
- Lift coefficient (C_L): The influence of the C_L on the C_D is assumed to be quadratic. Increments of the C_L turn into increments of the C_D , proportional to the square of the former increments. The relationship between both coefficients establishes the optimum drag-to-lift ratio. This ratio is defined by the point where a line from the origin of coordinates is tangent to the drag polar curve (at the considered Mach

number). Operating at the optimum drag-to-lift ratio ensures the maximum aerodynamic efficiency for the given flight conditions.

- High lift configuration parameter (δ_{HL}): These devices are used at low airspeeds to generate additional lift that compensates the aircraft weight at the considered flight conditions. The increment of the lift returns an increase of the drag because of the degradation of the aerodynamics' characteristics. The higher the deflection of the devices, the higher lift, leading therefore to higher C_D values.
- Speed breaks control parameter (δ_{SB}): These devices are used for quickly reducing the aircraft energy by generating an increase of the aerodynamic drag. They break the laminar boundary layer, provoking its separation from the wing surface and, thus, the reduction of the wing performance.
- Landing gear control parameter (δ_{LG}): The deployment of the landing gear worsens the airframe surface smoothness, generating an associated drag increase.
- Reynolds Number (Re): Its influence is almost negligible, especially at low airspeeds.

Contrary to the C_L , which is an input of the mathematical problem, the C_D can be obtained from the aircraft performance datasets once the C_L is known. When no manufacturers' data are available, another alternative is to leverage generalist performance models that provide the required information by approximating the drag polar curve by a mathematical model. This option will be adopted later in this chapter when a model of the aircraft performance uncertainties is proposed.

4.2.2 Propulsion

The force that moves the aircraft forward is the thrust. The thrust is produced by the power plant by means of a combination of combustion, compression, and expansion processes.

In commercial aviation, the power plants are air-breathing in all cases, meaning that the combustion process is created because of an air intake. The process aims at transforming the

internal fuel energy into an increase of the airflow kinetic energy, propelling the power plant in the opposite direction to the exhaust airflow (Newton's third law of motion).

Unlike piston engines that operate on a four-stroke cycle (inlet, compression, combustion, and exhaust), jet engines are designed for continuous operations, using independent chambers for each propulsion process.

Thrust is generated by a momentum¹⁵ increase of the air mass being taken into the power plant, the gas leaving the combustion chamber (notice that outlet mass flow is greater at the exhaust because, in addition to the incoming airflow, there is additional mass coming from the fuel combustion) and the airflow leaving the power plant. This force can be seen as the rate of momentum change of the gas (air plus combustion gases) as it passes through the engine.

The basic variables that affect the thrust generation are:

- Air density. This parameter depends on the atmosphere temperature and pressure. Since thrust is directly proportional to the inlet airflow, higher densities will return higher thrust values due to increased air mass introduced into the engine.
- Airspeed. The influence of the aircraft speed on thrust shows opposite effects:
 - Increases of airspeed imply increases of inlet air pressure, and therefore, greater air densities. This is usually referred to as the ram effect. This effect generates a quadratic thrust increase.
 - The momentum of air mass decreases because the difference between the inlet and outlet air mass speeds is reduced. The thrust provided by the engine decreases linearly due to this effect.

¹⁵ Momentum is defined as a measure of the motion of a body equal to the product of its mass and velocity.

The combination of both effects is depicted in Figure 4-3, where it is shown that the former is more noticeable at high speeds, while the latter is at higher speeds.

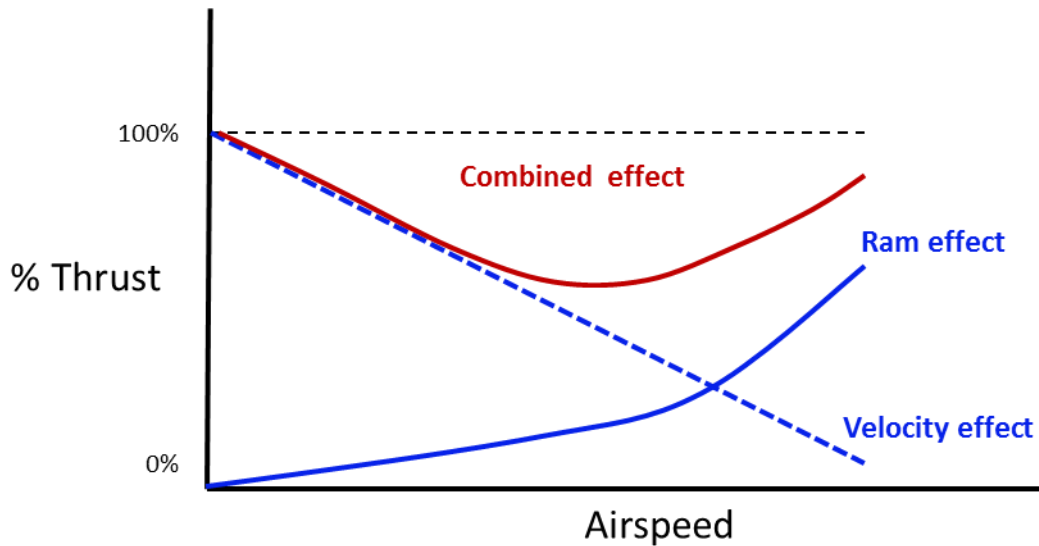


Figure 4-3 – Airspeed Effect on Thrust

At airspeeds usually around 400 kt, the ram effect compensates for loss of thrust due to increased airspeed in the way the negative effect is superseded by the positive influence produced by the high air pressure at the power plant inlet.

- Humidity. The increase of humidity causes a decrease in weight per unit volume of air within the (jet) engines. However, power plants usually operate with an air excess for completely combusting the injected fuel, so that any air weight lacking in the combustion air supply can be compensated. However, a reduction in overall performance is expected in high humidity conditions [90].
- Water injection. This is a method for augmenting the thrust used in multi-engine aircraft. The principle of the method is to inject water into the jet engine (into the compressor inlet in the diffuser section just ahead of the combustion chamber, or directly into the combustion chamber) to allow a higher fuel flow without exceeding the temperature limits of the power plant. This implies a higher mass flow and velocity of the exhaust gases, thereby increasing the thrust [91].

- Installation losses. The energy output by the installed power plant is not only used to generate thrust, but also to provide energy to other subsystems (e.g., hydraulic, air conditioning, electric, anti-icing). All those energy leakages impact negatively on the final thrust generated by the power plant.

As explained above, thrust is produced by the combustion of the fuel. Hence, the fuel flow injected into the combustion chamber is the key parameter that enables the generation of required thrust at each flight condition. For given aircraft weight, flight altitude, and Mach Number, the fuel flow is strongly dependent on the outside air temperature (OAT). It has a twofold effect on the fuel flow rate necessary to reach a certain level of thrust. For temperatures above ISA conditions, the drag needs to be augmented by Reynolds Number corrections. This additional drag needs to be compensated by the thrust from the increased fuel flow. In addition, the fuel flow depends directly on the OAT through the temperature ratio θ^{16} , so then the high temperature values will demand higher fuel flows for providing the same thrust. Approximately, a 3 percent fuel flow increase is necessary for every 10°C increment of temperature.

4.3 Aircraft Performance Modelling in Trajectory Prediction

Accurate aircraft performance data is paramount for efficient flight planning and operations. This information is used from the flight dispatcher during the strategic flight planning, to the FMS for commanding the aircraft during a flight. For instance, performance information is used on ground for calculating the optimal profiles to be flown in accordance with the airline's business requirements (expressed by the cost index [CI] value) and the expected environmental and traffic conditions. On board, the performance information is used for steering the aircraft following the air traffic regulations and restrictions, and respecting as much as possible the filed flight plan and the established CI.

¹⁶ $\theta = (T + 273.15)/(T_0 + 273.15)$ is the ratio of the air temperature at altitude to the standard air temperature at mean sea level $T_0 = 15$ °C.

The most accurate and up-to-date aircraft performance information is only available to the airlines. The aircraft manufacturers provide performance datasets that represent the performance of the airplanes as rolled out from the factory. This information is updated by the airlines as they operate and maintain their fleets.

However, for the majority of the ATM stakeholders (such as the ANSPs that might require performance data for accurately simulating, managing, and optimizing the traffic within an airspace block), there are no options for using manufacturers' or airlines' performance datasets due to the high business sensitivity of that information.

In order to overcome this lack of available inputs, the ATM community extensively uses aircraft performance models that can be utilised for traffic prediction and management or environmental impact analyses. Those models aim at representing the performance of each aircraft by means of mathematical formulations, which return information such as the drag, thrust, or fuel consumption as functions of the flight conditions.

For instance, the Integrated Noise Model (INM) developed by the US Federal Aviation Administration (FAA) instantiates the methods and algorithms exposed in SAE AIR 1845 [92] to predict aircraft noise levels in the vicinity of an airport. This standard proposes mathematical functions for calculating the drag and engine thrust, and subsequently the related noise footprint, based on knowledge of the flight conditions. Those methods and algorithms rely on a set of performance coefficients calculated for each aircraft type based on manufacturers' datasets.

Similarly in Europe, the Aircraft Noise and Performance (ANP) Database published by EUROCONTROL provides mathematical expressions for calculating aircraft performance and related noise impact contours [93] by means of a set of performance coefficients and a model specification.

In both cases, parabolic representations of the drag polar curve are used for determining the aerodynamic forces acting on the aircraft at each flight stage [94].

$$C_D = d_0 + d_1 C_L + d_2 C_L^2 \quad (4-3)$$

where d_i are the performance coefficients obtained by fitting such definition to the manufactures' data.

The thrust is usually described by two polynomials that represent the force provided by an engine at the flat-rated area and at the temperature-rated (or full-rated) area. The intersection of these two areas is established by the kink point (or thrust break temperature), which is the OAT that defines when the pressure in the combustion chamber (p_3) ends to limit the thrust provided by the engine, and the turbine temperature (T_4) starts to limit it (Figure 4-4).

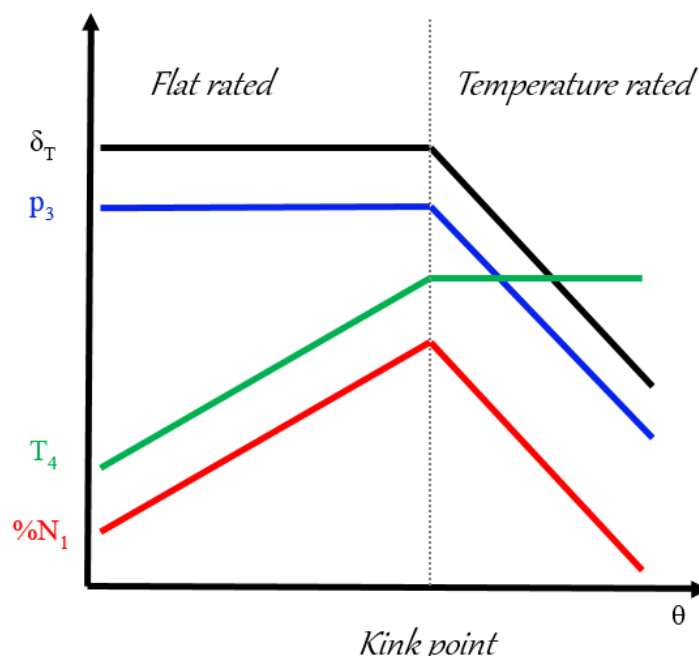


Figure 4-4 – Net Thrust Behaviour

The following Equation (4-4) represents the ANP formulation of the thrust provided by the engine operating at a specified rating.

$$\frac{F_n}{\delta} = a_0 + a_1 CAS + a_2 h + a_3 h^2 + a_4 T \quad (4-4)$$

when the ratio $\frac{F_n}{\delta}$, known as corrected net thrust, is a function of the calibrated airspeed (CAS), the geometric altitude (h), the air temperature (T), and the performance coefficients a_i (which characterise each aircraft type).

When the rotational speed of the engine's low-pressure compressor and turbine stages N_1 is used to set the thrust, the Equation (4-4) becomes

$$\frac{F_n}{\delta} = a'_0 + a'_1 CAS + a'_2 h + a'_3 h^2 + a'_4 T + a'_5 \frac{\%N_1}{\sqrt{\theta}} + a'_4 \left(\frac{\%N_1}{\sqrt{\theta}}\right)^2 \quad (4-5)$$

Regardless of the considered expression, the performance coefficients provided by the performance datasets will be different, depending on the model and the rated area in which the engine is being operated.

4.3.1 BADA Aircraft Performance Models

In support of advanced ATM capabilities and operational applications, EUROCONTROL BADA aircraft performance models provide sophisticated model specifications and datasets that enable highly accurate aircraft trajectories' modelling and simulations [95].

BADA provides an aircraft performance model suitable for ATM applications developed and maintained by EUROCONTROL through active cooperation with aircraft manufacturers. The information and data contained in BADA is designed for use in aircraft trajectory modelling, including simulation and analysis of air traffic operations and non-safety critical DSTs for air traffic control [96]. BADA is broadly considered as the international standard aircraft performance model for ATM applications, providing means for aircraft manufacturers to furnish the ATM community with accurate aircraft performance information in a manner that protects their sensitive proprietary information and within a framework validated and controlled by a neutral international entity.

Currently, there are two different model specifications and datasets that correspond to the BADA 3 and BADA 4 families. Each of those specifications has a list of available datasets comprising the performance coefficients required for instantiating the model for a specific aircraft type. The main differences between them are:

- Accuracy: For nominal operations, it has been proven that there are no relevant differences between the accuracy of the two families. However, for off-nominal conditions (trajectories close to the flight envelope boundaries), the accuracy of

BADA 3 models degrades dramatically while the high accuracy of BADA 4 models is almost not affected [97].

- Model dependencies: To precisely capture the aircraft performance under any flight conditions, the BADA 4 specification includes improvements to the models dependencies. For instance, the drag polar model proposed by BADA 4 includes the Mach number in addition to the lift coefficient C_L , contrary to BADA 3, which only considers the C_L . This means that the compressibility effects on the drag generated at high airspeeds are properly captured with the BADA 4 specification, which is not the case of BADA 3.
- Global fleet applicability: The BADA 3 family covers 90 percent of the current fleet, i.e., EUROCONTROL provides BADA 3 datasets for 90 percent of the aircraft types currently operating within the ECAC area, while BADA 4 family coverage is only 60 percent (including all Boeing and Airbus types). The difference is due to the fact that BADA 4 was released recently in comparison to the first release of BADA 3.

BADA 3 provides aircraft performance information within the nominal part of the flight envelope. Although its accuracy and flexibility are limited, it is considered the basic standard model to support the requirements of trajectory simulation applications addressing current air traffic operations.

Based on the high accuracy provided in all flight conditions, even in the vicinity of the flight envelope, the BADA 4.1 model specification and datasets have been selected as the most appropriate representation of aircraft performance to be used further in the development of this thesis.

4.3.2 Aerodynamic Model

The aerodynamics model is a model that provides information about the drag force D by means of the drag coefficient C_D as defined in Equation (3-4). The C_D is represented as a function of the aircraft configuration. Depending on that, the expression for calculating the C_D varies.

According to the BADA 4.1 specification [98], there are four expressions available for obtaining the C_D :

- Clean configuration for Mach Numbers below the maximum Mach number used for the generation of the performance datasets. The proposed expression considers both the Mach number and the lift coefficient C_L as main dependencies of the model.

$$\begin{aligned}
 C_D = & d_1 + \frac{d_2}{(1 - M^2)^{\frac{1}{2}}} + \frac{d_3}{(1 - M^2)^{\frac{2}{2}}} + \frac{d_4}{(1 - M^2)^{\frac{3}{2}}} + \frac{d_5}{(1 - M^2)^{\frac{4}{2}}} + \\
 & + (d_6 + \frac{d_7}{(1 - M^2)^{\frac{3}{2}}} + \frac{d_8}{(1 - M^2)^{\frac{6}{2}}} + \frac{d_9}{(1 - M^2)^{\frac{9}{2}}} + \frac{d_{10}}{(1 - M^2)^{\frac{12}{2}}}) C_L^2 + \quad (4-6) \\
 & + (d_{11} + \frac{d_{12}}{(1 - M^2)^{\frac{14}{2}}} + \frac{d_{13}}{(1 - M^2)^{\frac{15}{2}}} + \frac{d_{14}}{(1 - M^2)^{\frac{16}{2}}} + \frac{d_{15}}{(1 - M^2)^{\frac{17}{2}}}) C_L^6
 \end{aligned}$$

The expression is based on the Prandtl-Glauert compressibility correction [99], which allows solving compressible flow problems by incompressible-flow calculation methods. As depicted in Figure 4-5, the drag polar curve shows the effect of compressibility at high airspeeds, providing increased drag values for the same lift.

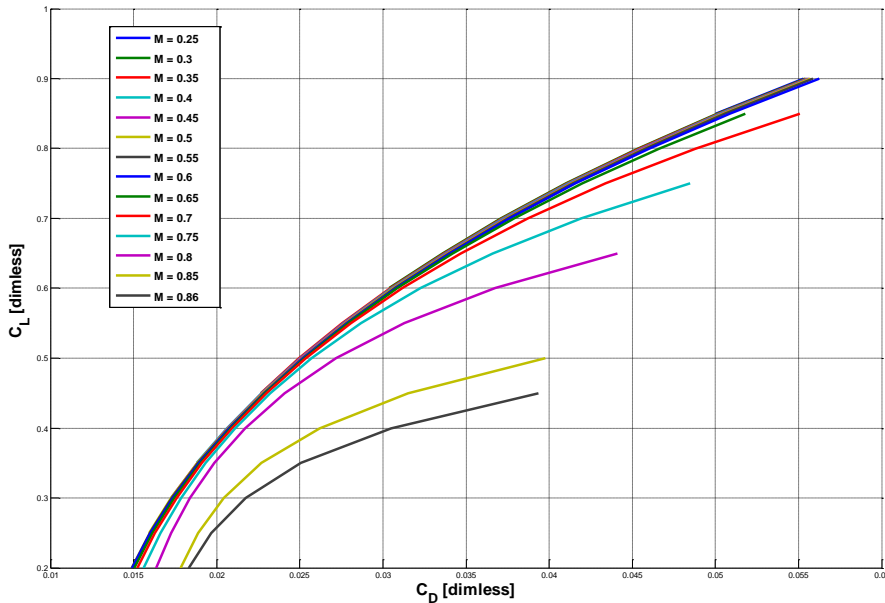


Figure 4-5 – Drag Polar Curve

- Clean configuration for Mach numbers above the maximum Mach number used for the generation of the performance datasets. An extrapolation formula is proposed for all cases in which the Mach number is higher than the values used during the identification of the drag polar coefficients d_i , defined in Equation (4-6).
- Non-clean configurations. Due to the existence of speed and altitude limitations for the use of high lift devices and landing gear, the expression used for describing C_D assumes the classic parabolic representation, ignoring the compressibility effect. This effect is almost negligible at the speeds allowed for the use of high lift devices or landing gear.

$$C_D = d_1^{\delta_{HL}, \delta_{LG}} + d_2^{\delta_{HL}, \delta_{LG}} C_L + d_3^{\delta_{HL}, \delta_{LG}} C_L^2 \quad (4-7)$$

- Transition between configurations. A linear interpolation between the values of C_D at the initial and final configurations is proposed for computing drag during the intermediate stages.

Additionally, the BADA 4.1 specification provides an expression for calculating the drag increment produced by the use of speed breaks. This increment should be summed to the drag coefficient obtained from the above mentioned BADA 4 drag formulations.

The coefficients d_i and $d_i^{\delta_{HL}, \delta_{LG}}$ are obtained from the corresponding BADA 4 performance datasets.

For the purpose of this thesis, only the clean configuration (clean drag polar model) will be taken into consideration because it provides sufficient information about the aerodynamics performance in support of the proposed research. Results obtained from this approach can be easily extrapolated to non-clean configurations.

4.3.3 Propulsion Model

The propulsive thrust can be modelled in accordance with the type of power plant with which the aircraft is equipped. The BADA 4.1 specification distinguishes among three alternatives: turbo fans, turbo props, and piston engines [77].

Regardless the engine type, the dependencies of the thrust model are the amount of fuel injected into the combustion chamber (modelled by the throttle parameter δ_T), the atmosphere conditions and the airspeed (through the Mach Number), as defined by Equation (3-7).

Although there are three separate expressions for obtaining the thrust parameter C_T based on the considered engine types, this thesis will consider exclusively the turbo fan models. Nevertheless, any of the performed analyses can be extrapolated to the case of turbo prop models and, with some additional adjustments, to the piston engine models.

The generalised thrust model provides the thrust coefficient C_T in all circumstances in which the engine is not operating in an idle rating. The throttle parameter can be input directly from the flight deck or can be computed by means of the turbo fan rating models, whenever the engine operates in one of the certified non-idle ratings¹⁷. The following Equation (4-8) determines the value of the C_T as a function of the Mach number and throttle parameter δ_T , where the coefficients a_i are provided by the corresponding BADA 4.1 performance dataset.

$$\begin{aligned}
 C_T = & a_1 + a_2 M + a_3 M^2 + a_4 M^3 + a_5 M^4 + a_6 M^5 + \\
 & + (a_7 + a_8 M + a_9 M^2 + a_{10} M^3 + a_{11} M^4 + a_{12} M^5) \delta_T + \\
 & + (a_{13} + a_{14} M + a_{15} M^2 + a_{16} M^3 + a_{17} M^4 + a_{18} M^5) \delta_T^2 + \\
 & + (a_{19} + a_{20} M + a_{21} M^2 + a_{22} M^3 + a_{23} M^4 + a_{24} M^5) \delta_T^3 + \\
 & + (a_{25} + a_{26} M + a_{27} M^2 + a_{28} M^3 + a_{29} M^4 + a_{30} M^5) \delta_T^4 +
 \end{aligned} \tag{4-8}$$

¹⁷ Maximum Take-Off (MTKF), Maximum Climb (MCMB), Maximum Continuous (MCNT), and Maximum Cruise (MCRZ).

$$+ (a_{31} + a_{32} M + a_{33} M^2 + a_{34} M^3 + a_{35} M^4 + a_{36} M^5) \delta_T^5$$

In the case of idle regimes, the model defined by Equation (4-9) does not depend of the δ_T and its only dependencies are the Mach number and the pressure ratio δ .

$$\begin{aligned} C_{Ti} = & \frac{ti_1}{\delta} + ti_2 + ti_3\delta + ti_4\delta^2 + \\ & + \left(\frac{ti_5}{\delta} + ti_6 + ti_7\delta + ti_8\delta^2 \right) M + \\ & + \left(\frac{ti_9}{\delta} + ti_{10} + ti_{11}\delta + ti_{12}\delta^2 \right) M^2 \end{aligned} \quad (4-9)$$

In addition, for a complete description of power plant performance, the BADA 4.1 specification includes a fuel consumption model for non-idle ratings and another, different model for idle ratings. The former depends on the Mach number and the calculated thrust coefficient C_T as described in Equation (4-10).

$$\begin{aligned} C_F = & f_1 + f_2 C_T + f_3 C_T^2 + f_4 C_T^3 + f_5 C_T^4 + \\ & + (f_6 + f_7 C_T + f_8 C_T^2 + f_9 C_T^3 + f_{10} C_T^4) M + \\ & + (f_{11} + f_{12} C_T + f_{13} C_T^2 + f_{14} C_T^3 + f_{15} C_T^4) M^2 + \\ & + (f_{16} + f_{17} C_T + f_{18} C_T^2 + f_{19} C_T^3 + f_{20} C_T^4) M^3 + \\ & + (f_{21} + f_{22} C_T + f_{23} C_T^2 + f_{24} C_T^3 + f_{25} C_T^4) M^4 \end{aligned} \quad (4-10)$$

The later only depends on the Mach number and pressure ratio δ , similar to the dependencies of the C_T for idle regimes. Equation (4-11) returns the fuel consumption at different airspeeds and atmosphere conditions.

$$\begin{aligned} C_{Fi} = & fi_1 + fi_2 \delta + fi_3 \delta^2 + \\ & + (fi_4 + fi_5 \delta + fi_6 \delta^2) M + \\ & + (fi_7 + fi_8 \delta + fi_9 \delta^2) M^2 \end{aligned} \quad (4-11)$$

The coefficients f_i and f_{i_i} , required for instantiating both fuel consumption models, are all included in the corresponding BADA 4.1 performance datasets.

Figure 4-6 depicts the behaviour of the fuel consumption coefficient C_F with variations of the Mach number and C_T for non-idle engine regimes.

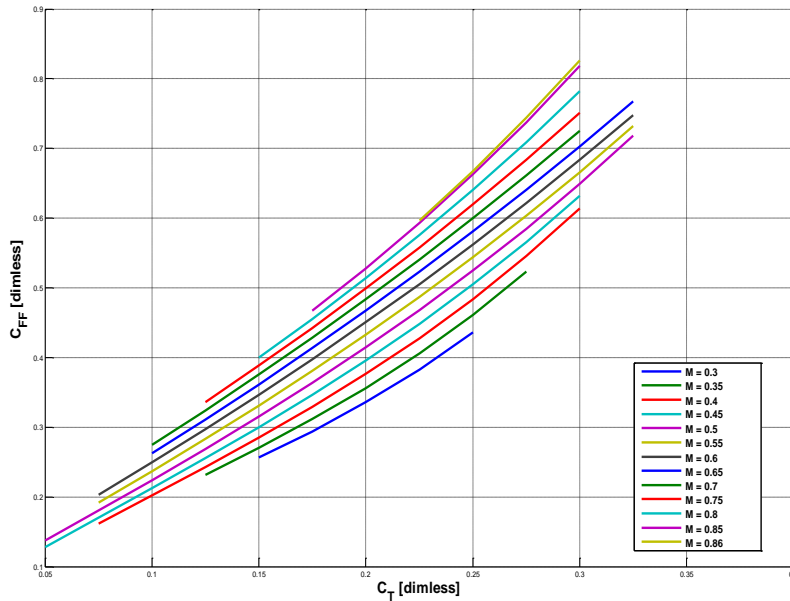


Figure 4-6 – Boeing 767-200 Fuel Consumption Coefficient for Non-Idle Regimes

In the case of idle regimes, Figure 4-7 shows how the fuel consumption coefficient C_F varies with the Mach Number and different pressure altitudes (identified by different pressure ratios).

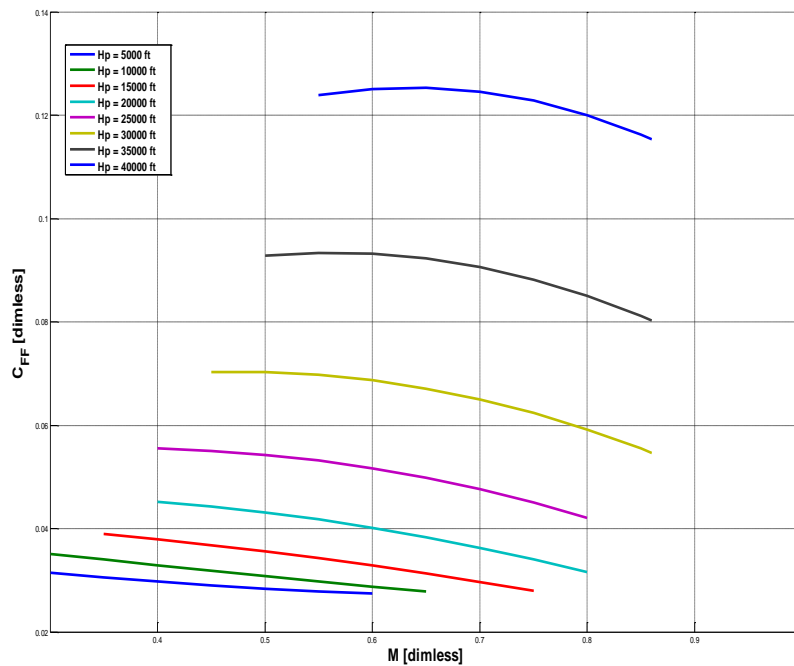


Figure 4-7 – Boeing 767-200 Fuel Consumption Coefficient for Idle Regimes

4.4 Aircraft Performance Modelling Uncertainty

The most accurate representation of the actual aircraft performance is only available to the FMS, which is capable of adjusting the performance information in its databases to better fit the actual performance by taking advantage of the real-time flight data provided by the systems on board. This typically results in a better representation of the actual performance because it takes into account the degradation in performance due to aircraft aging. However, this information is not accessible to other systems, especially those on ground in charge of managing the air traffic.

On the other hand, the use of parametric models entails considering the same performance for all aircraft of the same type, i.e., the average performance characteristics of an aircraft type are assumed for all individual aircraft considered to be of that type. Besides, the average performance captured by a parametric model typically reflects the performance of a brand new aircraft, as it is rolled out of the factory. Such average models are derived from manufacturers' data, without considering the performance degradation that occurs as the aircraft is operated by the airline.

The lack of access to actual performance data for each individual aircraft leads to the incapability of updating the datasets used for instantiating the parametric models. This condition results in an inherent level of uncertainty in the knowledge of the performance characteristics of specific aircraft for which a predicted trajectory is required, regardless of how accurately the average performance of the aircraft type had been modelled. Such uncertainty is produced by the following reasons:

- Accuracy of the models with respect to the performance reference datasets. The fitting process leads to differences between the reference and modelled data, which translates into performance modelling uncertainties
- Inherent variability in performance across individual aircraft of the same type. Aircraft age, maintenance, and operational history leads to different performance deviations with respect to the reference data used for identifying the model

Moreover, aircraft performance depends strongly on atmosphere conditions (e.g., there is a dependency of drag with speed of sound in actual atmosphere conditions through the Mach number). Thus, the uncertainty introduced by the description of atmosphere conditions propagates through to aircraft performance. However, this effect is not intrinsically considered as performance uncertainty, and therefore, it is not discussed in the rest of the chapter.

The actual aircraft performance deterioration endows two main origins, which at the end are considered performance uncertainty sources: engine performance degradation (fuel consumption increase for a given thrust) and aerodynamic deterioration (seals, doors, slats and flaps rigging, spoilers rigging, and the like) [100].

4.4.1 Aerodynamic Modelling Uncertainty

Airframe deterioration is the main cause that affects the aerodynamic characteristics of the aircraft. Deformed aerodynamic surfaces, missing or damaged seals, chipped paint or leaking doors are among most common causes of such deterioration. These spurious effects are rather complex for analytical quantification. Aircraft manufacturers provide some information that can be used for calculating the extra drag to be added to the data included in the performance manuals and datasets. For instance, Airbus reports an extra fuel

consumption of 90 kg in a 2,000-NM trip due to a slat miss-rigging of 15 mm. With this information, the extra drag coefficient to be considered would be approximately 0.06 [101]. Meanwhile, Boeing estimates the impact of areas of roughness surface between 0.93 and 1 m² in an extra fuel burn from 310 to 500 US gallons per year, which is approximately equivalent to a 0.4 percent drag increase [102].

The aerodynamics performance degradation can be expressed by an increase of the C_D which gathers all mentioned effects in a unique term ΔC_D^u . This term is applicable to all configurations and it can be assumed as strictly constant (no dependencies on airspeed or lift).

Leveraging the parametric description of the BADA 4.1 drag polar curve, it is straightforward to obtain a model of the degraded C_D by just adding such a constant term to the Equations (4-6) and (4-7). Thus, the degraded aerodynamics performance can be modelled, as shown in Equation (4-12).

$$C_D = C_D(M, C_L, \delta_{LG}, \delta_{HL}, \delta_{SB}) + \Delta C_D^u \quad (4-12)$$

However, the term ΔC_D^{dgr} varies according to the actual aircraft conditions. Its value cannot be considered for other aircraft even of the same type, and neither for the same aircraft after several operations or maintenance procedures.

The use of recorded flight data may help the process of calculating the actual value of ΔC_D^u . Appendix A proposes a method to derive the correction to the aircraft performance models from recorded flight data.

The BADA 4.1 performance datasets represent the performance of an aircraft at delivery, which can be considered the optimal values as the airframe is in its best condition. Hence, any degradation due to airframe aging can be translated to an increment ($\Delta C_D^u > 0$) of the drag values provided by the models built upon such reference data.

From the aircraft trajectory prediction perspective, updated information about airframe aerodynamic status is not commonly available. The deviations from the nominal values are

thus considered as the aerodynamic uncertainty and, therefore, the coefficient ΔC_D^u a representation of such uncertainty [103].

4.4.2 Propulsion Modelling Uncertainty

The aircraft engine performance is affected by many different factors (e.g., flight cycles, application of derate procedures, air pollution), which lead to a degradation of engine capabilities resulting, for instance, from fan blades leading edge erosion, blended blades, or nacelle air leakages.

Performance deterioration is mainly produced by losses of the rotatory elements (fans and turbines) and, to a lesser extent, of the non-rotatory elements such as the combustion chamber. The effect of the latter is usually negligible compared to the impact of the rotating component wear. This results in a reduction of the adiabatic efficiency, flow capacity, and an increase of the inner pressure that turns into a reduction of thrust provided by the engine and extra fuel consumption.

High fidelity deterioration models [104] differentiate between the diminished aerodynamic capabilities of the compressor rotor and stator airfoils (which limit the rise of total pressure at each stage), and the increased turbine tip clearance (due to rubbing wear and erosion associated with thermal growth during transients) and flow capacity (due to non-elastic deformation of the airfoils at high temperature and pressure loads). These models are used for engine performance monitoring, helping the airlines in the process of planning and executing their own maintenance procedures.

For applications that do not require such levels of sophistication, it is possible to describe an engine deterioration model taking advantage of thrust and fuel consumption models provided by the BADA 4.1 specification.

The degradation of engine performance is directly translated into variations of the engine rotation speed (N1) or the engine pressure ratio (EPR). In similar flight conditions, the engine needs to get additional fuel consumption to compensate for the degradation of its performance and, therefore, for providing the expected thrust [105]. Thus, it is possible to describe engine deterioration by means of an extra fuel consumption coefficient ΔC_F^u as shown in Equation (4-13).

$$C_F = C_F(M, C_T) + \Delta C_F^u \quad (4-13)$$

A similar expression can be posed by describing the fuel consumption model in idle conditions for degraded engines.

$$C_{Fi} = C_{Fi}(M, \delta) + \Delta C_{Fi}^u \quad (4-14)$$

Due to the specific BADA 4.1 coefficients obtained by fitting the model to reference manufacturers' data, it is not possible to determine ΔC_F^u or ΔC_{Fi}^u if no actual flight data are available. Thus, both coefficients can be seen as the representation of the propulsion uncertainty that affects the description of engine performance.

The assumption of modelling the engine degradation through extra fuel consumption considers that the reduction in the rate of climb capabilities is only produced by an increase of the drag.

4.5 Assessment of APM Uncertainty Impact on Prediction

The previous sections expose how aircraft performance uncertainty can be described by means of three separate coefficients that represent the uncertainty of the aerodynamics and propulsion performance. These coefficients can be estimated from the analysis of flight recorded data or by defining assumptions about maximum allowed performance degradation. Once those coefficients are obtained, the performance of any other aircraft of the same type may vary from the nominal values represented by BADA 4.1 datasets (equivalent to the aircraft performance at delivery) to the maximum degraded values represented by performance uncertainty coefficients ΔC_D^u , ΔC_F^u and ΔC_{Fi}^u .

Because recorded flight data are only at the disposal of the airlines or aircraft manufacturers, it is almost impossible to obtain a set of valid performance uncertainty coefficients for all aircraft types. However, due to the lack this type of information in most cases, additional hypotheses about performance degradation need to be established for calculating those performance uncertainty coefficients.

Based on the knowledge of performance uncertainty coefficients, the process of computing trajectory prediction uncertainty can be executed by using the following APMs:

- Nominal APM as provided by BADA 4.1.
- Synthetic APM generated by modifying the drag coefficient model, as described in Equation (4-12).
- Synthetic APM generated by modifying the fuel consumption models, as described in Equations (4-13) and (4-14).
- Synthetic APM generated by modifying the drag coefficient and fuel consumption models, as described in Equations (4-12), (4-13), and (4-14).

These four performance models will be used for computing four trajectory predictions that will determine the uncertainty boundaries. Any possible value of state variables will be contained in a plane defined by values of the considered variable, computed using the four mentioned APMs, and assuming that no additional uncertainty is introduced by other different sources.

Below, the proposed methodology to establish APM uncertainty bounds is demonstrated by means of an example using Monte Carlo simulations. In all studied examples, predicted trajectories consider flight segments at clean configuration with no wind, and neither temperature nor pressure deviations with respect to ISA conditions. The BADA 4.1 APM selected for the validation exercise was the B738W26, corresponding to a Boeing 737-800 equipped with the CFM56-7B26/27 made by CFM International with a thrust force of 26,000 pounds.

The Monte Carlo simulations define a set of stochastically generated models that are fed individually to the aircraft trajectory computation infrastructure proposed in Section 3.2. The stochastic generation of APMs is based on the limit values shown in Table 4-1, which were obtained following the next hypotheses [106]:

- Every 3,000 hours of flight time or 1,000 cycles, new airplanes lose about 1 percent of efficiency according to the nominal values during the cruise phase.

- Fuel burn tends to stabilise at 5 to 7 percent above the performance levels of a new aircraft.
- The influence of engine degradation is much higher (80 percent) than the influence of the aerodynamic degradation (20 percent)

Table 4-1 – Performance Uncertainty Coefficients

ΔC_D^u [dimless]	ΔC_{FF}^u [dimless]	ΔC_{FFi}^u [dimless]
$4.0563508424 \cdot 10^{-5}$	$3.2812823673 \cdot 10^{-2}$	$1.3947047356 \cdot 10^{-3}$

A triangular probability density function (PDF) is used for describing the variability of B738W26 performance between the nominal and maximum degraded values. It is assumed that the performance closer to the former is more probable than performance closer to the latter. Figure 4-8 shows the PDF used for generating the independent coefficient $f_1^+ = f_1 + \Delta C_F^u$, which will be used for instantiating the set of stochastically generated fuel consumption polynomials. Equivalent triangular distribution is used for generating the drag polar independent coefficient $d_1^+ = d_1 + \Delta C_D^u$.

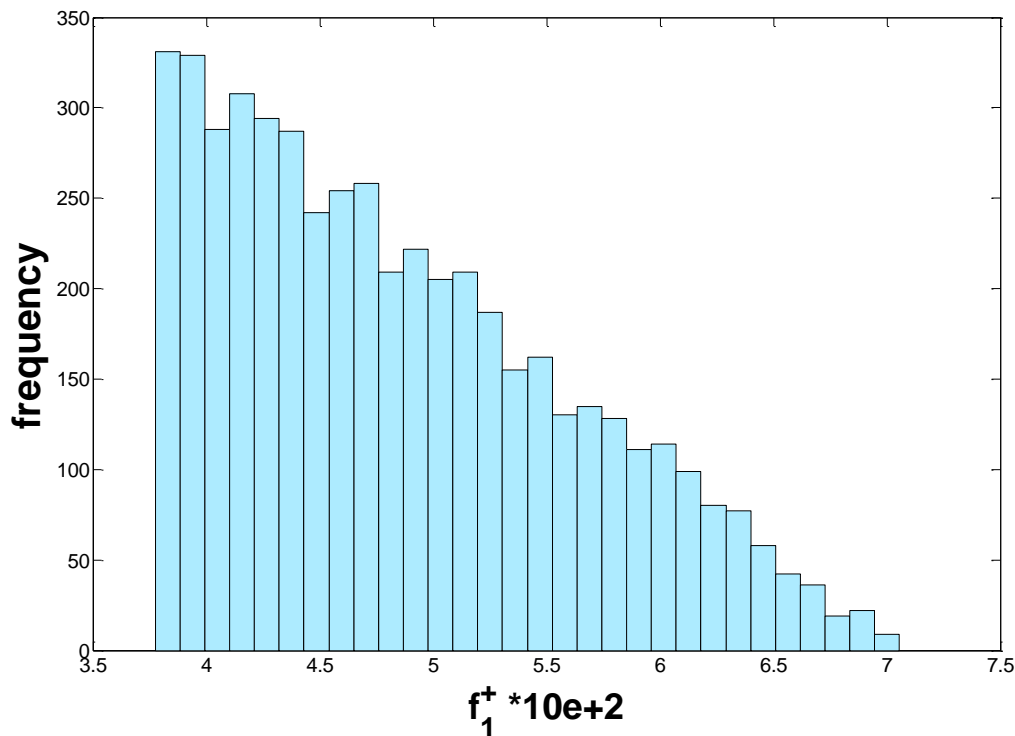


Figure 4-8 – Triangular Distribution of f_1^+

Nevertheless, other distributions could be valid as well for generating a set of probable aircraft performance models. Appendix B includes the outputs obtained with a uniform distribution, which would consider all possible performance as equally probable. The results in terms of trajectory prediction uncertainty are coherent with those obtained in the case of a triangular distribution of APMs.

4.5.1 Cruise

The cruise phase of a flight can be described by a segment at constant Mach speed and a constant pressure altitude along a lateral track. For simulation purposes, the lateral path is defined by a geodesic curve over the ellipsoid WGS84 between two designated waypoints.

Table 4-2 shows the initial conditions considered for predicting the described trajectory segment.

Table 4-2 – Cruise Phase Initial Conditions

Mass [kg]	Mach [dimless]	Hp [ft]
52,000	0.78	30,000

During cruise phases, it is assumed that engine thrust equals aerodynamic drag while the aircraft weight is compensated by the aerodynamic lift force. Hence, considering certain flight conditions, and with no weather variations to take into account, the only variable that supports performance uncertainties is fuel consumption (equivalent to the aircraft mass variation). All other state variables can be considered invariant with respect to the degradation of the aircraft performance.

The distribution of masses at the end of a flight segment of 100 sec of duration, considering the mentioned set of triangularly distributed APMs, is depicted in Figure 4-9 as function of the performance coefficients d_1^+ and f_1^+ . The blue diamond indicates where the mean value is located.

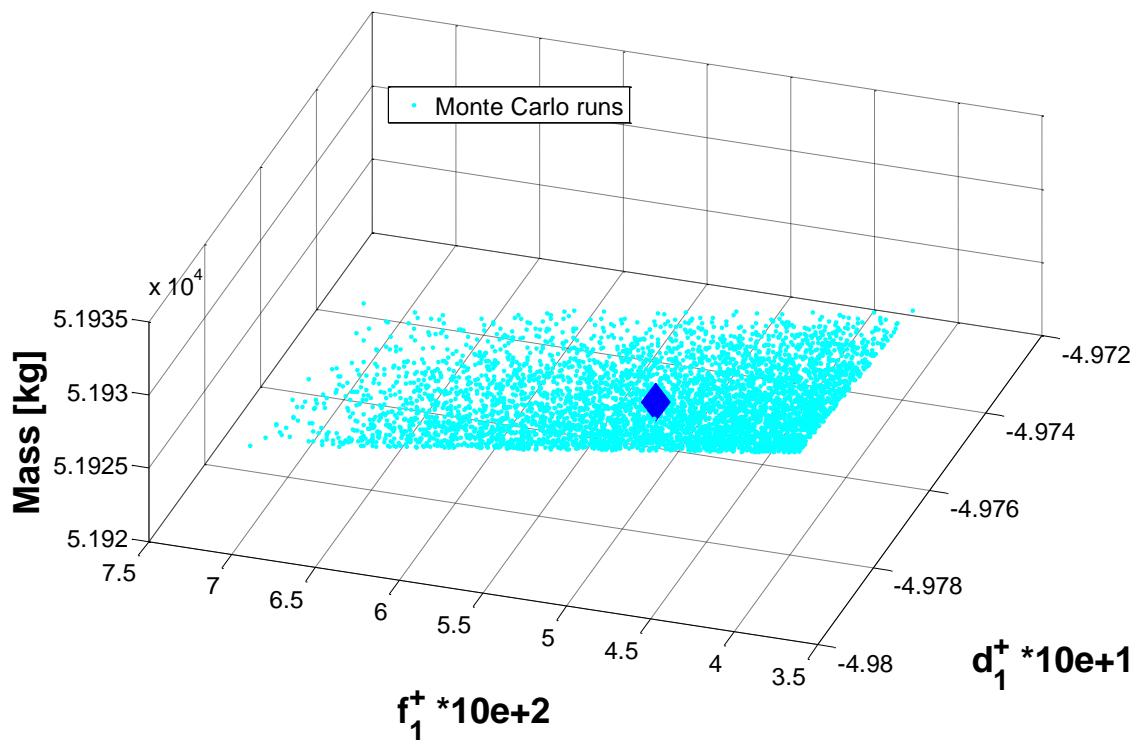


Figure 4-9 – Aircraft Mass Variability (Cruise Case)

Applying linear regression methods, the surface defined by the end masses corresponding to the trajectory computations performed with the set of stochastically generated APMs, is represented by the following expression.

$$mass [kg] = 5.068756 \cdot 10^4 - 2.283870 \cdot 10^3 d_1^+ - 1.614089 \cdot 10^2 f_1^+ \quad (4-15)$$

The root mean square error between the computed aircraft masses and the values calculated by the linear model at the end of the trajectory represents the excellence of fit.

$$RMS_{CRS_case} = 2.2177 \cdot 10^{-9} \quad (4-16)$$

4.5.2 Climb

There are several alternatives for defining a climb segment. For the purpose of analysing the impact of performance uncertainty in the trajectory prediction process, a climb at constant Mach speed and maximum climb rating following a geodesic path between two known waypoints with a target pressure altitude of 35,000ft was studied. Table 4-3 shows the initial conditions of the considered procedure.

Table 4-3 – Climb Phase Initial Conditions

Mass [kg]	Mach [dimless]	Hp [ft]
52,000	0.78	30,000

Different from the cruise case, several state variables are affected by uncertainty introduced by the variability of the aircraft performance model. In addition to the aircraft mass, the most relevant variables from the ATM point of view, influenced by the stochastic variability, are the elapsed time and the flown distance. Figure 4-10 shows the distributions of the elapsed times as function of the performance coefficients d_1^+ and f_1^+ . The blue diamond indicates where the mean value is located.

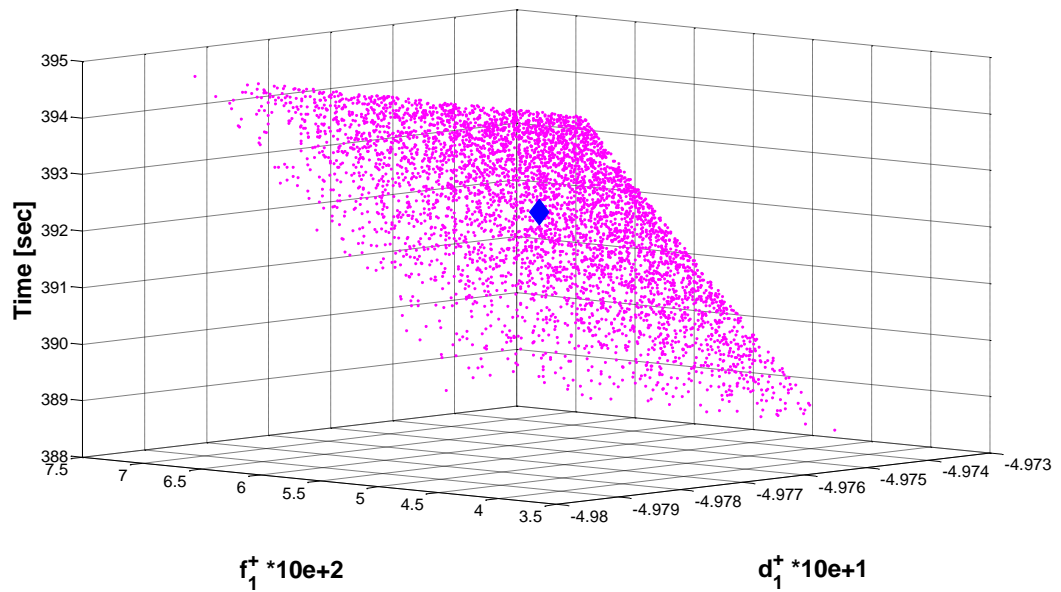


Figure 4-10 – Elapsed Time Variability (Climb Case)

Applying linear regression methods, the surface defined by the elapsed times corresponding to the trajectory computations performed with the set of stochastically generated APMs is represented by the following expression.

$$elpsd_t[sec] = 5.106295 \cdot 10^3 + 9.097844 \cdot 10^3 d_1^+ - 3.959943 \cdot 10^{-1} f_1^+ \quad (4-17)$$

The root means square error between the computed elapsed times and the values calculated by the linear model represents the excellence of fit.

$$RMS_{CMB_case} = 9.5135 \cdot 10^{-8} \quad (4-18)$$

A similar approach can be followed for characterising the distribution of any of the remaining state variables at the end of the considered flight segment.

4.5.3 Descent

Similar to the previous climb case, there are multiple alternatives for defining a descent manoeuvre. In this case, it was assumed a continuous descent at low idle regime at constant

Mach speed along a geodesic between two known waypoints during an interval of 150 sec. Table 4-4 shows the initial conditions of the considered procedure.

Table 4-4 – Descent Phase Initial Conditions

Mass [kg]	Mach [dimless]	Hp [ft]
52,000	0.78	35,000

The condition of computing a segment of 150 sec implies that uncertainty is supported by the final altitude, contrary to the climb case whose final altitude was established as a target condition. Figure 4-11 depicts the distribution of calibrated airspeed (CAS) at the end of the descent for the considered set of APMs. The red diamond indicates where the mean value is located.

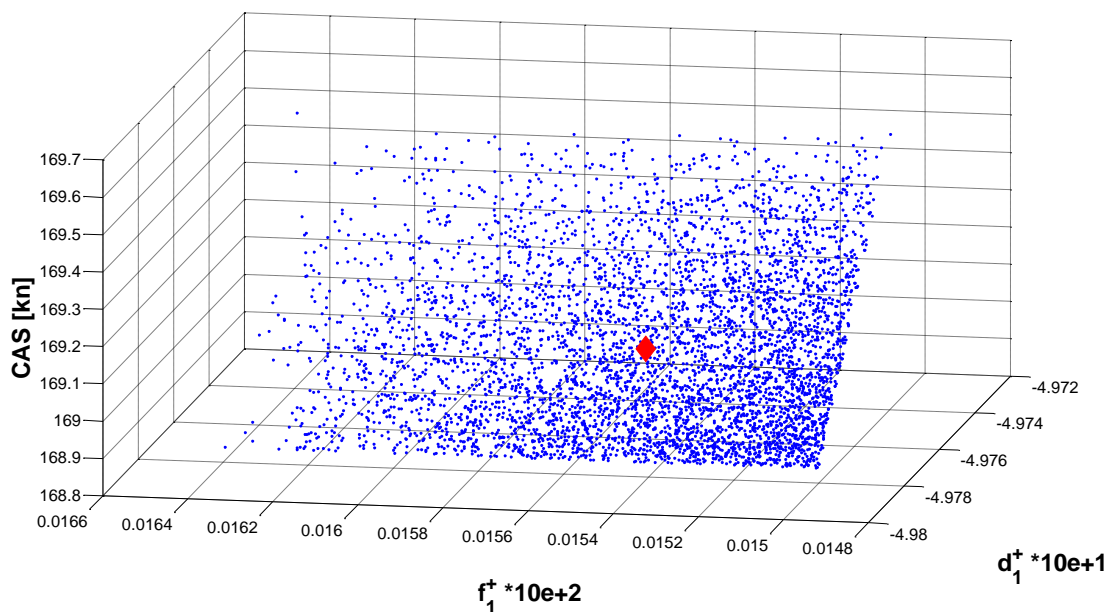


Figure 4-11 – CAS Variability (Descent Case)

Applying linear regression methods, the surface defined by the calibrated airspeeds corresponding to the trajectory computations performed with the set of stochastically generated APMs is represented by the following expression.

$$cas = 1.09776183 \cdot 10^3 + 1.70265964 \cdot 10^3 d_1^+ + 3.14557944 \cdot 10^{-1} f_{1i}^+ \quad (4-19)$$

The root means square error between the computed calibrated airspeeds and the values calculated by the linear model at the end of the trajectory represents the excellence of the fit.

$$RMS_{DES_case} = 5.8623 \cdot 10^{-10} \quad (4-20)$$

Similar to the previous study case, it is possible to apply this methodology to estimate the distribution of any state variable at the end of the predicted segment as function of the variation of drag and fuel consumption parameters.

4.6 Trajectory Prediction Uncertainty Model due to APM Uncertainty

Section 4.5 provided an assessment of the influence of aircraft performance uncertainty on trajectory prediction and exposed the relationship between distribution of the degradation models (drag and fuel consumption) and the aircraft state variables. Based on these results, the trajectory prediction uncertainty can be modelled as a function of the standard deviation of the probabilistic distributions that affect it.

It is assumed that degradation of the aerodynamic drag and increase of fuel consumption due to engine degradation are independent random variables. Hence, the probabilistic distribution of the aircraft state variables at the end of the predicted flight segment will be driven by the probabilistic characteristics (mean and standard deviation) of those two variables. According to this, the trajectory uncertainty represented by the standard deviation of the state variables can be expressed as follows in Equation (4-21) for those non-idle procedures

$$\sigma_{stv} = \sqrt{a^2 \sigma_{a_1^+}^2 + b^2 \sigma_{f_1^+}^2} \quad (4-21)$$

and by Equation (4-22) for idle procedures.

$$\sigma_{stv} = \sqrt{a^2 \sigma_{d_1^+}^2 + c^2 \sigma_{f_{1i}^+}^2} \quad (4-22)$$

Where σ_{stv} refers to the uncertainty of any state variable, $\sigma_{d_1^+}$, $\sigma_{f_i^+}$ and $\sigma_{f_{1i}^+}$ to the standard deviations of the drag and fuel consumption (non-idle and idle) model independent coefficients, and the coefficients a , b , c to those obtained previously as a result of linear regression fitting applied to the Monte Carlo simulation outputs.

Table 4-5 verifies this formulation comparing the standard deviation of the posterior state variable distributions of the Monte Carlo simulations presented in previous sections, with the values obtained following the proposed approach.

Table 4-5 –Prediction Uncertainty Due to APM Uncertainty

CASE	State Variable	σ_{MC}	σ_{Model}
CRUISE	mass	1.2901[kg]	1.2902[kg]
CLIMB	elapse time	0.0232[sec]	0.0232[sec]
DESCENT	CAS	1.0031[mps]	1.0027[mps]

The comparison between results obtained by Monte Carlo simulations and the ones obtained by the proposed model shows no differences. Hence, it can be concluded that the uncertainty model captures adequately the variability of the state variables due to the effect of the APM uncertainty.

4.7 Summary

This chapter analysed the aircraft performance information required to predict a trajectory using the formulation proposed in Section 3.4, and explored how to model the uncertainty related to the models used for representing the variability of aircraft performance. Such variability is generated by deviations of the aerodynamic characteristic of the airframe and engine capabilities with respect to nominal performance.

Aerodynamic performance entails the description of the lift and drag forces (or the respective C_L and C_D coefficients). The lift force is mainly produced by the different air pressure between the upper and lower wing surfaces. The lift is orthogonal to the airflow and basically

compensates the weight force. The drag represents the friction of the airflow on the airframe, which makes movement of the aircraft difficult. This force is parallel to the airflow and needs to be compensated by the thrust force provided by the engines.

Propulsion performance is described by those characteristics of the engine that define how thrust force is generated according to the flight requirements at the expense of burning fuel. The thrust is a force derived from the increase of the air mass momentum by means of combined processes of compression, combustion, and expansion. This force acts against the aerodynamic drag force propelling the aircraft forward. The energy required for producing such force is provided by the internal energy of the fuel injected into the combustion chamber. The fuel coefficient represents the quantity of fuel per unit of time required for providing certain levels of thrust under the considered flight conditions.

The most accurate representations for both the aerodynamic and propulsion performances are available in the manufacturers' performance datasets and manuals. However, this information is only accessible to the airlines and, therefore, is not typically available for ATM applications. An alternative to such data sources is the use of generalist performance models that represent the required inputs by means of mathematical expressions. These are approximations that fit the proposed formulation of each performance variable to a set of reference data. The most accurate and widely used by the ATM community models are the BADA 4.1 models released by EUROCONTROL.

The BADA 4.1 models comprise a model specification and the datasets corresponding to each aircraft type. The specification establishes the dependencies of the different performance parameters (e.g., the drag coefficient as a function of the aircraft configuration, the lift coefficient, and the Mach number), while the datasets provide the coefficients (obtained by fitting the models to manufacturers' reference data) required for instantiating the model of a specific aircraft type.

Based on the BADA 4.1 specification, a method for introducing the uncertainty to the performance models used in trajectory prediction has been proposed. The method relies on the definition of three performance uncertainty coefficients that are added to the drag polar model and to the fuel consumption models in no-idle and idle conditions. Those coefficients

represent deviations regarding the nominal BADA 4.1 datasets due to the aircraft performance degradation with time. The datasets released by EUROCONTROL represent the performance of an aircraft as delivered to the customer. Thus, the influence in performance of the number of operations, flight hours, or environmental conditions is not taken into account. These effects add uncertainty to the trajectory prediction process that can be emulated by the use of proposed performance uncertainty coefficients. Assuming some hypotheses about the aircraft performance aging leads to definition of the performance limits that determine the maximum performance degradation. It is supposed that in the case of aircraft operating beyond this performance limit, expedited maintenance would be required to regain the lost performance.

Given the description of performance uncertainties, a study of their impact on trajectory prediction uncertainty has been presented. The analysis considers three separate flight phases (cruise, climb, and descent at clean configuration) and assumes a triangular distribution of the aircraft performance between the nominal and maximum degraded values.

As discussed above in this chapter, the variability of the state variables at the end of the considered flight segment is contained in a plane surface defined by the values of that state variable computed with the designated four APMs (nominal plus three degraded models as discussed in Section 4.5). The state variables final values are distributed in the defined surface according to the selected distribution of the APMs. Appendix B provides the results obtained from a uniform PDF. The surface defined by fitting the computation outputs is the same as that calculated for the triangular distribution. Hence, independent of the hypotheses considered for modelling the distributions of degraded aircraft performance models, the trajectory uncertainty is limited by the computed trajectories obtained with the set of four intentionally designed APMs.

The uncertainty of the state variables is determined by the standard deviation of distribution that represents their variability. Based on the above, it is possible to analytically calculate such uncertainty as a function of the standard deviation of distributions that characterise the variability of the independent coefficients of drag and fuel consumption models.

CHAPTER 5

IMPACT OF WEATHER UNCERTAINTY ON TRAJECTORY PREDICTION

5.1 Introduction

Weather forecasting is the capability of predicting the status of the Earth's atmosphere at any given location based on physical models that analytically describe their evolutions from an initial state to a later state, over the course of time.

The atmosphere is considered as a compressible fluid, and therefore, any state can be calculated applying the thermodynamics and fluid dynamics equations with the addition of Coriolis and gravitational forces. Since the vertical dimension of the atmosphere is much smaller than the horizontal one (i.e., the height of the atmosphere is orders of magnitude smaller compared to the Earth's radius), it has been proven that the large-scale atmosphere satisfies the quasi-static equilibrium equation that provides the relationship between the atmosphere pressure P and density ρ .

$$\frac{\partial P}{\partial h} = -\rho g \quad (5-1)$$

Based on that assumption, the physics and dynamics of the atmosphere are mathematically formulated by the so-called Primitive Equations (PE), which describe the atmosphere motion and states by a system of nonlinear differential equations. PEs are also known as predictive equations of the following balance equations [107]:

- Continuity equation: Representing the conservation of mass applied to the air and water constituent parts of the atmosphere.

- Conservation of momentum: Consisting of a form of the 3D Navier–Stokes equations that describe the hydrodynamic airflow on the Earth’s surface under the assumption that vertical motion is much smaller than horizontal motion (hydrostasis) and that the fluid layer depth is small compared to the radius of the Earth.
- First law of thermodynamics: Relating the overall temperature of the system to heat flux per unit density, including solar heating, the albedo of the Earth, and molecular heating.
- Equation of state: Relationship among atmosphere state variables that describes the properties of the atmosphere (typically, the ideal gas law).

Additional transport equations for pollutants and other aerosols are included in the PE system for high-resolution models.

The numerical integration of this mathematical system of nonlinear partial differential equations relies on an initialisation process that generates a valid set of initial conditions from observed data gathered through different sources such as ground weather stations, radiosondes, meteorological radars, weather satellites, and aircraft sensors. The heterogeneity and diversity of these data sources impose a prior data assimilation process to assess the quality of data and to select a qualified subset that ensures a proper initialisation of the atmospheric model.

The system of equations only returns an analytical solution for some simplified cases. Thus, numerical methods need to be applied to obtain approximate outputs. Numerical Weather Predictions (NWP) approximate the atmosphere by using a 3D grid that covers the region of interest and provides values for the weather variables at each node of the grid at discrete times [108]. Global models (models of the whole atmosphere) usually exploit larger grid sizes [109], while regional and local models (models tailored to specific geographic regions) use shorter grid sizes because of the amount of data to be generated and because the forecast look-ahead times are orders of magnitude smaller than in global models [110].

Regardless of the numerical approach selected for computing a weather prediction [111] [112] [113], the basic information contained in a forecast includes the time evolution of the atmosphere pressure (P), density (ρ), temperature (T), and height, in addition to the wind components, vapour contents, and hydrometeors (e.g., rain, snow, cloud ice content). Other

subgrid-scale (unresolved by the model's resolution) meteorological processes, such as radiation, vertical turbulence, convection or clouds, may be provided as well. However, since they are not direct outputs computed by the numerical methods, a parameterisation procedure of the atmosphere model is required. For instance, cumulus cloud formation is a phenomenon of about 1 km in size, which is not properly captured by global models because of the larger grid edge [114]. Thus, explicit equations that relate the cloud water, ice, and cloud cover with atmosphere state variables are used for predicting the cloud formation.

This chapter is devoted to analysis of the influence of weather uncertainties on aircraft trajectory prediction.

After this introductory section, the main weather variables (wind, temperature, and pressure) required for trajectory prediction are presented, with a special focus on their influences on aircraft dynamics, aircraft performance, and speed and altitude transformations.

Next, an analysis of mechanisms for characterising weather uncertainties is discussed. The concept of forecast ensemble and the generation of time-lagged ensembles of ensembles are detailed for their relevance in the weather uncertainty characterisation, and their influence in the process of trajectory uncertainty characterisation.

This chapter proposes the use of forecast ensembles to evaluate the trajectory uncertainties introduced by weather variability based on the use of two consecutive weather forecast ensembles.

Finally, an assessment of trajectory prediction sensitivity to weather uncertainties is presented. Statistical analyses of relevant aircraft state variables at selected times illustrate how to obtain quantifications of the trajectory uncertainty as a result of the propagation of the weather uncertainties

5.2 Weather Data in Trajectory Prediction

Atmospheric conditions play a significant role in aviation because they constrain the aircraft flying capabilities. Not only may operational procedures be limited by exceptionally low ceilings, severe turbulences produced in thunderstorms, or the high likelihood of lightning

strikes, but also actual aircraft performance is dependent on the atmosphere temperature, pressure, and wind.

Meteorological information is critical to Trajectory Management. Weather forecasts are pivotal to enable precise trajectory prediction and efficient traffic flow optimisation from strategic trajectory negotiation and agreement, to tactical execution.

In addition to the evolution of atmosphere conditions (pressure, temperature, density, and wind) with time, weather forecasts also provide timely information on weather hazards, crucial to ensure operational safety and optimal airspace usage. Those hazards identify airspace volumes to be avoided during the flight. Their impact on trajectory prediction can be considered equivalent to imposing lateral and vertical restrictions to the planned trajectory.

5.2.1 Aircraft Dynamics

The influence of the atmospheric conditions on trajectory prediction can be clearly studied by analysing the system of equations that describe the aircraft motion (Equations [(3-11) to [(3-17)]. As stated in 3.4, aerodynamic, propulsive, and gravitational forces are referenced to the WFS, while the position of the aircraft centre of gravity is referenced to the GRS. This means that the aircraft movement is calculated in reference to the surrounding air mass, while the aircraft movement referenced to the ground is obtained considering the movement of the air mass in reference to the GRS by means of the wind.

The three components of the wind vector (w_1^{WFS} , w_2^{WFS} , w_3^{WFS}) affect the dynamic of the aircraft through their derivatives with time, according to Equations (3-11), (3-12) and, (3-13), while their effect on the motion of the aircraft centre of gravity with respect to the ground is considered through the navigation equations (3-15), (3-16), and, (3-17). The former effect reflects the influence of wind variations in the aircraft movement with respect to the surrounding air mass, while the latter affects the computation of the aircraft ground speed.

5.2.2 Aircraft Performance

Aerodynamic, propulsive, and gravitational forces are required for determining aircraft movement. The models used for representing these forces, in addition to the fuel consumption (3-14), show a dependency on atmosphere conditions, as described below.

- Pressure. Aerodynamic forces depend explicitly on atmosphere pressure as described by Equations (3-4) and (3-5). The propulsive force shows an explicit dependency with pressure in the definition of the thrust force F_n (3-7), and an implicit dependency in the description of the thrust coefficient C_T in the case of modelling a certified engine rating (3-8) through the description of the throttle coefficient δ_T . The throttle coefficient model that characterises each of the possible ratings shows an explicit dependency with atmosphere pressure for temperatures below¹⁸ the kink point (Figure 4-4). The fuel consumption also presents an explicit dependency as shown in Equation (3-9) and an implicit dependency through the definition of the C_T .
- Temperature. Propulsive force presents an implicit dependency with the atmosphere temperature through the rating engine models. If the thrust is defined setting the throttle coefficient δ_T , such dependency is null. It only appears when the throttle coefficient δ_T is modelled through one of the certified engine ratings, which show an explicit dependency with the temperature in the case of atmosphere temperatures higher than the kink point. In any other different case, the propulsive force does not depend on the atmosphere temperature. Its impact is also noticeable in the fuel consumption calculation, because the temperature is explicitly used in Equation (3-9).

5.2.3 Aircraft Speeds Transformations

The atmosphere conditions not only affect the aircraft performance as explained above, they are also used to calculate aircraft speeds based on the true airspeed, which is the state variable used in the formulation of the AMM. True airspeed is usually translated into other more operational aircraft speeds such as Mach number, calibrated airspeed, or estimated airspeed. These aircraft speeds are interrelated by Equations (3-26), (3-27), and (3-28), which show dependencies with the atmosphere speed of sound, pressure, and density. The dependency with temperature is implicit through the definition of the speed of sound in actual atmosphere

¹⁸ Current BADA 4.1 release only considers the dependency with pressure for the flat rated rating models. It is expected that in next BADA 4.2 release such dependency will be considered in the temperature rated rating models as well. This approach will provide higher accuracy for the complete flight envelope.

conditions as per Equation (3-23) and the ideal gas law that relates pressure, temperature, and density.

5.2.4 Altitude Transformations

In aviation, aircraft altitude is measured by the altimeter, which provides information about the actual air pressure. This pressure determines a geopotential pressure altitude or flight level (FL) referenced to the standard pressure, as opposed to the geodetic altitude referenced to the MSL. To obtain the geodetic altitude from altimeter pressure measurements, the altimeter must be recalibrated according to the local pressure and must consider its evolution with time and location¹⁹. This recalibration may lead to discrepancies between the geodetic altitudes obtained by neighbouring aircraft flying at the same FL, thereby jeopardising safety because aircraft might be flying at same altitude with disparate reported geodetic altitude due to erroneous or non-updated altimeter recalibrations. Thus, navigation is performed through pressure levels as reported straightforwardly by the altimeter regardless of the local MSL pressure, which is only required for obtaining the geodetic altitude. This approach is not valid during operations close to the ground where the geodetic altitude is necessary to ensure obstacle avoidance and an appropriate plan for descent, final approach, and landing procedures.

The correlation between geopotential pressure altitude H_p and geodetic altitude h is driven by the atmosphere conditions. The relationship can be expressed by means of an intermediate altitude defined as the geopotential altitude H by the following expression:

$$-f dh = -g_0 dH \quad (5-2)$$

where g_0 is the standard value of the constant gravitational acceleration and f is the geopotential acceleration that considers, simultaneously, both the gravitational and centrifugal accelerations. According to the expressions used for modelling the gravitational and centrifugal accelerations and the selected Earth model, the Equation (5-2) may range from a simple expression $h = H$ in the case of constant gravitational and null centrifugal

¹⁹ The altimeters are typically recalibrated by means of the QNH correction, which represents the barometric pressure adjusted to MSL, or the QFE correction, which adjusts the pressure to the local aerodrome elevation.

accelerations and spherical Earth, to a complex relation $h = f(\lambda, \phi, H)$ that relates both altitudes with the horizontal coordinates of the aircraft position in reference to the GRS (longitude and latitude) in the case of geoidal gravity, true centrifugal acceleration, and ellipsoidal Earth model.

Considering the quasi-static equilibrium of the atmosphere in the vertical direction (normal to the Earth surface) and the ideal gas law, the Equation (5-1) can be combined with Equation (5-2) as follows:

$$dP = -\rho f dh = -\rho g_0 dH = -\frac{P}{RT} g_0 dH \quad (5-3)$$

In the case of the standard atmosphere conditions (ISA conditions), the temperature T is equivalent to the temperature of the standard atmosphere T_{ISA} and the geopotential altitude H becomes the geopotential pressure altitude H_p .

$$dP = -\frac{P}{RT_{ISA}} g_0 dH_p \quad (5-4)$$

By combining Equations (5-3) and (5-4), it is possible to obtain the relationship between the geopotential and geopotential pressure altitudes,

$$\frac{dH}{dH_p} = \frac{T}{T_{ISA}} \quad (5-5)$$

which shows the ratio between altitude increments is equivalent to the ratio between the atmosphere temperature and the temperature of the standard atmosphere at the same point.

The expression that relates the geodetic and geopotential pressure altitudes is obtained as a result of introducing Equation (5-2) in Equation (5-5).

$$dh = \frac{T}{T_{ISA}} \frac{g_0}{f} dH_p \quad (5-6)$$

The description of the gravitational and centrifugal accelerations determine how to obtain one altitude from the other as a function of the temperature difference between the actual and ISA temperatures (T and T_{ISA} respectively).

Because of Equation (5-6), the forecast of atmosphere conditions significantly affects the transformation between altitudes and thus, affects trajectory predictions, especially in the computation of the vertical profile.

5.2.4.1 Tropopause

The tropopause is the separation between two different atmospheric layers: the troposphere, which is located below it, and the stratosphere, which is located above it. Its altitude H_{P_trop} is constant when expressed in terms of geopotential pressure altitude.

$$H_{P_trop} = 11,000 \text{ m} \quad (5-7)$$

The evolution of the atmosphere temperature is different up to and from the tropopause. This is why the definition of the transition between the aforementioned layers becomes crucial. Within the troposphere, temperature decreases with altitude as follows

$$dT = \beta_T dH_P \quad (5-8)$$

where β_T is equal to $-6.5 \cdot 10^{-3}$ K/m. Above the tropopause, the temperature is maintained constant, with no variability with altitude

$$dT = 0 \quad (5-9)$$

The highest flight efficiency is obtained at altitude proximate to the tropopause, while most meteorological hazards are circumscribed to the troposphere. For instance, the Polar jet stream in the North Atlantic, caused by the temperature gradient between the cold polar and warmer subtropical air masses occurs at or below the tropopause.

Considering the actual atmosphere conditions, the tropopause geopotential altitude will vary according to Equation (5-5).

5.3 Weather Forecast Uncertainty

The uncertainty of the weather predictions can be considered equivalent to the accuracy of the NWP's with respect to the actual weather conditions. As exposed above in Section 5.1, the most sophisticated weather models make use of assimilation techniques to introduce actual data in the initialisation of the models. This process adds fidelity to the predictions thanks to the consideration of real weather data. The intrinsic stochastic behaviour of the weather and the assumptions and hypotheses used for building the models unavoidable lead to deviations between the forecasted and actual states of the atmosphere.

Atmosphere conditions measured by onboard aircraft sensors are a paramount source of data used to initialise the NWP's. This information, which primarily encompasses actual winds and temperatures, may be accessible through the ACARS datalink [115]. In 2002, ACARS was added to the NOAA Observing System Architecture (NOSA) [116]. Since then, commercial aircraft act as weather data providers sending meteorological observations to be exploited in NWP's. The meteorological information contained in ACARS messages, in addition to other data sets coming from different data providers, are available through the Meteorological Assimilation Data Ingest System (MADIS)²⁰. The weather information sent using ACARS includes the aircraft position and time stamp in approximately 1-minute intervals. In general, the weather data is provided at arbitrary locations because aircraft usually fly fixed routes at defined flight levels in cruise or predefined Standard Instrument Departure (SID) or Standard Terminal Arrival Route (STAR) procedures for departures and arrivals. The information is only available at those spatial locations and times that are actually visited by any aircraft.

Contrary to the ACARS messages, which provide weather data almost in real time, there is an offline option of gathering actual weather information from aircraft recorded on flight. Flight Data Recorder (FDR) exports include, in addition to the aircraft location, heading and speed, information about wind speed and direction, and temperature.

²⁰ MADIS is a meteorological observational database and data delivery system that provides observations that cover the entire globe.

Regardless of the source of measured weather data, the comparison between actual and predicted weather conditions determines the accuracy, as well as the uncertainty, of the models. Depending on the weather model selected, the geographical area and time frame, deviations will vary. For instance, the distribution of wind speed deviations between the NOAA Rapid Update Cycle 60 km (RUC-1) weather forecast error of 6.14 m/s for a set of 1-year flights, when the Meteorological Data Collection and Reporting System (MDCRS)²¹ corrections are considered. These corrections to the RUC using near real-time MDCRS inputs improve the average error to 3.5 m/s [117].

In the case of temperature, the standard deviation of the errors, even in the most accurate forecasts, is approximately 2 K [118]. This deviation is usually considered independent of the time for a given aircraft and uncorrelated with the errors estimated by means of the information provided by other aircraft.

If the number of available weather data measurements is sufficiently high to the geographical area and time frame of interest, the assimilation techniques used for initialising the weather models may lead to short-term forecast (known as *nowcasts*) with standard deviations of wind errors less than 5 kt and temperature errors less than 1 K [120].

The uncertainty of the predictions, represented by those identified deviations, can be used for generating realistic weather profiles to be exploited in trajectory computation. For example, wind profiles can be defined by a deterministic wind components (forecast) and a stochastic component (forecast error), assuming that the stochastic component can be represented by a Gaussian distribution. The main consideration to take into account is the spatio-temporal correlation among wind speeds at proximate locations and times. Uncorrelated wind perturbation may lead to incoherent wind fields that exhibit physically infeasible behaviours (e.g., simultaneous head and tail winds at successive times, or completely different winds for trailing flights with respect to leading aircraft). This process requires comparing the actual and modelled data at several locations and times, generating

²¹ MDCRS collects ACARS reports, converts aircraft observations to the Binary Universal Form for Representation of Meteorological Data (BUFR) format, and disseminates and stores them [119].

a covariance matrix that represents the expected wind error correlation, and hence, the wind uncertainty [121].

The main drawback of this approach is that the weather uncertainty cannot be calculated for the complete airspace. Only uncertainty data related to those points for which measured data are available (e.g., points actually flown through by aircraft) can be computed. Moreover, the distribution of weather inputs provided by aircraft will be biased because the majority of reporting points will be at cruise altitudes, where aircraft fly most of the time. Climb and descent procedures are shorter and at lower altitudes, which imply that the available data will be scarce compared to those provided in cruise. The effect is even more noticeable because at high altitude, wind speeds are higher, and therefore, deviations and standard deviations of error are generally greater.

For obtaining more generic uncertainty quantifications that cover any location and future time, some weather forecast providers create a set of forecast ensembles. Ensembles represent the forecasts obtained by stochastically perturbing the model initialisation process. Due to the chaotic nature of the weather system, small differences in the initial conditions may produce significant discrepancies in time. Ensembles are considered among the best alternatives for predicting weather in the face of uncertainty [122].

5.3.1 Forecast Ensemble

The concept of forecast ensemble is based on the notion that erroneous forecasts are derived from a combination of deviations of the initial conditions with respect to the actual weather conditions and the simplifications and assumptions considered in the formulation of the PE. The former prevails in short-term predictions, while the latter becomes relevant in long-term predictions. Thus, a forecast ensemble is formed by a set of forecasts generated by perturbing the initial conditions used during the weather model initialisation. Because this process is computationally costly, the resolution of an ensemble member is typically lower than a deterministic forecast. As part of the ensemble, the weather forecast providers also generate a high resolution forecast (HRES forecast as denoted by the ECMWF), with a higher spatial resolution than the other members and a control forecast (CNTL forecast as denoted by the ECMWF), which uses the best current description of the model physics while discarding any

stochastic factor, and whose initial state is the most accurate estimate of the current conditions.

The process used by the ECMWF of perturbing the initial conditions around the most likely estimate of the true weather consists of three methods:

- Singular Vector (SV) technique, which computes the initial perturbation that maximises the perturbation growth rate on a 48-hour forecast.
- Ensemble of Data Assimilation (EDA), which generates an ensemble of data assimilations based on the known accuracy of the observations.
- Stochastic Perturbations Techniques, which randomly perturbs tendencies in the physical parameterisation schemes (stochastic physics) and the vorticity tendencies (stochastic backscatter).

The computation of the perturbed models lead to a forecast ensemble that represents the realistic variability of possible evolutions of the atmosphere with time and location. Each member is a priori equiprobable, although individual members are less skilful (i.e., provide larger average errors) than the unperturbed CNTL. Forecast skill represents the proportion of improvement of accuracy over the accuracy of a reference forecast. Single-value forecasts commonly use correlation, root mean squared error, mean absolute error, relative mean absolute error, bias or Brier (in the case of binary events, for instance, snow or no snow) scores. Probabilistic forecast skill scores rely on more sophisticated metrics such as the Relative Operating Characteristic (ROC), which determines the ability to reproduce hits (event observed and forecasted), correct rejection (event not observed nor forecasted), false alarms (event not observed but forecasted), and misses (observed event not forecasted) [123]. Probabilistic forecast skill scores also rely on the Reduced Centred Random Variable (RCRV), which compares the ensemble average with observed data, considering the observational and models errors [124].

In the short range, only a small number of the ensemble members are, on average, more skilful than the CNTL. However, their lack of individual skill can be compensated by their ability, as a whole, to make reliable probabilistic estimations of the uncertainty associated

with the prediction. Such estimations can be characterised by the ensemble mean (EM) and spread (ES).

EM represents the averaged atmosphere conditions among the ensemble members. The use of the EM reduces or even removes the effect of atmospheric features that significantly vary among members, often producing the weakness of some high-impact events. Hence, it is recommended to be applied to temperature and pressure variables, which usually have rather symmetric Gaussian distributions. Other variables, such as wind, show more skewed distributions and, therefore, the use of the median is more convenient. EM, CNTL and HRES forecasts provide similar accuracy in the short-term. Conversely, although ensemble averages do not constitute genuine representations of the atmosphere dynamic and are less able to capture extreme weather events, its use provides higher accuracies than those obtained from the CNTL or HRES forecasts in the long term [125].

ES reflects the difference between ensemble members by means of the standard deviation of such members with respect to EM. ES measures the diversity of all possible atmosphere evolutions and, therefore, the uncertainty related to the given deterministic forecast [126].

Both EM and ES convey forecast uncertainty information by quantifying the probability distributions of event occurrences. Such distributions are used for determining the likelihood of event occurrences at a given location within an interval or above/below a threshold, for instance, with the temperature between 2°C and 10°C, or wind speeds higher than 100 km/h.

5.4 Weather Forecast Uncertainty in Trajectory Prediction

Meteorological information is critical to Trajectory Management, as accurate and timely wind, pressure, and temperature forecasts are pivotal to enable precise trajectory prediction and efficient trajectory optimisation. In addition, timely dissemination of accurate information on weather hazards is crucial to ensure operational safety and optimize airspace usage. Thus, the uncertainty of meteorological conditions is one of the most important threats to the predictability of trajectories and the stability and robustness of the traffic solutions produced by Trajectory Management functions.

The most extended approach to model weather uncertainties, especially wind uncertainty, assumes Gaussian distributions and spatio-temporal wind uncertainty correlation (including altitude correlation, which accounts for wind-shear deviations). This type of wind uncertainty modelling has proven relevant for trajectory prediction, enabling improvements in along-track predictions from 40 percent with 20-minute look-ahead times to 70 percent with 5-minute look-ahead times [127].

The TESA²² project addresses the problem of characterising the impact on trajectory prediction of different a priori probability distributions of weather uncertainties. The sensitivity analysis carried out shows that along-track and cross-track wind components are the most relevant, impacting sources of uncertainty (in addition to the initial aircraft mass) [128]. However, this solution lacks information about the actual weather uncertainty distributions, which in most cases does not correspond to normal distributions around a mean value.

Time-lagged ensemble forecasts have been used for characterising wind uncertainty distributions, providing a better representation of the variability of wind inputs required in trajectory prediction. The uncertainty is measured by the spread among several successive forecasts of different lengths and valid at the same time. Unlike forecast ensembles described in 5.3.1, time-lagged ensembles are built by forecasts generated similarly but with different time spans, which avoids the high computational requirements necessary for generating a forecast ensemble. However, time-lagged ensembles show high correlations among members, while longer look-ahead members usually introduce larger errors and, therefore, increased levels of uncertainty. Results from applying this solution to en route flights demonstrate a strong correlation between wind and along-track predictions uncertainties [129].

Alternatively, the wind uncertainty that affects the prediction of a flight can be expressed as a function of the variance of the components of the wind error: representativeness error (associated with no modelling smaller and higher frequency effects), prediction error (occurring at model scale), and large-scale error (assumed to be a constant bias). By

²² Trajectory prediction and conflict resolution for En-route-to-en-route Seamless Air traffic management.

modelling those wind errors, it is possible to generate a signal that approximates the wind uncertainty encountered by an aircraft in level flight [130].

5.4.1 Forecast Ensembles in Trajectory Prediction

The impact of weather variability on trajectory prediction can be studied by using the forecast ensemble described in Section 5.3.1. Although ensembles do not provide explicit measures of the uncertainty distributions of weather variables, their use enables the capability of providing relevant uncertainty information [131]. In particular, it enables the characterisation of trajectory prediction uncertainty by generating an ensemble of trajectories (deterministic computations obtained from each individual forecast ensemble member) and evaluating the spread of the desired trajectory variables (Figure 5-1). The concept is not based on modelling the uncertainty of the weather forecast; rather, it relies on analysing the impact of each member of the ensemble on the relevant trajectory variables and evaluating the correlation between the spreads of forecasts and predictions creating an ensemble of trajectories [124].

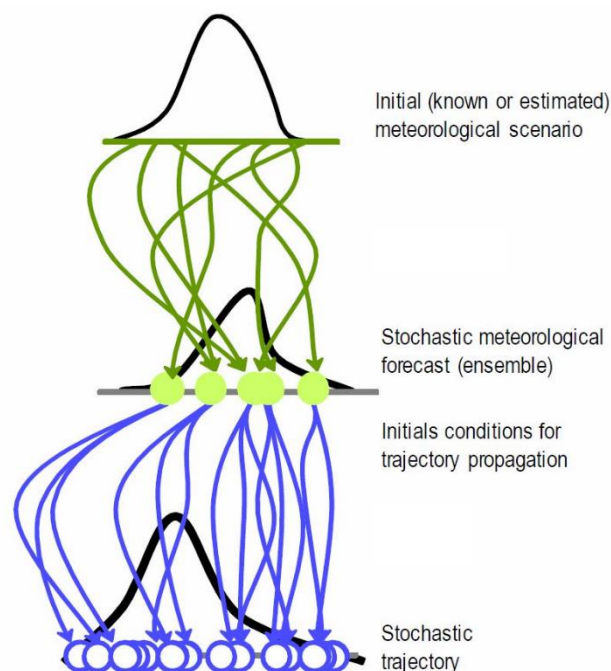


Figure 5-1 – Weather Uncertainty Propagation in Trajectory Prediction

The distribution of the trajectories within the trajectory ensemble will provide insight into the effect of weather uncertainties in the prediction process. The influence of weather uncertainty not only becomes noticeable in variations of aircraft performance or speeds

(especially ground speed), but also in modifications to the lateral profile because of the restriction of navigating through airspace areas, for instance, with high storm likelihood.

The aircraft state variables along the nominal predicted trajectory can be described by cumulative density functions that establish the likelihood of forecasted values above a threshold with certain level of confidence. The trajectory uncertainty will be determined by the spread of the state variables in accordance with such probabilistic distributions that represent their time evolution as a result of weather uncertainties.

5.5 Assessment of Trajectory Prediction Uncertainty due to Forecast Ensembles

As described in Section 5.2, weather uncertainties affect the computation of aircraft dynamics (including aircraft performance), the conversion of the TAS into other types of speeds (especially into ground speed), and the relationship between geodetic altitude and pressure levels. All those effects will turn into variability of aircraft state variables leading to trajectory prediction uncertainty.

Depending on the definition of the trajectory to be predicted, the effect of weather uncertainties will vary. For instance, if the aircraft holds the Mach speed during a level-off segment, the uncertainty of the temperature will affect the TAS computation. However, if the controlled speed during the same segment is TAS, the uncertainty will propagate into the CAS and Mach speed.

The effect of the wind is particularly relevant because its variation propagates directly into deviations of ground speed, which is the most important state variable from ATC's perspective, especially within the Terminal Manoeuvring Area (TMA). For example, the estimated time of arrival at a designated waypoint is calculated based on the ground speed. Thus, scheduling and sequencing procedures will rely on the capability of accurately estimating such time considering the effect of wind uncertainty into the ground speed prediction.

The approach followed in this section to analyse and model the influence of weather uncertainties combines two approaches discussed above: the use of weather forecast ensembles to capture the stochastic behaviour of the atmosphere and the generation of time-lagged ensembles to capture the evolution of weather conditions over time. The strategy

combines two sets of forecast ensembles to produce a new set of forecasts that consider simultaneously the weather uncertainty and the time-location variability (time-lagged ensemble of ensembles).

The NOAA's Global Ensemble Forecast System (GEFS) has been selected as a provider of forecast ensembles to illustrate the proposed approach by means of an example. GEFS is a weather forecast model made up of 21 separate forecasts, or ensemble members. The GEFS quantifies the amount of uncertainty in a forecast by generating an ensemble of multiple forecasts, each minutely different, or perturbed, from the original observations. GEFS is run four times a day, providing ensembles at 00:00, 6:00, 12:00 and 18:00 GMT with global coverage that is available through the NOAA National Operational Model Archive and Distribution System (NOMADS). Each member ensemble includes information up to 16 days, in time steps of 6 hours. The weather data is gridded with longitude and latitude resolutions of 1° in 28 pressure levels. Within the ensemble, there is a control forecast that represents the weather prediction obtained from unperturbed initial conditions. The remaining 20 members are generated by perturbing and rescaling the weather conditions used for their initialisation.

5.5.1 Trajectory Prediction Uncertainty Identification

The usage of weather forecast ensembles facilitates the process of identifying the boundaries within the aircraft state variables resulting from the weather influence on the trajectory. Based on the spread of trajectories obtained by considering each individual weather forecast ensemble member, the standard deviation and the confidence intervals of the state variables at the considered time can be computed straightforwardly.

The trajectories ensemble computed is characterised, for each aircraft state variables of interest, by the mean (average value among trajectories), the median (middle value that split the trajectories ensemble in two halves), and the standard deviation (measure of the spread among trajectories). This statistical metrics characterise the impact of the weather uncertainties on trajectory predictions due to weather variability.

The trajectory ensemble mean represents the average value of all trajectories computed from the weather forecast ensemble. Under some circumstance, this average trajectory might not

represent a realistic trajectory, as well as the forecast ensemble mean does not constitute realistic, dynamic three-dimensional representations of the atmosphere. However, it can be used for identifying the uncertainty affecting the aircraft state variables along the time interval of interest. For short look-ahead times, the trajectory ensemble mean will stay close to the trajectory computed using the control forecast, while for longer look-ahead times, the deviation between both will grow proportionally to the weather uncertainty (i.e., proportionally to the spread of the weather forecast ensemble). In the latter case, the weather forecast ensemble mean provides statistically more accurate predictions than the control forecasts [125]. Thus, the trajectories ensemble mean becomes more convenient for strategic decision-making processes such as traffic flow planning.

Similar to the probability of a weather event occurrence (e.g., wind speeds higher than 100 km/h, or precipitations between 5 and 8 mm/24h), a consistent way to convey trajectory uncertainty produced by weather uncertainty is through the definition of probability confidence intervals. This determines the probability of a state variable to exceed certain thresholds. The confidence interval represents a quantification of the trajectory uncertainty induced by weather uncertainties.

For the sake of clarity, the next example illustrates how trajectory prediction uncertainty can be derived from the use of weather forecast ensembles. The trajectory to be predicted is defined as follows:

- The selected aircraft type is the Boeing 737-800 identified by the BADA 4 designator B738W26.
- The aircraft intent defining the vertical profile is given by a sequence of chronologically ordered operations: maximum climb at constant CAS (245 kt), maximum climb at constant Mach (0.65), cruise at constant altitude (33,000 ft) and Mach (0.65), low idle descent at constant Mach (0.65), and low idle descent at constant CAS (250 kt) until reaching a geopotential pressure altitude of 10,000 ft at a metering fix point (MFP)
- The aircraft intent defining the horizontal profile is described by a single operation: constant course (-170°).

- The aircraft configuration is maintained clean along the trajectory.
- The initial aircraft state is determined by the initial mass (75,000 kg), initial latitude (59°), initial longitude (9°), initial heading (-170°), initial geopotential pressure altitude (3,000 ft), and initial time 5:20 GMT 2016, February 14.

It is possible to compute an ensemble of trajectories based on a time-lagged ensemble of forecast ensembles by individually entering the ensemble members provided by NOAA for the day of operation at 0:00 and 6:00 GMT. The trajectory computed from the control forecast will be the deterministic prediction, while the trajectories obtained from the forecast ensemble will represent the impact of weather uncertainty on the predicted trajectory. Figure 5-2 depicts the vertical profile (geodetic altitude [h] vs. time [t]) of the resulting ensemble of trajectories.

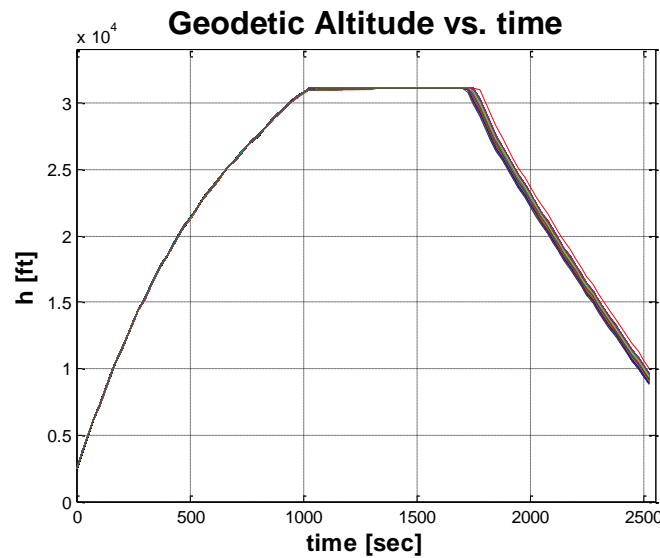


Figure 5-2 – Ensemble of Trajectories – h vs. t

The speed variability of the North and East components of the wind along the predictions are depicted in following Figure 5-3.

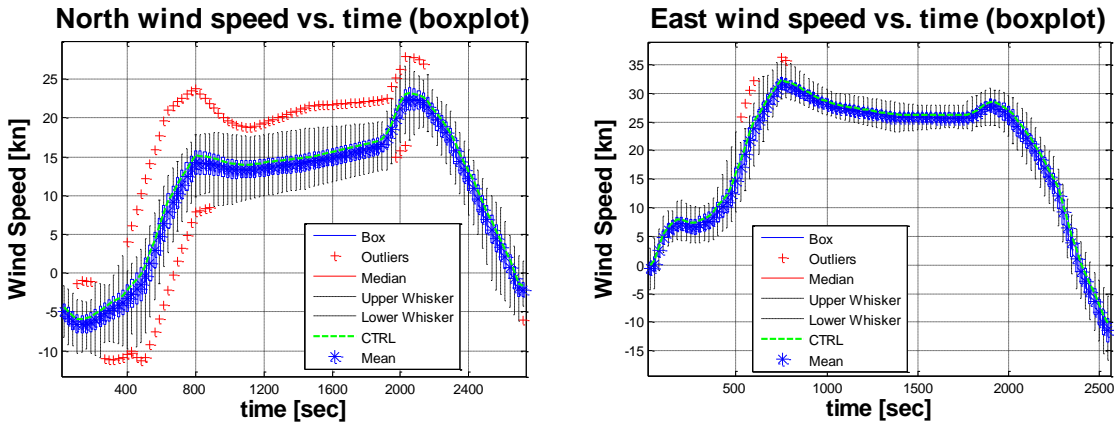


Figure 5-3 – North and East Wind Components Speed

A boxplot representation of the differences between the trajectories and the nominal prediction provides visual indications about the variability of the considered state variable (h) with the time. Figure 5-4 includes the mean and median values of these computed differences for the complete ensemble of trajectories, as well as the outliers and the interval that contain 99.3 percent of the values (equivalent to $\pm 2.7\sigma$ in a Gaussian distribution).

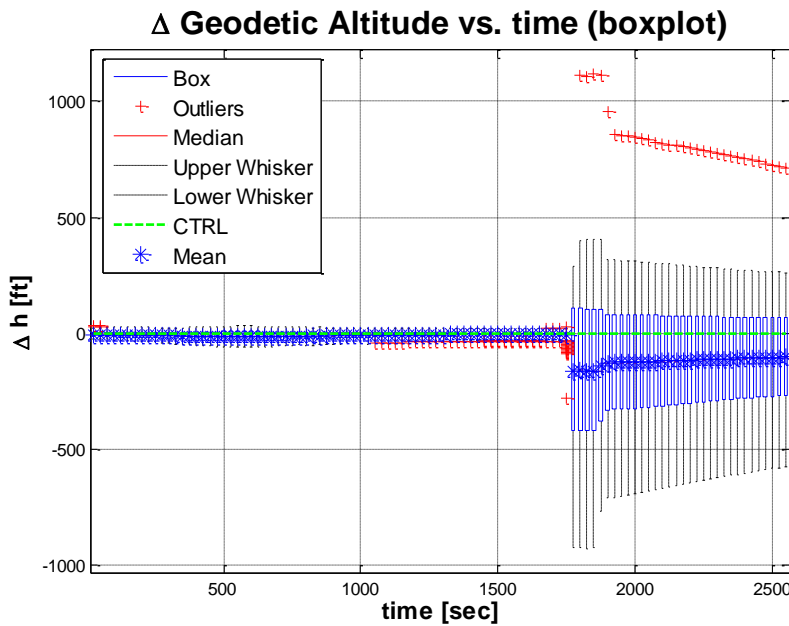


Figure 5-4– Ensemble of Trajectories – Δh Boxplot

In this particular example, the larger deviations with respect to the nominal prediction ($\Delta h = h - h_{nom}$) occur during the descent phase, where the effect of the weather uncertainty is more noticeable.

The confidence intervals, built upon the empirical cumulative density function (ECDF) generated from the predicted data, provide a quantification of the trajectory uncertainty. This information is highly valuable for determining, for instance, the maximum and minimum time deviations at the Top of Descent (TOD) or the geopotential pressure altitude differences at the metering fix point. Figure 5-5 shows the ECDFs that characterise the trajectory uncertainties at both the TOD and metering fix point.

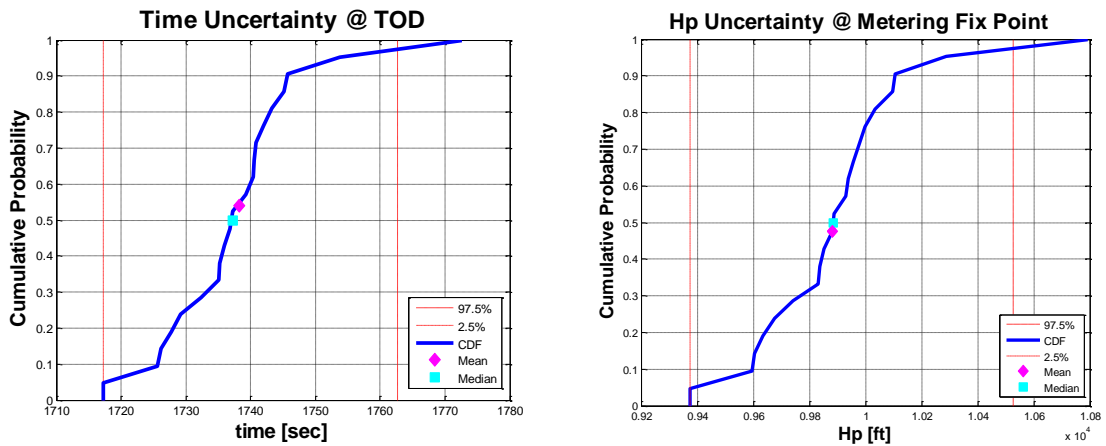


Figure 5-5 – Trajectory Uncertainty Described by ECDFs

Statistical information can be derived from the analysis of the ECDFs. Especially interesting are the mean and median values, and the upper and lower confidence interval limits according to the established confidence level. Table 5-1 provides the data for the examples described earlier.

Table 5-1 – Descent Phase Initial Conditions

	Mean	Median	97.5%	2.5%
Time @ TOD	1,738 sec	1,737 sec	1,762 sec	1,717 sec
Hp @ MFP	9,882 ft	9,885 ft	9,374 ft	10,527 ft

The main conclusions derived with 95 percent confidence level from this analysis are that the aircraft will initiate the descent at the designated TOD with a variability of ± 22.5 sec (confidence interval spread) and will reach the metering fix point with a geopotential pressure altitude variability of ± 576.5 ft, with respect to the median values because of the weather forecast uncertainties.

From the ATM perspective, the knowledge of estimated times of arrivals (ETAs) at principal waypoints in the trajectory is crucial for efficient and safe traffic management. This variable is directly related to the ground speed, which is strongly affected by weather and, especially, wind conditions. Hence, wind forecast uncertainties will determine the time prediction deviations with respect to nominal ETAs along the trajectory. The variability of ground speed is highly correlated with the variability of the along-track projection of the wind as depicted in Figure 5-6, where the standard deviations of both along-track wind and ground speed are plotted together for the study case proposed in this section.

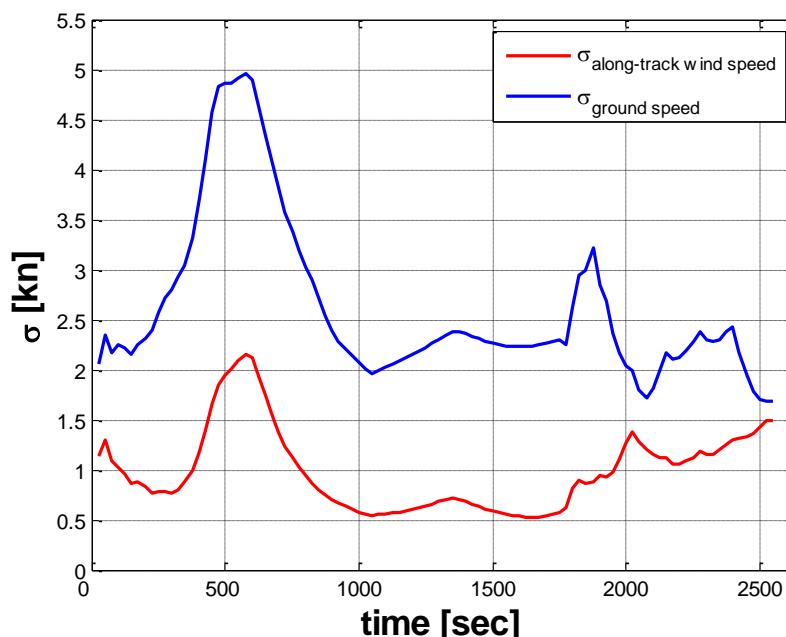


Figure 5-6 – Correlation Between Along-Track Wind Speed and Ground Speed Standard Deviations

Because of this correlation, it is possible to determine periods of high ground speed uncertainty based on knowledge of the wind speed uncertainties, calculated from weather forecast ensembles that cover the corresponding geographic area and timeframe in which the trajectory is to be predicted.

5.6 Summary

This chapter analyses the impact of weather uncertainties in trajectory prediction. The basic weather information required for computing a trajectory comprises the wind and the atmosphere temperature and pressure. These data are usually imported from NWP that provide gridded values for the weather variables at discrete times.

NWPs are deterministic representations of weather evolution from a set of initial and boundary conditions, and with measurements of the actual weather state. The accuracy of the models depends on the resolution of the selected grid and the physical assumptions considered for computing the predictions. However, NWPs are not able to provide any kind of information related to the uncertainty of the weather variables. To obtain such data, non-deterministic approaches need to be adopted. Forecast ensembles are sets of deterministic weather forecasts generated by perturbing the initial atmosphere state and the physical model that represent the atmosphere dynamic. These ensembles provide equally probable alternatives to the spatio-temporal weather evolution that determine the expected uncertainty of weather conditions when used in conjunction with each other.

The weather uncertainties in trajectory prediction basically affect the aircraft dynamics (the system of equations that represent the AMM requires the wind speed as input), the aircraft performance (drag, thrust, and fuel consumption models are dependent on atmosphere temperature and pressure), the transformation of the aircraft speeds (the AMM returns the TAS, although there are other types of speeds operationally more convenient such as CAS, Mach, or ground speed) and altitude definition (during cruise, aircraft fly at constant pressure levels, while during takeoff and landing the altitude control changes to geodetic altitude or elevation above runway. The relationship between pressure levels and geodetic altitude depends on the atmosphere conditions).

This chapter proposes the use of forecast ensembles to evaluate the trajectory uncertainties introduced by the weather variability. This approach generates trajectory ensembles that are obtained by entering each weather forecast ensemble member individually into the trajectory predictor ensemble member. The spread of the trajectory predictions provides a quantification of the trajectory uncertainties.

The forecast ensembles (e.g., provided by NOAA) are static snapshots of the atmosphere conditions. To include the evolution with time, it is necessary to consider at least two consecutive ensembles to generate a time-lagged ensemble of ensembles. This solution enables the capability of using weather information that captures the spatio-temporal variation of the weather conditions.

To exemplify the use of the time-lagged ensemble of ensembles, this chapter studies the effect of weather uncertainties in the prediction of a specific trajectory. The variability introduced by the ensemble members is directly transferred to the aircraft state variables. The statistical analysis of the predicted values of these variables quantifies the levels of uncertainty resulting from the weather forecast variability. For illustrative purposes, predicted time uncertainty at TOD and predicted geopotential pressure altitude uncertainty at a MFP have been analysed in detail, providing information about the spread of the aircraft state variables around the median values according to the considered confidence level.

Finally, thanks to the correlation between the standard deviation of the along-track wind speed and ground speed probability distributions, it has been shown how it is feasible to identify intervals of high ground speed uncertainty based on the knowledge of the along-track wind speed uncertainty.

CHAPTER 6

IMPACT OF AIRCRAFT INTENT UNCERTAINTY ON TRAJECTORY PREDICTION

6.1 Introduction

The aircraft intent (AI) describes the command and control actions issued by the pilot/FMS to operate the aircraft in accordance with the planned trajectory. An AI instance can be defined as the set of instructions that have to be provided to a TP in order to compute a trajectory in compliance with all the constraints and requirements defined by the client trajectory-based application. Instructions are conceived as atomic and indivisible inputs to the TP that provide all the necessary information required to integrate the AMM and obtain a predicted trajectory. The relationship between AI description and predicted trajectory is univocal, which makes it possible to conduct sensitivity assessments of trajectory predictions based on modelling the AI uncertainties.

The generation of a well-formed AI instance depends on the knowledge of how the aircraft is to be commanded to fulfil the defined trajectory requirements. The heuristics and methods applied to the AI generation process cannot be anticipated for all possible trajectory requirements and TP implementations. This process is subject to a high variability and, therefore, leads to broad levels of trajectory prediction uncertainty. The analyses of the trajectory prediction uncertainty are usually circumscribed to the evaluation of the impact of the stochastic behaviour of aircraft intent parameters, discarding all variability introduced by the AI generation process itself. This thesis is focused on the study of the trajectory prediction uncertainty introduced by a known instance of AI. The AI generation process is affected by other different stochastic parameters (e.g., user preferences variability), whose evaluation is considered out of the scope of the present research.

The remainder of the chapter will leverage the AIDL as a formal description of an AI instance, and will exploit its features to analyse the impact of AI uncertainty on trajectory prediction. The uncertainty will be limited to those parameters included in an AI instance formulated following the rules established by the AIDL.

The chapter first introduces the AIDL as a formal framework to describe well-formed AI to be used as a TP input.

Based on the lexical and grammar rules established by the AIDL, the most relevant parameters that can be considered as sources of AI uncertainty are identified.

Considering such sources of AI uncertainty, different polynomial models are proposed to evaluate the uncertainty in some aircraft state variables at the end of the trajectory segments generated from a given AI instance. These polynomials provide estimates for the standard deviation of state variables as a function of the standard deviations of the AI parameters considered as uncertainty sources.

This chapter ends with a discussion on the propagation of the uncertainty along a sequence of chronologically ordered AI instances describing a trajectory or flight segment.

6.2 The Aircraft Intent Description Language

The AIDL [57][71] has been designed as a formal language capable of describing an AI instance in a univocal, mathematically sound, and formalised manner. This language assumes a formulation of the AMM as explained in Section 3.4, where the mathematical formulation of the aircraft motion is posed as a DAE system. The solvability of such a system depends on how the three motion (3-19) and three configuration (3-20) constraints are defined. Both sets of algebraic constraints define an AI instance, with the AIDL defining the rules and restrictions required for those constraints to ensure a unique solution to the DAE system. A well-formed AI instance, according to the AIDL rules will include the necessary and sufficient information required to compute an aircraft trajectory unambiguously²³.

²³ The AIDL was thought to be used for describing airborne operations of civil fixed-wing commercial aircraft, including turbojet and turbofan powered aircraft. Its applicability to operations of other different aircraft has not been developed yet.

The AIDL is made up of an alphabet and a set of grammar rules (lexical and syntactical rules). The alphabet comprises the set of available instructions whose combination will form an AI instance. Each instruction represents an individual mathematical constraint to be applied to the DAE system. The grammar contains the rules that need to be observed for generating a correct AI instance. This is equivalent to ensuring that the mathematical constraints used in the AMM formulation allow the integration of the mathematical system of equations and the computation of a unique deterministic solution.

6.2.1 AIDL Alphabet

The AIDL alphabet (Σ_{AIDL}) includes a finite set of instructions that can be combined to describe an AI instance. Each instruction is characterised by two main features: effect and execution interval.

The effect represents the mathematical equation to be fulfilled by the aircraft motion (i.e., the algebraic equation defining the constraint encoded by the instruction), while the execution interval established the time period during which the effect is applicable.

An instruction effect is in turn made up of two elements:

- The constraint, which is an algebraic equation to be considered as part of the DAE system that describes the aircraft motion. A constraint relates different aircraft state variables with the aim of closing one of the AMM DoFs. A linear speed law between two different aircraft speeds is an example of a constraint.
- The specifier, which refers to the specific features of the state variables used for describing a constraint. The type of speed (e.g., Mach, CAS, TAS) to be controlled by a speed law is an example of a specifier.

The execution interval establishes the time period during which the instruction effect impacts the aircraft motion. Beyond this interval, the AMM needs to be defined again by means of a new set of instructions. This interval begins and ends when specific conditions on some of the aircraft state variables are met. Such conditions are known as triggers, which activate and deactivate the instruction effect. The triggers are grouped into two different categories:

- Explicit. These triggers define the end condition of the effect by means of an explicit equation. They can be *fixed* (specific time for the instruction activation or deactivation) or *floating* (target value to be fulfilled by a state variable or a combination of several of them).
- Implicit. The end condition cannot be explicitly formulated, as it requires additional information to be instantiated. There are three types of implicit triggers: *auto* (the end condition depends on an external variable that can only be solved at trajectory computation time), *linked* (the activation or deactivation condition is shared with the instruction at which the linked trigger is pointing) and *default* (the information required for defining this trigger is provided by the APM).

Examples of most common triggers would be:

- The initialisation of a climb procedure at $t = t_0$ (*fixed*).
- The end of an acceleration after reaching a Mach number $M = M_0$ (*floating*).
- The end of a climb procedure simultaneously with the end of the acceleration period (*linked*).
- The definition of the TOD under the condition of crossing a metering fix point at a predefined altitude $H_p = H_{p_0}$ (*auto*).
- The end of the transition between consecutive flaps retraction/deployment steps (*default*).

Five types of instructions are defined based on how the instruction influences and constrains the aircraft motion.

- *Set* instructions model short-term transitions between two aircraft states. These transitions are considered governed by the underlying aircraft performance model. Typical *set* instructions are those used for modelling the change in the power plant settings, landing gear retraction, or deployment.

- *Law* instructions model guidance and control modes. They are defined by uni- or multidimensional relationships between aircraft state variables that are assumed to be followed by the pilot/FMS. *Speed Laws* or *Altitude Laws* are examples of these types of instructions.
- *Track* instructions describe geometrical paths to be followed by the aircraft. The Track Lateral Path instruction describes the horizontal projection of the trajectory that will determine the route flown by the aircraft.
- *Hold* instructions maintain constant the initial value of a state variable throughout the execution interval. *Hold Altitude* and *Hold Speed* instructions can be used for describing the cruise. Their effect on the trajectory will be a segment of constant altitude and aircraft speed equal to the values at the TOC.
- *Open loop* instructions are used for modelling the direct input of the pilot on the controls at his/her disposal. The dependency of these instructions is not with any of the state variables, just with the time.

The complete list of instructions, which entails the AIDL alphabet Σ AIDL, is included in Appendix C.

Table 6-1 – AIDL Instruction Groups and Profiles

Type	Profile	Keyword	Group	Instruction	Target Value
MOTION	SPEED	SG	Speed Guidance	SL, HS	V_{TAS}
		HSG	Horizontal Speed Guidance	HSL, HHS	$V_{TAS} \cos \gamma_{TAS}$ γ_{TAS}
	SPEED/ VERTICAL	EG	Energy Guidance	EL, HE	dV_{TAS}/dh
	VERTICAL	VSG	Vertical Speed Guidance	VSL, HVS	$V_{TAS} \sin \gamma_{TAS}$
		PAC	Path Angle Control	SPA, PAL, HPA, OLPA	γ_{TAS}
		AG	Altitude Guidance	AL, HA	h
		VPG	Vertical Positional Guidance	TVP	h, λ, ϕ
	PROPULSIVE	TC	Throttle Control	ST, TL, HT, OLT	δ_T
	LATERAL	LDC	Lateral Directional Control	SBA, BAL, HBA, OLBA	μ_{TAS}
		LDG	Lateral Directional Guidance	CL, HC	χ_{TAS}
		LPG	Lateral Positional Guidance	TLP	λ, ϕ
	CONFIGURATION	HIGH LIFT	HLC	High Lift Configuration	SHL, HLL, HHL
SPEED BREAKS		SBC	Speed Breaks Configuration	SSB, SBL, HSB, OLSB	δ_{SB}
LANDING GEAR		LGC	Landing Gear Configuration	SLG, HLG	δ_{LG}

Finally, the AIDL instructions are also categorised into groups that facilitate definition of the grammar rules necessary for generating valid instances of AI. These groups are defined by state variables affected by the instruction. Instructions can be further classified into

profiles that are more intuitive representations of their effect on the aircraft behaviour. Table 6-1 shows how the instructions are organised in groups and profiles.

6.2.2 AIDL Grammar

The rules that govern how to combine instructions to generate a well-formed AI instance comprise the AIDL grammar. A grammatically correct AI instance enables the computation as it defines all the motion and configuration constraints (AIDL instructions) required for posing a closed mathematical system of DAE equations. The six (three motion and three configuration) instructions that determine the behaviour of the aircraft during a given time interval cannot be defined independently. They must obey certain rules to ensure that AMM DoFs are properly closed and define a solvable mathematical problem. The grammar rules effectively regulate the combination to limit the effect of the instructions on aircraft motion, thus avoiding the possibility of more than one instruction affecting the same aircraft state variable at the same time.

The computed trajectory is the result of applying the restrictions defined by the instructions to the aircraft motion. A set of six simultaneously active valid instructions that describe the AI during a period of time is called an operation. Every operation represents elementary aircraft behaviours that result from the effects defined by the active instructions. The instructions are sequentially concatenated along the three motion threads (two longitudinal, which describe the aircraft motion in the vertical plane and one lateral, which describe it in the horizontal plane) and three configuration threads (landing gear, high lift devices, and speed breaks).

The AIDL grammar rules establish the criteria to correctly choose the six instructions for each operation and to sequentially concatenate operations along the six threads to generate a description of a complete AI.

Lexical rules establish the criteria that ensure the proper combination of simultaneously active AIDL instructions to result in a valid operation.

Table 6-2 – AIDL Lexical Rules

#	Rule
LR1	An operation shall be formed by six overlapping instructions
LR2	Each instruction of an operation shall belong to a different profile
LR3	One instruction from each of the following groups must be present: HLC, LGC and SBC
LR4	Three instructions must be from the following groups: LDG, LPG, LDC, TC, SG, HSG, VSG, PAG, AG and VPG
LR5	Only one instruction must be from the following groups: LDG, LPG, and LDC
LR6	Instructions from group SG cannot be simultaneously present with instructions from group HSG
LR7	Instructions from groups VSG, PAG, AG, and VPG cannot be simultaneously present.
LR8	Instructions from groups VPG can only be present if an instruction from group LPG is also present

Syntactical rules govern the sequential concatenation of instructions along the different threads.

Table 6-3 – AIDL Syntactical Rules

#	Rule
SR1	A valid AI instance must be constituted by six threads
SR2	The lateral, landing gear, high lift devices, and speed break threads can only contain instructions from their respective profiles
SR3	The two longitudinal threads can only contain instructions from the speed, vertical, and propulsive profiles

Any AI instance formulated in accordance with the above-mentioned lexical and syntactical rules determines a valid input to a TP and, therefore, identifies a unique trajectory that can be predicted by the computation of the related AMM.

6.3 Description of AI Uncertainties

The study of AI uncertainty presented here is restricted to those cases where a deterministic, well-formed AI instance has already been defined (i.e., a nominal predicted trajectory can be computed based on a planned AI). In such cases, possible stochastic variations of some, or all, of the AI elements can be modelled and their impact on the predicted trajectory analysed. Modifications of the planned intent due to external actions such as ATC interventions, e.g., path stretching, vectoring, or altitude changes, are not considered as prediction uncertainties in this research. These tactical interventions issued to solve possible

conflicts or to improve traffic flow efficiency cannot be modelled as variations in AI parameters. They represent modifications to the original AI description, resulting in changes to the AI structure, instructions, and the like.

Thus, the analysis of AI uncertainty assumes that a nominal AI is known a priori and is circumscribed to the analysis of the propagation of stochastic effects on AI input into trajectory output.

Based on the AIDL alphabet and grammar, it is possible to isolate the influence of different elements that compose a well-formed AI operation and to address their influence individually and collectively.

According to AIDL syntactical rules, a valid AI instance requires definition of three motion and three configuration profiles. The latter ones establish the aerodynamic configuration of the aircraft for the trajectory segment during which the operation is active. The variability of the instructions belonging to the *HL*, *SB*, and *LG* profiles only affect the aircraft configuration and, therefore, its aerodynamic performance. Consequently, their effect can be accounted for as aircraft performance uncertainty rather than AI uncertainty.

The AI uncertainty analysis has then been reduced to the study of variability introduced by the instructions, relative to the motion profiles (*Speed*, *Vertical*, *Propulsive*, and *Lateral*).

Since the AI is specified by a chronologically ordered set of operations, there are three aspects to be considered for an uncertainty assessment: instruction uncertainty, initial conditions uncertainty, and continuity uncertainty.

6.3.1 Instruction Uncertainty

The instruction uncertainty is the stochastic variability of the elements that characterised an AIDL instruction. The instruction effect, specifier, and trigger are the parameters to be considered. However, not all of them show a stochastic behaviour.

The instruction effect univocally defines a motion constraint to be applied to the mathematical formulation of the AMM. Modifications of such constraint may lead to a different formulation of the problem and, therefore, a different solution. Depending on the

instruction type, it is possible to classify the effect of stochastic variation on the trajectory. Table 6-4 shows the relationship between AIDL instruction type and prediction uncertainty.

Table 6-4 – Impact of Instruction Type on Uncertainty

Instruction Type	Impact on Uncertainty
SET	The transitions between two states are modelled with this type of instruction. A <i>SET</i> instruction fixes the value of the state variable at the end of the instruction interval and it is concluded that these instructions do not contribute to aircraft intent uncertainty; it is assumed that the state variable reaches the target value defined by the instruction with no variability.
LAW	These instructions define functions that describe the evolution of a state variable with time. The stochastic variability of those functions represents the uncertainty related to the instruction effect.
TRACK	The instruction effect is described by a geometric function. Deviations due to inaccurate aircraft control derive into prediction uncertainty.
HOLD	The variability of the affected state variable will be maintained from the initial state while the instruction is active. Thus, from the uncertainty point of view, this type of instruction does not introduce additional uncertainty besides the uncertainty in the initial state when the instruction becomes active.
OPEN LOOP	The variability in how the pilot acts on the aircraft controls leads to uncertainty in the resulting trajectory.

In summary, the effect of certain types of instructions is assumed not to increase the uncertainty of the prediction process (*SET* and *HOLD*), while other types (*LAW*, *TRACK*, and *OPEN LOOP*) may affect the trajectory uncertainty.

The instruction's specifier defines the variable affected by the instruction's effect. Not all instructions admit all possible specifiers. However, from the point of view of uncertainty assessment, the specifier does not show stochastic behaviour. Changes in the specifier used for defining an instruction lead to a different AI and, thus, a different trajectory. For instance, a *HOLD SPEED* instruction with a *CAS* specifier determines part of the vertical profile of a trajectory that would be very different from the trajectory obtained if the selected specifier was *MACH*, as in the case of climbs or descents. Hence, variability in the specifiers is not considered as AI.

Triggers define the time interval during which the instruction effect is active. The end trigger sets the condition at which the instruction has to be deactivated and indicates the start of the next instruction in the thread. Hence, the initial trigger is defined by the final state of the previous instruction (continuity requirement). The variability of the initial triggers can be

considered equivalent to the analysis of the initial conditions and the continuity requirements required for describing a well-formed AI instance. The variability of the end triggers represents those cases where the instruction is deactivated earlier or later, or alternatively, where the actual trajectory goes below or above the target value defined by that trigger. This effect introduces a variability that translates directly into prediction uncertainty.

6.3.2 Initial Conditions Uncertainty

As mentioned above, an operation is a group of six AIDL instructions that determines a solvable DAE system by modelling the behaviour of the aircraft during a time interval. For the integration of the mathematical problem, a set of initial conditions describing the initial aircraft state from which the trajectory will be predicted are necessary. There is no need for an initial definition of all possible state variables, only those related to the instructions used for defining the AI instance need to be provided, because the remaining ones can be calculated from this initial subset. For instance, the initial aircraft mass is always required but the initial heading might be unnecessary in the case of predicting a cruise segment along a geodesic.

The definition of a consistent set of initial conditions depends on the formulation of the DAE system. Unlike ODE systems, where the initial conditions can be chosen arbitrarily within certain bounds, in DAE systems the set of initial conditions must comply not only with the explicit set of constraints but also with the so-called hidden constraints. These are additional algebraic equations obtained by differentiating the explicit constraints [133]. The hidden constraints are kinematic constraints, not explicitly formulated, which are obtained from the derivation of the geometric constraints. For example, an altitude constraint $g_1(h) = 0$ leads to a hidden path angle constraint $\gamma_{TAS} = 0$, in case of zero wind. Since a DAE system is not solvable for any set of initial conditions, its selection determines the capability of obtaining a unique solution (strong solvability²⁴).

²⁴ A DAE system has strong solvability when there is a unique solution for a set of consistent initial values and the solution coincides with those values at the initial time t_0 .

The variability of the initial conditions is propagated throughout the instruction interval in accordance with the definition of the AI. In the case of *HOLD* type instructions, the variability of the initial value of the state variable to be controlled is maintained until the instruction deactivation. For *LAW* type instructions, the initial condition may be superseded by the initial value of the law. Although the uncertainty will be removed, this would generate a discontinuity in the variable that should be addressed during the AI modelling. *TRACK* and *OPEN LOOP* type instructions show the same behaviour as *LAW* instructions, while *SET* type instructions constrain the uncertainty because the end aircraft state is defined by the value of the state variable that will be set.

6.3.3 Continuity Uncertainty

The AIDL imposes certain continuity requirements in the form of additional algebraic equations at the end of an instruction to ensure the continuity of certain variables in the transition between two instructions. These equations associate the value of certain state variables at the beginning of an instruction with their corresponding values from the previous instruction.

An AI is a sequence of chronologically ordered operations. Each operation represents a solvable Trajectory Prescribed Path Control (TPPC) problem (definition used for identifying the problem of flying vehicles trajectories subject to constraints [134]). For every TPPC problem, it is required to identify a set of initial conditions consistent with the system of equations. As explained in Section 6.3.2, consistent initial conditions are those that satisfy the geometric, kinematic, configuration, and hidden constraints. The output of the precedent TPPC problem is used to initialise the consistency system of equations as depicted in Figure 6-1.

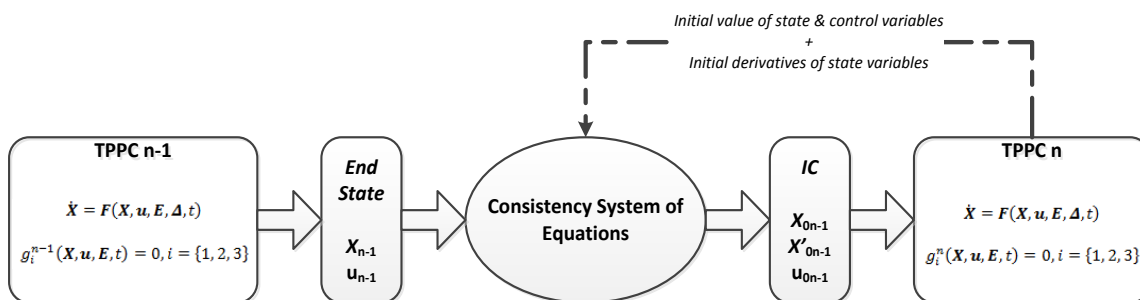


Figure 6-1 – Initialisation of a TPPC Problem

The consistency system includes the constraints and hidden constraints that do not include control variables (State Initialisation Subsystem [SIS]) and the remaining constraints that do

contain control variables (Control Variable Subsystem [CVS]). The former provides the initial values of the state variables, while the latter gives the initial value of the control variables and the initial derivatives of the state variables. Both systems are decoupled, and therefore, \mathbf{X}_0 can be obtained separately from \mathbf{u}_0 and $\dot{\mathbf{X}}_0$.

The same approach can be applied to obtain the initial configuration state Δ_0 considering the three configuration constraints $d_i(\delta_i) = c_i(\mathbf{X}, \mathbf{E}, t)$.

The variables that can be chosen for initialising the following TPPC problem will depend on the type and number of constraints and hidden constraints. Details of the process of selecting an adequate set of initial conditions are included in “Definition of an aircraft intent description language for air traffic management applications.” [71].

Hence, the uncertainty of the output (end state) of the n TPPC problem will affect the initialisation of the following TPPC problem. The calculation of the consistent initial conditions to be used for solving a given TPPC problem (a given operation) will be influenced by the accumulated uncertainty propagated from all previously solved TPPC problems. Hence, the effect on prediction of continuity uncertainties can be considered as a particular case of the effect of the initial conditions uncertainties on a single operation.

6.4 AI Uncertainty Modelling

This section presents an AI uncertainty model based on the discussion of the previous section. This model facilitates the quantitative analysis of the impact of AI uncertainties on trajectory prediction.

The stochastic parameters of an AI instance considered to introduce uncertainty in the trajectory prediction process are the instruction end trigger, its effect, and the initial conditions

6.4.1 Instruction Uncertainty Model

The two instruction elements considered as sources of uncertainty are the end trigger and the instruction effect.

6.4.1.1 Trigger Uncertainty Model

Regardless of the type of trigger, during the trajectory computation, all triggers are transformed into *fixed* triggers. This transformation allows chronologically ordering the sequence of triggers to be executed. Hence, once computed, the trajectory can always be described by a set of operations with known execution intervals. For instance, a *floating* trigger such as the altitude of the TOC would translate into the time at which the trajectory computation reaches the cruise altitude. This transformation facilitates the process of studying and modelling the uncertainty related to triggers by reducing it to the analysis of variability during the time at which certain state variables reach a target value.

Considering the above, trigger uncertainty can be modelled by probability density functions that in most cases will be centred on a nominal value. This assumption considers that it is equally probable to get the target value earlier versus than later. The standard deviation of those distributions represents a measurement of the trigger uncertainty.

The chronological sequence of triggers determines the sequence of AI operations that univocally describe the aircraft trajectory. Then, the influence of the triggers' uncertainty can be evaluated at each individual AI operation independently. The propagation of uncertainty transmitted from one AI operation to the next will be studied later in the chapter as part of the initial conditions uncertainty.

To assess the impact of trigger uncertainty on trajectory prediction, a series of Monte Carlo runs have been conducted. The experiments considered a set of AI operations that describe typical operational procedures. This approach can be straightforwardly applied to any valid AI that describes a trajectory or trajectory segment.

The Monte Carlo runs were designed as follows:

- The selected aircraft type is a Boeing 737-800 (B738W26 BADA 4.1 designator).
- The atmosphere is considered in standard condition with null wind.
- Trajectories are computed considering clean configuration in all cases.
- Trajectories are described by the AI instances summarised in Table 6-5.

- The variability that describes the trigger uncertainty is approximated by Gaussians distributions. These distributions are symmetric with respect to the nominal value and considered equally probable to get the target value earlier versus later. This assumption is accepted with regard to model intrinsic uncertainties in the flight mode transitions [135].

Table 6-5 – Trigger Uncertainty - AI Descriptions Used in Monte Carlo Runs

Flight Phase	CASE		AI DESCRIPTION ²⁵
CRUISE	CRZ1	Constant speed & altitude	HS(Mach) + HA(Hp) + HC(geo)
	CRZ2	Constant acceleration @ constant altitude	SL(Mach) + HA(Hp) + TLP(circ_arc)
	CRZ3	Constant deceleration @ constant altitude	SL(Mach) + HA(Hp) + TLP(circ_arc)
CLIMB	CMB1	Constant speed @ Maximum Climb rating	HS(Mach) + TL(MCMB)+ TLP(geodesic)
	CMB2	Constant speed @ constant path angle	HS(Mach) + PAL(geo) + TLP(geodesic)
	CMB3	Constant acceleration @ Maximum Climb rating	TL(MCMB)+ SL(Mach) + TLP(circ_arc)
	CMB4	Constant acceleration @ linear altitude law	SL(Mach) + AL(Hp) + TLP(circ_arc)
DESCENT	DES1	Constant speed @ Low Idle rating	TL(LIDL)+ HS(Mach) + HC(geo)
	DES2	Constant speed @ linear path angle law	HS(Mach) + PAL(geo) + TLP(circ_arc)

The nominal trigger value (μ_{tr}) is set to 150 sec, while the initial masses, altitudes, and speeds, as well as the standard deviation (σ_{tr}) of the Gaussian distributions that identify the trigger uncertainty, normalised with respect to the nominal coefficient of variation ($CV_{tr} = \frac{\sigma_{tr}}{\mu_{tr}}$), are selected from the ranges shown in Table 6-6.

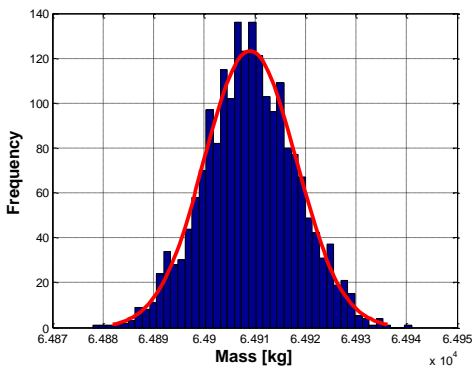
²⁵ Because the aircraft is considered as always flying at clean configuration, the information about the three AIDL configuration threads was not included. For all cases, they are described by the following instructions HHL(HL=0), HSB(SB=0) and HLG(LG=0).

Table 6-6 – Trigger Uncertainty – Monte Carlo Parameters Ranges

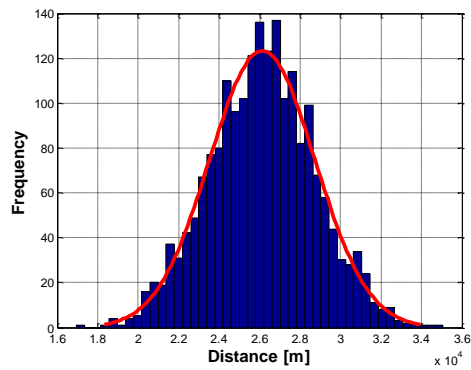
	Mass [tons]	Altitude [ft]	Speed [Mach]	CV _{tr} [%]
CRUISE	65 – 74	20,000 – 33,000	0.55 – 0.775	0 – 25
CLIMB	71 - 80	3,000	0.35 – 0.44	0 – 25
DESCENT	75 – 71	33,000	0.705 – 0.75	0 – 25

CRZ1

(a) Final Mass Distribution

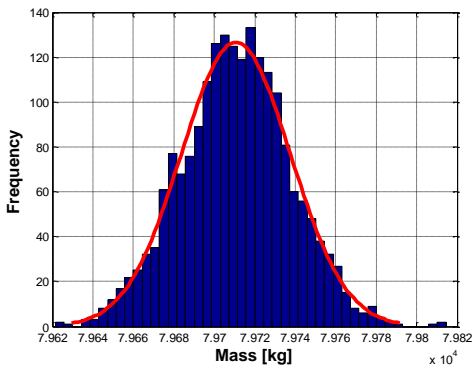


(b) Final Flown Distance Distribution

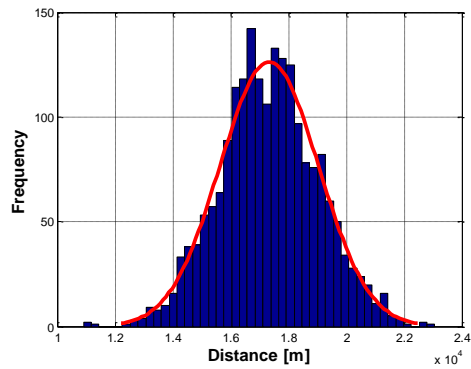


CMB1

(c) Final Mass Distribution

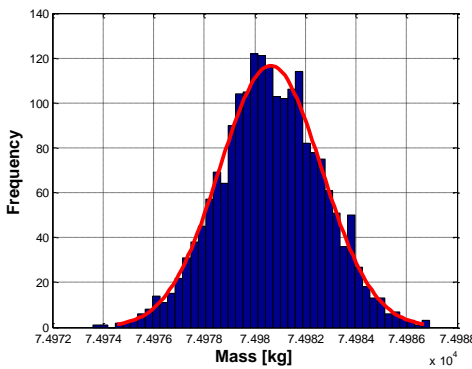


(d) Final Flown Distance Distribution



DES1

(e) Final Mass Distribution



(f) Final Flown Distance Distribution

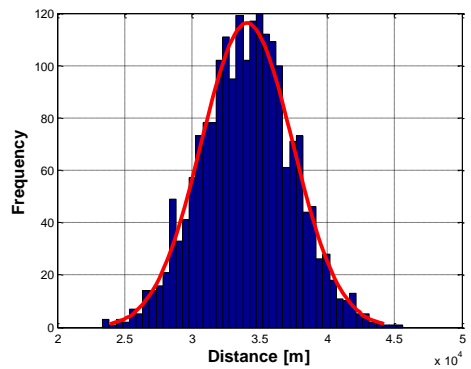


Figure 6-2 – Mass and Flown Distance Uncertainty Distributions at the End of the Execution Interval due to Gaussian Trigger Uncertainty

The first conclusion derived from the analysis of the Monte Carlo runs is that the variation of the state variables at the end of the execution interval corresponds to a Gaussian distribution. Figure 6-2 shows that variability of the aircraft mass (m) and flown distance (d) for the CRZ1, CMB1, and DES1 cases, when σ_{tr} is set to 15 sec (10 percent with respect to the nominal value) and the initial masses, speeds, and altitudes are 67 tons – 0.6 Mach – 23,000 ft; 78 tons – 0.37 Mach – 3,000 ft; and 74 tons – 0.74 Mach – 33,000 ft, respectively.

Thus, the trajectory uncertainty (measured by means of the standard deviations of distributions that represent the variability of the state variables at the end of the execution interval) can be expressed as a function of the trigger uncertainty. Considering that all remaining AI parameters are known and do not introduce uncertainty to the process (trajectory uncertainty sensitivity to trigger uncertainty), this trajectory uncertainty is characterised by the nominal trigger value (μ_{tr}) that describes the execution interval. Denoting the variability of the output state variables as σ_{sv} , where sv represents any state variable (e.g., geodetic altitude, true airspeed, mass), the model that returns σ_{sv} is proposed in Equation (6-1).

$$\sigma_{sv} = A |\mu_{sv} - iv_{sv}| \cdot \frac{\sigma_{tr}}{\mu_{tr}} \quad (6-1)$$

This model is a function of the following parameters:

- The absolute difference between the initial value of the state variable (iv_{sv}) and the mean value (μ_{sv}) of the distribution that identify the state variable values at the end of the execution interval.
- The trigger uncertainty σ_{tr} .
- The execution interval μ_{tr} .

The coefficient A is specific to each state variable and depends on the aircraft type and the information encoded in the AI.

This model ensures that in the case of null trigger uncertainty ($\sigma_{tr} = 0$), the uncertainty of the state variables at the end of the execution interval will also be null ($\sigma_{sv} = 0$).

A subset of all possible state variables, as shown in Table 6-7, has been selected to illustrate the accuracy of the proposed model with respect to the outputs generated by the Monte Carlo runs.

Table 6-7 – Subset of Studied Aircraft State Variables

STATE VARIABLE			
d	Flown distance	m	Aircraft mass
TAS	True Airspeed	Hp	Pressure altitude
χ	Heading	γ	Geometric path angle

The relative root mean square error (rRMSE) is used as a metric to assess how well the model fits the data. The rRMSE is a percentage of the difference between σ_{sv} and the estimation provided by the model ($\widehat{\sigma}_{sv}$) referred to σ_{sv} that can be calculated as follows:

$$rRMSE = \sqrt{\frac{\sum_1^n \left(\frac{\widehat{\sigma}_{sv} - \sigma_{sv}}{\sigma_{sv}}\right)^2}{n}} \cdot 100 \quad (6-2)$$

where n is the number of Monte Carlo runs.

This metric indicates the average errors provided by the proposed uncertainty model within the envelope of data used for the identification. For each proposed case, the coefficient A has been identified by a linear fitting process. Table 6-8 summarises the rRMSE obtained for the selected state variables.

Table 6-8 –Trigger Uncertainty Propagation Model - RMSE Metric

CASE		d	m	TAS	Hp	y	x
CRZ1	RMSE [%]	3.1e-5	6.1e-3	-	-	-	-
CRZ2	RMSE [%]	0.137	1.314	2.2e-12	-	-	0.123
CRZ3	RMSE [%]	0.148	3.307	2.2e-12	-	-	0.347
CMB1	RMSE [%]	0.157	1.025	1.138	0.944	4.971	0.096
CMB2	RMSE [%]	0.022	0.817	0.024	0.026	7.4e-13	0.076
CMB3	RMSE [%]	0.380	0.823	0.784	0.310	4.277	0.263
CMB4	RMSE [%]	0.134	0.968	1.015	2.0e-14	0.987	0.154
DES1	RMSE [%]	0.057	0.282	0.964	1.016	2.467	-
DES2	RMSE [%]	0.024	1.194	0.024	0.042	1.1e-12	0.135

The following Figure 6-3 depicts a graphical comparison between the computed and modelled data for CMB3 case. The plots of all remaining cases are included in Appendix D-1.

Based on the numerical and graphical comparisons, it can be concluded that the proposed model approximates with high accuracy the uncertainty propagated to the state variables as a consequence of the trigger uncertainty. This model is valid for all possible combinations of AIDL instructions.

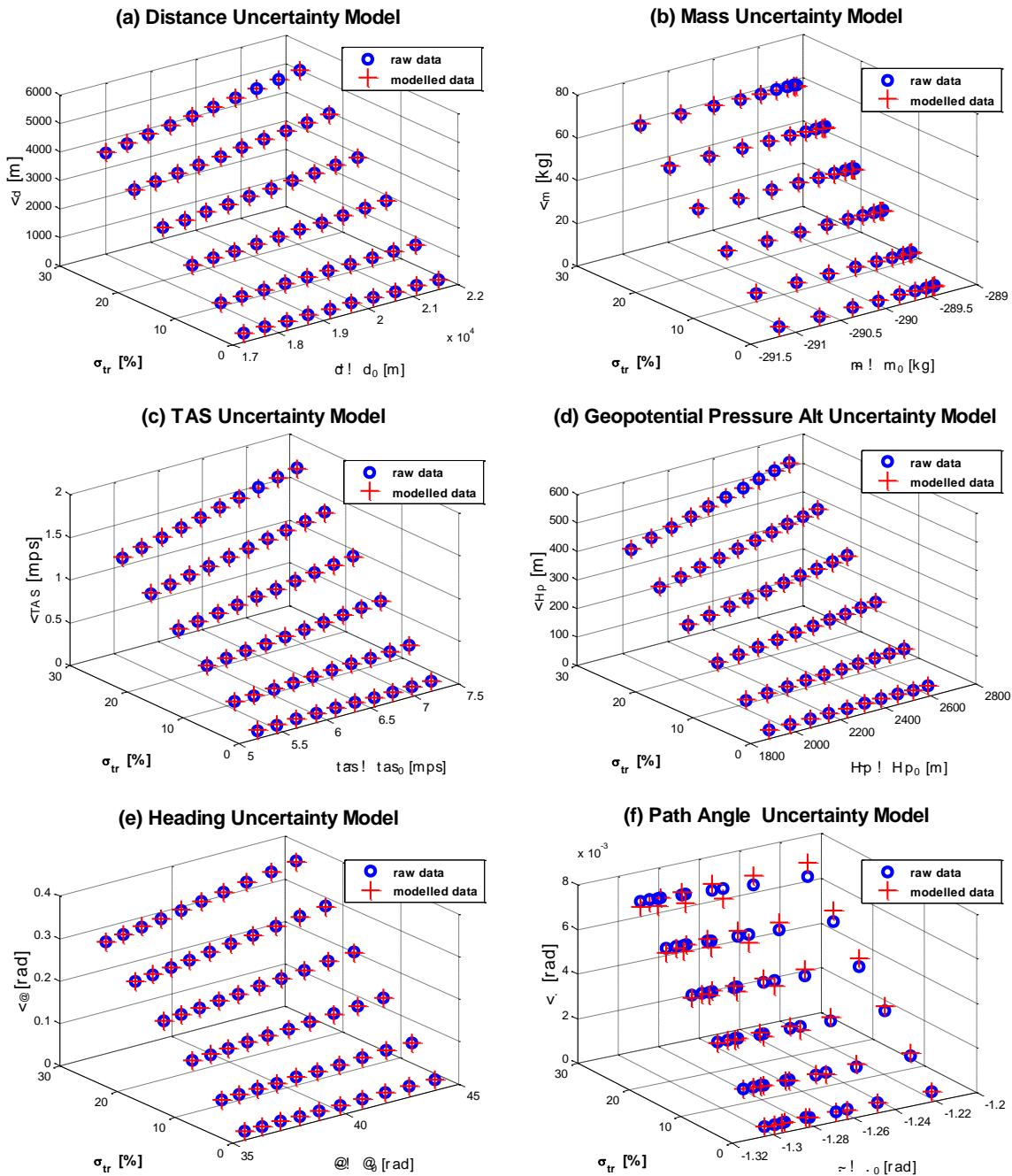


Figure 6-3 – CMB3 – Comparison Between Modelled and Raw Uncertainty Data due to Trigger Uncertainty

6.4.1.2 Effect Uncertainty Model

The instruction effect is given by an algebraic relationship between state variables enforced during the execution interval. Depending on the type of instruction, the impact of the effect on trajectory prediction uncertainty varies according to Table 6-4. *SET* instructions are not considered as sources of AI uncertainty because their effect is defined by the aircraft performance model. *HOLD* instructions do not contribute to AI uncertainty because their effect is reduced to maintain certain state variable constant throughout the instruction

interval and no tracking error is assumed. Thus, only *LAW*, *TRACK*, and *OPEN LOOP* instructions are considered for evaluating the uncertainty introduced by the instruction effect.

Analogously to the process as described in the previous section, a series of Monte Carlo simulations were conducted to evaluate how the effect uncertainty is propagated to the state variables at the end of the execution interval.

The selected aircraft type and atmosphere conditions are the same as defined in Section 6.4.1.1. The aircraft is always considered as operating in clean configuration. The descriptions of the AI instances used for running the Monte Carlo simulations are summarised in Table 6-9.

Table 6-9 – Effect Uncertainty - AI Descriptions Used in Monte Carlo Runs

Flight Phase	CASE		AI DESCRIPTION ²⁶
CRUISE	CRZ2	Constant acceleration @ constant altitude	SL(Mach) + HA(Hp) + TLP(circ_arc)
	CRZ3	Constant deceleration @ constant altitude	SL(Mach) + HA(Hp) + CL(geo)
CLIMB	CMB3	Constant acceleration @ Maximum Climb rating	TL(MCMB)+ SL(Mach) + TLP(circ_arc)
	CMB4	Constant acceleration @ linear altitude law	SL(Mach) + AL(Hp) + TLP(circ_arc)
	CMB5	Constant speed @ linear path angle law	HS(Mach) + PAL(geo) + CL(geo)
	CMB6	Constant acceleration @ linear path angle law	SL(Mach) + PAL(geo) + CL(geo)
DESCENT	DES2	Constant speed @ linear path angle law	HS(Mach) + PAL(geo) + TLP(circ_arc)
	DES3	Constant deceleration @ linear path angle law	HS(Mach) + PAL(geo) + CL(geo)

The effect variability is modelled through the variability of the slope that describes the constant accelerations or decelerations, linear altitude laws, and linear path angle laws. This

²⁶ As explained in Section 6.4.1.1, the aircraft is considered as always flying at clean configuration and, therefore, the three AIDL configuration threads are described by the following instructions: HHL(HL=0), HSB(SB=0), and HLG(LG=0) in all cases.

variability may be potentially characterised by any probability distribution. To exemplify the modelling process, it has been assumed as represented by a Gaussian distribution. Other alternatives to model the effect uncertainty can also be adopted, although they would not affect the applicability of the proposed methodology in this section.

The Monte Carlo runs selected the initial aircraft masses, speeds, altitudes, and standard deviations (σ_{eff}) of the Gaussian distributions that identify the effect uncertainty (equal to the slope variability in this particular case), normalised with respect to the nominal value (μ_{eff}) of the considered parameter (in this case, the nominal slope of the linear functions that describe the evolution of a state variable between the initial and final values), from the operational ranges shown in Table 6-10 according to the type of trajectory segment to be predicted in steps of 0.025 Mach for cruise cases and 0.01 for climb and descent cases; 1 ton for all cases; 1,500 ft for cruise cases and 5 percent of variability for all cases respectively.

Table 6-10 – Effect Uncertainty – Monte Carlo Parameters Ranges

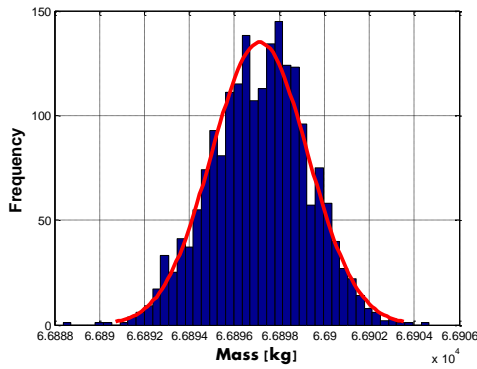
	Mass [tons]	Altitude [ft]	Speed [Mach]	CV_{eff} [%]²⁷
CRUISE	65 – 74	20,000 – 33,500	0.55 – 0.775	0 – 25
CLIMB	71 – 80	3,000	0.35 – 0.44	0 – 25
DESCENT	70.5 – 75	33,000	0.705 – 0.75	0 – 25

As a result of the analysis of the simulation outputs, it is possible to conclude that the distribution of state variables at the end of the execution interval is Gaussian as well. Figure 6-4 depicts the variability of the aircraft mass (m) and flown distance (d) for the CRZ2, CMB5, and DES3 cases, when the coefficient of variation $CV_{\text{eff}} = \frac{\sigma_{\text{eff}}}{\mu_{\text{eff}}}$ is set to a 15 percent, and the initial mass, speed, and altitude are 67 tonnes – 0.57 Mach – 23,000 ft; 78 tons – 0.37 Mach – 3,000 ft; and 74 tons – 0.74 Mach – 33,000 ft, respectively.

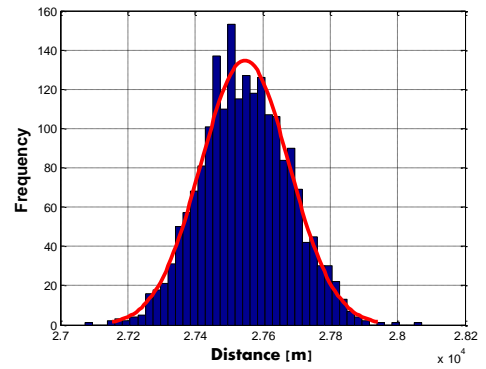
²⁷ The variability of CV_{eff} should be established as a result of the analysis of empirical data, if available.

CRZ2

(a) Final Mass Distribution

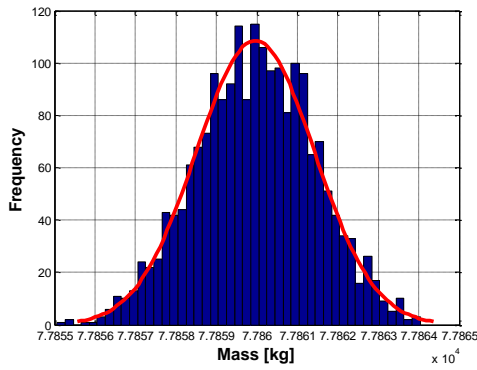


(b) Final Flown Distance Distribution

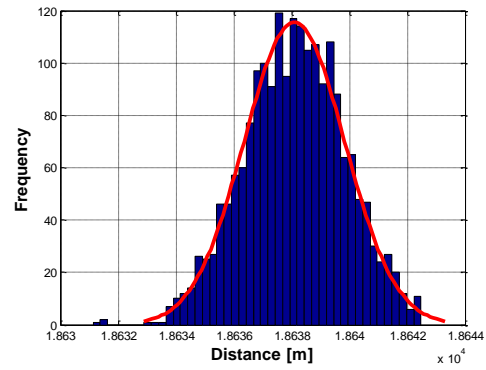


CMB5

(c) Final Mass Distribution

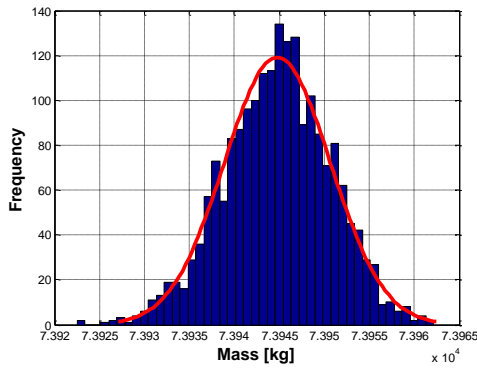


(d) Final Flown Distance Distribution



DES3

(e) Final Mass Distribution



(f) Final Flown Distance Distribution

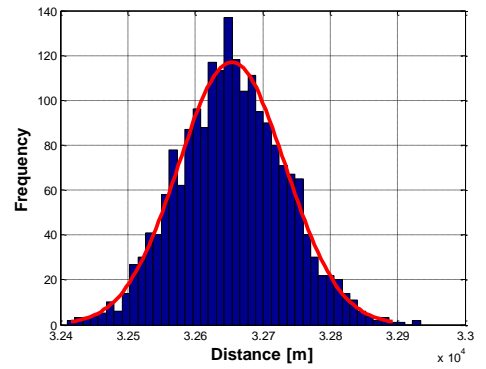


Figure 6-4 – Mass and Flown Distance Uncertainty Distributions at the end of the Execution Interval due to Gaussian Effect Uncertainty

Thus, it is possible to conclude that there is a relationship between the standard deviation of the Gaussian distribution that describes the effect uncertainty and the standard deviation of the Gaussian distributions that describe the uncertainty of the state variables at the end of the execution interval.

Considering that all remaining AI parameters are known and do not introduce uncertainty to the process (trajectory uncertainty sensitivity to instructions' effect uncertainty), the proposed model relates σ_{eff} and the mean value of the distribution that describes the variability of the considered state variable (μ_{sv}) at the end of the execution interval according to the following expression:

$$\sigma_{sv} = B\sigma_{eff} + C \left(\frac{\sigma_{eff}}{\mu_{sv}} \right) \quad (6-3)$$

The coefficients B and C are specific for each state variable and depend on the aircraft type and the information encoded in the AI.

This model ensures that in the case of null effect uncertainty ($\sigma_{eff} = 0$), the uncertainty of the state variables at the end of the execution interval will also be null ($\sigma_{sv} = 0$).

The list of state variables studied to evaluate the accuracy of the proposed model is the same as those included in Table 6-7.

The accuracy of the model with respect the data generated by the Monte Carlo simulations is measured through the rRMSE as defined in Equation (6-2). This metric indicates the average error of the proposed uncertainty model within the envelope of data used for the identification. For each proposed case, the coefficients B and B have been identified by a linear fitting process.

Table 6-11 summarises the rRMSE obtained for the selected state variables.

Table 6-11 –Effect Uncertainty Propagation Model - RMSE Metric

CASE		<i>d</i>	<i>m</i>	<i>TAS</i>	<i>Hp</i>	<i>y</i>	<i>X</i>
CRZ2	RMSE [%]	0.1322	8.0906	0.0529	-	0.3572	0.7987
CRZ3	RMSE [%]	0.5615	1.8055	0.0520	-	0.0176	0.0001
CMB3	RMSE [%]	0.7966	1.7378	0.2431	1.2471	7.6229	0.4215
CMB4	RMSE [%]	0.0727	0.5461	0.0635	8.4e-15	0.0751	0.0727
CMB5	RMSE [%]	0.0818	0.6623	0.0192	0.0345	0	2.8e-5
CMB6	RMSE [%]	0.13217	8.0906	0.05290	-	0.3572	0.7987
DES2	RMSE [%]	0.5615	1.8055	0.0520	-	0.0176	0
DES3	RMSE [%]	0.2866	0.1394	0.0087	1.3e-14	0.004	0.2866

Figure 6-5 depicts a graphical comparison between the computed and modelled data for CMB3 case. The plots of all remaining cases are included in Appendix D-2.

Based on the numerical and graphical comparisons, it can be concluded that the proposed model approximates with high accuracy the uncertainty propagated to the state variables because of the uncertainty introduced by the instructions' effect. This model is valid for all possible combinations of AIDL instructions.

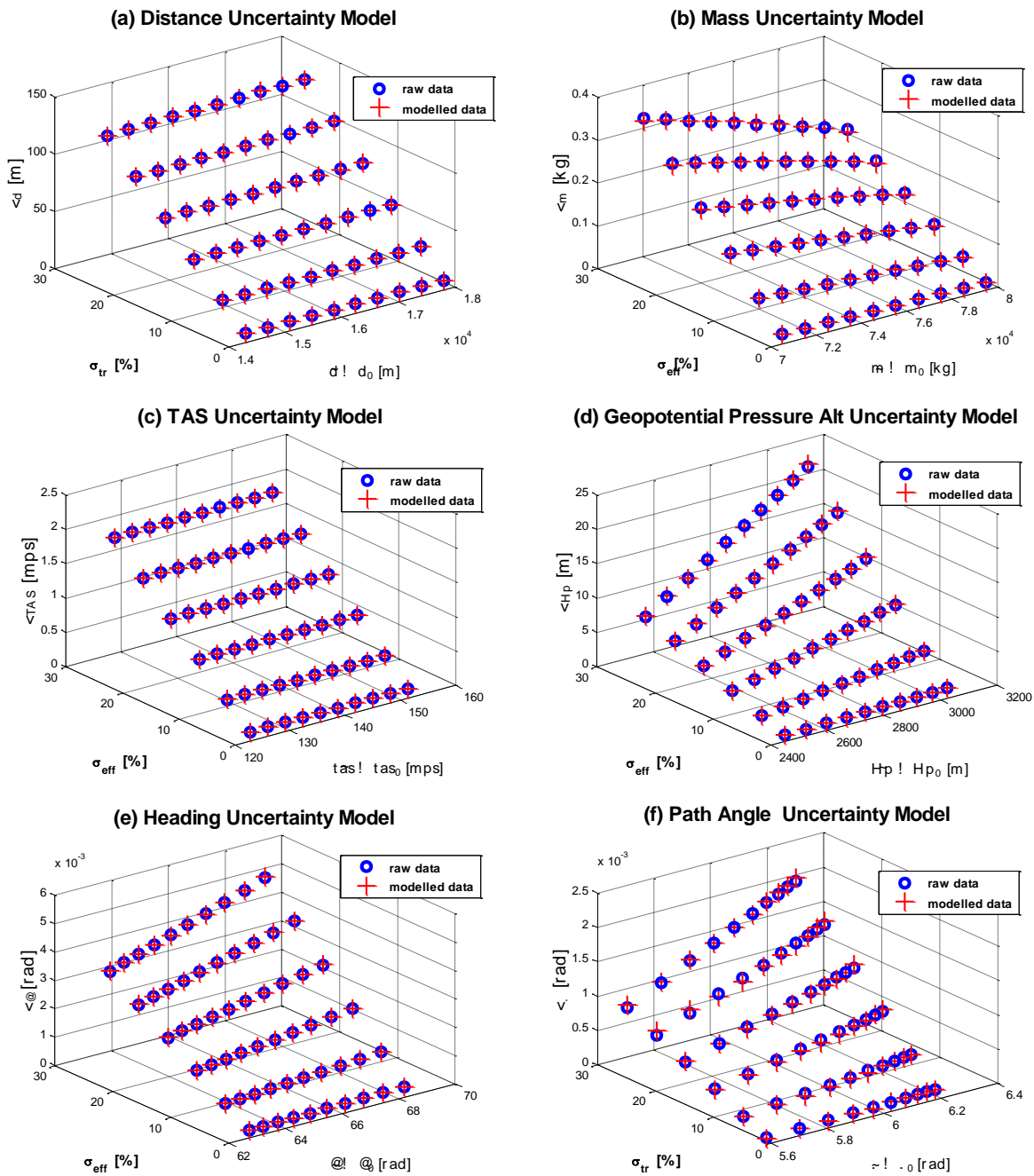


Figure 6-5 – CMB3 – Comparison Between Modelled and Raw Uncertainty Data due to Effect Uncertainty

6.4.2 Initial Conditions Uncertainty Model

As explained in Section 6.3.2, the initial conditions at the start of an operation must comply with certain geometric, kinematic, configuration, and hidden constraints to ensure the solvability of the DAE system that describes the aircraft motion within the corresponding execution interval (Section 6.3.3).

The set of required initial conditions includes the aircraft position (latitude, longitude, and altitude), the aircraft speed, the initial mass, and the aerodynamic configuration (position of

flaps, speed breaks, and landing gear). In some cases, and depending on the AI instance, other additional conditions may be required. For instance, in the case of *Hold Path Angle (HPA)* instructions, the initial value of the path angle needs to be provided in addition to the previous ones. Similarly, in the case of non-geometric lateral instructions such as *Course Law (CL)* or *Hold Course (HC)*, the initial heading is required for initialisation the mathematical system of equations.

Without considering the type of trigger that establishes the end of the instruction interval, the uncertainty introduced by the inputs is straightforwardly propagated to the outputs by the integration process. The trigger plays a significant role because it may produce a reduction of the uncertainty of some state variables at the cost of transferring it to others. This impact is analysed later when the continuity uncertainty modelling is discussed. Thus, the model of initial condition uncertainties is studied considering only their propagation with time according to the system of equations that describe the aircraft motion.

Because the lateral and longitudinal²⁸ profiles are decoupled with respect to the definition of the AI, it is possible to study them separately. The following sections analyse their propagation considering that the AI is known and defined without uncertainty (no stochastic parameters). Additionally, it assumed that the APM does not add uncertainty to the prediction and that the weather conditions are known and do not vary (standard atmosphere and no wind).

6.4.2.1 Lateral Profile

The state variables that determine the initial conditions of the aircraft in the horizontal plane are related to the state variables affected by the definition of the corresponding motion constraints (AIDL lateral instructions). As shown in Table 6-1, those state variables are latitude (λ), longitude (φ), heading (χ_{TAS}), and bank angle (μ_{TAS}). A lateral instruction requires the definition of at least a subset of them (latitude and longitude) to properly define a solvable DAE system.

²⁸ The longitudinal profile describes the trajectory in the vertical plane. This is defined by AIDL instructions belonging to the Vertical, Speed, and Propulsion profiles.

For *HOLD* and *OPEN LOOP* instructions, the variability of the initial conditions (measured through the standard deviation [σ_{sv}] of the distribution that characterises their variability normalised with respect to the distribution mean value [μ_{sv}]) is directly propagated to the outputs as follows:

$$CV_{final}^{initial} = CV_{final}^{final} \rightarrow \frac{\sigma_{sv}^{initial}}{\mu_{sv}^{initial}} = \frac{\sigma_{sv}^{final}}{\mu_{sv}^{final}} \quad (6-4)$$

Figure 6-6 shows how the uncertainty in initial altitude and speed is propagated for an aircraft flying in cruise conditions (constant Mach and geopotential pressure altitude).

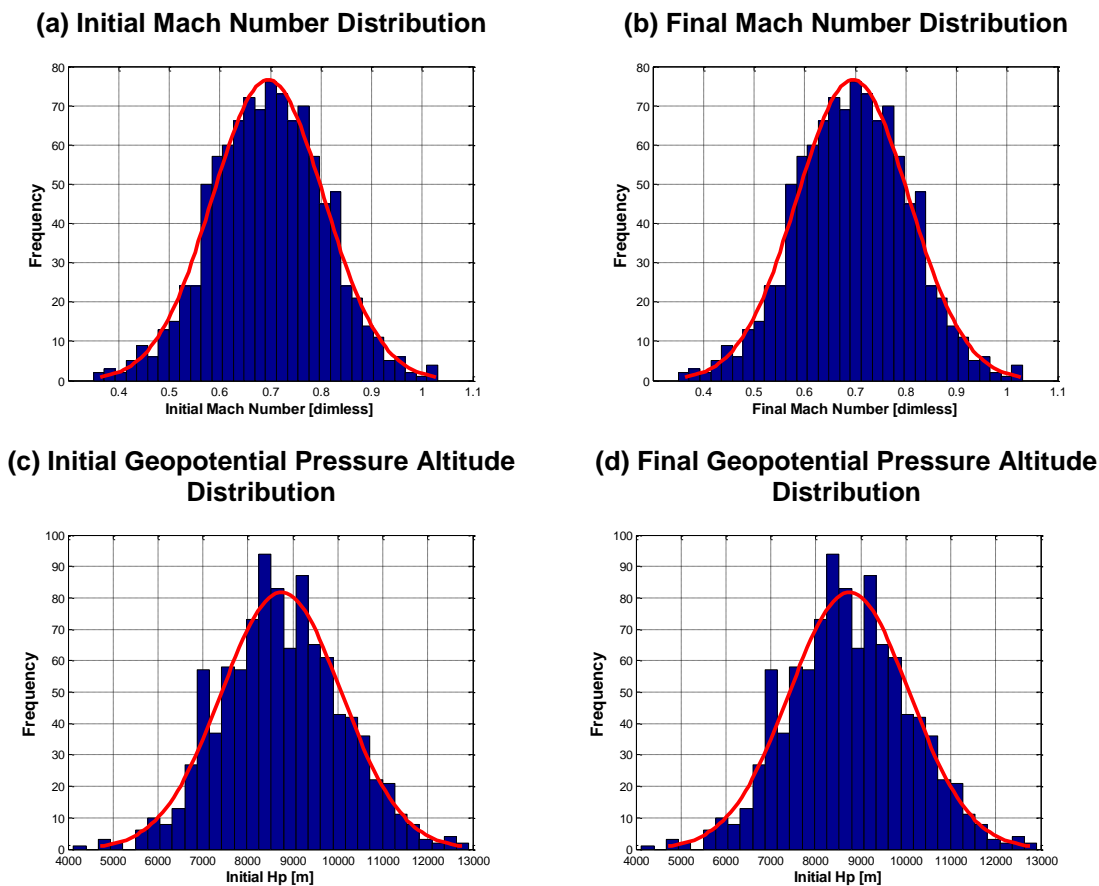


Figure 6-6 – Propagation of Initial Speed and Altitude Uncertainties in Cruise Trajectory Prediction at Constant Speed

In the case of *TRACK* instructions (*TLP* in the case of the Lateral profile), the mathematical formulation of the motion constraint will determine how the uncertainty is propagated. There are two *TLP* specifiers that relate the evolution of latitude and longitude: geodesic or circular arc. Both can be defined by following different alternatives (e.g., geodesic defined by initial and final points, or initial point and initial heading; circular arc of radius R between 2 points,

or initial point and heading, and final point and heading). All possibilities propagate the uncertainty following the Equation (6-4), except those that use the final point to define the corresponding geometry. For such cases, the uncertainty diminishes with the time (or the flown distance) until becoming null at the final point. Figure 6-7 depicts two examples of this behaviour for the geodesic and circular arc specifiers.

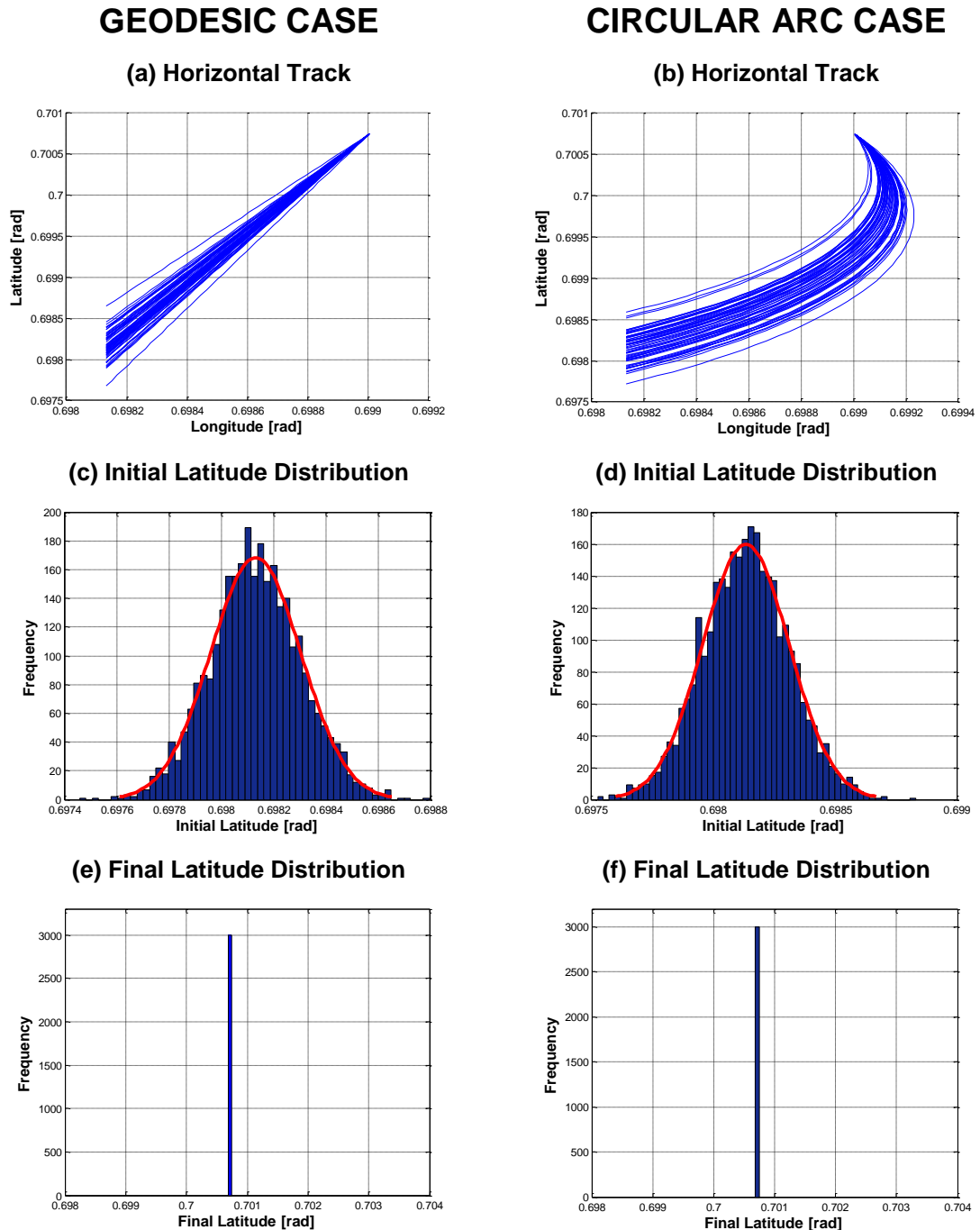


Figure 6-7 – TLP - Position Uncertainty

LAW instructions show similar behaviour as *TRACK* instructions. If the equation that describes the motion constraint is defined by a transition between an initial condition and a target value (for instance, a linear *CL* with target course of 10°), the uncertainty related to the constrained state variable decreases until reaching the target value (the heading uncertainty at the end of the operation is null as depicted in Figure 6-8). For the remaining state variables, the uncertainty propagation is driven by the Equation (6-4).

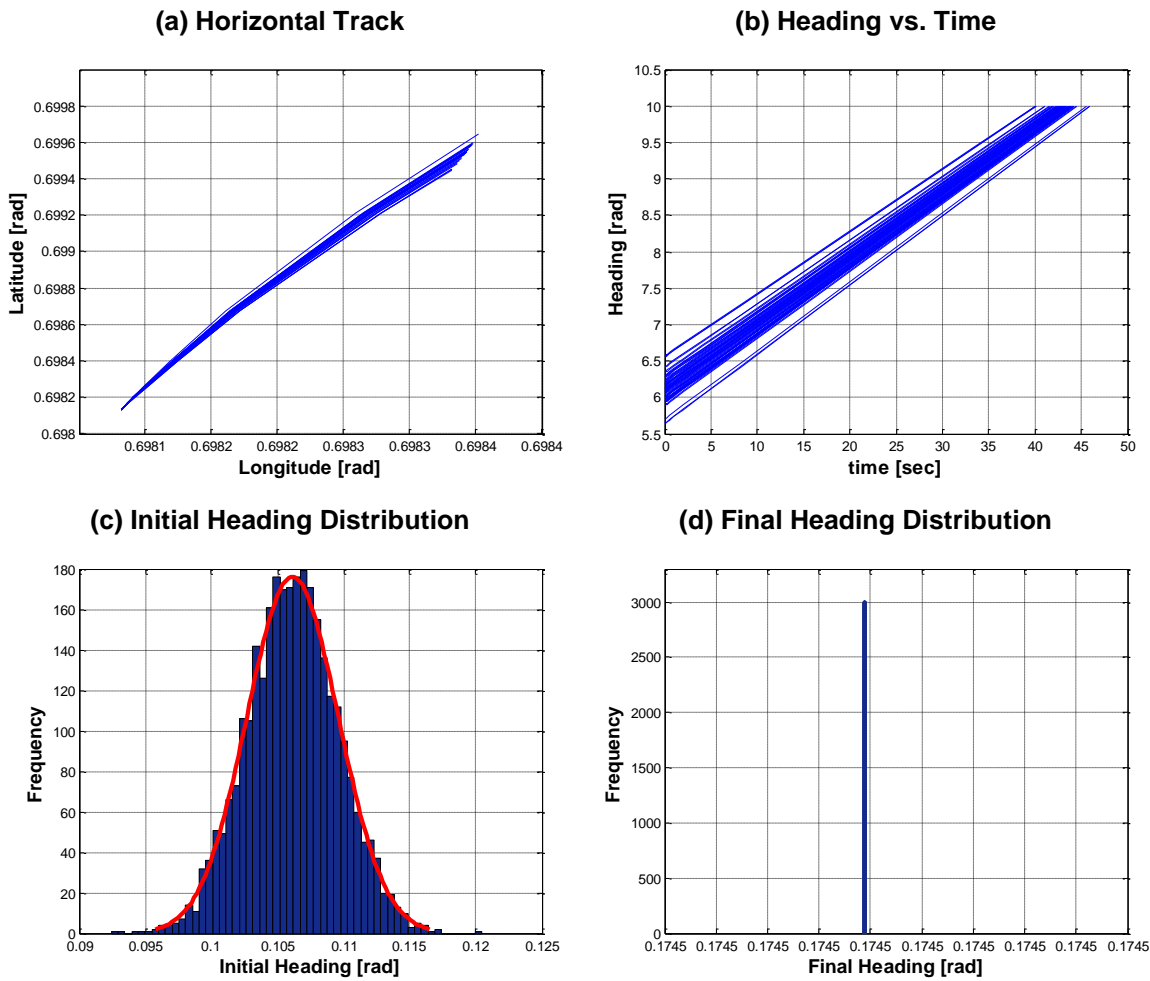


Figure 6-8 – Heading Uncertainty in CL Instructions

Of particular interest is the relationship between initial heading and position uncertainties. The initial heading uncertainty is propagated to the final position uncertainty, which means that the final longitude and latitude uncertainties are driven by the uncertainty of the initial heading. However, the uncertainty of the initial position does not affect the heading uncertainty. Therefore, the variability of the initial longitude and latitude do not add any uncertainty either to the initial or to the final heading.

6.4.2.2 Vertical Profile

The vertical profile is defined by two AIDL instructions belonging to the speed, vertical, or propulsion AIDL profiles. The initial conditions required for posing a solvable aircraft motion problem will depend on how those instructions are selected. The basic set of longitudinal initial conditions will contain the altitude (h), speed (V_{TAS}), and aircraft mass²⁹ (m) at the initial instant. Additionally, based on the state variables affected by the considered vertical profile instructions, information related to the initial value of those state variables will be required as well.

As stated in Table 6-1, the remaining state variables that might require initialisation by an initial condition value are: the acceleration factor ($\frac{V_{TAS}}{g} \frac{dV_{TAS}}{dh}$), the path angle (γ_{TAS}), the rate of climb ($V_{TAS} \sin \gamma_{TAS}$), and the throttle parameter (δ_T).

The evolution of the uncertainty will depend on the combination of the two selected instructions, which finally determine the type of trajectory to be executed by the aircraft.

According to the flight conditions, it is possible to group the trajectories into two types: level segments (in which the altitude is constant) and climbs/descents (in which the altitude varies). For each group, the uncertainty propagation is studied independently as described below.

- Level segments. These trajectory segments are defined by a combination of a *Hold Altitude* (HA) instruction and an instruction belonging to the AIDL *Speed* or *Propulsive* profiles. The uncertainty throughout the considered interval will be directly propagated for the altitude, speed, and throttle parameter variables according to Equation (6-4), as in the cases of *Hold Speed* (HS), *Hold Horizontal Speed* instruction, *Throttle Law* (TL), *Hold Throttle* (HT), or *Open Loop Throttle* (OLT) instructions. The uncertainties supported by the acceleration factor, path angle, and rate of climb will be null due to the invariability of the altitude.

²⁹ The aircraft mass is a state variable that affects both the lateral and longitudinal profiles' initialization.

The mass uncertainty should be driven by the mass, speed, and altitude uncertainties at the initial state. At different altitudes and speeds, the fuel burnt by the engine is different, and therefore, affects aircraft mass at the final state. However, the influence of the two latter is much lower than the impact of the initial mass uncertainty.

The following Equation (6-5) relates the uncertainty of the initial Mach number (M), geopotential pressure altitude (Hp), and mass,

$$\left(\frac{\sigma_{mass}}{\mu_{mass}}\right)_{final} = a_1 \left(\frac{\sigma_M}{\mu_M}\right)_{initial} + a_2 \left(\frac{\sigma_{Hp}}{\mu_{Hp}}\right)_{initial} + a_3 \left(\frac{\sigma_{mass}}{\mu_{mass}}\right)_{initial} \quad (6-5)$$

The coefficients a_i , which is dependent of the aircraft type and flying conditions, can be computed by a fitting process with respect to the data obtained by means of a series of Monte Carlo simulations. The Monte Carlo runs have been designed considering the following hypotheses:

- The selected aircraft type is a Boeing 737-800 (B738W26 BADA 4.1 designator).
- The trajectory is described by a constant flight level of FL260 and Mach speed of 0.65.
- The initial aircraft mass is 69,000 kg.
- The variability of the initial altitude, speed, and mass is considered Gaussian. The extrapolation of the proposed method to other different probability distributions is direct.
- The altitude and speed uncertainties defined by standard deviations of the distributions that characterise them (σ_M and σ_{Hp} respectively) with respect to the nominal value (μ_M and μ_{Hp} respectively) are set to 15 percent, while the mass uncertainty (σ_{mass}) normalised respect to the nominal mass value (μ_{mass}) is set to 5 percent.

Table 6-12 summarises the values obtained for the coefficients of the proposed model after fitting them to the outputs of Monte Carlo simulations.

Table 6-12 – Values of the Identified Mass Uncertainty Model Coefficients

a_1	a_2	a_3
0.0053	-0.0032	0.99

The rRMSE of the proposed mass uncertainty model with respect to the data produced by the Monte Carlo runs is 4.3 percent. This results shows that the mass uncertainty model is slightly dependant of the initial speed and altitude uncertainties. Their impact on the variability of the aircraft mass at the end of the execution interval can be dismissed compared to the initial mass uncertainty. Therefore, the mass uncertainty model can be simplified to that described in Equation (6-4). The rRMSE in this case is 3.9 percent, which represents even an improvement of the accuracy for this particular case.

- Climb and descent segments. These trajectories are characterised by an altitude change between the initial and final aircraft states. Depending on the type of AIDL instructions used for modelling such segments, the output state variables will support differently the uncertainty propagation. *HOLD* and *OPEN LOOP* instructions will conserve the inputs uncertainty, while the effect of *LAW* instructions will vary according to the description of the instruction effect. For instance, in the case of *LAW* instructions defined between the initial conditions and a target value, the uncertainty will decrease reaching the imposed target value and will increase from then on. *TRACK* instructions are limited to just one in the longitudinal profile: *Track Vertical Path (TVP)*. This instruction is used for describing geometry on the vertical plane. Considering that this geometry is adequately defined to reach a fixed altitude at a designated waypoint, the impact of this instruction in the altitude uncertainty will be a reduction with respect to the initial altitude uncertainty.

The altitude and speed uncertainties are propagated through the state variables not constrained by the instruction effect. Regardless of the description of the climb/descent segments, the following Equation (6-6) establishes a model of the uncertainty induced by the speed and altitude uncertainties on the other state variables at the end of the execution interval.

$$\begin{aligned}
\left(\frac{\sigma_{stv}}{\mu_{stv}}\right)_{final} &= b_1 \left(\frac{\sigma_M}{\mu_M}\right)_{intial}^3 + b_2 \left(\frac{\sigma_{Hp}}{\mu_{Hp}}\right)_{intial}^3 + b_3 \left(\frac{\sigma_M}{\mu_M}\right)_{intial}^2 \\
&+ b_4 \left(\frac{\sigma_{Hp}}{\mu_{Hp}}\right)_{intial}^2 + b_5 \left(\frac{\sigma_M}{\mu_M}\right)_{intial} \left(\frac{\sigma_{Hp}}{\mu_{Hp}}\right)_{intial} \\
&+ b_6 \left(\frac{\sigma_M}{\mu_M}\right)_{intial} + b_7 \left(\frac{\sigma_{Hp}}{\mu_{Hp}}\right)_{intial}
\end{aligned} \tag{6-6}$$

The coefficients b_i , which are dependent on the aircraft type and the initial operational conditions, can be obtained by fitting the model to the outputs generated in a series of Monte Carlo runs. The Monte Carlo runs have been designed considering the following hypotheses:

- The selected aircraft type is a Boeing 737-800 (B738W26 BADA 4.1 designator).
- The trajectory is described by a climb at Maximum Climb rating and constant Mach 0.39.
- The initial geopotential pressure altitude is 3,000 ft.
- The initial aircraft mass is 76,000 kg.
- The variability of the initial altitude and speed is considered Gaussian. The extrapolation of the proposed method to other different probability distributions is direct.
- The altitude and speed uncertainties defined by standard deviations of the distributions that characterise them (σ_M and σ_{Hp} respectively) with respect to the nominal value (μ_M and μ_{Hp} respectively) range from 0 up to 15 percent.

Figure 6-9 depicts the modelled and raw data for the following state variables: acceleration factor (AF), aerodynamic path angle, and rate of climb (ROC). The model returns an rRMSE of 2.8 percent, 7.7 percent, and 6.8 percent respectively.

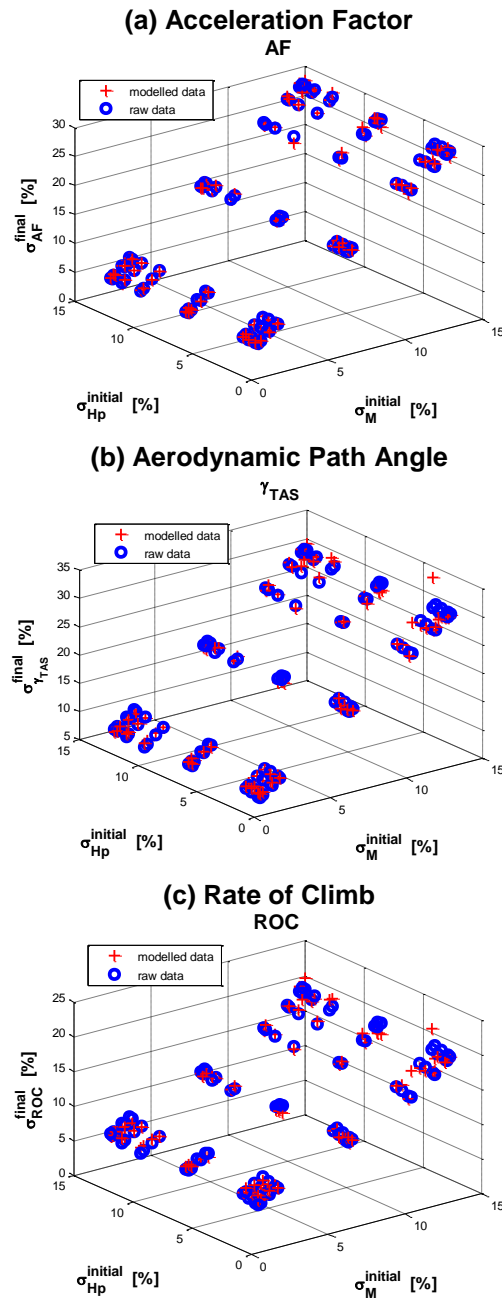


Figure 6-9 – AF, γ_{TAS} and ROC Uncertainties in Climbs at Constant Speed

Analogously to the climb example, the validity of the proposed model has been studied in a descent case. The Monte Carlo simulations were designed according to the assumptions described below:

- The selected aircraft type is a Boeing 737-800 (B738W26 BADA 4.1 designator).

- The trajectory is described by a descent at Low Idle (LIDL) rating and constant Mach 0.73.
- The initial geopotential pressure altitude is 33,000 ft.
- The initial aircraft mass is 73,000 kg.
- The variability of the initial altitude and speed is considered Gaussian.
- The altitude and speed uncertainties (σ_M and σ_{Hp} respectively) with respect to the nominal value (μ_M and μ_{Hp} respectively) range from 0 up to 15 percent.

As shown in Figure 6-10, the uncertainty model fits the outputs obtained from the Monte Carlo runs with high accuracy. The rRMSEs for the state variables AF, γ_{TAS} , and ROC are 6.2 percent, 8.3 percent, and 7.8 percent respectively, which are of the same order as those obtained in the climb case.

In these cases, the altitude and speed uncertainties impact the propagation of the mass uncertainty, although the main factor is the mass uncertainty at the initial aircraft state, as happened in the previous level segment case. Thus, the model proposed in Equation (6-4) is the best alternative to calculate the mass uncertainty at the final aircraft state. Figure 6-11 includes the plots showing the evolution of the final mass uncertainty as a function of the initial mass uncertainty for both climb and descent cases.

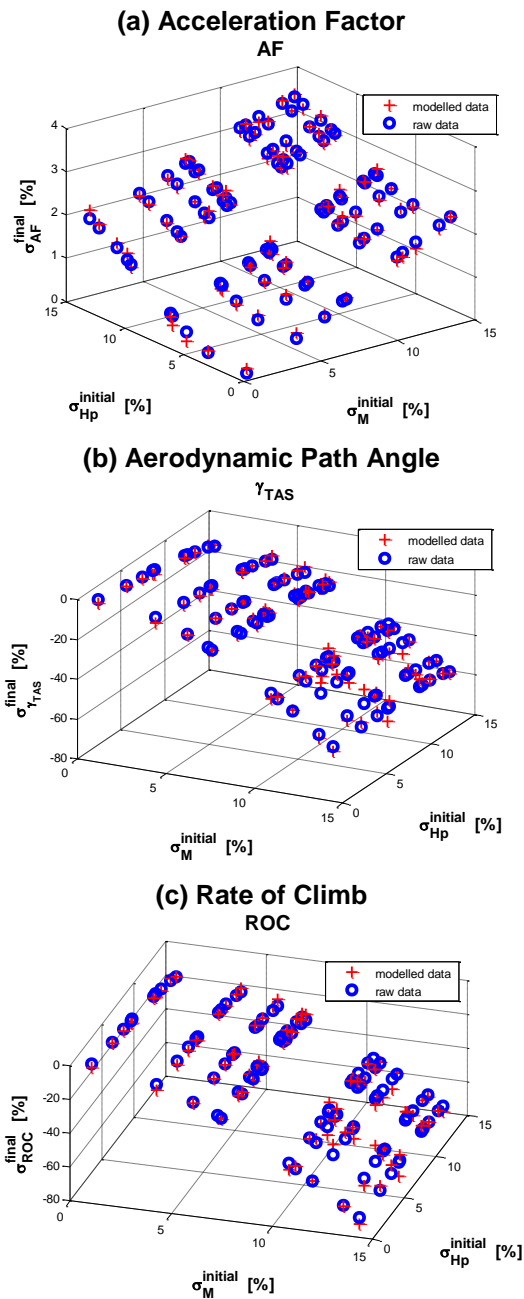
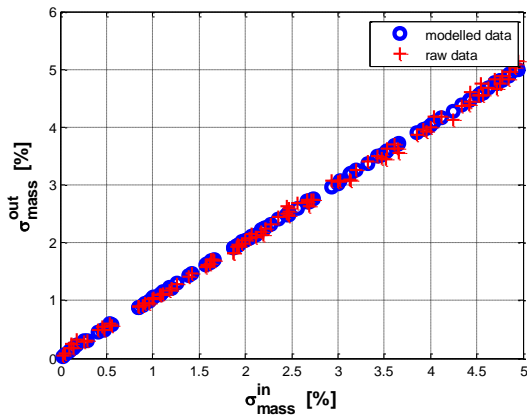


Figure 6-10 – AF, γ_{TAS} and ROC Uncertainties in Descents at Constant Speed

(a) Climb at MCMB rating and constant Mach speed



(b) Descent at LIDL rating and constant Mach speed

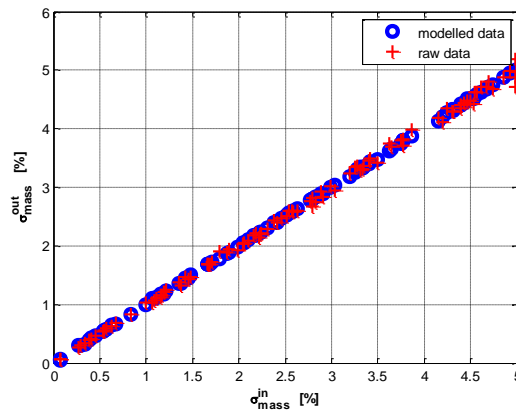


Figure 6-11 – Mass Uncertainties in Climbs and Descents at Constant Speed

6.5 Uncertainty Propagation between Operations

Since a trajectory can be described as a chronologically ordered sequence of operations, the initial conditions of each operation (solvable DAE system) in the sequence will be affected by the uncertainty in the output of the previous operation. The so-called continuity uncertainty models show uncertainty is transferred from one operation to the following operation in the chronological sequence.

As stated in Section 6.3.2, the initial conditions must comply with the geometric, kinematic, configuration, and hidden constraints. The first three constraint types are explicit constraints that define the AIDL instructions and whose effect on uncertainty prediction was studied previously in Section 6.4.1. The last constraint type represents mathematical conditions that ensure the solvability of the DAE system. These constraints limit the variability of some state variables whose effect is a reduction of the uncertainty related to such state variables.

Following the example proposed in Section 6.3.2, a level trajectory segment can be described by imposing an altitude constraint $g_1(h) = 0$. This explicit geometric constraint leads to a hidden constraint that limits the value of the path angle to zero ($\gamma_{TAS} = 0$). Hence, independently of the uncertainty in the path angle coming from the output of the previous DAE system, the path angle uncertainty introduced to following DAE system will be null by the effect of the hidden constraint.

For each type of solvable DAE system, there is a set of hidden constraints that will remove the uncertainty of the state variables affected by those hidden constraints. This may generate a singularity in the variable affected by the hidden constraint. *SET* instructions are used to introduce transition phases that avoid such discontinuities in the affected state variable. For instance, level segments are typically preceded by climb/descent segments. The transition between them can be modelled by a Set Path Angle (SPA) instruction that describes the evolution of the path angle from the climb/descent value up to zero. This instruction ensures the continuity of the path angle throughout the complete trajectory.

As described above in Section 6.3.1, the outcome of using *SET* instructions is a reduction of the uncertainty related to the state variable affected by the instruction effect.

The propagation of uncertainty between consecutive operations is thus governed by the hidden constraints, which restrict the variability of certain state variables at the beginning of the next operation in the sequence. They limit the uncertainty propagation constraining its growth with time.

6.6 Summary

In this chapter, different sources of AI uncertainty were identified based on the elements that encompass the AIDL. Two main AI uncertainty elements were studied: instruction's effect and trigger. This approach considers an AI instance as described by a set of six known compatible AIDL instructions. The instructions' specifiers are assumed to be known, as well. Variations of the instruction type or specifier correspond to descriptions of other different AI instances and, therefore, to descriptions of other different trajectories. Thus, the uncertainty analysis provided in this chapter is circumscribed to the study of a known description of a trajectory subject to those two aforementioned sources of uncertainty.

In addition, although they are not intrinsically considered as part of an AI description, the initial conditions' uncertainty has been also studied in this chapter because of its strong relationship with the AIDL instructions. The instruction effect propagates the uncertainty of the initial conditions in accordance with the mathematical formulation of the constraint it represents.

The uncertainty analysis and modelling provided in this chapter is circumscribed to the study of a known description of an AI subject to the aforementioned sources of uncertainty.

The uncertainty has been modelled through the standard deviations of the probabilistic density functions used for describing the variability of the considered parameters. For illustrative purposes, the distributions selected were Gaussian, although the same methodology would be applicable to any other type of probability distribution that characterises the uncertainty of the different parameters studied in this chapter.

The proposed uncertainty models are polynomial representations that relate the standard deviation of the distribution of the output state variables to the standard deviations of the uncertainty sources. The models coefficients were identified against a set of trajectories computed according to the definition of several Monte Carlo experiments. For each source of uncertainty and operational condition, the polynomial that best represents the uncertainty effect of the final aircraft state variables was identified. To apply the proposed method in practice, the polynomial coefficients identification process would have to be extended to a representative set of operational conditions, generating a database of coefficients that provides the optimal polynomial depending on the actual aircraft weight, position, and speed.

Finally, the propagation of the uncertainty through a complete trajectory described by a chronologically ordered sequence of AIDL operations is driven by continuity uncertainty. This uncertainty represents how the output uncertainty of an operation is transferred to the next one in the sequence. This propagation is limited by the hidden constraints of the DAE system, establishing the process of obtaining the initial conditions of the next operation as a function of the final aircraft state of the previous one.

CHAPTER 7

QUANTIFICATION OF TRAJECTORY PREDICTION UNCERTAINTY

7.1 Introduction

Previous chapters of this dissertation provided individual models to quantify the uncertainty introduced by input parameters to the prediction of an aircraft trajectory. CHAPTER 4 proposes a method to evaluate the impact of using generic aircraft performance models that do not capture the actual aerodynamic and power plant performance. The impact on the predicted trajectory can be measured assuming constant deviations of the drag polar and fuel consumption polynomial models. The relationship between degraded performance and prediction outputs are described by linear models of the considered deviations. CHAPTER 5 analyses the effect of weather forecast uncertainty, with a special focus on using weather forecast ensembles. The trajectory prediction uncertainty due to weather stochasticity is a function of the variation of temperature, pressure, and wind conditions with time, location, and altitude. The use of forecast ensembles provided by the meteorological agencies leads to an ensemble of trajectory predictions that represent the trajectory variability introduced by the uncertainty of weather models. Finally, CHAPTER 6 discusses how aircraft intent uncertainties affect trajectory prediction and it provides models that represent the impact of different elements of an aircraft intent description, including the initial conditions, on the final aircraft state.

All of those individual analyses can be used simultaneously to evaluate the uncertainty of a prediction. However, it is a prerequisite to have a database with the coefficients that identify the polynomial approximations representing the uncertainty of different sources for each aircraft type and operational conditions. This means that the models proposed in Sections 4.5 and 6.4 need to cover the complete flight and environmental envelopes. Thus, although theoretically this approach would return a quantification of the prediction uncertainty of any possible trajectory, in practical terms it becomes almost inapplicable. For instance, an ANSP

would have to own a database for any potential aircraft that operates within the airspace under its responsibility. This database should encompass the polynomial descriptions of any possible trajectory in the range of all possible aircraft masses. In addition, the resulting models should be combined with the weather uncertainty represented by the time-lagged ensemble of ensembles to obtain a complete representation of prediction uncertainty.

To overcome all of the drawbacks revealed by this approach, this chapter proposes a quantification method based on the use of the Polynomial Chaos theory. Polynomial Chaos Expansion is presented as the most suitable technique compliant with expected flexibility and efficiency. A summary of the PCE theoretical basis, with a special focus on arbitrary PCE, is followed by its application to trajectory uncertainty quantification. In addition, a sensitivity analysis based on a set of Sobol indices computed directly from the polynomial expansions is also introduced.

The applicability of this method is analysed through an extensive case study, considering different uncertainty sources. The results are compared with those obtained from a Monte Carlo simulation, as a verification exercise.

Finally, two examples of how to make use of the proposed uncertainty quantification process based on PCE are presented.

7.2 Uncertainty Quantification Based on Polynomial Chaos Expansions

The prediction of an aircraft trajectory is determined by the model used to describe aircraft motion (Section 3.4), a representation (polynomial or data tables) of aircraft performance (Section 3.7), a description of aircraft intent (Section 3.9), an estimate of the initial state (Section 3.3), and a forecast of weather conditions (Section 3.8). Although methodologies and techniques were developed to accurately define those elements, the intrinsic stochastic nature of the prediction problem leads to unavoidable deviations between actual and predicted trajectories.

A PC expansion is a way of representing a random variable as a function of the other random variables identified by a probability distribution described by a polynomial expansion [136]. PCE enables the capability of studying non-linear effects with high accuracy in a very efficient manner (especially compared with Monte Carlo approaches, which are usually more inefficient to analyse very large and complex systems). PCE represents a mathematical

representation of a system response in the form of a high dimensional polynomial of uncertain parameters.

The application of PCE discriminates between intrusive [137] and non-intrusive methods [138][139]. The intrusive methods, like Galerink projection, require a manipulation of the equations that describe the system behaviour. This approach usually implies an increase in complexity of the problem formulation, which leads to arduous resolution processes. Non-intrusive or data-driven methods, like sparse quadrature or probabilistic collocation, make use of selected system outputs to identify the corresponding polynomial expansion. These methods treat the system as a black box that generates a set of outputs that are used afterward to estimate the polynomial coefficients by, for instance, regression techniques [140].

Originally, PCE was applied to model normally distributed random variables. To cope with different input distributions, PC methods evolved to the generalised PC (gPC). These solutions rely on the Askey scheme of orthogonal polynomials and extend the usability of this technique to other non-Gaussian parametric distributions like Uniform, Gamma, or Beta [141] (Appendix E-1). These alternatives require exact knowledge of the involved distributions, which is not the case in most real systems. In these situations, the lack of complete input information may introduce additional uncertainty in the identification of the output distributions. To manage incomplete or/and implicit distributions only defined by their moments, the use of Gram-Schmidt orthogonalisation led to the definition of the arbitrary PC (aPC) method [142]. In aPC, the exact probability description of the inputs is not strictly necessary. For a finite-order expansion, only a finite number of statistical moments are required. This method enables data-driven applications of the PC theory, in which data samples with limited size allow the inference of the polynomial description of the system outputs as a result of the impact of uncertain inputs described by arbitrary distributions (e.g., discrete, continuous, discretised continuous).

It should be noted that the PCE methodology has been extensively applied to different research fields like petroleum engineering [143], fluids dynamics [144], aerodynamic design [145], stochastic finite elements [146], micro-electromechanical systems (MEMS) [147] and vehicle dynamics [148], among others. These applications have illustrated the potential power of this technique and thus indicated its usefulness for the work presented here.

7.2.1 One-dimensional PCE

Considering the stochastic process in the probability space (Ω, A, Γ) with space of events Ω , σ -algebra A and probability measure Γ , the stochastic model $\Psi = f(\xi)$ with model input and model output Ψ can be expanded as follows:

$$\Psi = \sum_{i=0}^{\infty} A_i P^i(\xi) \quad (7-1)$$

For practical reasons, the series are usually truncated to a finite number of terms as follows:

$$\Psi \approx \sum_{i=0}^d A_i P^i(\xi) \quad (7-2)$$

where d is the order of the expansion, A_i are the expansion coefficients and $P^{(i)}$ are the polynomials of order i that define the orthogonal (or orthonormal) basis $\{P^{(0)}, \dots, P^{(d)}\}$ with respect to the measure Γ . Contrary to other PC methods in which Γ must have a known form, in aPC, Γ can have any arbitrary form and, therefore, the basis $\{P^{(0)}, \dots, P^{(d)}\}$ needs to be specifically found. If Ψ is expanded in this orthonormal basis, the statistical properties of Ψ can be evaluated directly from the expansion coefficients \bar{a}_i using the following expressions:

$$\text{mean}(\Psi) = A_0 \quad (7-3)$$

$$\text{std}(\Psi) = \sum_{i=1}^{\infty} A_i^2 \approx \sum_{i=1}^d A_i^2 \quad (7-4)$$

These results are based on the orthonormality of the basis used to define the expansion.

7.2.2 Multi-dimensional PCE

One-dimensional aPCs are only used to model the response of systems with a unique stochastic input, which restricts significantly its applicability. Real systems are affected by multiple stochastic factors that influence the system response differently. Thus, a stochastic process Ψ can be described by a multivariate polynomial expansion of n input parameters $\{\xi_1, \dots, \xi_n\}$ as follows:

$$\Psi(\xi_1, \dots, \xi_n) \approx \sum_{i=0}^m B_i \Phi_i(\xi_1, \dots, \xi_n) \quad (7-5)$$

In this case, Φ_i represents the multivariate polynomials that constitute the orthogonal basis for the input variables $\{\xi_1, \dots, \xi_n\}$ and m is the size of the polynomial basis (number of coefficients of the expansion).

Assuming the independence of the input variables, the multivariate polynomials are obtained by the combination of univariate polynomials:

$$\Phi_i = \prod_{j=1}^n P_j^{(o_j^k)}(\xi_1, \dots, \xi_n) \quad (7-6)$$

where o_j^k is an integer that represents the combination of all possible products of individual univariate basis (Appendix E-2) and satisfies the following expression:

$$\sum_{j=1}^n o_j^k \leq \bar{q} \quad (7-7)$$

$$k = 1, \dots, m$$

The number of input parameters n and the order of the expansion d establish the size of the polynomial basis and, therefore, the number m of B coefficients to be identified as follows:

$$m = \binom{d+n}{d} = \frac{(d+n)!}{d! n!} \quad (7-8)$$

As stated above, the presented approach assumes that the stochastic parameters are independent or, at most, linearly correlated. In this latter case, a pre-process for removing the correlation, for instance by a linear transformations, is required prior to the identification of the PCE.

7.2.3 PCE Based on Statistical Moments

Contrary to gPC, where the orthonormal basis is known according to the distribution that characterises the stochastic input parameters, aPC methods require construction of such a basis of polynomials for every set of input parameters [149]. Depending on the type of the input distributions and the available knowledge of them, the orthonormal basis will take different forms. The orthogonality between polynomials of order q and r are defined as:

$$\frac{1}{\|P^{(q)}\|^2} \int_{\xi \in \Omega} P^{(q)}(\xi) P^{(r)}(\xi) d\Gamma(\xi) = \delta_{qr} \quad (7-9)$$

$$\forall q, r \in [0, d]$$

where δ_{qr} is the Kronecher delta and $\|P^{(q)}\|^2$ is the norm of the polynomial $P^{(q)}$ used to generate an orthonormal basis.

Considering that the univariate polynomial $P^{(q)}$ of order q can be expressed as follows:

$$P^{(q)}(\xi) = \sum_{i=0}^q C_i^{(q)} \xi^i \quad (7-10)$$

$$\forall q \in [0, d]$$

where $C_i^{(q)}$ are the coefficients of the polynomial $P^{(q)}$, the orthogonal condition of this polynomial with all lower-order polynomials, assuming that the coefficients of highest order of all polynomials are equal to 1 ($C_q^{(q)} = 1$), is defined by the following system of equations:

$$\int_{\xi \in \Omega} C_0^{(0)} \left[\sum_{i=0}^q C_i^{(q)} \xi^i \right] d\Gamma(\xi) = 0$$

$$\int_{\xi \in \Omega} \left[\sum_{i=0}^1 C_i^{(1)} \xi^i \right] \left[\sum_{i=0}^q C_i^{(q)} \xi^i \right] d\Gamma(\xi) = 0 \quad (7-11)$$

$$\vdots$$

$$\int_{\xi \in \Omega} \left[\sum_{i=0}^{q-1} C_i^{(q-1)} \xi^i \right] \left[\sum_{i=0}^q C_i^{(q)} \xi^i \right] d\Gamma(\xi) = 0$$

$$C_q^{(q)} = 1$$

This system is closed and determines the coefficients $C_i^{(q)} \forall i \in [0, q]$ of the considered orthogonal basis. Substituting the first equation into the second, the first and the second into the third, and so on, it is possible to reformulate the system of equations in a more suitable fashion:

$$\int_{\xi \in \Omega} \sum_{i=0}^q C_i^{(q)} \xi^i d\Gamma(\xi) = 0$$

$$\int_{\xi \in \Omega} \sum_{i=0}^q C_{i+1}^{(q)} \xi^{i+1} d\Gamma(\xi) = 0$$

$$\vdots$$

(7-12)

$$\int_{\xi \in \Omega} \sum_{i=0}^q C_{i+q-1}^{(q)} \xi^{i+q-1} d\Gamma(\xi) = 0$$

$$C_q^{(q)} = 1$$

On the other hand, the q^{th} raw moment μ_q of the random variable ξ is defined by the following expression:

$$\mu_q = \int_{\xi \in \Omega} \xi^q d\Gamma(\xi) \quad (7-13)$$

This expression can be used for rearranging the system of equations (7-13) as follows:

$$\begin{aligned}
\sum_{i=0}^q C_i^{(q)} \mu_i &= 0 \\
\sum_{i=0}^q C_{i+1}^{(q)} \mu_{i+1} &= 0 \\
&\vdots \\
\sum_{i=0}^q C_{i+q-1}^{(q)} \mu_{i+q-1} &= 0 \\
C_q^{(q)} &= 1
\end{aligned} \tag{7-14}$$

This rearrangement represents a system of linear equations that can be written in a more convenient matrix form:

$$\begin{bmatrix}
\mu_0 & \mu_1 & \cdots & \mu_q \\
\mu_1 & \mu_2 & \cdots & \mu_{q+1} \\
\vdots & \vdots & \ddots & \vdots \\
\mu_{q-1} & \mu_q & \cdots & \mu_{2q-1} \\
0 & 0 & \cdots & 1
\end{bmatrix}
\begin{bmatrix}
C_0^{(q)} \\
C_1^{(q)} \\
\vdots \\
C_{q-1}^{(q)} \\
C_q^{(q)}
\end{bmatrix}
=
\begin{bmatrix}
0 \\
0 \\
\vdots \\
0 \\
1
\end{bmatrix} \tag{7-15}$$

The condition to obtain the coefficients $C_i^{(q)}$ requires that the matrix of moments is not singular. This condition is satisfied if the number of support points in the distribution ξ is greater than q , and all moments up to $2q-1$ exist and are finite. The basis of orthogonal polynomials $\{P^{(0)}, \dots, P^{(q)}\}$ of order q is obtained by solving the system defined in Equation (7-15) for each individual stochastic parameter ξ .

Thus, this approach avoids the need of having a complete representation of any input distribution ξ . It is only necessary to calculate a finite number of moments from the raw data. This condition assumes that any deviation between the actual distribution and raw data represented by moments of higher order than $2q-1$ will not be captured by the identified PCE.

7.2.4 Non-intrusive Determination of PCE Coefficients

Once the orthogonal basis of polynomials is set for each stochastic input parameter ξ_i as explained in Section 7.2.3, the multivariate PCE is determined by the identification of coefficients B_i in Equation (7-5).

Probabilistic Collocation Method (PCM) is a non-intrusive technique that provides values for the referred coefficients by evaluating a finite set of the system outputs. This method considers the system as a black box that produces a set of outputs from intentionally selected sets of inputs. The PCM returns a list of p sets of collocation points $(\xi_1^1, \dots, \xi_n^1) \dots (\xi_1^p, \dots, \xi_n^p)$ at which the system requires to be evaluated, generating the associated set of p outputs (Ψ^1, \dots, Ψ^p) with $p \geq n$. These sets of inputs and outputs are used to estimate the multivariate expansion coefficients B_i .

This process leads to definition of the following system of p equations with m unknown coefficients:

$$\begin{aligned} \Psi^1 &= \sum_{i=1}^m B_i \Phi_i(\xi_1^1, \dots, \xi_n^1) \\ &\vdots \\ \Psi^p &= \sum_{i=1}^m B_i \Phi_i(\xi_1^p, \dots, \xi_n^p) \end{aligned} \tag{7-16}$$

where the combinations of multivariate polynomials Φ_i are defined by Equation (7-6) from the individual orthogonal basis obtained by solving the system of equations described in Equation (7-15) for each stochastic input parameter.

The collocation points are represented by the roots of the univariate polynomial of one order higher $(d+1)$ than the order of the univariate PCE (d) . In the case of multivariate problems with n independent variables, the number of collocation points reaches up to $p = (d+1)^n$ corresponding to the n combinations of the $(d+1)$ roots of the univariate polynomial expansions. In this case, this number p is much higher than the minimum necessary m as

defined by Equation (7-8), so a selection of the optimal collocation points would increase the efficiency of the identification process by reducing to the minimum the number of points at which the multivariate expansion needs to be evaluated.

Any subset of collocation points obtained from the roots of the polynomials is suitable to estimate the B_i coefficients. However, to obtain the values that best estimation of the statistical characteristics of the outputs (especially, the mean and standard deviation), the optimal approach is to strategically select the collocation points from most probable regions of the inputs' distributions. The process of selecting those points [150] can be described as follows:

- Generate of possible combinations of polynomials of order 0 to d for n polynomial basis (corresponding to n PCE of the input variables (ξ_1, \dots, ξ_n) . Following matrix depicts the case of $d = 1$ and $n = 2$.

$$\begin{bmatrix} 0 & 0 \\ 1 & 0 \\ 0 & 1 \\ 1 & 1 \\ 1 & 2 \\ 2 & 1 \\ 2 & 2 \\ 2 & 0 \\ 0 & 2 \end{bmatrix} \quad (7-17)$$

- Sort previously generated combinations of polynomials from lower or higher order of the expected multivariate PCE.

$$\begin{bmatrix} 0 & 0 \\ 1 & 0 \\ 0 & 1 \\ 2 & 0 \\ 0 & 2 \\ 1 & 1 \\ 2 & 1 \\ 1 & 2 \\ 2 & 2 \end{bmatrix} \quad (7-18)$$

- Rank the roots of the input variables (ξ_1, \dots, ξ_n) according to the distance to the mean values of the distributions that characterize the inputs variability. Following the aforementioned case of $d = 1$ and $n = 2$,

$$\begin{bmatrix} \xi_1^{root\ 1} & \xi_1^{root\ 2} & \xi_1^{root\ 3} \\ \xi_2^{root\ 1} & \xi_2^{root\ 2} & \xi_2^{root\ 3} \end{bmatrix} \quad (7-19)$$

- Build the initial set of collocation points by combining the ranked roots as defined in Equation (7-23) with the sorted matrix of polynomial combinations described in Equation (7-24).

$$\begin{bmatrix} \xi_1^{root\ 1} & \xi_2^{root\ 1} \\ \xi_1^{root\ 2} & \xi_2^{root\ 1} \\ \xi_1^{root\ 1} & \xi_2^{root\ 2} \\ \xi_1^{root\ 3} & \xi_2^{root\ 1} \\ \xi_1^{root\ 1} & \xi_2^{root\ 3} \\ \xi_1^{root\ 2} & \xi_2^{root\ 2} \\ \xi_1^{root\ 3} & \xi_2^{root\ 2} \\ \xi_1^{root\ 2} & \xi_2^{root\ 3} \\ \xi_1^{root\ 3} & \xi_2^{root\ 3} \end{bmatrix} \quad (7-20)$$

- Generate the optimal set of collocation points by removing all possible combination of polynomials that lead to a multivariate polynomial of higher order than d . Due to the matrix shown in Equation (7-20) is ordered, this is equivalent to keep the first m rows as stated by Equation (7-8) and removing the remaining ones.

$$\begin{bmatrix} \xi_1^{root\ 1} & \xi_2^{root\ 1} \\ \xi_1^{root\ 2} & \xi_2^{root\ 1} \\ \xi_1^{root\ 1} & \xi_2^{root\ 2} \\ \xi_1^{root\ 3} & \xi_2^{root\ 1} \\ \xi_1^{root\ 1} & \xi_2^{root\ 3} \\ \xi_1^{root\ 2} & \xi_2^{root\ 2} \end{bmatrix} \quad (7-21)$$

- The outcome of the process is a ranked matrix of size $n \times m$, containing the optimal set of collocation points at which the system will be evaluated to obtain the set of m outputs (Ψ^1, \dots, Ψ^m) required by Equation (7-16).

The use of the set of optimal collocation points obtained following the aforementioned process ensures that the solution of Equation (7-16) provides the values of coefficients B_i that statistically best fit the behaviour of the output multivariate polynomial expansions.

Regardless if the set of collocation points is the optimal ($p = m$) or not ($p > m$, or $p = m$ but randomly selected), the coefficients B_i can be identified by regression methods, spline interpolation or any other fitting technique.

7.3 Global Sensitivity Analysis Based on Polynomial Chaos Expansions

Assessing the impact of parameters variation on the model response is a key process to understand the propagation of uncertainty from inputs to outputs. In most cases, it is very useful to quantify and rank the impact of individual inputs. This process, known as Sensitivity Analysis (SA), is used to identify most influencing parameters and, therefore, to establish strategies to reduce or limit their impact.

According to their scope, SA methods are classified in two categories:

- Local SA (LSA), which studies the impact of inputs locally. These methods rely on the computation of the gradient of the model response with respect to the input parameters around a nominal (local) value.
- Global SA (GSA), which aims at determining how output uncertainties can be apportioned to input uncertainties [151] and quantifying the relative importance of each individual parameter in the model response.

Performing GSA usually requires evaluating the model at many points that cover the complete operational range. For this purpose, Monte Carlo simulations have proven to be a versatile approach to obtain the mean value of the outputs or to characterise the probability distribution of outputs. However, this approach usually requires a very high computational effort due to the large number of evaluation points required for completing a global assessment.

An advantage of GSA based on PCE is that this alternative explicitly offers a method to choose the optimal set of evaluation points based on the generalised mathematical theory of Gaussian integration. This leads to a computationally more efficient and flexible analyses, as opposed to other Monte-Carlo-based techniques (e.g., regression-based methods, variance-based methods, stochastic finite element methods, or structural reliability methods) [152].

7.3.1 Sobol Sensitivity Indices

Classical PCE has already been used for sensitivity analyses in multiple applications making use of an analytical computation of Sobol's indices [153]. To compute these sensitivity indices, it is required to obtain Sobol's decomposition of the polynomial expansion.

Considering the probability space (Ω, A, Γ) defined in Section 7.2.1, and the multivariate function $\Psi = \Psi(\xi_1, \dots, \xi_n)$ defined in Section 7.2.2, Sobol's decomposition of Ψ can be expressed as follows:

$$\Psi = f_0 + \sum_{i=1}^n f_i(\xi_i) + \sum_{1 \leq i < j \leq n} f_{i,j}(\xi_i, \xi_j) + \dots + f_{i,j,\dots,n}(\xi_1, \dots, \xi_n) \quad (7-22)$$

where f_0 is a constant, while the integral of each summand over any independent variable is zero, i.e.,

$$\int_0^1 f_{i_1, \dots, i_s}(\xi_{i_1}, \dots, \xi_{i_s}) d\xi_{i_k} = 0 \text{ for } 1 \leq k \leq s \quad (7-23)$$

The expression (7-23) ensures the orthogonality of the polynomials in the following sense:

$$\int_{\xi \in \Omega} f_{i_1, \dots, i_s}(\xi_{i_1}, \dots, \xi_{i_s}) f_{j_1, \dots, j_t}(\xi_{j_1}, \dots, \xi_{j_t}) d\xi_1 \dots d\xi_n = 0 \quad (7-24)$$

for $\{i_1, \dots, i_s\} \neq \{j_1, \dots, j_t\}$

The term f_0 is considered the mean value, while the terms $f_i(\xi_i)$ represent the variation of the output Ψ due to changes of the input variable ξ_i . The terms $f_{i,j}(\xi_i, \xi_j)$ represent the variation of the output Ψ due to the combined effect of variables ξ_i and ξ_j and the terms $f_{i,j,\dots,n}(\xi_1, \dots, \xi_n)$ represent the variation of the output Ψ due to the combined effect of all variables.

Assuming the independence of the input variables $\{\xi_1, \dots, \xi_n\}$, the variance of the output $V[\Psi]$ is determined by:

$$V[\Psi] = \sum_{i=1}^n V_i + \sum_{i=1}^n V_{ij} + \cdots + V_{1,\dots,n} \quad (7-25)$$

The first-order Sobol Index (S) is defined by the ratio between the variance of the output and the variation of each individual input, disregarding the effect of the remaining inputs and the combined effects as follows:

$$S_i = \frac{V_i}{V[\Psi]} \quad (7-26)$$

While higher order interaction Sobol indices, which represent the contribution of combined inputs into the output, can be obtained following same formulation:

$$\begin{aligned} S_{ij} &= \frac{V_{i,j}}{V[\Psi]} \\ &\vdots \\ S_{i\dots n} &= \frac{V_{i\dots n}}{V[\Psi]} \end{aligned} \quad (7-27)$$

The definition of these sensitivity indices leads to the following expression:

$$\sum_{i=1}^n S_i + \sum_{i<j}^n S_{ij} + \cdots + S_{1\dots n} = 1 \quad (7-28)$$

The Total Sobol Index (S_T) is defined to measure the contribution of ξ_i to the output variance, including all variance caused by its interactions, of any order, with any other input variables. This index is built by considering all terms in Equation (7-25) in which variable ξ_i appears.

$$S_{T_i} = \frac{V[\Psi]|\xi_i}{V[\Psi]} \quad (7-29)$$

Due to the fact that the interaction effect between ξ_i and ξ_j is counted in both S_{T_i} and S_{T_j} , the sum of total sensitivity indices $\sum_{i=1}^n S_{T_i}$ will only be equal to one when all higher order interaction indices are null for all possible interaction among inputs ($S_{ij} = S_{ijk} = \cdots = S_{1\dots n} = 0$). In any other circumstance, $\sum_{i=1}^n S_{T_i} > 1$.

Comparing Equations (7-5) and (7-22) it is straightforward to deduce how to obtain the Sobol indices corresponding to a PCE. Considering the orthogonality of the polynomial chaos basis, the mean and variance of the output distribution is calculated by:

$$E[\Psi] = B_0$$

$$V[\Psi] = \sum_{i=1}^n B_i^2 \quad (7-30)$$

Substituting the definition of $V[\Psi]$ provided by Equation (7-30) in Equations (7-26), (7-27), and (7-29), it is possible to obtain the Sobol indices as a function of the coefficients of PCE that characterise the system output [154].

$$S_{i_1, \dots, i_s} = \frac{\sum_{i=2}^n \lambda_j B_i^2}{\sum_{i=2}^n B_i^2} \quad \text{where } \lambda_j = \begin{cases} 1 & \text{if } o_j^k > 0 \forall j \in (i_1, \dots, i_s) \\ 0 & \text{if } \exists j \in (i_1, \dots, i_s) / o_j^k = 0 \end{cases}$$

$$S_{T_j} = \sum_{(i_1, \dots, i_s): j \in (i_1, \dots, i_s)} S_{i_1, \dots, i_s} \quad (7-31)$$

The index represents the sum of all Sobol indices in which the variable ξ_j contributes to the variation of the output, considering simultaneously its individual contribution and its interactions with all the remaining variables.

7.4 Application of PCE-based Uncertainty Quantification to Trajectory Prediction

The methodology presented in the previous section, based on aPCE, is applied to the quantification of uncertainty in multiple dynamic systems. A main novelty proposed in this dissertation is the application of this technique to the aircraft motion problem to derive quantitative representations of trajectory prediction uncertainties.

To illustrate how to apply the uncertainty quantification process described in Section 7.3 and the sensitivity analysis proposed in Section 7.3, a case study will be analysed in this section. This case study will be used to evaluate the effect of different sources of uncertainty that affect trajectory prediction by means of a polynomial description that will enable the

analytical calculation of the output spread (characterised by the standard deviation of the output distributions) as a function of the input variability.

7.4.1 Case Study Description

The trajectory to be analysed is described by means of the AIDL. Using the framework proposed by this language, the trajectory proposed in this case study is described by the aircraft intent description depicted in Figure 7-1.

The horizontal profile is defined by the lateral thread (third motion profile), which indicates that the aircraft is flying a geodesic described by the initial position (i.e., initial latitude and longitude), and the initial heading, until reaching a waypoint located 300 km away (*trigger K*). At this WP, the aircraft initiates a turn with an 8-km radius. The turn finishes when the aircraft heading is -5° (*trigger L*). At this instant, the aircraft starts following the geodesic determined by its current position and the Metering Fix Point (MFP) of coordinates 7.25°N 57.50°E (*trigger H*), which represents the end trigger of the sequence of instructions and, therefore, the end of the prediction.

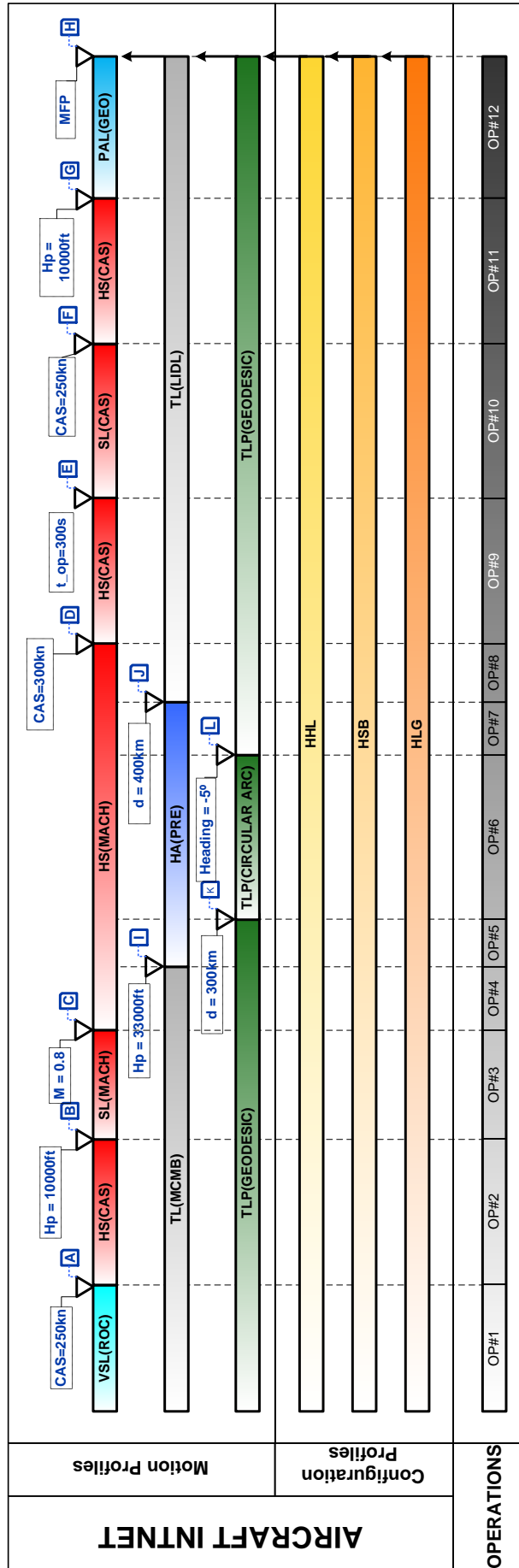


Figure 7-1 – Case Study – Aircraft Intent Description

The vertical profile is defined by the longitudinal threads (first and second motion profiles) as follows:

- Initially, the aircraft is climbing at maximum climb (MCMB) engine regime while maintaining a constant rate of climb of 2,000 ft/min. This operation ends when the CAS reaches 250 kt (*trigger A*).
- The climb continues at MCMB until crossing a geopotential altitude of 10,000 ft (*trigger B*).
- Above this altitude, the operational restriction of 250 kt CAS is not applicable and the aircraft accelerates to a cruise Mach of 0.8 (*trigger C*) with an acceleration rate of 0.005 Mach per second.
- After this event, the aircraft continues climbing at MCMB until the TOC (*trigger I*) at FL 330.
- From this point, the aircraft maintains cruise Mach and flight level until the TOD point located 400 km away from the trajectory beginning (*trigger J*).
- The descent phase is initiated then, setting the engine regime at LIDL while holding the cruise Mach speed until reaching a CAS of 300 kt (*trigger D*).
- This speed is maintained during a time interval of 5 minutes (*trigger E*).
- To respect the speed restriction below 10,000 ft, a deceleration phase is planned to reduce CAS to 250 kt (*trigger F*) with a deceleration rate of 0.02 kt/ft.
- This speed is held until crossing a geopotential altitude of 10,000 ft (*trigger G*).
- From this point, the aircraft starts a descent at a constant path angle of 2.5° until reaching the MFP (*trigger H*), the final event of the predicted trajectory.

Finally, the configuration profiles describe the aircraft configuration through the predicted trajectory. In this case study, it was considered that the configuration of the aircraft does not change from the initial state, assuming that the aircraft is in clean configuration at any time.

To compute a prediction based on the above described aircraft intent, it is required to determine the APM corresponding to the aircraft that will execute the planned trajectory, the initial conditions, and the weather model that will provide information about the expected atmosphere conditions for the day of operation:

- The selected aircraft is a Boeing 737-800, whose BADA 4.1 designator is B738W26.
- The conditions that represent the initial aircraft state are shown in Table 7-1.

Table 7-1 – Case Study – Initial Aircraft State

Time	5:20 GMT, 2016 February 14
Longitude	9° N
Latitude	58° E
Mass	70,000 kg
Mach	0.3
Geopotential Altitude	1,000 ft
Heading	-170°

- The day of operation is 2016 February 14, and NOAA-generated forecasts were selected to compute the prediction.

7.4.1.1 Sources of Uncertainty

Once the nominal description of the trajectory is formulated and the necessary initial conditions, APM and Weather Model (WM) are set, the next step is the identification and characterisation of the sources of uncertainty that affect the prediction.

According to the set of inputs described above, uncertainties can be classified according to the parameter categories described below.

- **AI Uncertainties.** This category collects all parameters that introduce uncertainty to the AI description as explained in Section 6.3.1. In this particular case study, the sources of uncertainty are shown in Table 7-2, Table 7-3, Table 7-4 and Table 7-5.

Table 7-2 – Case Study – AI Uncertainties (Triggers A to D)

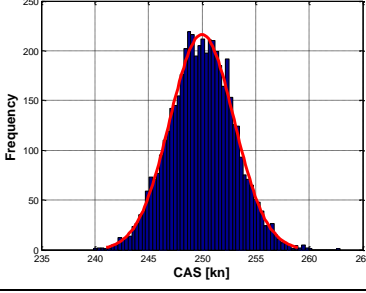
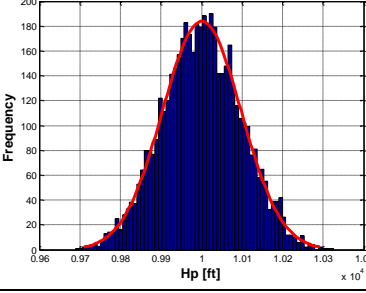
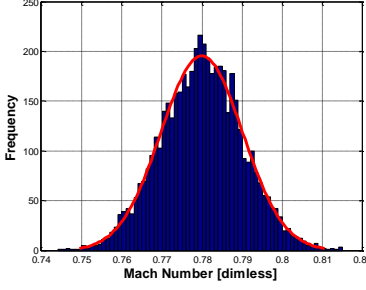
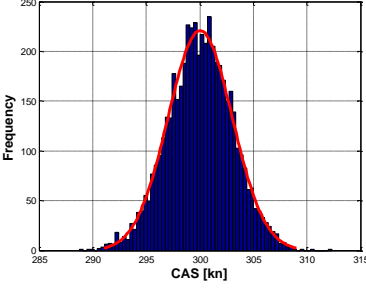
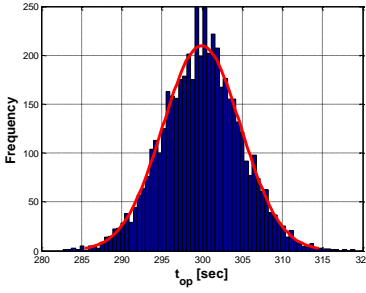
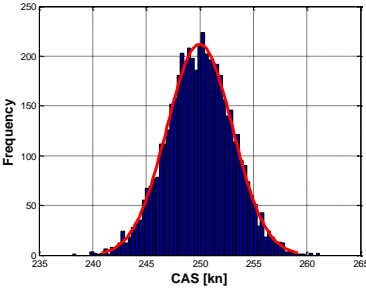
Trigger	Distribution	Trigger	Distribution
A	$\mathcal{N}(250, 3)$ 	B	$\mathcal{N}(10,000, 100)$ 
C	$\mathcal{N}(0.78, 0.01)$ 	D	$\mathcal{N}(300, 3)$ 

Table 7-3 – Case Study – AI Uncertainties (Triggers E to K)

Trigger	Distribution	Trigger	Distribution
E	$\mathcal{N}(300, 5)$ 	F	$\mathcal{N}(250, 3)$ 
G	$\mathcal{N}(10,000, 100)$	H	$TRI(7.235, 7.25, 7.265)$

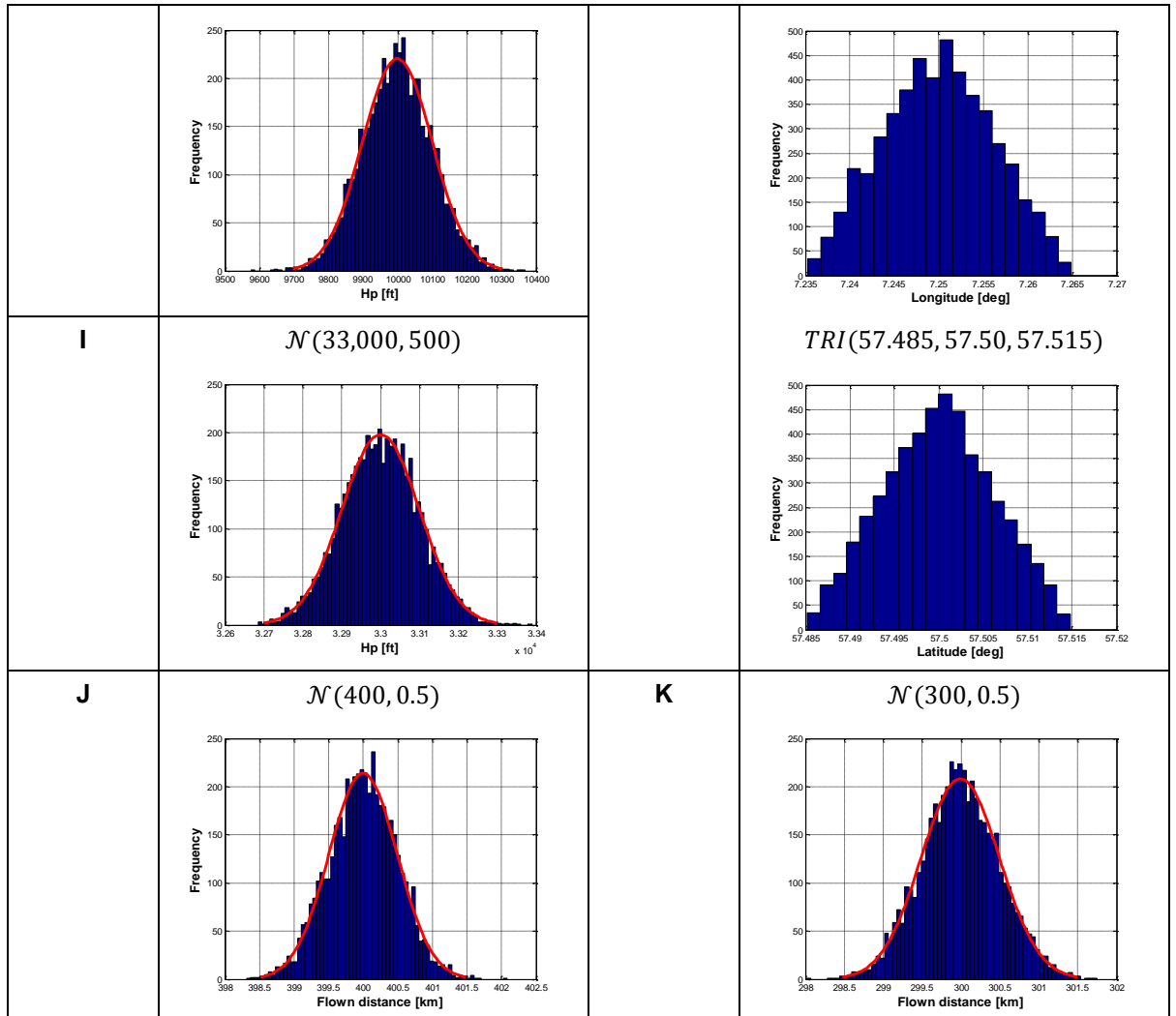


Table 7-4 – Case Study – AI Uncertainties (Triggers L)

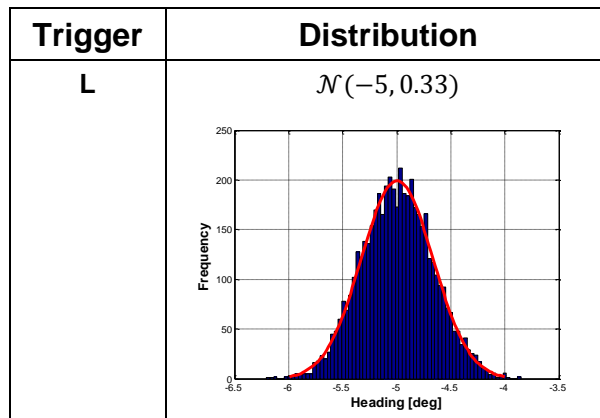
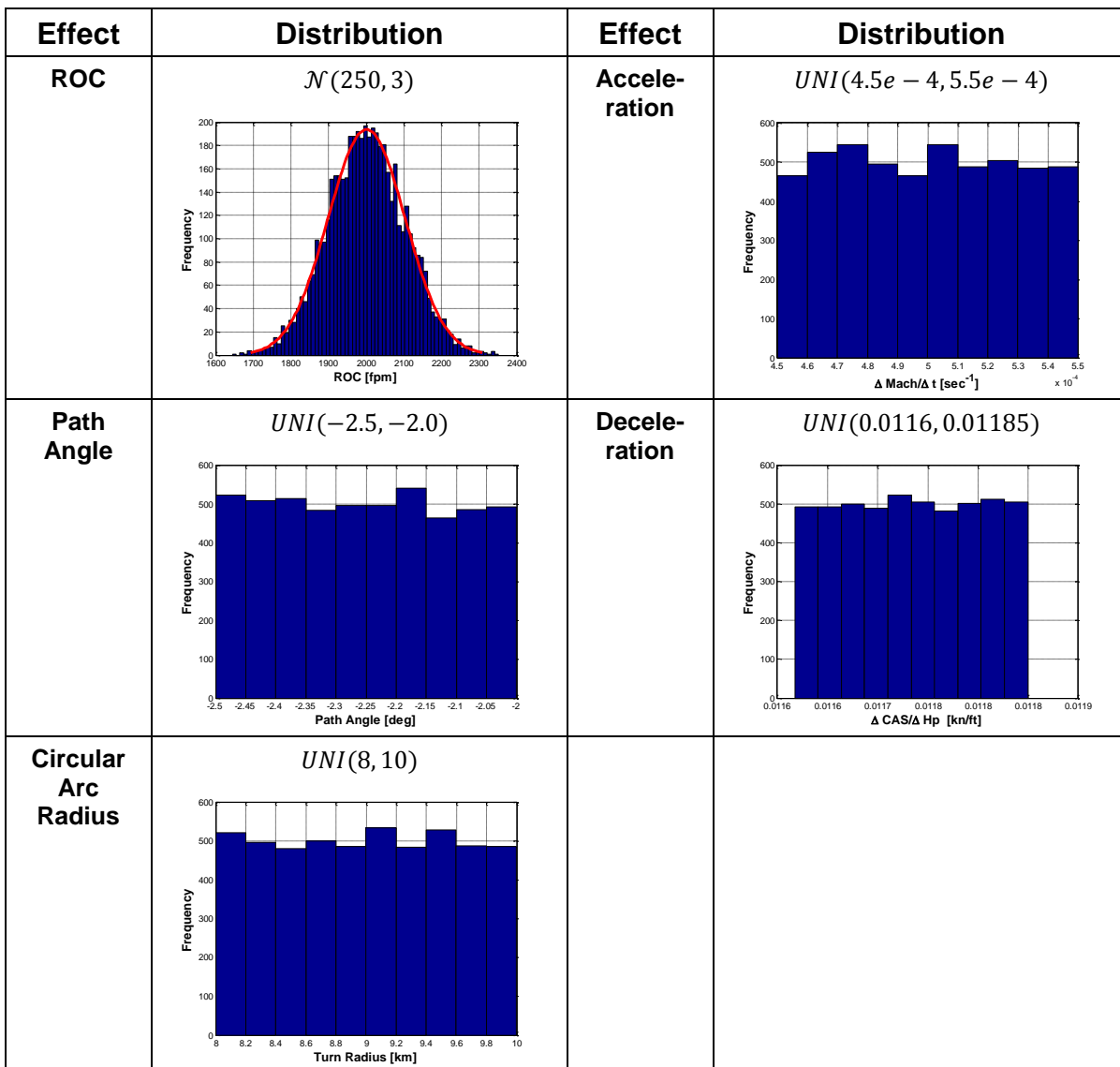
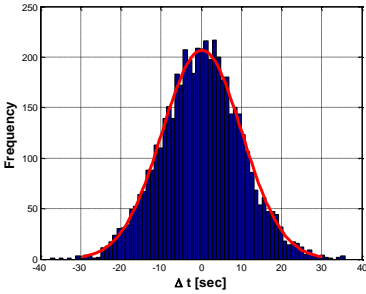
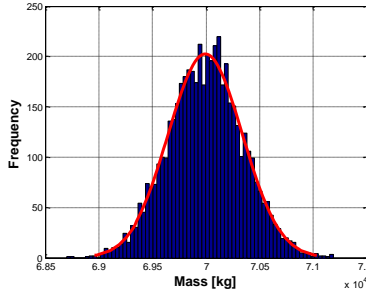
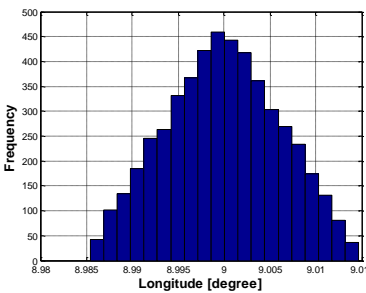
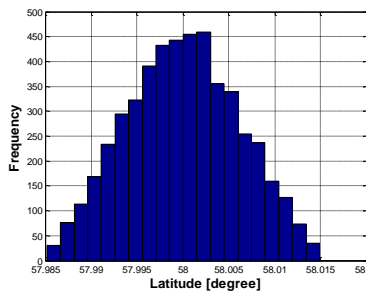
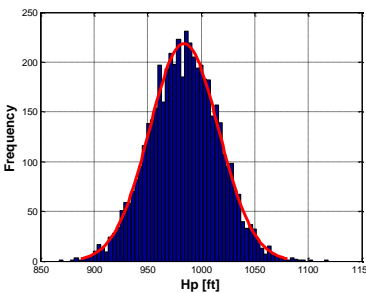
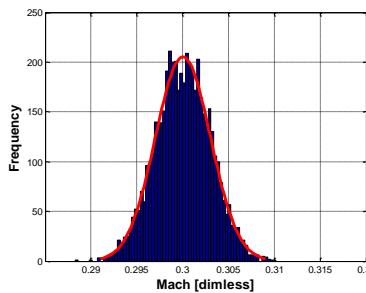
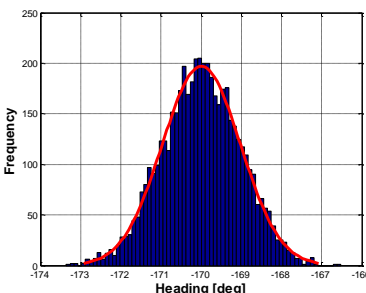


Table 7-5 – Case Study – AI Uncertainties (Instructions Effects)



- Initial Conditions Uncertainties. This category includes uncertainties introduced by the variability of the initial state used for trajectory prediction (Table 7-6).

Table 7-6 – Case Study – Initial Conditions Uncertainties

Variable	Distribution	Variable	Distribution
Time	$\mathcal{N}(t_0, 10)$ 	Mass	$\mathcal{N}(70,000, 350)$ 
Longitude	$TRI(8.985, 9, 9.015)$ 	Latitude	$TRI(57.985, 58, 58.015)$ 
Geo-potential Pressure Altitude	$\mathcal{N}(984, 33)$ 	Mach	$\mathcal{N}(0.3, 3e - 3)$ 
Heading	$\mathcal{N}(-170, 1)$ 		

- **APM Uncertainties.** The parameters that represent a variability of the nominal aircraft performance are included in this category. The drag polar, non-idle fuel consumption and idle fuel consumption models presented in Section 4.4 represent the APM uncertainties considered in this case study. The triangular distributions proposed in Section 4.5 represent the admissible variability of these inputs and, therefore, a measure of the uncertainty introduced by them.
- **WM Uncertainties.** Section 5.4.1 proposed the use of a forecast ensemble to capture weather uncertainty in a way that can be used in trajectory prediction. Although this approach has been proven as an effective solution to analyse the influence of the atmosphere variability, it cannot be directly applied to an aPCE-based trajectory prediction uncertainty characterisation. aPCE allows the use of discrete variables because it is only necessary to have the capability of computing the statistical moments up to $2\alpha-1$ (Section 7.2.3). However, to calculate the optimal set of collocation points, it is more suitable to have a mechanism to reproduce weather forecasts that represent the roots of the univariate expansion that characterize the weather variability. In addition to the forecast ensembles, weather forecast providers (especially NOAA) generate the mean forecast that identifies the average values of all ensemble members and the associated standard deviations of the atmosphere properties at each grid point [155]. Thus, assuming that the variability among ensemble members can be represented by a variable uniformly distributed, any possible forecast can be reproduced by the mean forecast and the standard deviation, multiplied by the value of this uniform variable. This hypothesis relies on the fact that any uniform distribution can be assimilated to a uniform distribution between -1 and +1 by just scaling it. The variability obtained from this distribution can be transformed into the real variability by moving the mean value from zero to the original average value, and multiplying the original standard deviation by 2. The mean and variance of a uniform distribution is defined as follows:

$$\mu = \frac{1}{2}(a + b)$$

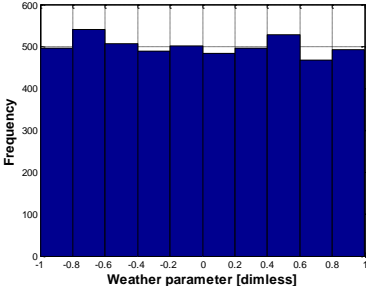
$$\sigma = \frac{1}{\sqrt{12}}|b - a| \quad (7-32)$$

Then, the relationship between the points of any uniform distribution and that defined between -1 and +1 reads as follows:

$$X = \mu + \sigma x$$

$$X_{[-1,1]} = 0 + \frac{2}{\sqrt{12}} x \quad \Rightarrow \quad X = \mu + \frac{|b - a|}{2} X_{[-1,1]} \quad (7-33)$$

Table 7-7 – Case Study – Initial Conditions Uncertainties

Variable	Distribution
WM Parameter	<p>$UNI(-1, 1)$</p> 

7.4.2 Numerical Results

The study case proposed in previous Section 7.4.1 describes a nominal trajectory and the sources of uncertainty that affect the prediction. These sources are modelled by probability density functions that characterise their variability. Relying on that nominal trajectory description and these functions, a typical Monte Carlo simulation is used to assess the stochastic behaviour of the predicted aircraft state variables. The obtained results will be compared with those generated by the aPCE solution, using the same models of the trajectory description and uncertainty sources.

7.4.2.1 Results from Monte Carlo Simulation

The total number of Monte Carlo runs are set to 5,000. In each run, the values of the uncertain variables are randomly selected from the previously described probability density functions. Table 7-8 shows the mean and standard deviation of the distribution of selected state variables at the end of each AI operation.

Table 7-8 – Monte Carlo Simulation Results

		Mass [kg]	Flown Distance [km]	Elapsed Time [sec]	Geopotential Altitude [ft]
OP#1	μ	69,841	5.85	49	2,629
	σ	352.22	0.66	5.4	252
OP#2	μ	69,580	24.5	183	9,998
	σ	351.51	0.70	2.6	100
OP#3	μ	68,662	142.5	841	29,339
	σ	353.17	8.7	43.6	888
OP#4	μ	68,479	178	1,004	32,999
	σ	342	5.4	18.5	103
OP#5	μ	68,079	300	1,559	32,999
	σ	346	0.5	28.7	103
OP#6	μ	67,992	325.11	1,671	32,999
	σ	346	1.7	30	103
OP#7	μ	67,778	400	1,985	32,999
	σ	346	0.5	29	103
OP#8	μ	67,769	416	2,055	29,323
	σ	346	4	39.7	794
OP#9	μ	67,725	482	2,355	17,881
	σ	346	4	39.8	899
OP#10	μ	67,691	516	2,551	13,611
	σ	346	5	44.9	1,129
OP#11	μ	67,663	538	2,698	10,001
	σ	346	4	32.8	99.7
OP#12	μ	67,634	557	2,844	7,359
	σ	346	2	25.8	607

The computational cost of computing the trajectory outputs for each individual run is 0.197 sec³⁰, hence, the total time required for evaluating the impact of uncertainty sources in this particular case is 985 sec.

³⁰ The trajectory predictions have been computed by means of a C++ library developed in BR&T-E. This library represents an implementation of an ADL-based trajectory prediction. The Monte Carlo simulations have been run in a MacBook Pro 2.5 GHz quad-core Intel Core i7.

7.4.2.2 Results from aPCE Method

The aPCE methods require data points obtained from the probability distributions of inputs to compute the statistic moments of each individual uncertainty source. In this case, the same set of 5,000 data points randomly selected in the Monte Carlo simulation is used.

The number of input parameters n in the proposed study case is 29. To avoid extremely large expansions, the order \bar{q} of the PCE was set to 2. Further, in this section the analysis of the results will support this decision. Solutions of higher order are possible as well, although the increased computational effort does not return significant improvements in expansions accuracy. Thus, the number of coefficients \bar{a}_i that characterise the PCE for each of the considered outputs as per Equation (7-8) is 465.

By applying the non-intrusive determination of the expansion coefficients proposed in Section 7.2.4, it is possible to build a linear system of 465 equations that leads to the computation of 465 \bar{a}_i coefficients that determine the PCE of every output variable. The mean and standard deviation can be obtained directly from the set of identified coefficients by applying the relationships exposed in Equation (7-30). Table 7-9 summarises the results obtained for the same state variables as those studied in Section 7.4.2.1.

Table 7-9 – aPCE Results

		Mass [kg]	Flown Distance [km]	Elapsed Time [sec]	Geopotential Altitude [ft]
OP#1	μ	69,903	5.93	49.2	2,631
	σ	348	0.8	5.3	249
OP#2	μ	69,642	24.9	183	10,000
	σ	347	2	2.8	99.9
OP#3	μ	68,722	145	840	29,351
	σ	348	16.2	44	900
OP#4	μ	68,542	180.7	1,002	32,997
	σ	338	13.7	23.9	101
OP#5	μ	68,153	300	1,542	32,997
	σ	347	0.5	97.7	101.14
OP#6	μ	68,066	325	1655	32,997
	σ	347	1.7	99.6	101
OP#7	μ	67,850	400	1970	32,997
	σ	346	0.5	88.6	101
OP#8	μ	67,841	416	2040	29,312
	σ	346	4.2	95.7	797
OP#9	μ	67,797	481	2340	17,827
	σ	346	7.8	96	921
OP#10	μ	67,763	515	2537	13,568
	σ	346	8.8	91.2	1,149
OP#11	μ	67,735	536.6	2683	10,001
	σ	346	9.9	89.5	98.6
OP#12	μ	67,702	557.9	2846	7,109
	σ	344	2	29	674

Compared to the 5,000 runs computed in the Monte Carlo simulation, the current aPCE alternative reduces this number to just 465 runs. The extra computational effort is dedicated to generating the orthonormal basis of each individual input parameter and the identification of optimal collocation points. Both processes are proportional to the number of considered inputs.

The total computational time applying this technique is 186 sec³¹.

7.4.2.3 Comparison of Results

The numerical results shown in Table 7-8 and Table 7-9 show that the aPCE reproduces the results obtained by a classical Monte Carlo simulation with high accuracy at a lower computational cost. However, assessing the fidelity of both approaches requires evaluating their capability of reproducing the initial aircraft state. Table 7-1 shows the comparison of both approaches with respect to the input distributions described in Section 7.4.1.1.

Table 7-10 – Case Study – Initial Aircraft State

		Input	Monte Carlo	aPCE
Longitude [deg]	μ	9	8.99	8.99
	σ	6.1e-3	6.3e-3	6.1e-3
Latitude [deg]	μ	58	58	57.99
	σ	6e-3	6e-3	6.1e-3
Mass [kg]	μ	70,000	70,024	70,000.5
	σ	350	354	349.8
Mach [dimless]	μ	0.3	0.299	0.299
	σ	3e-3	2.9e-3	3e-3
Geopotential Altitude [ft]	μ	984	983.2	984.4
	σ	33	33.3	32.7

The data presented for both Monte Carlo and aPCE approaches are obtained by processing the initial point of the computed trajectories in the former case and, generating the corresponding polynomials in the latter.

³¹ In addition to the C++ library used for computing the trajectory predictions, the proposed approach uses an implementation of the aPCE algorithms developed in Matlab.

Although both alternatives show high accuracy, the fidelity of the aPCE option is slightly higher. These results support the hypothesis of considering a polynomial expansion of order 2 posed in previous section.

7.4.2.4 Sensitivity Analysis

A main advantage of aPCE over Monte Carlo is the capability of straightforwardly assessing the sensitivity of outputs by computing the Sobol indices as explained above in Section 7.3.1.

The most interesting index is the ST as defined by Equations (7-29) and (7-31), which measures the contribution of each individual input to the variance of the considered output state variable. Table 7-11 presents the total indices computed for the following subset of state variables: mass, flown distance, elapsed time and geopotential pressure altitude.

Based on the analysis of the Total Sobol indices, it can be concluded that for the proposed study case:

- The aircraft mass uncertainty and, therefore, the fuel consumption uncertainty are mainly driven by the uncertainty of the initial mass.
- The flown distance uncertainty is strongly influenced by the latitude of initial and end points, and the location of the point at which the aircraft will initiate the planned turn, as well as by the selected turn radius.
- The ETA at the MFP is mainly driven by the Mach speed at cruise determined by trigger C, the location of the point at which the aircraft will initiate the planned turn and the selected turn radius, and how fast the aircraft accelerates from 250 kt CAS at 10,000 ft to the cruise Mach speed.
- The uncertainty of the geopotential pressure altitude depends on the variability of the initial aircraft mass, the Mach speed at cruise and the Mach/CAS profile designed for the initial part of the descent, the deviations of the drag polar and idle fuel consumption models (i.e., the variation of aircraft mass along the descent affects the variability of the vertical profile), the description of the acceleration segment planned during the climb, and the radius of the planned turn. The radius plays also a role because the TOD is set by a flown distance from the origin, and the trajectory end point is determined

by the location of a fix waypoint (i.e., the MFP). For longer radius, the TOD is reached at a longer distance away from the MFP and, therefore, the descent phase until the end of the trajectory will last longer, which impacts the variability of the geopotential pressure altitude along the descent.

Table 7-11 – Sensitivity Analysis Based on Total Sobol Indices

	$S_{T_{mass}} \times 100$	$S_{T_{dist}} \times 100$	$S_{T_{time}} \times 100$	$S_{T_{Hp}} \times 100$
IC_{time}	0.0000	0.0000	0.0000	0.0000
IC_{mass}	97.5090	0.0000	2.4540	12.8123
IC_{Hp}	0.1031	0.0000	0.8228	4.8826
IC_{Mach}	0.0832	0.0000	0.6908	4.0581
IC_{longitude}	0.1082	0.5667	1.0213	5.1588
IC_{latitude}	0.1049	9.0002	3.1926	5.2111
IC_{heading}	0.8093	0.0000	5.6585	3.7263
Trigger A	0.0776	0.0000	4.5508	3.4913
Trigger B	0.0700	0.0000	0.4582	3.2239
Trigger C	0.2956	0.0000	39.2574	7.6314
Trigger D	0.0255	0.0000	0.2750	6.1265
Trigger E	0.0639	0.0000	0.4797	2.8883
Trigger F	0.0480	0.0000	1.1479	2.7874
Trigger G	0.0900	0.0000	0.5639	4.3856
Trigger H	Long	0.0566	0.0092	0.4381
	Lat	0.1037	11.5710	4.0617
Trigger I	0.1006	0.0000	1.5035	5.7805
Trigger J	0.0992	0.0000	1.5521	5.1234
Trigger K	0.0428	24.1291	8.4668	3.5715
Trigger L	0.0521	0.0000	0.3566	2.4157
ΔC_D^u	0.2283	0.0000	1.5907	10.7024
ΔC_{FF}^u	0.8844	0.0000	0.5859	3.5044
ΔC_{FFi}^u	0.1552	0.0000	1.1784	6.9551
WM parameter	0.0395	0.0000	0.2765	1.8434
ROC	0.0255	0.0000	0.1878	1.1693
Acceleration	0.1992	0.0000	9.7307	9.6163
Deceleration	0.0394	0.0000	0.2765	1.8370
Path Angle	0.0399	0.0000	0.7830	3.4153
Circular Arc Radius	0.1377	54.7240	20.3204	10.3478

7.5 Trajectory Prediction Uncertainty in Decision Support Tools

The main function of DSTs (current or planned in future TBO paradigm) is to assist humans in the process of managing traffic flow, delivering to the greatest possible extent the expected quality of service in terms of capacity, flexibility, predictability, efficiency, cost effectiveness, safety, and environmental impact. The warnings, alerts, or indications provided by DSTs rely on predicting the trajectories of planned and current air traffic with accuracy. Hence, prediction uncertainties directly affect the ability of DST to generate valuable outputs that help air traffic management.

aPCE technique may improve the capability of introducing prediction uncertainty information into DST processes because

- It provides an analytical representation of uncertainty based on a polynomial expansion that can be easily managed by any algorithm.
- Computing an expansion is very fast and can be considered a pseudo-real time process.
- Sensitivity assessments are immediate.

The following examples illustrate how aPCE can provide valuable uncertainty quantifications for three different applications. The AI description, APM, and day of operations (which determines the weather forecasts to be used to predict the trajectory) are the same as those proposed in Section 7.4.1. Unlike the previous study case, the sources of uncertainty considered in these examples are only a subset of those originally analysed in Section 7.4.1.1. From the DST perspective, the uncertainty introduced by some inputs may not affect their processes (e.g., initial aircraft mass in case of conflict detection in cruise), or cannot be modelled properly due to the lack of reliable information (e.g., aircraft performance in case of demand and capacity balancing).

The next sections present two examples of DSTs and how they can make use of the uncertainty quantification obtained from applying the aPCE methodology.

7.5.1 Demand and Capacity Balancing

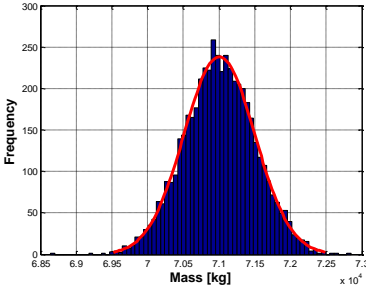
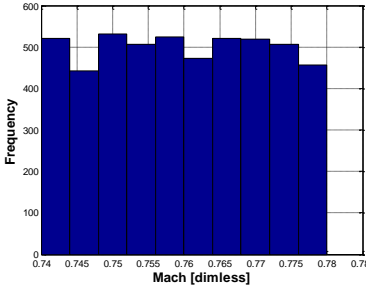
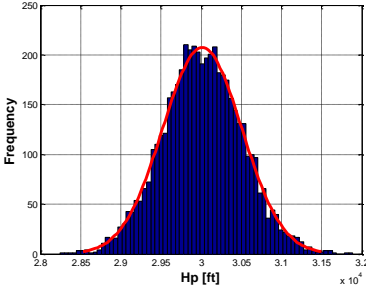
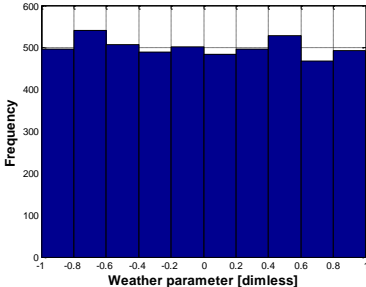
Demand and Capacity Balancing (DCB) encompasses all processes and procedures necessary to assess the traffic load within a sector to ensure that capacity is not exceeded, which would increase the controllers’ workload.

The main information required by DCB tools is the estimated entry and exit times to an airspace volumen. The knowledge of these times enables assessing the expected traffic load as it evolves over time and taking actions in advance if some thresholds are breached.

The application of the proposed aPCE methodology can provide valuable uncertainty information that can be used by DCB tools in pseudo-real time.

Table 7-12 gathers the description of modelled uncertainty sources that were used to quantify the trajectory prediction uncertainty exploited by subsequent DSTs.

Table 7-12 – DCB - Uncertainty Sources

Variable	Distribution	Variable	Distribution
Mass	$\mathcal{N}(71,000, 500)$ 	Cruise Mach Speed	$UNI(0.74, 0.78)$ 
Cruise Altitude	$\mathcal{N}(30,000, 500)$ 	WM Parameter	$UNI(-1, 1)$ 

In addition, the time of departure is a key variable for most DSTs. This variable is usually represented by a Poisson distribution indicating that late departures are more likely than early departures [156]. The shape of the distribution will depend on the airport characteristics, the planned traffic pattern within the TMA, or unexpected events (e.g., runway closure). Table 7-13 shows a typical case that represents the distribution used in the following analyses.

Table 7-13 – Departure Time Uncertainty

Variable	Distribution
Departure Time	<p><i>Poisson(10, 0)</i></p>

Figure 7-2 depicts the uncertainty boundaries around the computed nominal prediction based on generated polynomial expansions of the estimated time and elapsed time variables. In this example, the entry and exit points to the sector are designed by the end of operations OP#4 (*trigger K*) and OP#8 (*trigger J*).

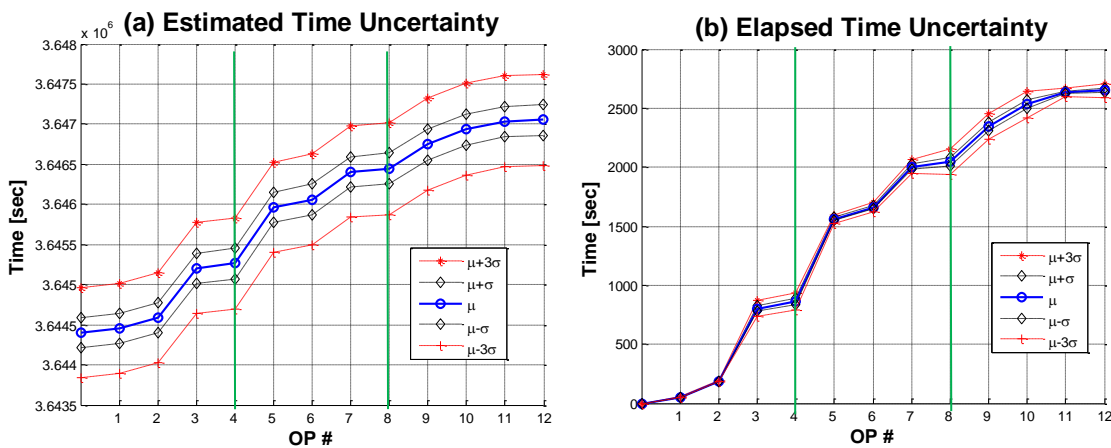


Figure 7-2 – DCB - Estimated Time and Elapsed Time Uncertainties

From the analysis of the previous figures, it can be concluded in this example that the uncertainty of departure time is maintained constantly throughout the trajectory. The planned

trajectory does not present the capability of reducing this uncertainty and, therefore, it is directly propagated without attenuation.

A very useful analysis is to assess the influence of input variability in the estimated times at the entry and exit points. This sensitivity analysis is immediate thanks to the computation of the Sobol indices.

Table 7-14 – DCB – Sensitivity Analysis

	$S_{T_{time}}^{entry} \times 100$	$S_{T_{time}}^{exit} \times 100$
Departure Time	99.9892	99.0074
Mass	0.0108	0.0004
Cruise Mach Speed	0.0000	0.9914
Cruise Altitude	0.0000	0.0008
WM Parameter	0.0000	0.0000

As expected, the major contribution to the ETA at the entry and exit points is the uncertainty of the departure time, although in the case of the exit point, the cruise Mach speed also plays a role. Typically, cruise speed can be used to partially reduce the effect of departure delays.

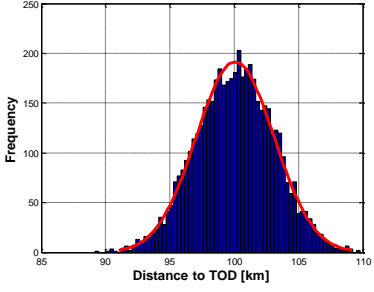
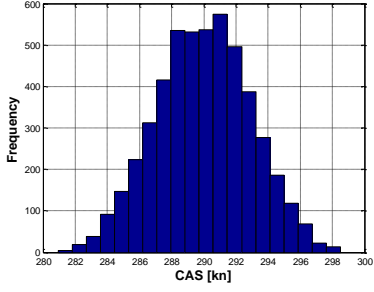
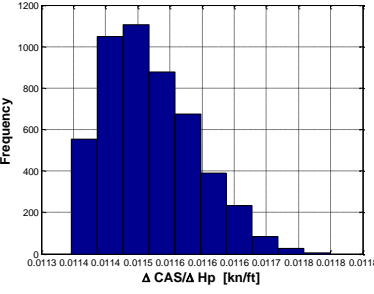
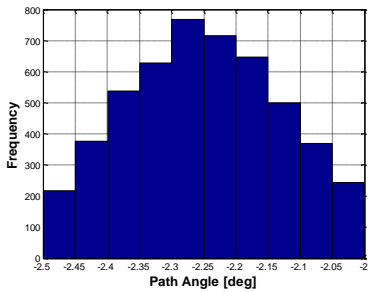
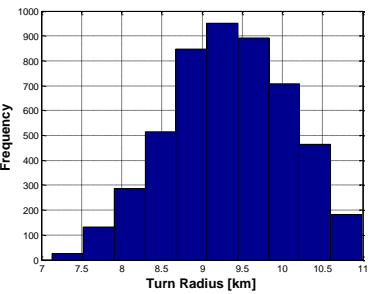
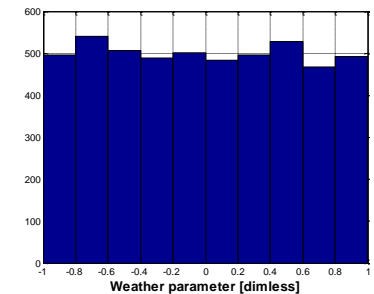
The computational time required to obtain the polynomial expansions and the Sobol indices used in the sensitivity analysis was 2.54 sec.

7.5.2 Arrival Manager

Arrival Managers (AMAN) provide electronic assistance to manage the flow of arriving traffic within an airspace, to particular points such as runway thresholds or metering points. The AMAN system provides a sequenced traffic pattern and estimated times at designated fixes.

In this particular example, the beginning of the trajectory is considered at the TOC and, hence, it is assumed that there is no uncertainty in the initial conditions. The aircraft position, altitude, and speed are considered known (e.g., obtained from surveillance systems like ADS-B), while it is assumed that an estimation of the aircraft mass is available to the AMAN (for instance, reported by the aircraft through the Extended Projected Profile [EPP] [157]).

The uncertain variables selected to illustrate this example are presented in Table 7-12.

Variable	Distribution	Variable	Distribution
TOD	$\mathcal{N}(100, 3)$ 	Initial Descent CAS	<i>Unknown</i> 
De-celeration Rate	$Beta(5, 2)$ 	Path Angle	$\mathcal{N}(-2.25, 0.15)$ <i>truncated between $[-2.5, -2]$</i> 
Turn Radius	<i>Unknown</i> 	WM Parameter	$UNI(-1, 1)$ 

After computing the corresponding polynomial expansions, it is possible to depict the combined variation of state variables with the flown distance. Figure 7-3 shows the plot generated for fuel burnt and pressure altitude uncertainties.

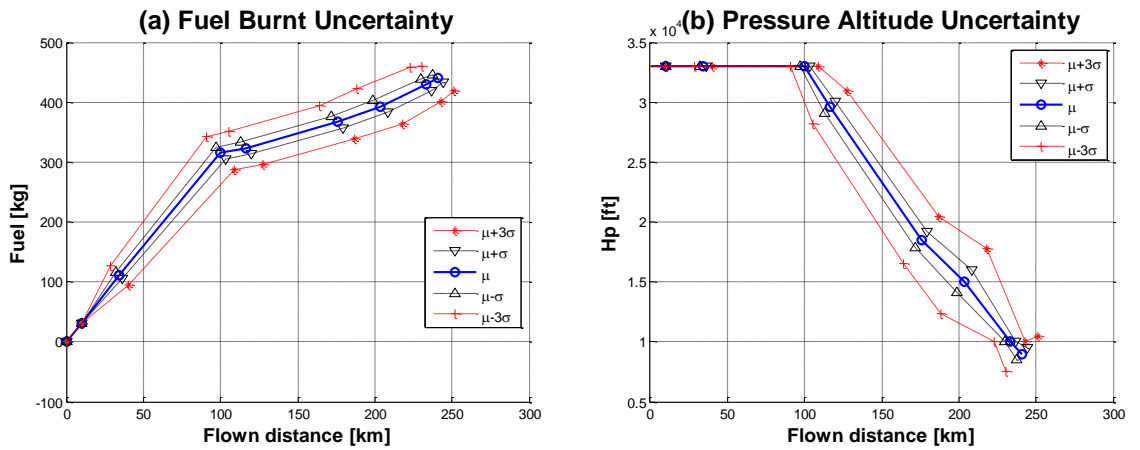


Figure 7-3 – AMAN – Fuel Burnt and Pressure Altitude Uncertainties

Additional state variables of interest for an AMAN system are CAS and ground speed, especially at the MFP. Figure 7-4 plots the associated uncertainty of these two variables with respect to the flown distance.

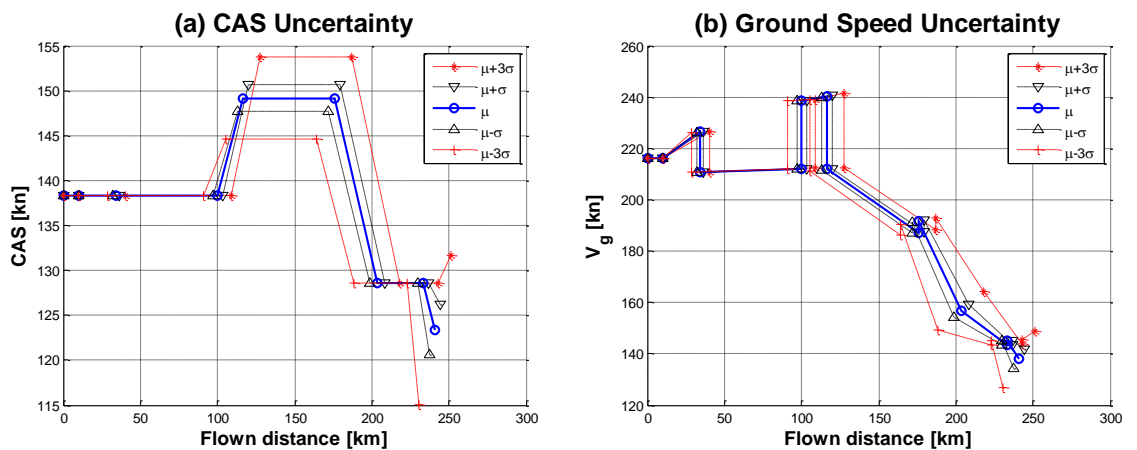


Figure 7-4 – AMAN – CAS and Ground Speed Uncertainties

The plots included in Figure 7-3 and Figure 7-4 show that uncertainty fluctuates around the nominal prediction, but does not increase uncontrollably with time. On the contrary, the trigger G, which defines the end of the instruction $HS(CAS = 250 \text{ kt})$ and the beginning of the PAL instruction, clearly determines a bottleneck for the uncertainty propagation in all state variables.

From the AMAN perspective, the geopotential pressure altitude, ETA, and CAS at the MFP are the state variables of highest interest. Table 7-15 presents the Sobol indices-based sensitivity analysis of the proposed example.

Table 7-15 – AMAN – Sensitivity Analysis

	$S_{T_{Hp}} \times 100$	$S_{T_{ETA}} \times 100$	$S_{T_{CAS}} \times 100$
TOD	69.5500	7.0930	60.1895
Initial Descent CAS	27.1489	91.4565	23.2921
Deceleration Rate	0.0006	0.0028	0.0005
Path Angle	1.4684	0.0121	18.1637
Turn Radius	2.1020	1.4576	1.8188
WM Parameter	0.0000	0.0000	0.0000

The variability of the Mach/CAS transition that describes the descent profile is the major contributor to the ETA uncertainty, while it also significantly impacts the Hp and CAS uncertainties. In these latter cases, a more important factor is the location of the TOD, because it determines the distance with respect to the MFP at which the descent at LIDL rating is initiated.

The CAS uncertainty is also affected by the path angle set to describe the vertical path from 10,000 ft to the MFP. The variability of this angle strongly influences the aircraft speed at the end of the trajectory, as it is shown in Figure 7-4.

The computational time required to obtain the polynomial expansions and the Sobol indices used in the sensitivity analysis was 2.95 sec.

7.6 Summary

This chapter has reviewed current approaches used to quantify the uncertainty of a trajectory prediction based on knowledge of the input variability. Some solutions, based on Monte Carlo simulations, are computationally costly. Others, based on a linearisation of motion equations and control laws, return approximate values of prediction uncertainties.

To address the problem of trajectory prediction uncertainty quantification, a novel approach based on the arbitrary PCE methodology has been described. PCE was applied in dynamic systems to evaluate the uncertainty of parameters that characterise the system by means of a polynomial description of the variability of inputs. The advantage of using aPCE relies on the capability of describing the input distributions driven by data. This method does not require an analytical description of input distributions, it is only necessary to have the possibility of computing the statistical moments up to a certain order (which will determine the maximum order of the polynomial expansion). With this information, it is possible to identify the polynomial expansion of the inputs and, based on this, to obtain the expansion of the outputs.

In addition to the theoretical formulation of the proposed method, this chapter defines a study case to evaluate its suitability. The trajectory used in the study case is represented by climb, cruise, and descent phases in which each individual source is modelled separately to obtain their PCEs. These expansions are used afterwards to characterise the output uncertainty. The numerical results provided in this chapter are compared with the results from a Monte Carlo simulation, proving that it is possible to obtain slightly better results with a much lower computational effort (i.e., the computational time required in the case of aPCE is 186 sec, compared to the 985 sec in the case of Monte Carlo for the same size of data samples).

Moreover, the computed coefficients that identify the polynomial expansions of the outputs provide an immediate sensitivity assessment thanks to the definition of the Sobol indices. These indices are used to rank the influence of the inputs in the output uncertainty, providing a relative quantification of such influences.

This chapter also discusses how DSTs can leverage the uncertainty quantification generated by the aPCE method, which can be considered as pseudo-real time if the number of uncertain inputs is limited. To illustrate this process, examples of a DCB tool and an AMAN were studied. In the latter case, it was tested against a set of uncertainty sources characterized by known and unknown probability density functions. This example demonstrates that it is possible to obtain a quantification of the prediction uncertainty regardless the type of input distribution. Only a sufficient set of data is necessary to apply the aPCE method as described.

The main advantages of aPCE-based uncertainty quantification is that it provides the flexibility of studying any type of trajectory with an unrestricted number of uncertain inputs, while at the same time it provides high accuracy with a low computational effort (orders of magnitude lower than Monte Carlo simulations).

The proposed methodology shows an unprecedented capability to quantify the impact of uncertainty sources on trajectory predictions by means of a non-intrusive process that can potentially be applied to any TP. At the same time, it facilitates the process of identifying most influencing uncertainty sources that can be used for robust decision making processes.

CHAPTER 8

CONCLUSIONS AND FUTURE WORK

8.1 Conclusions

The research presented in this thesis proposes a novel approach to quantify the uncertainty associated with aircraft trajectory prediction. This approach is based on applying PCE techniques to describe the variability in the inputs to the trajectory prediction process. The main result of this research is a methodology to describe the uncertainty in those inputs by means of orthonormal univariate polynomials and to derive from them multivariate polynomials that represent the uncertainty in the output trajectory.

The first stage of the research focused on the identification, description, and classification of the different sources of uncertainty that affect trajectory prediction (RO#1). Regardless of the TP architecture considered, CHAPTER 3 groups the different uncertainty sources into four generic categories: APM uncertainties, weather forecast uncertainties, initial conditions uncertainty, and AI description uncertainties.

This thesis have provided practical methods to assess the impact of the stochastic factors affecting the process of predicting an aircraft trajectory (RO#2) that are used to identify the individual uncertainty models the characterize the prediction uncertainty as function of the variability of prediction inputs (RO#3).

In CHAPTER 4, the influence of the APM uncertainties is modelled by the variability of the independent coefficients of the drag polar and fuel consumption models (non-idle and idle models). The prediction uncertainty derived from the effect of these uncertainty sources is bounded within the plane surface. This surface can be computed by the predictions generated from four APMs: the nominal and three degraded models as explained in Section 4.5. Based on the computation of this plane surface, this chapter described a method to obtain a measurement of the prediction uncertainty due to the effect of the APM uncertainties.

CHAPTER 5 discussed approaches to manage weather forecast uncertainty. The trajectory predictions are influenced by the atmosphere conditions (temperature and pressure) and especially by the wind. The variability of these parameters not only affects the aircraft dynamics, but also impacts the aircraft performance, the aircraft speed transformations, and the definition of the geopotential pressure altitude. This chapter proposed the use of time-lagged ensemble of ensembles to characterise the prediction uncertainty introduced by the used of weather forecasts.

CHAPTER 6 studied the influence of the AI description making use of the framework defined by the AIDL. The AIDL is a formal language used to describe AI instances, which univocally identifies a trajectory (or a flight segment). This language encompasses an alphabet (set of instructions that when properly combined determine the aircraft motion) and the grammar (lexical and syntactical rules that govern the combination of instructions). This chapter studied the effect of the variability of AI instances formulated by means of the AIDL. Regression methods were applied to identify the models that represent the prediction uncertainty in case of trigger uncertainty, effect uncertainty, and initial conditions uncertainty.

The analysis of the impact of each individual uncertainty source on the predicted trajectory resulted in very complex models that can only be used in limited cases. These models are dependent on the aircraft type and operational conditions, which reduces their usability and restricts their applicability. Due to these reasons, a formal framework to characterise the prediction uncertainty in generic and flexible fashion have been proposed (RO#4).

In CHAPTER 7 of this thesis, the application of the aPCE methodology to the quantification of trajectory prediction uncertainty is presented. DSTs, especially in the future TBO context, will demand extended trajectory information to improve their processes. DSTs will require a prediction uncertainty quantification independent of the type of TP used: in pseudo-real time; capable of being applied to any ATM procedure; capable of managing multiple sources of uncertainty simultaneously; that enables sensitivity assessment capabilities without increased computational requirements; that does not require modifications of native prediction architectures; that returns accurate representations of the uncertainty propagation; and finally, that facilitates the process of ranking the most impacting input variables in the overall prediction uncertainty.

All these requirements are fulfilled by the proposed PCE methodology, based on the polynomial description of inputs variability, which is used to compute the polynomial description of outputs variability.

PCE was originally applied to model Gaussian processes in a variety of scientific fields. The need to model non-Gaussian processes caused the development of gPCE, an extension of the methodology to other known distributions (e.g., Gamma, Beta, Uniform, Poisson, or Binomial). Nevertheless, actual processes commonly do not respond like analytically known distributions. To overcome this drawback, aPCE proposes a data-driven alternative that only requires a set of data samples to compute the statistical moments of the real distributions up to certain order. Based on these statistical moments, it is possible to build the orthonormal basis of polynomials that characterise the variability of the considered parameters.

Numerical results obtained from the application of this methodology to a typical trajectory prediction problem are compared against the results generated by Monte Carlo simulation. The main conclusion of this assessment is that aPCE provides better accuracy than Monte Carlo, even for low order polynomials, with a much lower computational effort. Moreover, aPCE enables the possibility of performing a sensitivity assessment by means of the identified coefficients of the expansion (RO#5).

The benefits obtained from the application of the aPCE-based uncertainty quantification are manifold:

1. This solution can potentially be applied to any trajectory predictor without modifications.
2. The prediction uncertainty models obtained can be used by DSTs in the current ATM environment, or by a future advanced DST designed to operate in the future TBO context.
3. The prediction uncertainty models are analytical representations formed by polynomial expansions that can be easily processed by computer-based CDM processes.

4. It is a fast and computationally efficient procedure, especially when compared with classical approaches like Monte Carlo, and can be considered as a pseudo-real time process taking into account typical look-ahead trajectory prediction times.
5. It is a data-driven process, which means that it does not require analytical representations of the probability distributions characterising the inputs uncertainty.
6. PCE provides the capability of straightforward sensitivity assessments due to the relationship between polynomial expansion coefficients and total Sobol indices.

Overall the work completed in this research has shown that it is possible to apply the PCE theory to the quantification of aircraft trajectory prediction uncertainty in the context of ATM applications. Numerical results have demonstrated the suitability of the proposed method, especially compared to the results obtained by Monte Carlo simulation. The use of aPCE to describe the stochastic behaviour of output variables enables the capability of exploiting trajectory prediction uncertainty in pseudo-real time, which is crucial for the development of advanced DSTs in future TBO environment.

8.2 Future Work

The main contribution of this thesis is a description of a process to formally quantify trajectory prediction uncertainty independently of the TP framework considered. In the future ATM environment, advanced DST will be able to manage uncertainty prediction information to improve CDM processes. However, detailed analysis about how to exploit this information will be required. Each DST has its own requirements and, therefore, will use this information in different manners. The applicability of the proposed method and the ability to use the generated prediction uncertainty representation in an effective way have not tackled by this thesis and, therefore, need to be researched prior to their applicability in real scenarios.

Among potential follow-up research efforts to the work presented in this thesis, the following can be highlighted:

1. *Application of PCE to the Intent Generation Process.* aPCE has been applied to a TP considering that a univocal description of the trajectory exists, i.e., an AI description exists that is available to the TP. However, the process of predicting a trajectory

typically lacks a complete description of the AI that identifies the trajectory. In most common situations, the available information is that contained in the FP or in an instance of an FI. This set of data does not univocally represent a trajectory; on the contrary, there is potentially an infinite number of trajectories compliant with the considered FP/FI. The IGP is the process that completes the information contained in the FP/FI and generates a valid AI instance to be computed by the TP. All models and datasets used for this purpose introduce uncertainty into the prediction process that can potentially be modelled by applying PCE techniques.

2. *Integration with DSTs.* The use of uncertainty information is paramount to improve the efficiency of ATM procedures. The integration of the proposed aPCE-based uncertainty quantification method with different DSTs is an interesting challenge that will provide relevant conclusions about the foreseen enhanced features obtained from its application. The sensitivity analysis derived from the use of this methodology can help focus on key parameters affecting trajectory uncertainty in different operational scenarios.
3. *Application of PCE to traffic prediction uncertainty.* The ability to predict the evolution of a traffic pattern could be improved by the quantification of the traffic uncertainty by the use of PCE techniques.
4. *Robust trajectory design.* PCE is used in robust design optimisation. Its applicability to trajectory prediction optimisation may provide robust predictions against variations of most influencing parameters. It would be possible to describe a trajectory by means of an AI instance that minimizes the effect of uncertain inputs on certain state variables (for instance, on fuel consumption).

This page intentionally left blank

REFERENCES

1. Mueller, K. Tysen, John A. Sorenson, and George J. Couluris. "Strategic aircraft trajectory prediction uncertainty and statistical sector traffic load modeling." In AIAA Guidance, Navigation, and Control Conference and Exhibit, p. 4765. 2002.
2. Paielli, Russell A., and Heinz Erzberger. "Conflict probability for free flight." *Journal of Guidance, Control, and Dynamics* 20, no. 3: 588-596. 1997.
3. Torres, Sergio. "Trajectory Accuracy Sensitivity to Modeling Factors." In 15th AIAA Aviation Technology, Integration, and Operations Conference (ATIO). 2015.
4. Torres, Sergio. "Accuracy impact of trajectory sampling and representation for Trajectory-Based Operations." In Digital Avionics Systems Conference (DASC), 2013 IEEE/AIAA 32nd, pp. 5D2-1. IEEE. 2013.
5. Swierstra, Sip, and Steven Green. "Common trajectory prediction capability for decision support tools." In 5th USA/Eurocontrol ATM R&D Seminar, Budapest, Hungary. 2003.
6. Commission of the European Communities. "White Paper: Air Traffic Management – Freeing Europe’s Airspace." COM (96) 57 Final. 1996.
7. National Air Traffic Controllers Association (NATCA). "A History of Air Traffic Control." 2010.
8. Civil air regulations. Part 60, Air traffic rules / Civil Aeronautics Board. Oct. 8, 1947.
9. Gilbert, Glen. "Historical development of the air traffic control system." *Communications, IEEE Transactions on* 21, no. 5: 364-375. 1973.
10. Stevens, Michael C. *Secondary surveillance radar*. Artech House on Demand, 1988.
11. Kraus, Theresa L. *The Federal Aviation Administration: A Historical Perspective, 1903-2008*. US Department of Transportation, Federal Aviation Administration, 2008.
12. EUROCONTROL. "1960 – 1970: Building the foundations." EUROCONTROL website. <http://www.eurocontrol.int/articles/1960-%E2%80%93-1970-building-foundations>. Last accessed on March 31, 2016.
13. Israel, David R. "THIRD GENERATION AIR TRAFFIC CONTROL SYSTEM." *Transportation Research Board Special Report 159* (1975).
14. Hink, L. L. "Automation in air traffic control." In *Decision and Control including the 13th Symposium on Adaptive Processes, 1974 IEEE Conference on*, pp. 545-547. IEEE, 1974.

15. EUROCONTROL. "Principles of Mode S Operation and Interrogator Codes." Edition 2.3. 2003.
16. EUROCONTROL. "1972 – 2012. Forty years of vision. The EUROCONTROL Maastricht UAC story." 2012.
17. EUROCONTROL. "1980 – 1990: Capacity challenges." EUROCONTROL website. <http://www.eurocontrol.int/articles/1980-%E2%80%93-1990-capacity-challenges>. Last accessed on February 14, 2016.
18. EUROCONTROL. "1960s-1990s: leading up to the last decade." Skyway Magazine (Special Edition). Volume 11, Number 46. Autumn/Winter 2007.
19. Universal Avionics. "Understanding the Future Air Navigation System (FANS) 1/A Operations and Regulatory Requirements." White Paper WHTP-2013-18-10. October 2013.
20. European Commission. "Communication from the Commission to the council and the European parliament - The creation of the Single European Sky." COM 1999 – 614.
21. EUROCONTROL. "ATM Strategy for the Years 2000+." 2003 Edition.
22. EUROCONTROL. "European ATM Master Plan." eATM Portal website. 2016. <https://www.atmmasterplan.eu/oisteps>. Last accessed on February 14, 2016.
23. JPDO. "NextGen Concept of Operations V2.0." June 2007.
24. JPDO. "NextGen Enterprise Architecture V2.0." June 2007.
25. NextGen & SESAR. "State of Harmonization Document." 2015.
26. Australian Strategic Air Traffic Management Group (ASTRA). "The ATM Strategic Plan (Part A)." 2007.
27. Fukuda, Yutaka. "ATM Research in Japan." In Tenth USA/Europe Air Traffic Management Research and Development Seminar. Plenary Session. 2013.
28. ICAO. "Global Air Traffic Management Operational Concept." Doc 9854, AN/458. First Edition. 2005.
29. FAA. "FAA's NEXTGEN Implementation Plan." March 2011.
30. EC Directorate-General for Research and Innovation and Directorate General for Mobility and Transport. "Flightpath 2050 Europe's Vision for Aviation." March 2011.
31. SESAR. "Trajectory Management Document." Project ID B.04.2 Edition 00.02.90. September 2010.
32. SESAR Factsheet. "System Wide Information Management (SWIM)." No. 01/2011. 2011.

33. Wilber, Rick. "NextGen architectures to include pilots in collaborative decision making." In Digital Avionics Systems Conference (DASC), 2014 IEEE/AIAA 33rd, pp. 1E1-1. IEEE. 2014.
34. MITRE Center for Advanced Aviation System Development "Report NextGen Independent Assessment and Recommendations." October 2014.
35. SESAR. "Trajectory Management Document." Project ID B.04.2 Edition 00.02.90. September 2010.
36. EUROCONTROL. "Network Operations Portal." EUROCONTROL website. <https://www.public.nm.eurocontrol.int/PUBPORTAL/gateway/spec/>. Last accessed on February 15, 2016.
37. EUROCONTROL. "Mission Trajectory Detailed Concept." DDS/CM/SPM/SESAR/12-042. Release 1.0. October 22, 2012.
38. Billings, Charles E. Aviation automation: The search for a human-centered approach. 1997.
39. FAA/EUROCONTROL. "ACTION PLAN 16: Trajectory Prediction-Related Terminology." 2010.
40. RTCA SC-214/ EUROCAE WG78. "4D Trajectory Data Link Operational Service Description." August 2009.
41. Mondoloni, Stéphane, and Sipke Swierstra. "Commonality in disparate trajectory predictors for air traffic management applications." In Digital Avionics Systems Conference, 2005. DASC 2005. The 24th, vol. 1, pp. 3-C. IEEE. 2005.
42. Graves, Debra J., Rolf Stefani, William Brian Pemberton, Alan Martin Williard, and Ernest Joseph Siegrist. "ACARS messages over iridium." U.S. Patent 7,904,081, issued March 8, 2011.
43. Warren, Anthony. "Trajectory prediction concepts for next generation air traffic management." In 3rd USA/Europe ATM R&D Seminar. 2000.
44. Frontera, Guillermo, Juan A. Besada, Ana M. Bernardos, Enrique Casado, and Javier Lopez-Leones. "Formal Intent-Based Trajectory Description Languages." Intelligent Transportation Systems, IEEE Transactions on 15, no. 4: 1550-1566. 2014.
45. BR&T-E, D. F. S. "Avtech." COURAGE: Domain Analysis. 2006.
46. Besada, Juan A., Guillermo Frontera, Joao Bernardo Crespo, Enrique Casado, and Javier Lopez-Leones. "Automated aircraft trajectory prediction based on formal intent-related language processing." Intelligent Transportation Systems, IEEE Transactions on 14, no. 3: 1067-1082. 2013.

47. Torres, Sergio, Jon Dehn, Edward McKay, Mike M. Paglione, and Brian S. Schnitzer. "En-Route Automation Modernization (ERAM) trajectory model evolution to support trajectory-based operations (TBO)." In 2015 IEEE/AIAA 34th Digital Avionics Systems Conference (DASC), pp. 1A6-1. IEEE, 2015.
48. Walker, Marilyn Gisk. "A Benefits Assessment of the User Request Evaluation Tool (URET)." *Air Traffic Control Quarterly* 10, no. 4. 2002.
49. Volpe National Transportation System Center. "Enhanced Traffic Management System (ETMS) Functional Description, Version 5.0." Report DTS56-TMS-002. US Department of Transportation. June 1995.
50. Walter, Randy. "Flight Management Systems." *The Avionics Handbook*: 264-288. 2001.
51. Slattery, Rhonda, and Yiyuan Zhao. "Trajectory synthesis for air traffic automation." *Journal of Guidance, Control, and Dynamics* 20, no. 2: 232-238. 1997.
52. Glover, Willian, and John Lygeros. "A multi-aircraft model for conflict detection and resolution algorithm evaluation." HYBRIDGE Deliverable D 1. 2004.
53. EUROCONTROL. "Impact assessments for noise, gaseous and particulate emissions, and local air quality." Eurocontrol website. <http://www.eurocontrol.int/services/impact>. Last accessed on February 14, 2016.
54. Schnitzer, Brian S., Young, Christina M., Paglione, Mike and Chu Yao. "Evaluation of a Kinetic Modeling Approach to Aircraft Trajectory Prediction in the En-Route Automation Modernization System." DOT/FAA/TC-TN15/5. March 2015.
55. Vivona, Robert A., Karen T. Cate, and Steven M. Green. "Abstraction techniques for capturing and comparing trajectory predictor capabilities and requirements." In AIAA Guidance, Navigation, and Control Conference, Honolulu, HI. 2008.
56. Leclaire, C., P. Q. Nguyen, and T. Mandon. "CITRAC: Common Interface for Trajectory Computation." Orly (France), Centre d'Etudes de la Navigation Aerienne (CENA). 1995.
57. Lopez-Leones, Javier, Miguel Vilaplana, Eduardo Gallo, Francisco Navarro, and Carlos Querejeta. "The aircraft intent description language: a key enabler for air-ground synchronization in trajectory-based operations." In Digital Avionics Systems Conference, 2007. DASC'07. IEEE/AIAA 26th, pp. 1-D. IEEE. 2007.
58. López, Javier, Miguel Vilaplana, Ibrahim Bayraktutar, Joel Klooster, José Manuel Asensio, Greg McDonald, and Peter Kappertz. "Towards an open test bed for the study of trajectory synchronization in the future ATM system: The ASIS Initiative." In Integrated Communications, Navigation and Surveillance Conference, 2009. ICNS'09, pp. 1-14. IEEE. 2009.

59. Mondoloni, Stephane, Sipke Swierstra, and Mike Paglione. "Assessing trajectory prediction performance-metrics definition." In Digital Avionics Systems Conference, 2005. DASC 2005. The 24th, vol. 1, pp. 3-C. IEEE. 2005.
60. Ryan, Hollis F., Mike Paglione, and Steven M. Green. "Review of trajectory accuracy methodology and comparison of error measurement metrics." In Proceedings American Institute of Aeronautics and Astronautics (AIAA) Guidance, Navigation, and Control Conference, Providence, Rhode Island. 2004.
61. Torres, Sergio. "Determination and ranking of trajectory accuracy factors." In Digital Avionics Systems Conference (DASC), 2010 IEEE/AIAA 29th, pp. 1-C. IEEE. 2010.
62. Knorr, Dave, and Leif Walter. "Trajectory Uncertainty and the Impact on Sector Complexity and Workload." SESAR Innovation Days. 2001.
63. Copenbarger, Richard A. "Climb trajectory prediction enhancement using airline flight-planning information." In AIAA Guidance, Navigation, and Control Conference, p. 170. 1999.
64. Jackson, Michael R., Yiyuan J. Zhao, and Rhonda A. Slattery. "Sensitivity of trajectory prediction in air traffic management." *Journal of Guidance, Control, and Dynamics* 22, no. 2 (1999): 219-228.
65. Navarro, Francisco, Ernesto Valls, Miguel Vilaplana, Piero Chessa, and Carlos Querejeta. "System and method for defining and predicting aircraft trajectories." EP2889579, application published July 1, 2015.
66. Jackson, Michael Rollin Charles. "Sensitivity of trajectory prediction in air traffic management and flight management systems." PhD diss., University of Minnesota. 1997.
67. Yepes, Javier Lovera, Inseok Hwang, and Mario Rotea. "New algorithms for aircraft intent inference and trajectory prediction." *Journal of guidance, control, and dynamics* 30, no. 2: 370-382. 2007.
68. EUROCONTROL Experimental Center, "User Manual for the Base of Aircraft Data (BADA) Family 4", Technical/Scientific Report No. 12/11/22-58. April 2014.
69. Vilaplana, Miguel A., and Francisco A. Navarro. "COURAGE: Key Performance Indicators for Aircraft Intent Description Models." 2005.
70. Hall, Timothy, Stephen Mackey, Steven Lang, and Jeffrey Tittsworth. "Localizer Flight Technical Error measurement and uncertainty." In Digital Avionics Systems Conference (DASC), 2011 IEEE/AIAA 30th, pp. 4A3-1. IEEE. 2011.
71. Lopez Leones, Javier. "Definition of an aircraft intent description language for air traffic management applications." PhD diss., University of Glasgow. 2008.

72. Hangos, Katalin M., József Bokor, and Gábor Szederkényi. Analysis and control of nonlinear process systems. Springer Science & Business Media. 2006.
73. Vilaplana, Miguel, Eduardo Gallo, Francisco Navarro, and Sip Swierstra. "Towards a formal language for the common description of aircraft intent." In Digital Avionics Systems Conference, 2005. DASC 2005. The 24th, vol. 1, pp. 3-C. IEEE. 2005.
74. Boyle, M. J. Department of Defense World Geodetic System 1984-It's definition and relationship with local geodetic systems. DMA Technical Report 83502.2., Washington, DC, 1987.
75. National Geospatial-Intelligence Agency. "Office of Geomatics: World Geodetic System 1984 (WGS 84)." 2014. <http://earth-info.nga.mil/GandG/wgs84/index.html>. Last accessed on February 14, 2016.
76. Lemoine, Frank G., Steve C. Kenyon, John K. Factor, Ronald G. Trimmer, Nikolaos K. Pavlis, Douglas S. Chinn, Christopher M. Cox et al. "The development of the joint NASA GSFC and the National Imagery and Mapping Agency (NIMA) geopotential model EGM96." (1998).
77. EUROCONTROL. "Base of Aircraft Data (BADA)." Eurocontrol Research & SESAR website. 2015. <https://www.eurocontrol.int/services/bada>. Last accessed on February 15, 2016.
78. Nuic A.; Poinot C.; Iagaru M.G.; Gallo E.; Navarro F.A.; Querejeta C.; "Advanced Aircraft Performance Modeling For ATM: Enhancements To The BADA Model," 4th Digital Avionics System Conference, Washington D.C. October 30 – November 3, 2005.
79. Green, Steven M., Michael P. Grace, and David H. Williams. "Flight test results: CTAS and FMS cruise/descent trajectory prediction accuracy." In 3rd USA/Europe Air Traffic Management R&D Seminar, Napoli, Italy. 2000.
80. Mondoloni, Stephane, Mike Paglione, and Steve Green. "Trajectory modeling accuracy for air traffic management decision support tools." In ICAS 2002 Congress, Toronto, ON. 2002.
81. NOAA. "The Rapid Update Cycle." NOAA website, Earth System Research Laboratory. 2012. <http://ruc.noaa.gov/>. Last accessed on February 15, 2016.
82. Lygeros, John, and Maria Prandini. "Aircraft and weather models for probabilistic collision avoidance in air traffic control." In IEEE Conference on Decision and Control, vol. 3, pp. 2427-2432. IEEE; 2002.
83. Lee, Alan G., Stephen S. Weygandt, Barry Schwartz, and James R. Murphy. "Performance of trajectory models with wind uncertainty." In AIAA Modeling and Simulation Technologies Conference, Chicago, Illinois. 2009.
84. MacGarvin, Malcolm. Late lessons from early warnings: the precautionary principle 1896-2000. Office for Official Publications of the European Communities. 2001.

85. Moreno, Carolina, Oliver Todt, and José Luis Luján. "The context (s) of precaution: Ideological and instrumental appeals to the precautionary principle." *Science Communication* 32, no. 1: 76-92. 2010.
86. Johnson, C. W., and A. Jeunemaitre. "Future directions for contingency planning in European Air Traffic Management: a response to the April 2010 Eyjafjallajökull volcano eruption." 2010.
87. Walker, Warren E., Poul Harremoës, Jan Rotmans, Jeroen P. van der Sluijs, Marjolein BA van Asselt, Peter Janssen, and Martin P. Kraymer von Krauss. "Defining uncertainty: a conceptual basis for uncertainty management in model-based decision support." *Integrated assessment* 4, no. 1: 5-17. 2003
88. Zipfel, Peter H. "Modelling and simulation of aerospace vehicle dynamics." American Institute of Aeronautics and Astronautics. 2000.
89. Mukai, Conrad, and George Hunter. "A higher fidelity point-mass simulation of aircraft dynamics." In *AIAA Guidance, Navigation and Control Conference*, San Diego, CA. 1996.
90. Federal Aviation Administration. "Pilot's Handbook of Aeronautical Knowledge – Chapter 10: Aircraft Performance." FAA-H-8083-25A. 2008.
91. Daggett, David L., Silvio Ortanderl, David Eames, Jeffrey J. Berton, and Christopher A. Snyder. *Revisiting Water Injection for Commercial Aircraft*. NASA/CR-2004-212957, Copyright© 2004 SAE International, 2004.
92. Society of Automotive Engineers (SAE), Committee A-21, Aircraft Noise; "Procedure for the Computation of Airplane Noise in the Vicinity of Airports", Aerospace Information Report No. 1845, Warrendale, PA: Society of Automotive Engineers Inc., March 1986.
93. European Civil Aviation Conference (ECAC) Doc 29 "Report on Standard Method of Computing Noise Contours around Civil Airports", 3rd Edition, Volume 1: Applications Guide. 2005.
94. Su, Wei-Nian. "Evaluation of aircraft performance algorithms in Federal Aviation Administration's Integrated Noise Model." PhD diss., Massachusetts Institute of Technology. 1999.
95. EUROCONTROL. "Base of Aircraft Data (BADA)." Eurocontrol Research & SESAR website. 2015. <https://www.eurocontrol.int/services/bada>. Last accessed on February 16, 2016.
96. Poles, Damir, Angela Nuic, and Vincent Mouillet. "Advanced aircraft performance modeling for ATM: Analysis of BADA model capabilities." In *Digital Avionics Systems Conference (DASC)*, 2010 IEEE/AIAA 29th, pp. 1-D. IEEE. 2010.

97. Gallo, Eduardo, Francisco Navarro, Angela Nuic, and Mihai Iagaru. "Advanced Aircraft Performance Modelling for ATM: BADA 4.0 Results." In 25th Digital Avionics Systems Conference, 2006 IEEE/AIAA, pp. 1-12. IEEE. 2006.
98. Nuic, Angela, Chantal Poinot, Mihai-George Iagaru, Eduardo Gallo, Francisco A. Navarro, and Carlos Querejeta. "Advanced aircraft performance modelling for ATM: enhancements to the BADA model." In 24th Digital Avionics System Conference, Washington D.C. 2005.
99. Vos, Roelof, and Saeed Farokhi. *Introduction to Transonic Aerodynamics*. Vol. 110. Springer. 2015.
100. AIRBUS Customer Services Directorate, "Getting to grips with aircraft performance monitoring." 2002.
101. Filippone, Antonio. *Advanced aircraft flight performance*. Vol. 34. Cambridge University Press. 2012.
102. Longmuir, Mark, and Na A. Ahmed. "Commercial aircraft exterior cleaning optimization." *Journal of Aircraft* 46, no. 1: 284-290. 2009.
103. Casado, Enrique, Miguel Vilaplana, and Colin Goodchild. "Sensitivity of Trajectory Prediction Accuracy to Aircraft Performance Uncertainty." AIAA Infotech@Aerospace (I@A) Conference, Guidance, Navigation, and Control and Co-located Conferences, Boston (MA). 2013.
104. Zaita, Anthony V., Greg Buley, and Glen Karlsons. "Performance deterioration modeling in aircraft gas turbine engines." In ASME 1997 International Gas Turbine and Aeroengine Congress and Exhibition, pp. V004T16A007-V004T16A007. American Society of Mechanical Engineers. 1997.
105. Krajčėk, Karolina, Dario Nikolić, and Anita Domitrović. "AIRCRAFT PERFORMANCE MONITORING FROM FLIGHT DATA." *Technical Gazette* 19, no. 4: 709-715. 2013.
106. Fueri, Monique. "Aircraft Performance Degradation", 16th Airbus Performance and Operations Conference. May 2009.
107. Lions, Jacques-Louis, Roger Temam, and Shouhong Wang. "New formulations of the primitive equations of atmosphere and applications." *Nonlinearity* 5, no. 2 (1992): 237.
108. Mason, John. "Numerical weather prediction." In *Proceedings of the Royal Society of London A: Mathematical, Physical and Engineering Sciences*, vol. 407, no. 1832, pp. 51-60. The Royal Society, 1986.
109. Kalnay, E., M. Kanamitsu, and W. E. Baker. "Global numerical weather prediction at the National Meteorological Center." *Bulletin of the American Meteorological Society* 71, no. 10 (1990): 1410-1428.

110. Mass, Clifford F., and Ying-Hwa Kuo. "Regional real-time numerical weather prediction: Current status and future potential." *Bulletin of the American Meteorological Society* 79, no. 2 (1998): 253.
111. White, P. W. "Finite-difference methods in numerical weather prediction." In *Proceedings of the Royal Society of London A: Mathematical, Physical and Engineering Sciences*, vol. 323, no. 1553, pp. 285-292. The Royal Society, 1971.
112. Bourke, William. "A multi-level spectral model. I. Formulation and hemispheric integrations." *Monthly Weather Review* 102, no. 10 (1974): 687-701.
113. Tanguay, M., A. Staniforth, and A. Simard. "A three-dimensional semi-Lagrangian scheme for the Canadian regional finite-element forecast model." *Monthly weather review* 117, no. 8 (1989): 1861-1871.
114. Frank, William M. "The cumulus parameterization problem." *Monthly weather review* 111, no. 9 (1983): 1859-1871.
115. Moninger, William R., Richard D. Mamrosh, and Patricia M. Pauley. "Automated meteorological reports from commercial aircraft." *Bulletin of the American Meteorological Society* 84, no. 2 (2003): 203.
116. O'Connor, Lauraleen. "NOAA's observing requirements collection process—making a global difference." In *21st International Conference on Interactive Information Processing Systems*. 2005.
117. Cole, R. E., C. Richard, S. Kim, and D. Bailey. "Assessment of the 60 km Rapid Update Cycle (RUC) with Near Real-Time Aircraft Reports." 1998.
118. Chaloulos, Georgios, and John Lygeros. "Wind Uncertainty Correlation and Aircraft Conflict Detection based on RUC-1 Forecasts." In *AIAA Guidance, Navigation and Control Conference and Exhibit*, p. 6870. 2007.
119. Martin, R. C., M. M. Wolfson, and R. G. Hollowell. "MDCRS: Aircraft observations collection and uses." In *Preprints, 5th Int. Conf. on Aviation Weather Systems*, Vienna, VA, p. 317. 1993.
120. Robert, Emilien, and David de Smedt. "Comparison of operational wind forecasts with recorded flight data." In *10th USA/Europe ATM R&D Seminar*. 2013.
121. Tandale, Monish D., S. S. Vaddi, P. Sengupta, and S. Lin. "Spatio-temporally correlated wind uncertainty model for simulation of terminal airspace operations." In *13th Aviation Technology, Integration, and Operations (ATIO) Conference*, Los Angeles, CA, pp. 12-14. 2013.

122. Parker, Wendy S. "Predicting weather and climate: Uncertainty, ensembles and probability." *Studies in History and Philosophy of Science Part B: Studies in History and Philosophy of Modern Physics* 41, no. 3 (2010): 263-272.
123. Zhu, Yuejian, Zoltan Toth, Richard Wobus, David Richardson, and Kenneth Mylne. "The economic value of ensemble-based weather forecasts." *Bulletin of the American Meteorological Society* 83, no. 1 (2002): 73.
124. Cheung, Jacob, Alan Hally, Jaap Heijstek, Adri Marsman, and Jean-Louis Brenguier. "Recommendations on trajectory selection in flight planning based on weather uncertainty." In *5th SESAR Innovation Days*, Bologna, Italy. 2015.
125. Persson, Anders. "User Guide to ECMWF forecast products." 2001.
126. Cheung, Jacob, Jean-Louis Brenguier, Jaap Heijstek, Adri Marsman, and Helen Wells. "Sensitivity of Flight Durations to Uncertainties in Numerical Weather Prediction." In *4th SESAR Innovation Days*, Madrid, Spain. 2014.
127. Mondoloni, Stephane, and Dianna Liang. "Improving trajectory forecasting through adaptive filtering technique." *Proceedings of 5th USA-Europe ATM Seminar*. 2003.
128. Schuster, Wolfgang. "Trajectory Prediction Algorithms." SESAR TESA project, D1.2. 2012.
129. Lee, Alan G., Stephen S. Weygandt, Barry Schwartz, and James R. Murphy. "Performance of trajectory models with wind uncertainty." In *AIAA Modeling and Simulation Technologies Conference*, Chicago, Illinois. 2009.
130. Mondoloni, Stéphane. "A multiple-scale model of wind-prediction uncertainty and application to trajectory prediction." In *6th AIAA Aviation Technology, Integration and Operations Conference (ATIO)*, pp. 1-14. 2006.
131. Steiner, Matthias, and J. Krozel. "Translation of ensemble-based weather forecasts into probabilistic air traffic capacity impact." In *Digital Avionics Systems Conference, 2009. DASC'09. IEEE/AIAA 28th*, pp. 2-D. IEEE. 2009.
132. Slattery, Rhonda, and Yiyuan Zhao. "Trajectory synthesis for air traffic automation." *Journal of Guidance, Control, and Dynamics* 20, no. 2: 232-238. 1997.
133. Schwarz, Diana Estévez, and René Lamour. "The computation of consistent initial values for nonlinear index-2 differential-algebraic equations." *Numerical Algorithms* 26, no. 1: 49-75. 2001.
134. Brenan, Kathryn Eleda. "Stability and convergence of difference approximations for higher index differential algebraic systems with applications in trajectory control." PhD diss. 1983.

135. Liu, Weiyi, and Inseok Hwang. "Probabilistic trajectory prediction and conflict detection for air traffic control." *Journal of Guidance, Control, and Dynamics* 34, no. 6: 1779-1789. 2011.
136. Wiener, Norbert. "The homogeneous chaos." *American Journal of Mathematics* 60, no. 4 (1938): 897-936.
137. Vazquez, Rafael, and Damián Rivas. "Propagation of initial mass uncertainty in aircraft cruise flight." *Journal of Guidance, Control, and Dynamics* 36, no. 2 (2013): 415-429.
138. Berveiller, Marc, Bruno Sudret, and Maurice Lemaire. "Stochastic finite element: a non-intrusive approach by regression." *European Journal of Computational Mechanics/Revue Européenne de Mécanique Numérique* 15, no. 1-3 (2006): 81-92.
139. Togawa, Kanali, Andrea Benigni, and Antonello Monti. "A MATLAB graphical user interface for nonintrusive polynomial chaos theory." In *Complexity in Engineering (COMPENG)*, 2012, pp. 1-6. IEEE, 2012.
140. O'Hagan, Anthony. "Polynomial chaos: A tutorial and critique from a statistician's perspective." *SIAM/ASA J. Uncertainty Quantification* 20 (2013): 1-20.
141. Xiu, Dongbin, and George Em Karniadakis. "The Wiener--Askey polynomial chaos for stochastic differential equations." *SIAM journal on scientific computing* 24, no. 2 (2002): 619-644.
142. Oladyshkin, Sergey, and Wolfgang Nowak. *Polynomial Response Surfaces for Probabilistic Risk Assessment and Risk Control via Robust Design*. INTECH Open Access Publisher, 2012.
143. Li, Heng, Pallav Sarma, and Dongxiao Zhang. "A comparative study of the probabilistic-collocation and experimental-design methods for petroleum-reservoir uncertainty quantification." *SPE Journal* 16, no. 02 (2011): 429-439.
144. Najm, Habib N. "Uncertainty quantification and polynomial chaos techniques in computational fluid dynamics." *Annual Review of Fluid Mechanics* 41 (2009): 35-52.
145. Dodson, Michael, and Geoffrey T. Parks. "Robust aerodynamic design optimization using polynomial chaos." *Journal of Aircraft* 46, no. 2 (2009): 635-646.
146. Ghanem, Roger, and P. D. Spanos. "Polynomial chaos in stochastic finite elements." *Journal of Applied Mechanics* 57, no. 1 (1990): 197-202.

147. Agarwal, Nitin, and N. R. Aluru. "A data-driven stochastic collocation approach for uncertainty quantification in MEMS." *International Journal for Numerical Methods in Engineering* 83, no. 5 (2010): 575-597.
148. Kewlani, Gaurav, Justin Crawford, and Karl Iagnemma. "A polynomial chaos approach to the analysis of vehicle dynamics under uncertainty." *Vehicle System Dynamics* 50, no. 5 (2012): 749-774.
149. Oladyshkin, S., and W. Nowak. "Data-driven uncertainty quantification using the arbitrary polynomial chaos expansion." *Reliability Engineering & System Safety* 106 (2012): 179-190.
150. Li, Heng, and Dongxiao Zhang. "Probabilistic collocation method for flow in porous media: Comparisons with other stochastic methods." *Water Resources Research* 43, no. 9 (2007).
151. Saltelli, Andrea, Marco Ratto, Terry Andres, Francesca Campolongo, Jessica Cariboni, Debora Gatelli, Michaela Saisana, and Stefano Tarantola. "Global sensitivity analysis: the primer." John Wiley & Sons, 2008.
152. Garcia-Cabrejo, Oscar, and Albert Valocchi. "Global sensitivity analysis for multivariate output using polynomial chaos expansion." *Reliability Engineering & System Safety* 126 (2014): 25-36.
153. Sudret, Bruno. "Global sensitivity analysis using polynomial chaos expansions." *Reliability Engineering & System Safety* 93, no. 7 (2008): 964-979.
154. Xie, Qimiao, Shouxiang Lu, Daniel Cóstola, and J. Hensen. "An Arbitrary Polynomial Chaos-Based Approach to Analyzing the Impacts of Design Parameters on Evacuation Time under Uncertainty." *Fire Safety Science* 11 (2014): 1077-1090.
155. National Centers for Environmental Predictions Products Inventory. GFS Ensemble Forecast System. <http://www.nco.ncep.noaa.gov/pmb/products/gens/>. Last accessed on March 26, 2016.
156. Mueller, Eric R., and Gano B. Chatterji. "Analysis of aircraft arrival and departure delay characteristics." In *AIAA aircraft technology, integration and operations (ATIO) conference*. 2002.
157. Radio Technical Commission for Aeronautics. *Safety and Performance Standard for Baseline 2 ATS Data Communications (Baseline 2 Interop Standard) Initial Release (DO-350/ED228)*. Washington DC: RTCA (2013).
158. Xiu, Dongbin, and George Em Karniadakis. "The Wiener--Askey polynomial chaos for stochastic differential equations." *SIAM journal on scientific computing* 24, no. 2 (2002): 619-644.

APPENDIX A

AIRCRAFT PERFORMANCE DEGRADATION MODELLING USING RECORDED FLIGHT DATA

The recorded flight data are a source of information that is extensively exploited by airlines for maintenance purposes. However, it is possible to use it for updating the performance models available to the ground-based trajectory prediction tools to enhance their prediction capabilities, and, for instance, to improve the flight planning processes. The procedure showed in Figure A-1 represents a solution to the problem of modelling the degradation of the aircraft performance. The procedure outputs are the uncertainty performance coefficients defined in Section 4.4. With these values, it is possible to build improved APMs based on the polynomial description of the aircraft performance stated by the BADA 4.1 specification.

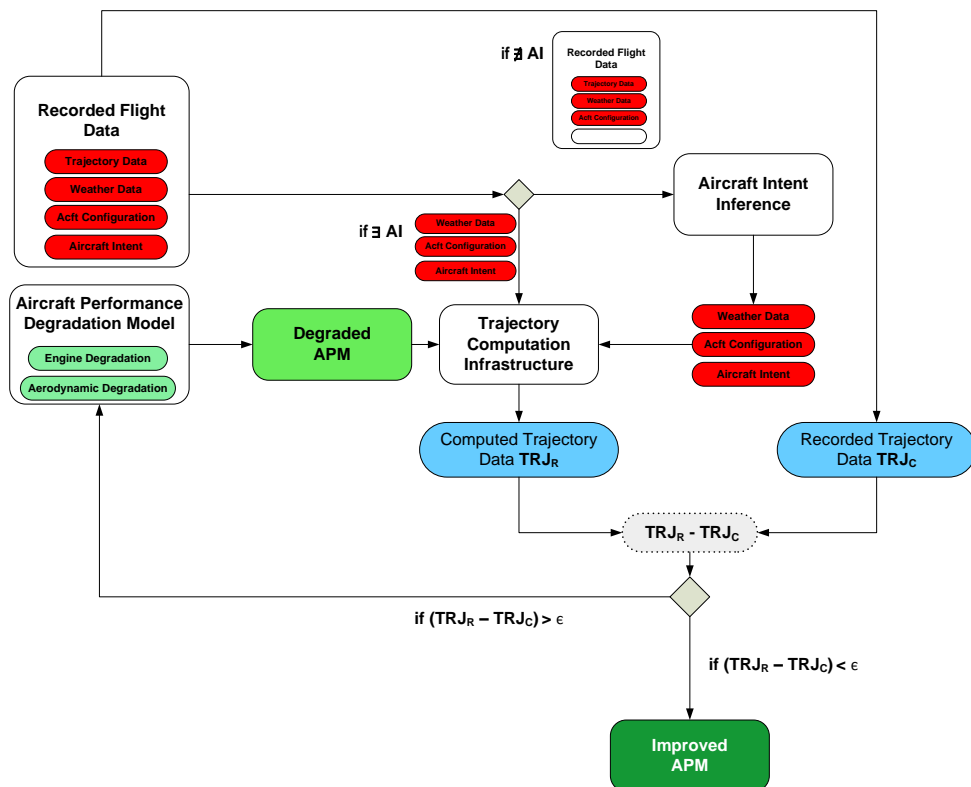


Figure A-1 – Aircraft Performance Degradation Modelling

The procedure requires the following elements.

- **Recorded Flight Data.** Information about the state variables of a real flight recorded by the Flight Data Recorder System (FDRS) on board. This set of data contains information related to the 4D trajectory, aircraft configuration, and actual weather conditions faced by the aircraft during the flight.
- **Aircraft Performance Degradation Model (APDM).** The APDM mainly relates the extra fuel consumption produced by the aerodynamics and propulsion performance degradation with the polynomial description of the drag polar curve and the engine thrust curve. This model represents how performance degrades with time and operations.
- **Degraded APM.** This is made by polynomial descriptions of aircraft performance including the degradation effects described by the APDM. The hypotheses provided by the APDM are translated into the coefficients that improve the nominal performance descriptors (e.g., BADA polynomial models).
- **Trajectory Computation Infrastructure.** Computational infrastructure required for calculating an aircraft trajectory based on the set of required inputs (Aircraft Intent, Weather Model, Initial Conditions, and APM).
- **Aircraft Intent Inference Engine.** Infrastructure capable of deducing aircraft intent that corresponds to the flown trajectory by inferring it from the recorded flight data. This model provides the altitude and speed laws that describe the vertical profile of the trajectory, and a function of the geographic latitude and longitude for determining the lateral profile.
- **Improved APM.** Improved polynomial description of the aircraft performance that provides the model that best represents the actual aircraft performance.

The output of the process is an enhanced APM, which can be considered as the final instance of the APM obtained after an iterative process that best fits the performance of a real aircraft.

The complete process is described in the following list.

- With the APDM hypothesis related to the degradation of aircraft performances, a degraded APM is generated. The APDM identifies the coefficients of the polynomial descriptions of the drag polar curve and engine thrust curve that can represent the degradation of performances. The nominal values of such coefficients are replaced by values that approximate such degradation. With the new polynomial description of the aircraft performances provided by the APDM, a degraded APM is generated.
- This degraded APM is used for computing a trajectory.
- Making use of the degraded APM, a new computation is launched to compare the data with recorded trajectory information. If the recorded data includes information about the flown aircraft intent, the computation process is straightforward. If not, a process for inferring the aircraft intent needs to be executed. This process provides the aircraft intent by analysing the trajectory data.
- Then, the computed (TRJC) and the real (TRJR) trajectories are compared.
- If the difference of target state variables (basically, fuel consumption) between the nominal and degraded cases is negligible, an enhanced APM is obtained. If not, an iterative process that implies a modification of the APDM is followed until such difference meets the defined threshold (ϵ).

The process can be executed for each available set of recorded flight data of the same aircraft. This process would ensure that the aircraft performance modelling gathers the most updated information about the considered aircraft.

This page intentionally left blank

APPENDIX B

TRAJECTORY PREDICTION UNCERTAINTY DUE TO UNIFORMLY DISTRIBUTED APM UNCERTAINTY

Section 4.5 presents the impact on aircraft trajectory uncertainty of the aircraft performance degradation, assuming a triangular distribution of drag and fuel consumption coefficients between the nominal and maximum degraded values.

The following section gathers the results obtained with a uniform distribution of the aforementioned coefficients. In this case, all possible values are considered as equally probable. Figure B-1 depicts the distribution of the fuel consumption coefficients.

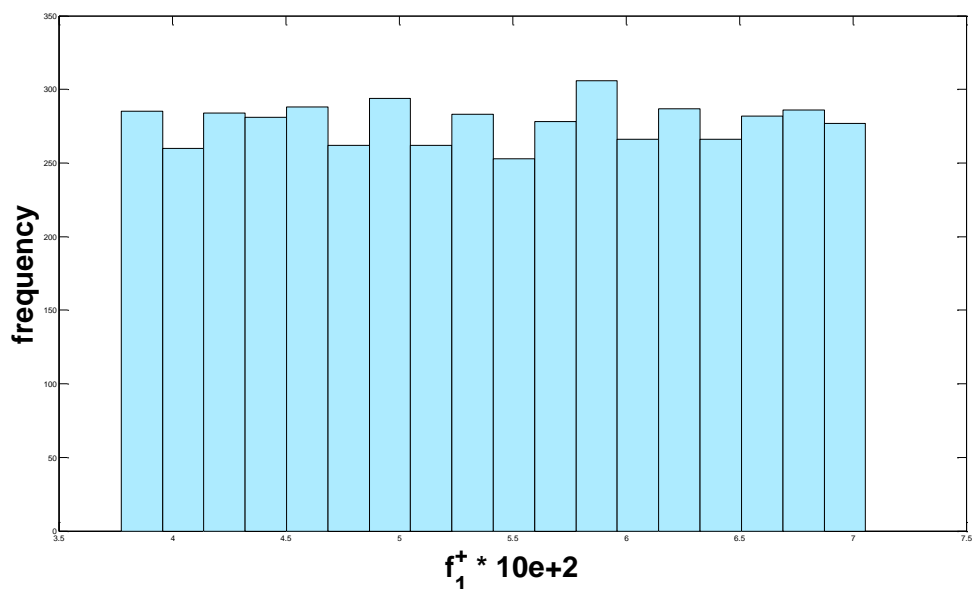


Figure B-1 – Uniform Distribution of f_1^+

B-1. Cruise

The distribution of masses at the end of a flight segment identical to that described in 4.5.1, considering the mentioned set of uniform distributed APMs, is depicted in Figure B-2 as

function of the performance coefficients d_1^+ and f_1^+ . The blue diamond indicates where the mean value is located.

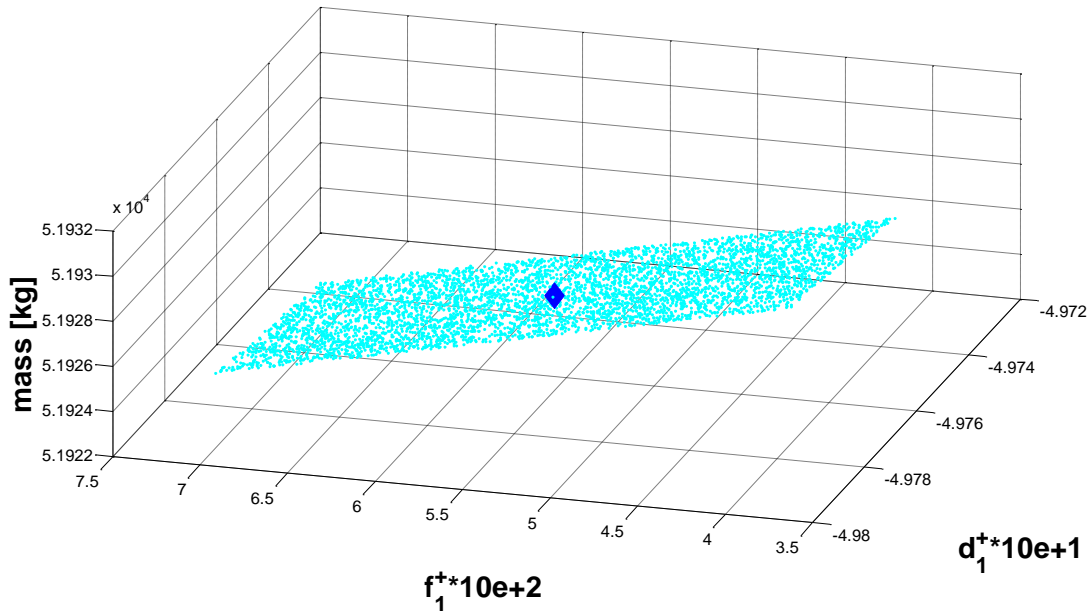


Figure B-2 – Aircraft Mass Variability (Cruise Case)

The resulting linear fitting provides the same result as shown in Section 4.5.1, while the root mean square error represents the excellence of the fit.

$$mass = 5.068400 \cdot 10^4 - 2.290394 \cdot 10^3 d_1^+ - 1.614089 \cdot 10^2 f_1^+ \quad (0-1)$$

$$RMS_{CRS_case} = 2.7019 \cdot 10^{-9} \quad (0-2)$$

B-2. Climb

The distribution of elapsed times at the end of a flight segment identical to that described in 4.5.2 is depicted in Figure B-3. The blue diamond indicates where the mean value is located.

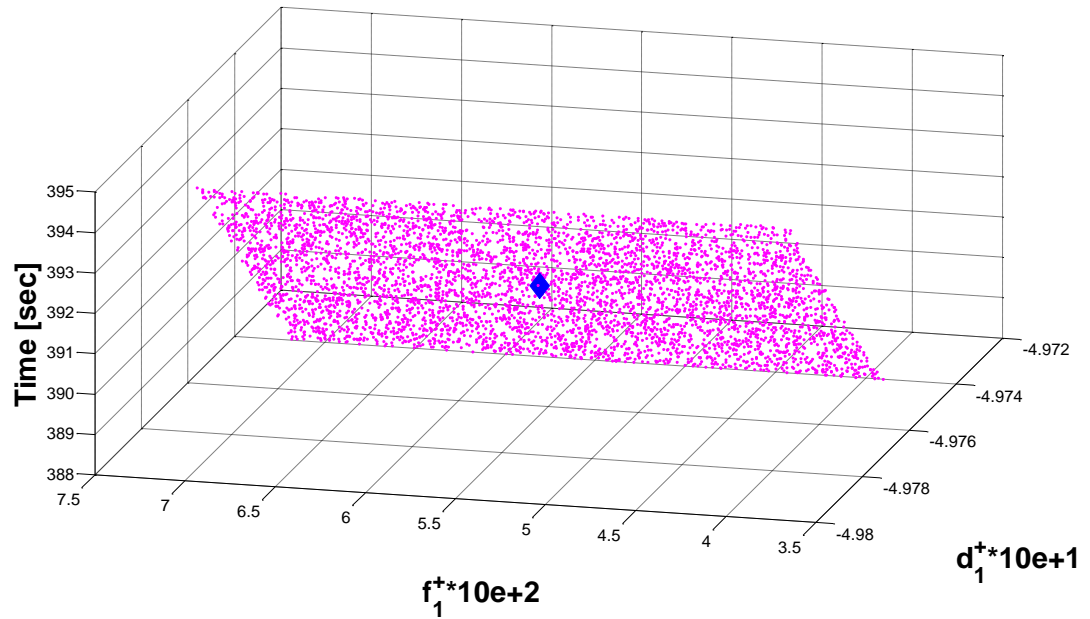


Figure B-3 – Elapsed Time Variability (Climb Case)

The resulting linear fitting provides the same result as shown in Section 4.5.2, while the root mean square error represents the excellence of the fit.

$$elpsd_t = 5.256416 \cdot 10^3 + 9.372825 \cdot 10^3 d_1^+ - 3.959850 \cdot 10^{-1} f_1^+ \quad (0-3)$$

$$RMS_{CMB_case} = 1.1593 \cdot 10^{-7} \quad (0-4)$$

B-3. Descent

The distribution of CAS at the end of a flight segment identical to that described in Figure 4-11 is depicted in Figure B-4. The red diamond indicates where the mean value is located.

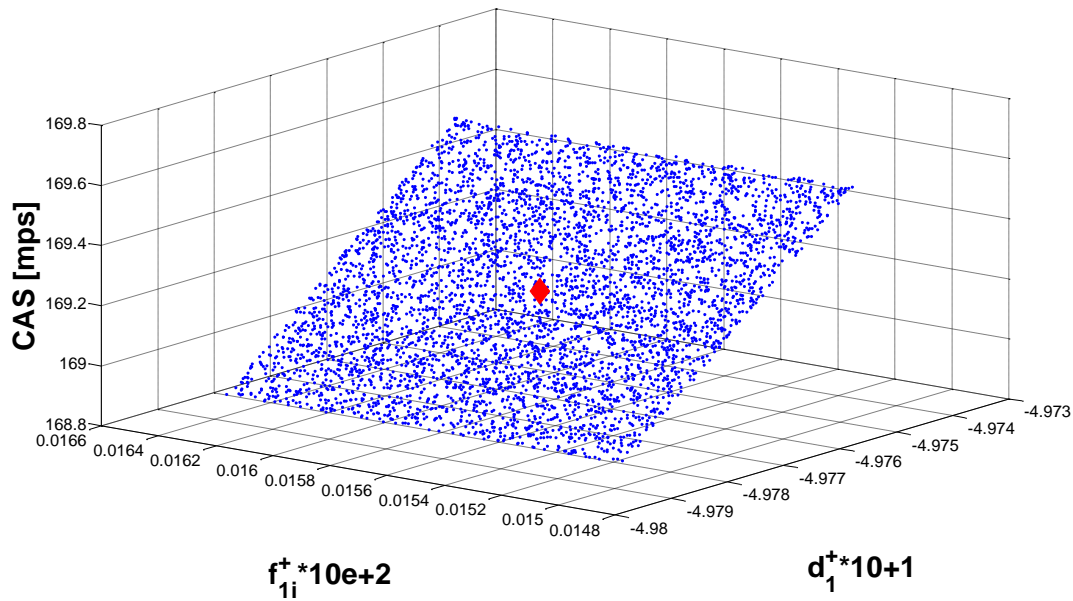


Figure B-4 – CAS Variability (Descent Case)

The resulting linear fitting provides the same result as shown in Section 4.5.3, while the root mean square error represents the excellence of the fit.

$$cas = 1.09587 \cdot 10^3 + 1.692207 \cdot 10^3 d_1^+ + 3.145595 \cdot 10^{-1} f_{1i}^+ \quad (0-5)$$

$$RMS_{DES_case} = 7.8290 \cdot 10^{-10} \quad (0-6)$$

APPENDIX C

AIDL ALPHABET & GRAMMAR SUMMARY

AIDL Alphabet

Set Law/Track	Speed	Vertical	Propulsive	Lateral	Configuration Profiles
SL HS HSL HHS EL HE VSL HVS SPA PAL HPA OLPA VSL HVS SPA PAL HPA OLPA VSG PAG AG VPG TC ST TL HT OLT LDC SBA BAL HBA OLBA LDG CL HC LPG TLP HLC SHL HLL HHL HLG SBC SSB SBL HSB OLSB LGC	SG HSG EG	VSG PAG AG VPG	TC ST TL HT OLT	LDG CL HC LPG TLP	HLC SBC LGC

Open loop input

#	Keyword	Instruction	Target
1	SL	Speed Law	
2	HS	Hold Speed	v_{TAS}
3	HSL	Horizontal Speed Law	
4	HHS	Hold Horizontal Speed	$v_{TAS} \cos \gamma_{TAS}$
5	EL	Energy Law	
6	HE	Hold Energy	dh_{TAS}/dt
7	VSL	Vertical Speed Law	
8	HVS	Hold Vertical Speed	$v_{TAS} \sin \gamma_{TAS}$
9	SPA	Set Path Angle	
10	PAL	Path Angle Law	
11	HPA	Hold Path Angle	γ_{TAS}
12	OLPA	Open Loop Path Angle	
13	AL	Altitude Law	
14	HA	Hold Altitude	h
15	TVP	Track Vertical Path	λ, ϕ, h
16	ST	Set Throttle	
17	TL	Throttle Law	
18	HT	Hold Throttle	δ_T
19	OLT	Open Loop Throttle	
20	SBA	Set Bank Angle	
21	BAL	Bank Angle Law	
22	HBA	Hold Bank Angle	μ_{TAS}
23	OLBA	Open Loop Bank Angle	
24	CL	Course Law	
25	HC	Hold Course	χ_{TAS}
26	TLP	Track Horizontal Path	λ, ϕ
27	SHL	Seth High Lift devices	
28	HLL	High Lift devices Law	δ_{HL}
29	HHL	Hold High Lift devices	
30	SSB	Set Speed Brakes	
31	SBL	Speed Brakes Law	
32	HSB	Hold Speed Brakes	δ_{SB}
33	OLSB	Open Loop Speed Brakes	
34	SLG	Set Landing Gear	
35	HLG	Hold Landing Gear	δ_{LG}

AIDL Lexicon

- 6 instructions, each from a different group
- Of the 6, 3 must belong to the motion profiles and 3 to the configuration profiles
- The 3 motion instructions must belong to different motion profiles
- Of the 3 motion instructions, 1 must come from the lateral profile

AIDL Syntax

- Lateral instructions can only be followed by lateral instructions
- Instructions from the configuration groups can only be followed by instructions from the same group
- Instructions from vertical, speed and propulsive profiles can only be followed by instructions of those profiles

This page intentionally left blank

APPENDIX D

TRIGGER AND EFFECT UNCERTAINTY MODELS

D-1 Trigger Uncertainty Modelling

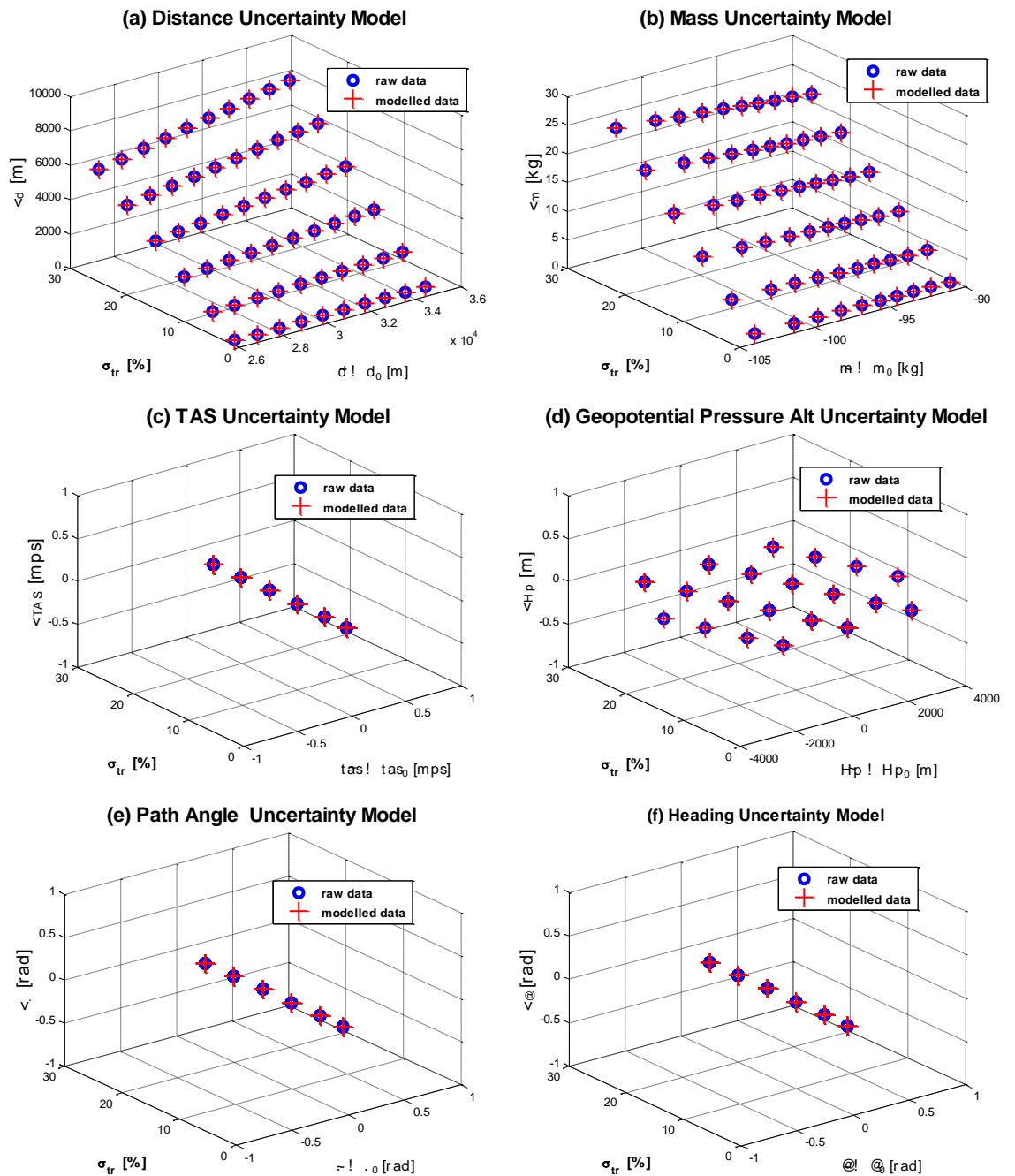


Figure D-1 – CASE CRZ1

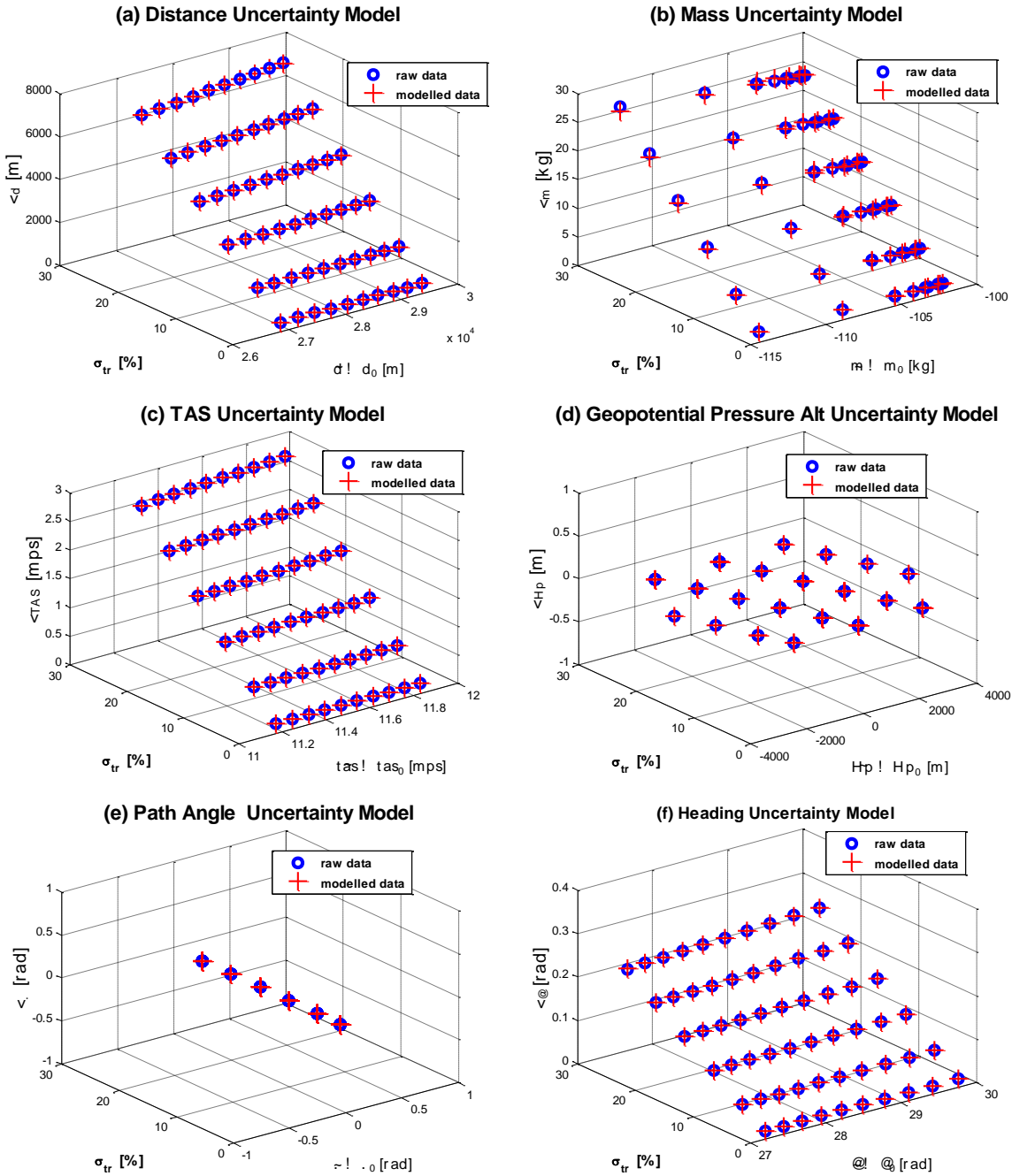


Figure D-2 – CASE CRZ2

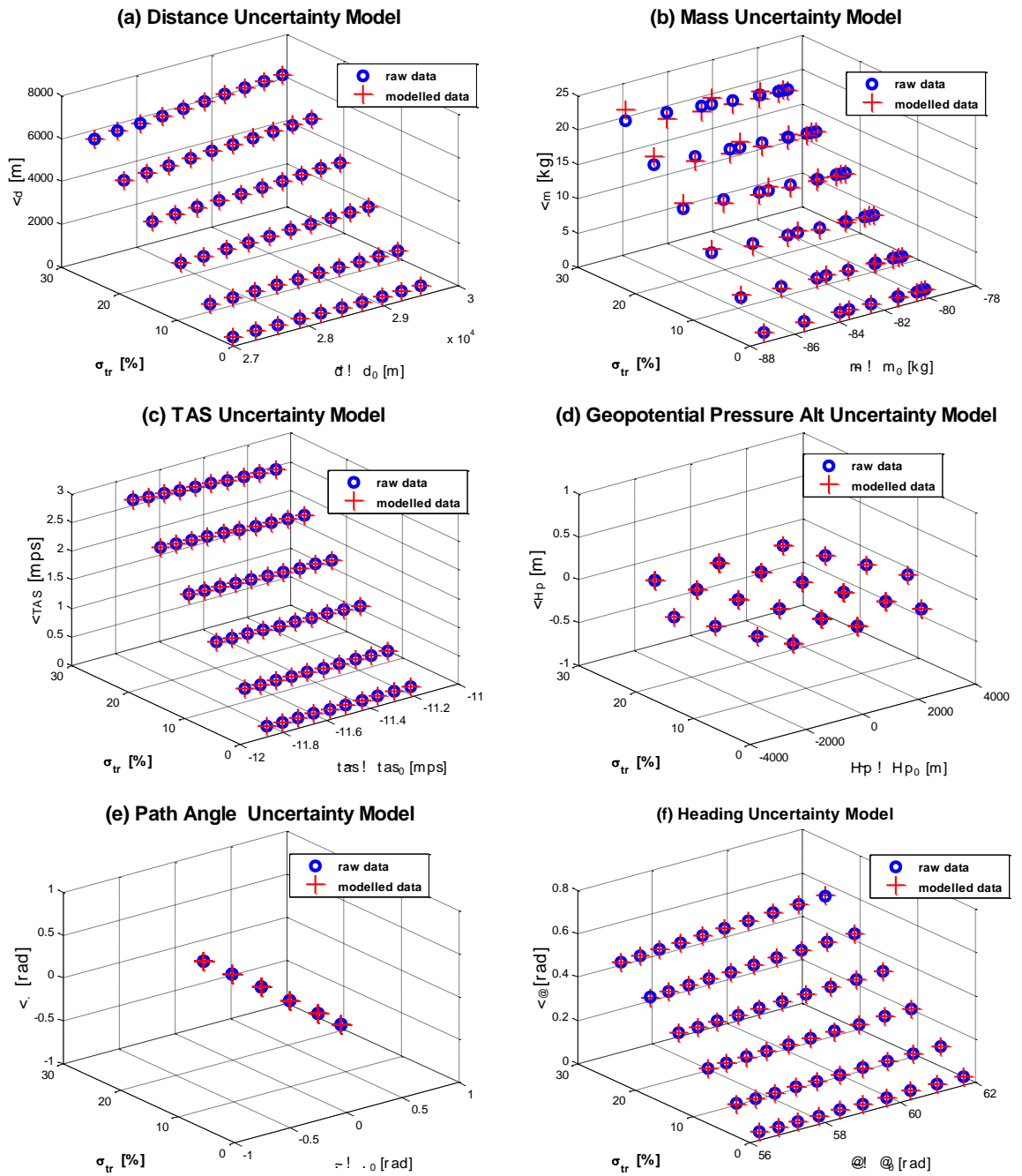


Figure D-3 – CASE CRZ3

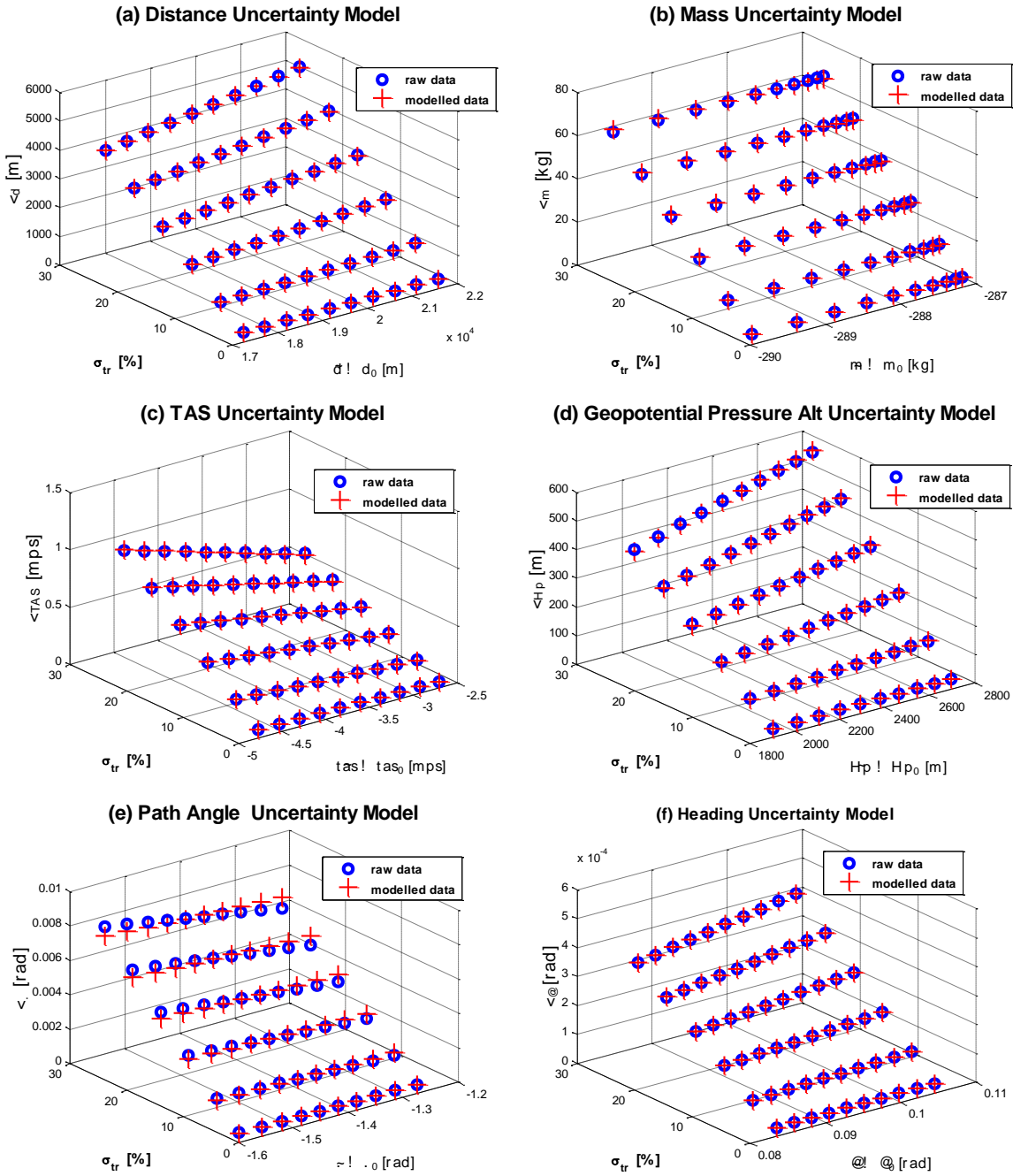


Figure D-4 – CASE CMB1

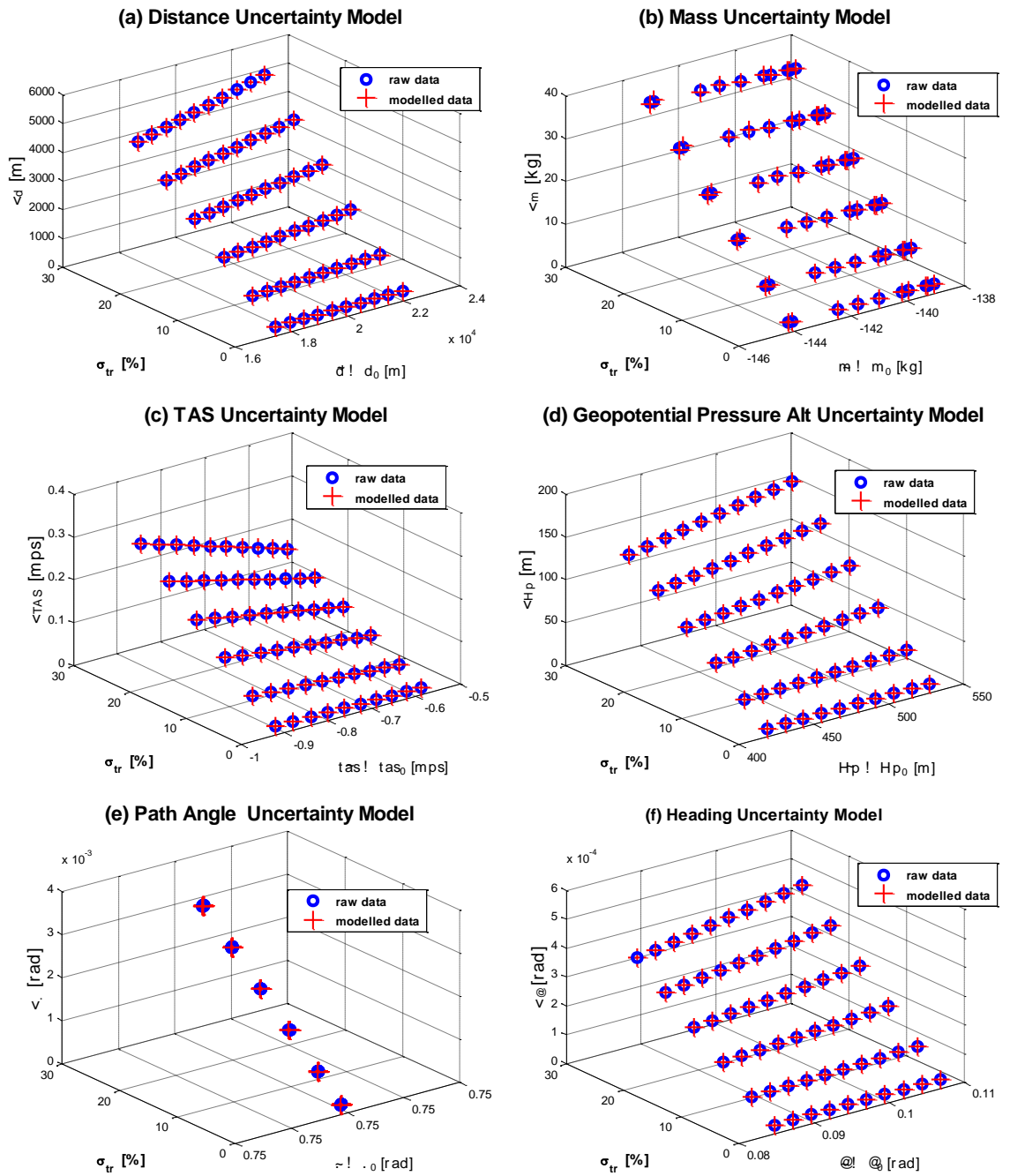


Figure D-5 – CASE CMB2

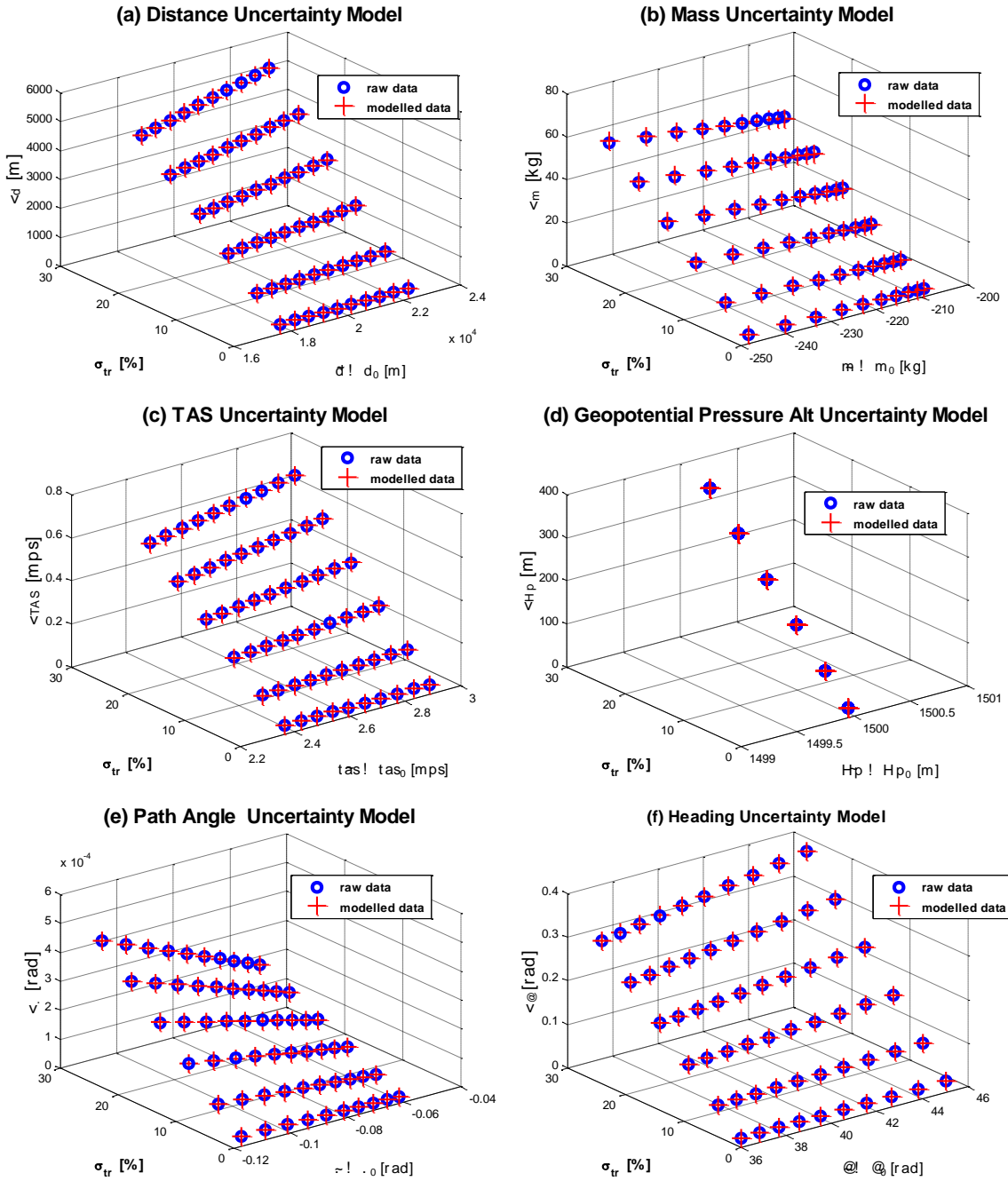


Figure D-6 – CASE CMB4

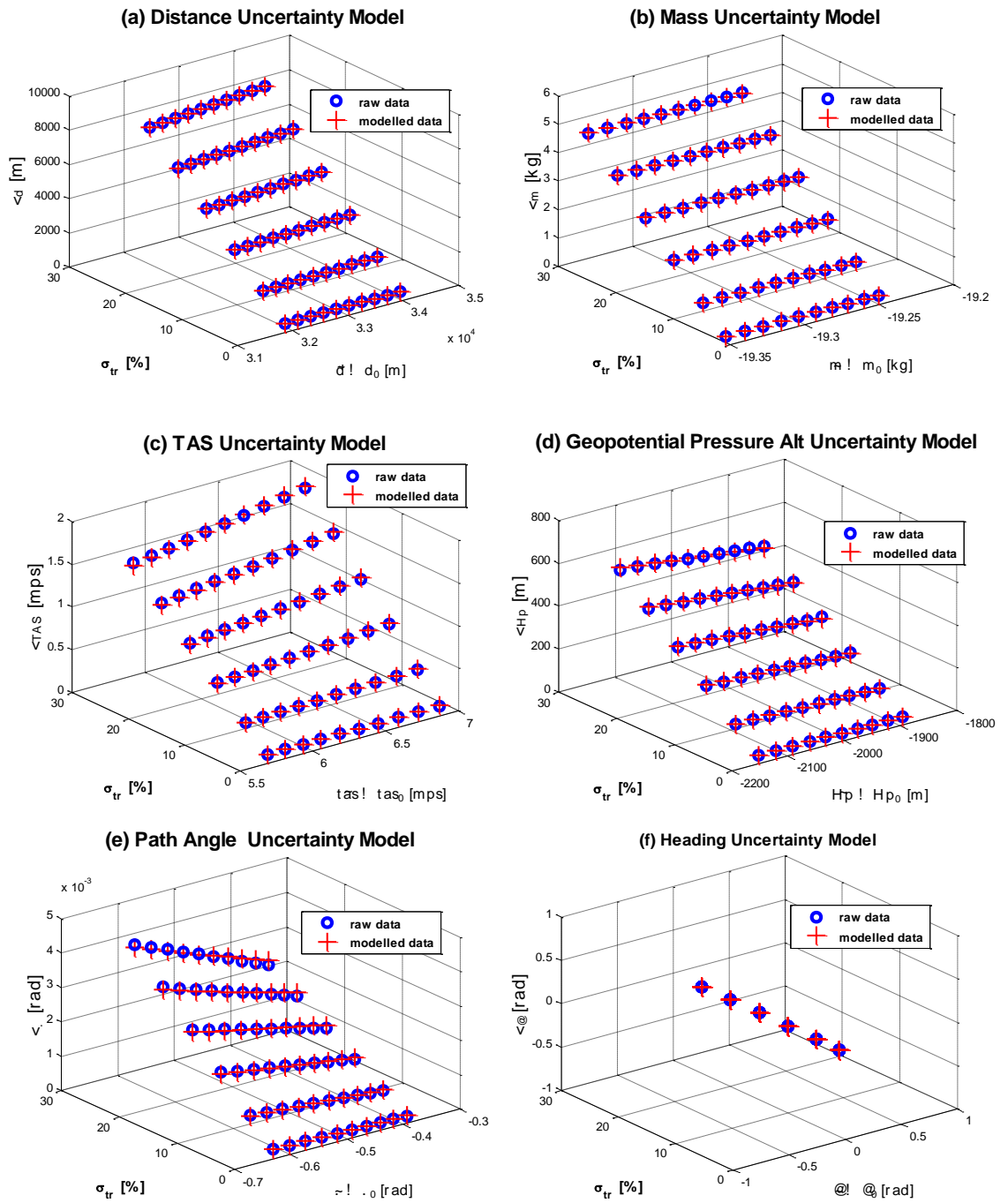


Figure D-7 – CASE DES1

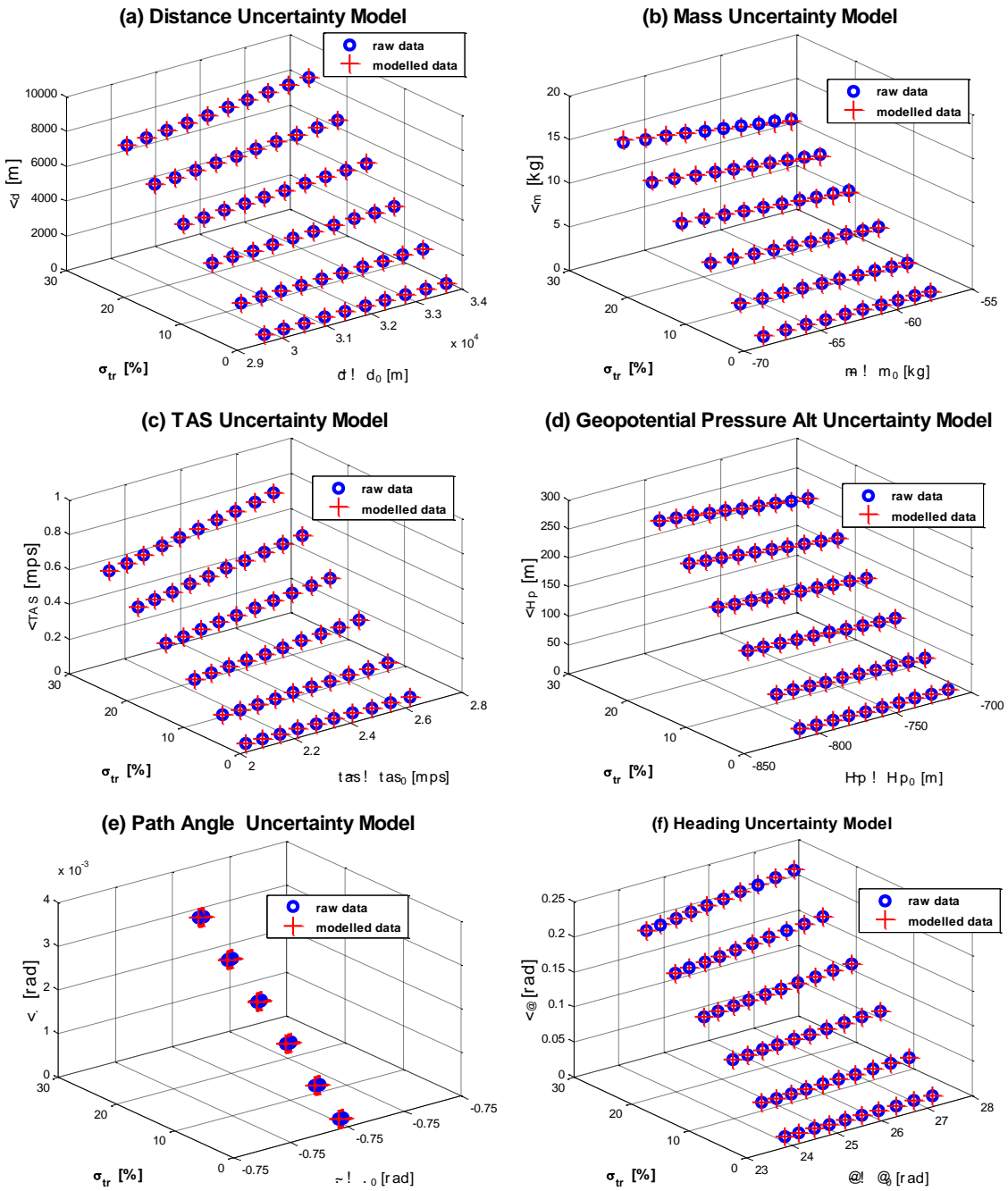


Figure D-8 – CASE DES2

D-2 Effect Uncertainty Modelling

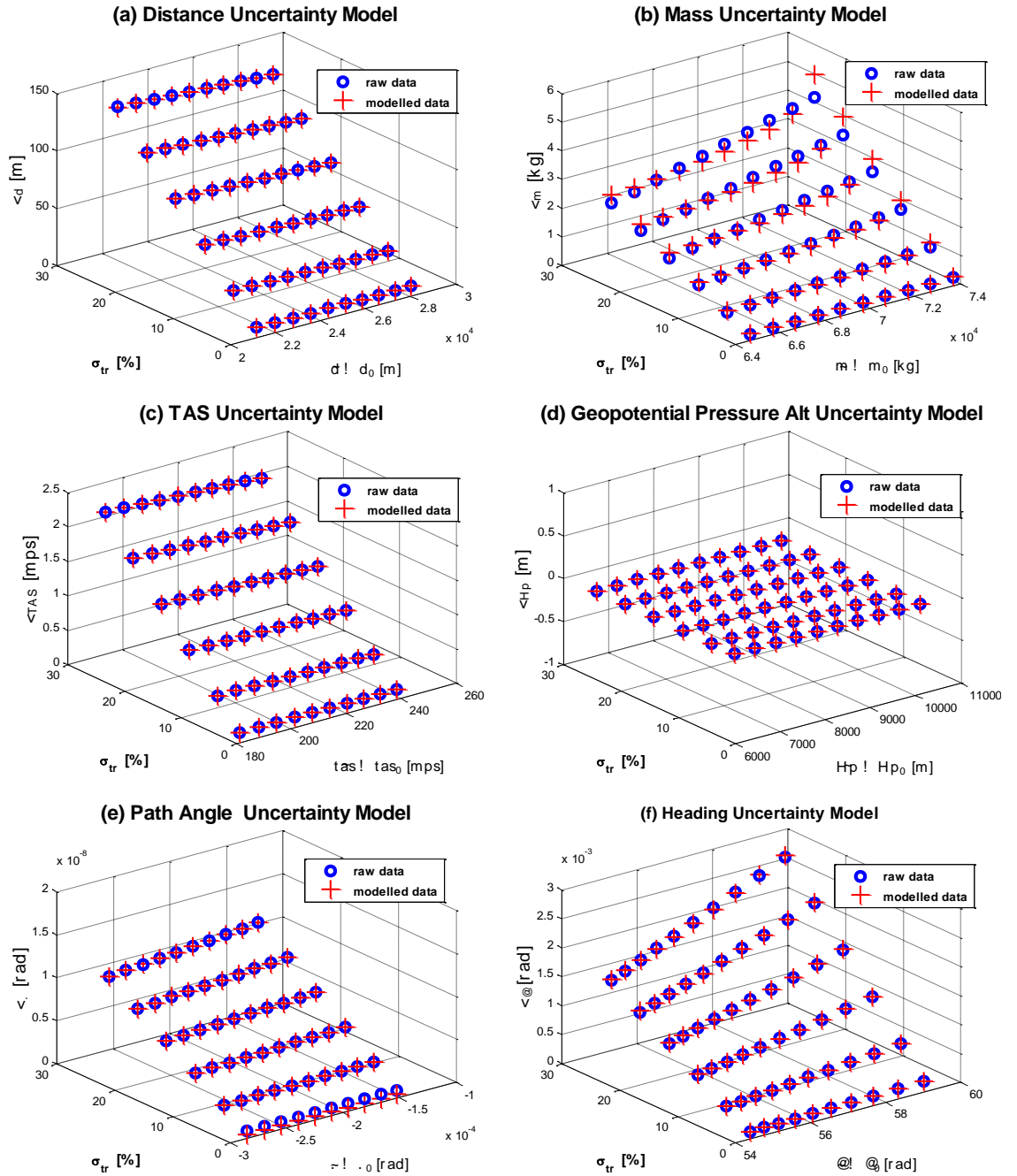


Figure D-9 – CASE CRZ2

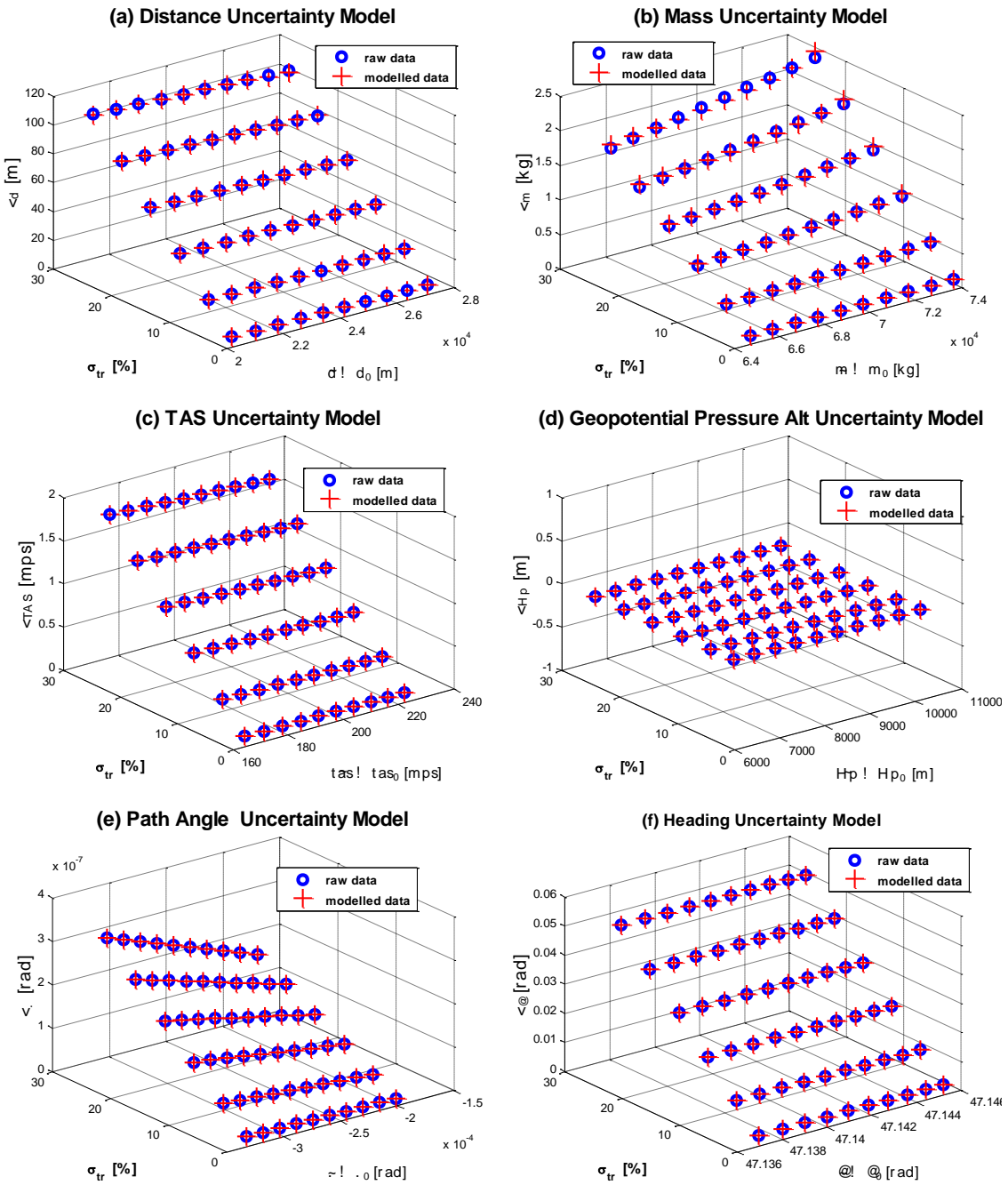


Figure D-10 – CASE CRZ3

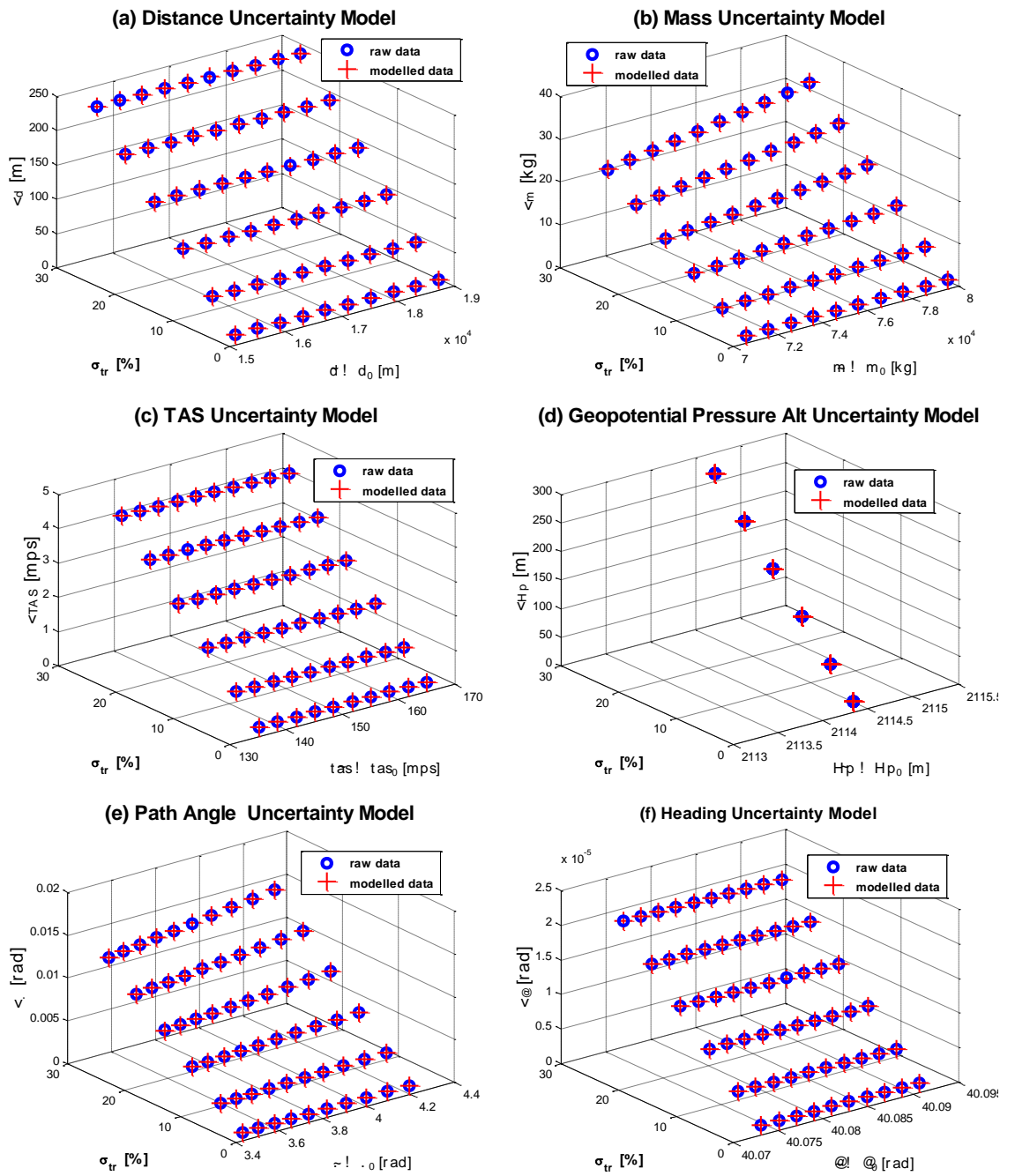


Figure D-11 – CASE CMB4

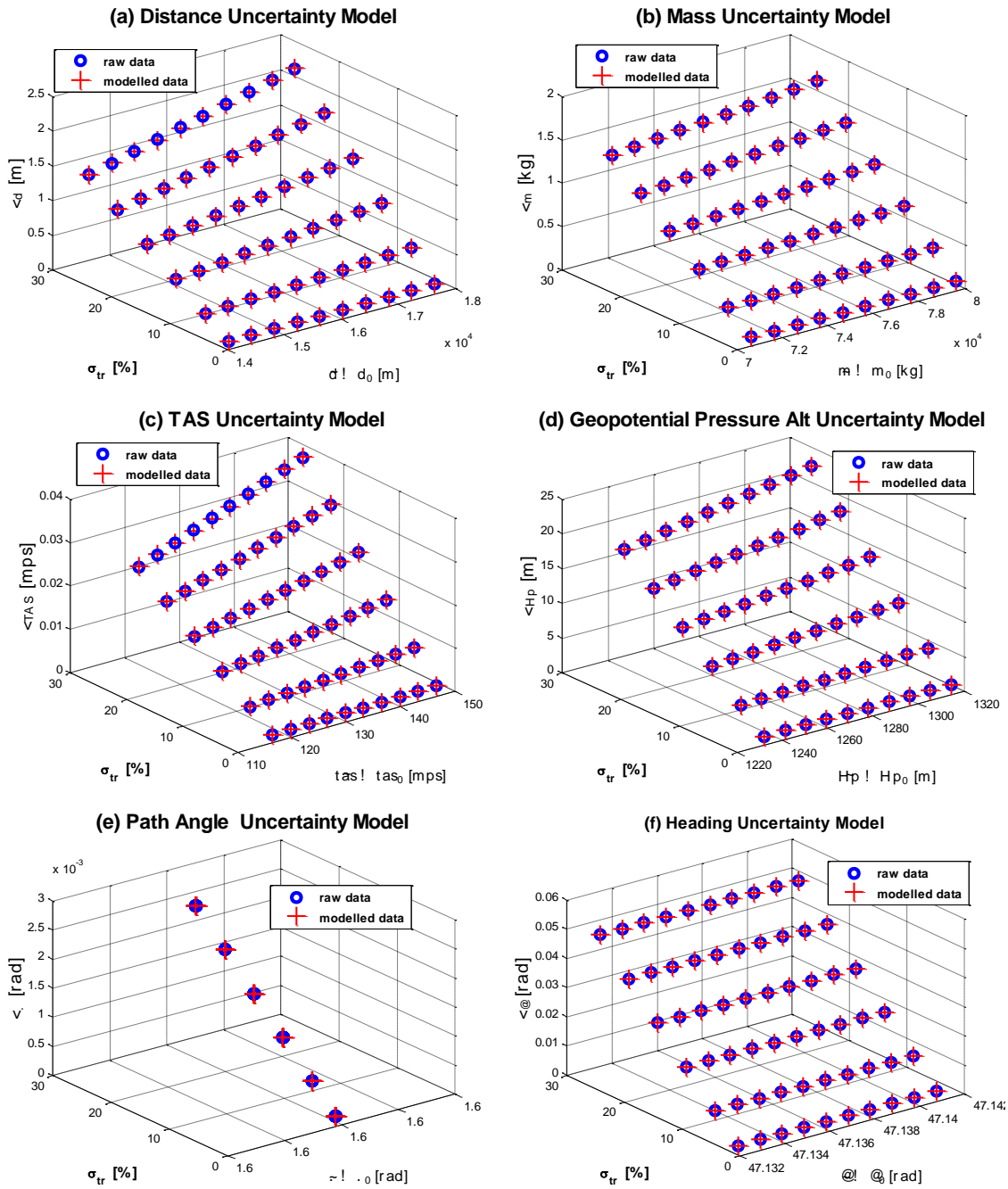


Figure D-12 – CASE CMB5

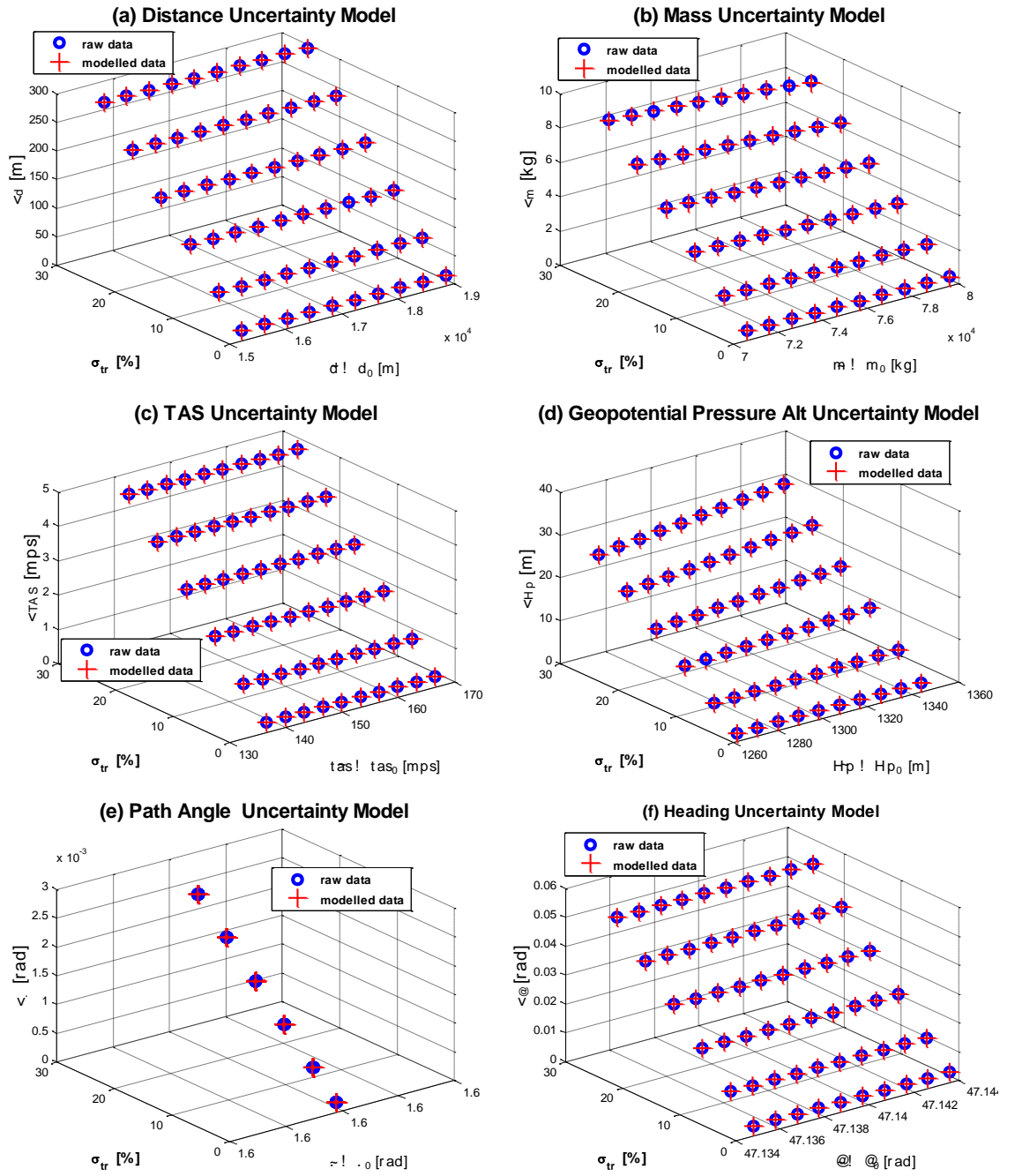


Figure D-13 – CASE CMB6

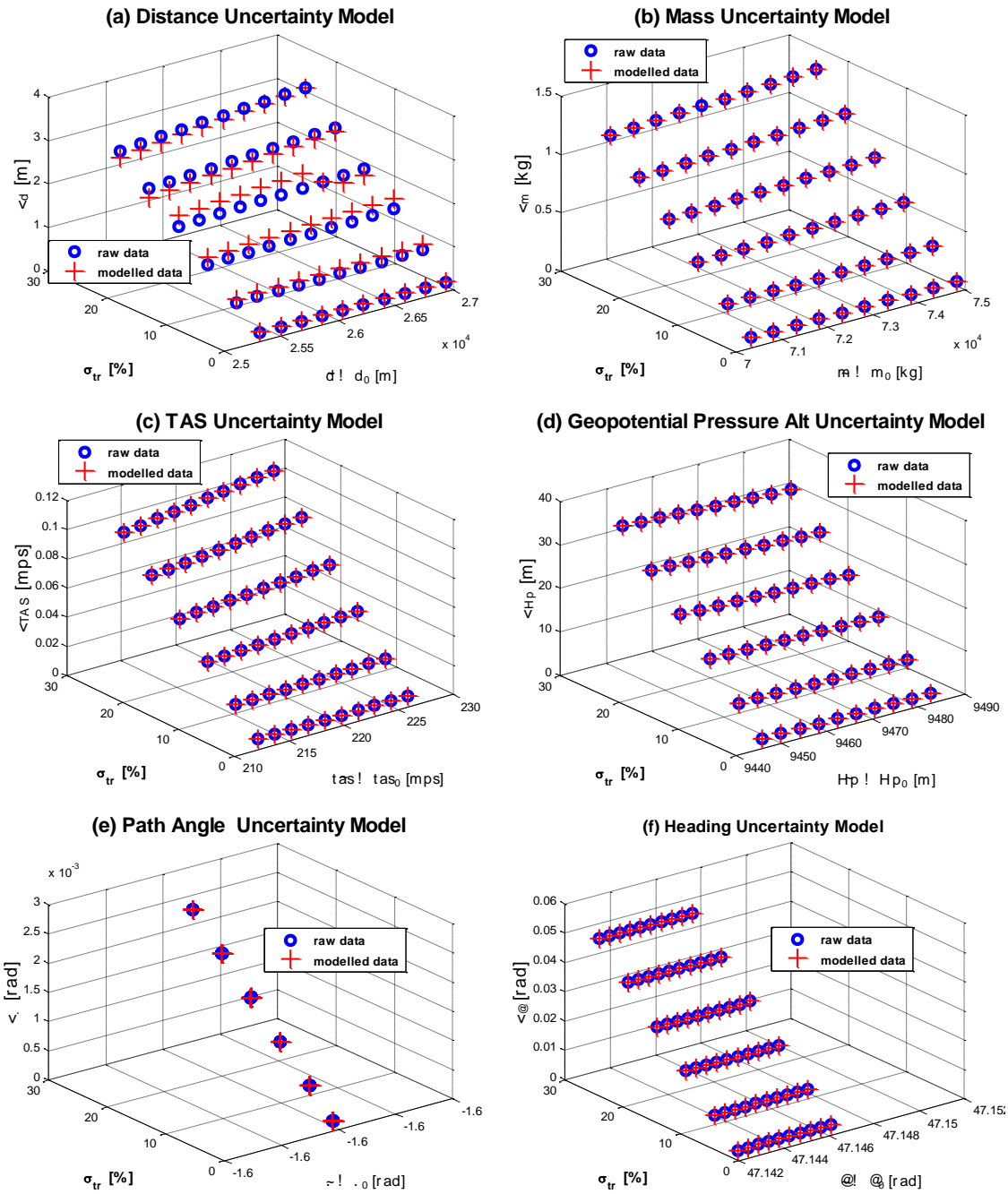


Figure D-14 – CASE DES2

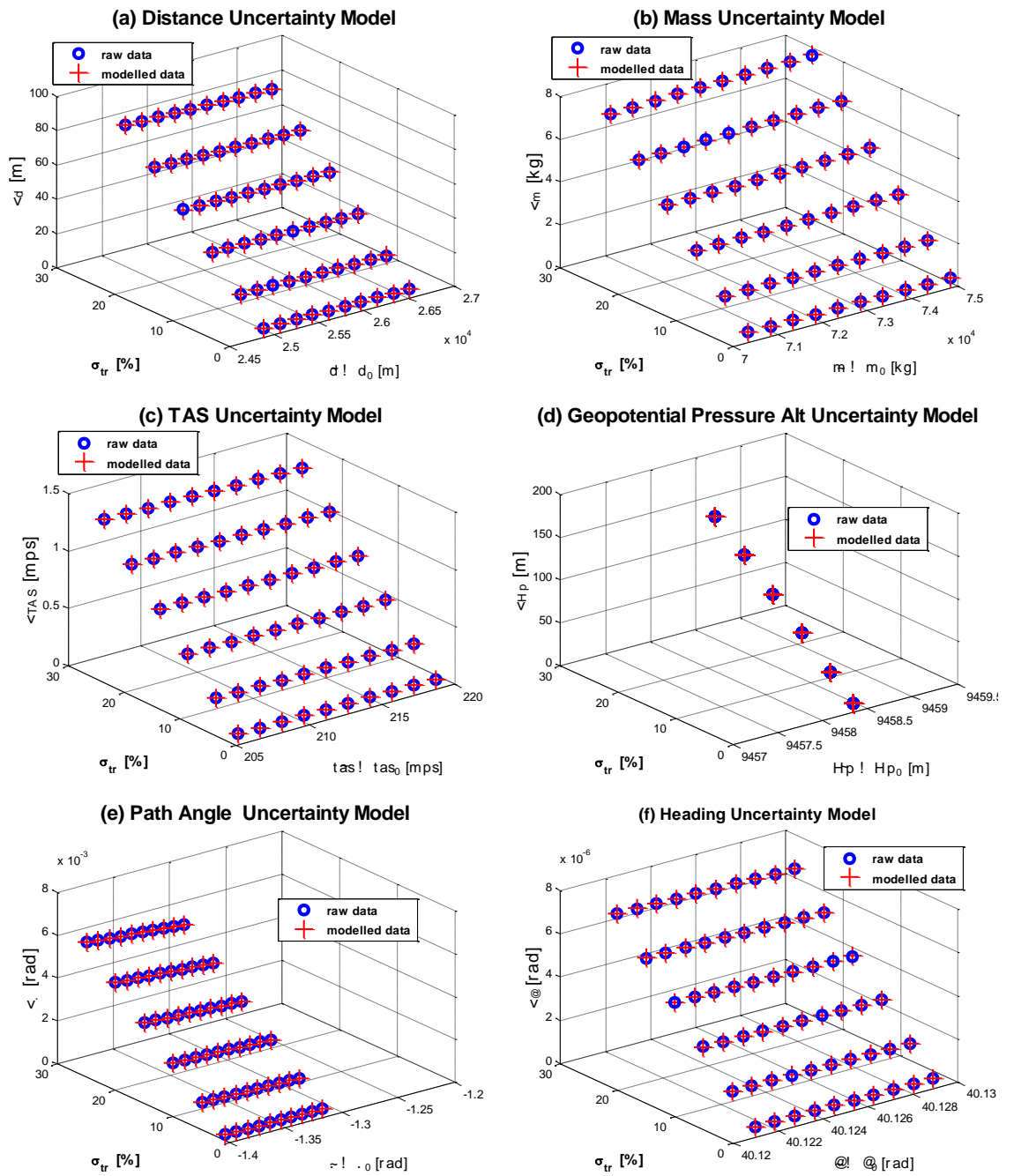


Figure D-15 – CASE DES3

This page intentionally left blank

APPENDIX E

POLYNOMIAL CHAOS EXPANSIONS DETAILS

E-1 Orthonormal Basis Used in gPCE

Generalized PCE was developed to extend its applicability to input variables whose variability did not correspond to a Gaussian process. The following Table E-1 shows the orthogonal polynomial basis associated with the random variables with predefined probability density functions as defined by Xiu [158].

Table E-1 – Case Study: Initial Aircraft State

	Random Variable ξ	Orthogonal Polynomials Φ	Support
Continuous Variables	Gaussian	Hermite	$(-\infty, \infty)$
	Gamma	Laguerre	$[0, \infty)$
	Beta	Jacobi	$[a, b]$
	Uniform	Legendre	$[a, b]$
Discrete Variables	Poisson	Charlier	$\{0, 1, 2, \dots\}$
	Binomial	Krawtchouk	$\{0, 1, 2, \dots, n\}$
	Negative Binomial	Meixner	$\{0, 1, 2, \dots\}$
	Hypergeometric	Hahn	$\{0, 1, 2, \dots, n\}$

The relationship between random variables and types of polynomials is obtained from the Askey scheme of orthogonal polynomials, and extends the Wiener description of PCE.

E-2 Determination of integers o_j^k

The combination of the univariate orthonormal basis used for describing the variability of the inputs leads to the definition of the multivariate polynomial expansion as defined in Equation (7-6). The order q and the number of variables n of the polynomial expansion will determine the combination of univariate polynomials. Following Table E-2 illustrates the matrix of integers o_j^k in case of $d = 2$ and $n = 5$, which corresponds to an expansion of 21 coefficients.

Table E-2 – Matrix of Integers o_j^k

o_j^k					k	$\sum_{j=1}^n o_j^k$	ϕ_i
0	0	0	0	0	1	0	$P_1^0 \cdot P_2^0 \cdot P_3^0 \cdot P_4^0 \cdot P_5^0$
0	0	0	0	1	2	1	$P_1^0 \cdot P_2^0 \cdot P_3^0 \cdot P_4^0 \cdot P_5^1$
0	0	0	1	0	3	1	$P_1^0 \cdot P_2^0 \cdot P_3^0 \cdot P_4^1 \cdot P_5^0$
0	0	1	0	0	4	1	$P_1^0 \cdot P_2^0 \cdot P_3^1 \cdot P_4^0 \cdot P_5^0$
0	1	0	0	0	5	1	$P_1^0 \cdot P_2^1 \cdot P_3^0 \cdot P_4^0 \cdot P_5^0$
1	0	0	0	0	6	1	$P_1^1 \cdot P_2^0 \cdot P_3^0 \cdot P_4^0 \cdot P_5^0$
0	0	0	0	2	7	2	$P_1^0 \cdot P_2^0 \cdot P_3^0 \cdot P_4^0 \cdot P_5^2$
0	0	0	2	0	8	2	$P_1^0 \cdot P_2^0 \cdot P_3^0 \cdot P_4^2 \cdot P_5^0$
0	0	2	0	0	9	2	$P_1^0 \cdot P_2^0 \cdot P_3^2 \cdot P_4^0 \cdot P_5^0$
0	2	0	0	0	10	2	$P_1^0 \cdot P_2^2 \cdot P_3^0 \cdot P_4^0 \cdot P_5^0$
2	0	0	0	0	11	2	$P_1^2 \cdot P_2^0 \cdot P_3^0 \cdot P_4^0 \cdot P_5^0$
1	1	0	0	0	12	2	$P_1^1 \cdot P_2^1 \cdot P_3^0 \cdot P_4^0 \cdot P_5^0$
1	0	1	0	0	13	2	$P_1^1 \cdot P_2^0 \cdot P_3^1 \cdot P_4^0 \cdot P_5^0$
1	0	0	1	0	14	2	$P_1^1 \cdot P_2^0 \cdot P_3^0 \cdot P_4^1 \cdot P_5^0$
1	0	0	0	1	15	2	$P_1^1 \cdot P_2^0 \cdot P_3^0 \cdot P_4^0 \cdot P_5^1$
0	1	0	0	1	16	2	$P_1^0 \cdot P_2^1 \cdot P_3^0 \cdot P_4^0 \cdot P_5^1$
0	0	1	0	1	17	2	$P_1^0 \cdot P_2^0 \cdot P_3^1 \cdot P_4^0 \cdot P_5^1$
0	0	0	1	1	18	2	$P_1^0 \cdot P_2^0 \cdot P_3^0 \cdot P_4^1 \cdot P_5^1$
0	0	1	1	0	19	2	$P_1^0 \cdot P_2^0 \cdot P_3^1 \cdot P_4^1 \cdot P_5^0$
0	1	0	1	0	20	2	$P_1^0 \cdot P_2^1 \cdot P_3^0 \cdot P_4^1 \cdot P_5^0$
0	1	1	0	0	21	2	$P_1^0 \cdot P_2^1 \cdot P_3^1 \cdot P_4^0 \cdot P_5^0$